SYNTHESIS AND CHARACTERIZATION OF 1,8-NAPHTHALIMIDE AND NAPHTHOTHIADIAZOLE DERIVATIVES AS LIGHT-EMITTING MATERIALS FOR ORGANIC LIGHT-EMITTING DIODES

Sumita Boonnab

A Thesis Submitted in Partial Fulfillment of the Requirements for the
Degree of Doctor of Philosophy in Chemistry
Suranaree University of Technology
Academic Year 2019

การสังเคราะห์และพิสูจน์เอกลักษณ์อนุพันธ์ของ 1,8-แนฟทาลิไมด์และแนฟโธไทไดเอโซลเพื่อใช้เป็นสารเปล่งแสงสำหรับไดโอดเปล่งแสงอินทรีย์

นางสาวสุมิตา บุญแนบ

วิทยานิพนธ์นี้เป็นส่วนหนึ่งของการศึกษาตามหลักสูตรปริญญาวิทยาศาสตรดุษฎีบัณฑิต
สาขาวิชาเคมี
มหาวิทยาลัยเทคโนโลยีสุรนารี
ปีการศึกษา 2562

SYNTHESIS AND CHARACTERIZATION OF 1,8-NAPHTHALIMIDE AND NAPHTHOTHIADIAZOLE DERIVATIVES AS LIGHT-EMITTING MATERIALS FOR ORGANIC LIGHT-EMITTING DIODES

Suranaree University of Technology has approved this thesis submitted in partial fulfillment of the requirements for the Degree of Doctor of Philosophy.

Thesis Examining Committee

(Prof. Dr. James R. Ketudat-Cairns)

Chairperson

(Asst. Prof. Dr. Thanaporn Manyum)

Member (Thesis Advisor)

(Prof. Dr. Vinich Promarak)

Member

(Asst. Prof. Dr. Tinnagon Keawin)

Member

Chanokbhorn Phaosiri

(Asst. Prof. Dr. Chanokbhorn Phaosiri)

Member

Theeranun Siritanon

(Asst. Prof. Dr. Theeranun Siritanon)

Member

(Assoc. Prof. Flt. Lt. Dr. Kontorn Chamniprasart)

Vice Rector for Academic Affairs

and Internationalization

(Assoc. Prof. Dr. Worawat Meevasana)

Dean of Institute of Science

สุมิตา บุญแนบ : การสังเคราะห์และพิสูจน์เอกลักษณ์อนุพันธ์ของ 1,8-แนฟทาลิไมด์และแนฟโธไทอะไดเอโซลเพื่อใช้เป็นวัสดุเปล่งแสงสำหรับไดโอดเปล่งแสงอินทรีย์ (SYNTHESIS AND CHARACTERIZATION OF 1,8-NAPHTHALIMIDE AND NAPHTHOTHIADIAZOLE DERIVATIVES AS LIGHT-EMITTING MATERIALS FOR ORAGNIC LIGHT-EMITTING DIODES) อาจารย์ที่ปรึกษา : ผู้ช่วยศาสตราจารย์ ดร.ธนพร แม่นยำ, 179 หน้า

งานวิจัยนี้เป็นการศึกษาเกี่ยวกับการสังเคราะห์อนุพันธ์ของ 1,8-แนฟทาลิไมด์ ไทอะไดเอโซล และแนฟโธ[2,3,-ซี][1,2,5]ไทอะไดเอโซล เพื่อทำหน้าที่เป็นวัสดุเปล่งแสงสำหรับไดโอดเปล่งแสงอินทรีย์ อนุพันธ์ของ 1,8-แนฟทาลิไมด์ ที่ใช้เป็นวัสดุเปล่งแสง ซึ่งได้แก่สารประกอบ **49**, **50** และ **51** ได้รับการออกแบบและสังเคราะห์ให้เป็นตัวให้อิเล็กตรอน-ตัวรับอิเล็กตรอน พบว่าสารประกอบ **51** เมื่อนำไปใช้ในอุปกรณ์ให้ผลการทดลองดีที่สุด โดยมีค่าประสิทธิภาพภายนอกสูงสุดเท่ากับ 1.42 % อนุพันธ์ของ 1,8-แนฟทาลิไมด์ ที่ใช้เป็นวัสดุเปล่งแสงและโฮลทรานสปอร์ตภายในสารเดียวกัน ซึ่งได้แก่สารประกอบ **53**, **54**, **55** และ **56** ได้รับการออกแบบและสังเคราะห์ให้เป็นตัวให้อิเล็กตรอน-ตัวรับไพอิเล็กตรอน สารเหล่านี้มีค่าระดับพลังงานโฮโมและลูโม ซึ่งได้จากไซคลิกโวลทาโมแกรมเท่ากับ -5.06 และ -2.59, -4.62 และ -2.32 -4.56 และ-2.18 และ -4.88 และ -2.18 อิเล็กตรอนโวลต์ ตามลำดับ อนุพันธ์ของไทอะไดเอโซล ที่ใช้เป็นวัสดุเปล่งแสงและโฮลทรานสปอร์ตภายในสารเดียวกัน ซึ่งได้แก่สารประกอบ **63**, **64**, **65** และ **66** ได้รับการออกแบบและสังเคราะห์ให้เป็นตัวให้อิเล็กตรอน-ตัวรับไพอิเล็กตรอน สารเหล่านี้มีค่าระดับพลังงานโฮโมและลูโม ซึ่งได้จากไซคลิกโวลทาโมแกรมเท่ากับ -5.11 และ -3.21, -5.18 และ -3.20, -5.13 และ -3.19 และ -5.20 และ -3.20 อิเล็กตรอนโวลต์ ตามลำดับ อนุพันธ์ของแนฟโธ-[2,3,-ซี][1,2,5]ไทอะไดเอโซล ที่ใช้เป็นวัสดุเปล่งแสงและโฮลทรานสปอร์ตภายในสารเดียวกัน ซึ่งได้แก่สารประกอบ **67** และ **68** ได้รับการออกแบบและสังเคราะห์ให้เป็นตัวให้อิเล็กตรอน-ตัวรับไพอิเล็กตรอน สารเหล่านี้มีค่าระดับพลังงานโฮโมและลูโม ซึ่งได้จากไซคลิกโวลทาโมแกรมเท่ากับ -5.31 และ -3.55 และ -5.17 และ -3.48 อิเล็กตรอนโวลต์ ตามลำดับ

สาขาวิชาเคมี
ปีการศึกษา 2562

ลายมือชื่อนักศึกษา
ลายมือชื่ออาจารย์ที่ปรึกษา

SUMITA BOONNAB : SYNTHESIS AND CHARACTERIZATION OF
1,8-NAPHTHALIMIDE AND NAPHTHOTHIADIAZOLE
DERIVATIVES AS LIGHT-EMITTING MATERIALS FOR ORGANIC
LIGHT-EMITTING DIODES. THESIS ADVISOR : ASST. PROF.
THANAPORN MANYUM, Ph.D. 179 PP.

1,8-NAPHTHALIMIDE / THIADIAZOLE / NAPHTHO[2,3-C][1,2,5]THIADIAZOLE

This research involves the study of the syntheses of the derivatives of 1,8-naphthalimide, thiadiazole, and naphtho[2,3-c][1,2,5]thiadiazole as light-emitting materials for organic light-emitting diodes. The 1,8-naphthalimide derivatives to be used as emissive materials, including compounds **49**, **50**, and **51** were designed and synthesized as electron donor-electron acceptors. It was found that the compound **51** had the best performance in the device with a maximum EQE value of 1.42%. The 1,8-naphthalimide derivatives to act as single emissive and hole transport materials, including compounds **53**, **54**, **55**, and **56** were designed and synthesized as electron donor-π-electron acceptors. Their HOMO and LUMO energy levels obtained from the cyclic voltamograms were equal to -5.06 and -2.59, -4.62 and -2.32, -4.56 and -2.18, and -4.88 and -2.18 eV, respectively. The thiadiazole derivatives to act as single emissive and hole transport materials, including compounds **63**, **64**, **65**, and **66** were designed and synthesized as electron donor-π-electron acceptors. Their HOMO and LUMO energy levels obtained from the cyclic voltamograms were equal to -5.11 and -3.21, -5.18 and -3.20, -5.13 and -3.19, and -5.20 and -3.20 eV, respectively. The naphtho[2,3-c][1,2,5]thiadiazole derivatives to act as single emissive and hole transport materials, including compounds **67** and **68** were designed and synthesized as electron donor-π-electron acceptors. Their HOMO and LUMO energy levels obtained from the cyclic voltamograms were equal to -5.31 and -3.55, and -5.17 and -3.48 eV, respectively.

School of Chemistry
Academic Year 2019

Student's Signature Sumita.b
Advisor's Signature T. Juyen

ACKNOWLEDGEMENTS

I would like to express the deepest appreciation to my advisor, Asst. Prof. Dr. Thanaporn Manyum and Prof. Dr. Vinich Promarak for the continuous support of my Ph.D study and research, for his patience, motivation, enthusiasm, and immense knowledge. His guidance helped me in all the time of research and writing of this thesis.

I am so grateful to the National Science and Technology Development Agency (NSTDA) scholarship scheme and the Nakhonratchasima Ratjabhat University for making it possible for me to study here. I would like to thank my thesis committee Prof. Dr. James R. Ketudat-Cairns, Asst. Prof. Dr. Tinnagon Keawin, Asst. Prof. Dr. Chanokbhorn, Phaosiri and Asst. Prof. Dr. Theeranun Siritanon for their encouragement, insightful comments.

I would like to thank Mr. Chirawat Chitpakdee from National Science and Technology Development Agency (NSTDA), Mr. Wachara Benchaphanthawee from Chiang mai University and Mr. Pongsakorn Chasing from Vidyasirimedhi Institute of Science and Technology (VISTEC) for Density functional theory (DFT). I would like to thank Mr. Chaiyon Chaiwat for device fabrication.

I would like to thank my family for all the encouragement and support for everything.

Sumita Boonnab

CONTENTS

CHAPTER

CONTENTS (Continued)

CONTENTS (Continued)

CONTENTS (Continued)

Page

CONTENTS (Continued)

LIST OF TABLES

LIST OF FIGURES

LIST OF FIGURES (Continued)

Figure **Page**

LIST OF FIGURES (Continued)

Figure **Page**

LIST OF FIGURES (Continued)

LIST OF FIGURES (Continued)

LIST OF ABBREVIATIONS

Al	Aluminum
Ca	Calcium
$C_4H_4BrNO_2$	*N*-Bromosuccinimide
CaH_2	Calcium hydride
CH_2Cl_2	Dichloromethane
C_3H_7NO	Dimethylformamide
C_6H_{14}	Hexane
CH_3OH	Methyl alcohol
C_4H_8O	Tetrahydrofuran
C_7H_8	Toluene
CIE	Commission International de I’Eclairage
DFT	Density functional theory
DSC	Differential Scanning Calorimeter
EL	Electroluminescence
EML	Emissive layer
ETL	Electron transport layer
HBL	Hole blocking layer
HTL	Hole transport layer
HIL	Hole injection layer
ISC	Intersystem crossing
ITO	Indium tin oxide
LCDs	Light-emitting diodes

LIST OF ABBREVIATIONS (Continued)

$MgSO_4$	Magnesium sulfate
Na_2SO_4	Sodium sulfate
ns	nanosecond
OLEDs	Organic light emitting diodes
QYs	Quantum yields
TGA	Thermogravimetric Analysis

CHAPTER I

INTRODUCTION

1.1 OLEDs

Organic molecules are generally considered to be insulators. This general concept has been changing since the discovery of conducting polymers in 1977s by A. J. Heeger, A.G. MacDiarmid, and H. Shirakawa. In 1987, a semiconducting organic small molecule was found to be emissive with film layers under the application of an electric field (Tang T.W. and VanSlyke, S.A. 1987). Organic light-emitting diodes (OLEDs) have attracted increasing interest over the last few years because of their potential to achieve low-cost, full-color and flat-panel displays (Shirota *et al.*, 2000). One of the key developments in OLED display technology can be attributed to the discovery of the guest-host doped emitter system in which a single host material with optimized transport and luminescent properties may be used together with a variety of highly fluorescent guest dopants, leading to its electroluminescence (EL) of desirable hues with very high efficiencies (Hung *et al.*, 2002). However, phosphorescent materials containing noble metals are difficult for OLEDs to become competitive in the markets because these materials are rather expensive and unsustainable. Therefore, a new method for obtaining materials with high external EL efficiency is required (Gaj *et al.*, 2015 and Lee, Park *et al.*, 2016).

1.2 Structures of organic light emitting diodes (OLEDs)

An OLED is a thin film optoelectronic device, consisting of a single layer, double layer or multi-layer of organic materials sandwiched between two electrodes, one of which must be transparent, as shown in Figure 1.1. The emissive layer comprises of a thin film of an organic compound such as a small molecule, dendrimer or polymeric substance that allows the deposition. OLEDs can be used in light sources for general space illumination (Thejokalyani and Dhoble, 2014).

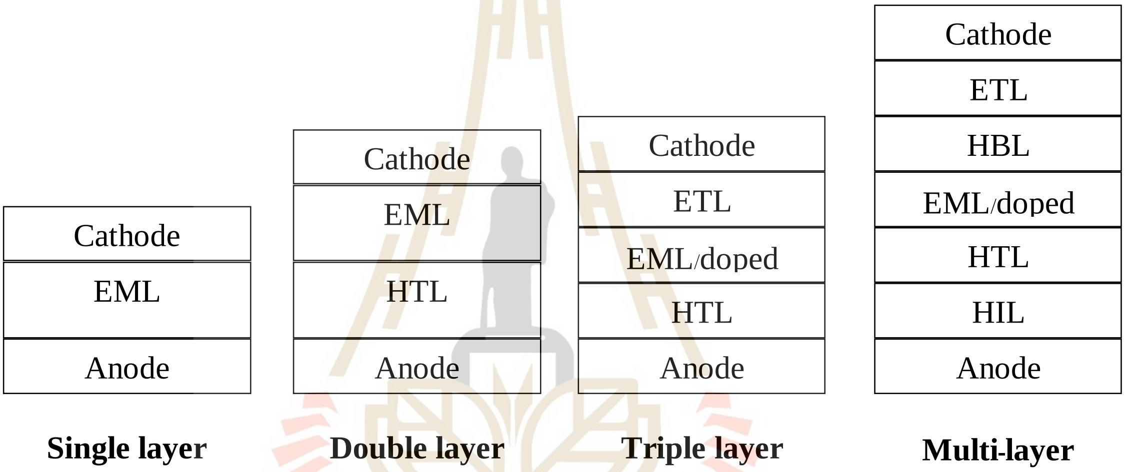

Single layer **Double layer** **Triple layer** **Multi-layer**

Figure 1.1 The general structures of OLED devices where ETL stands for electron transport layer, HBL for hole blocking layer, EML for emissive layer, HTL for hole transport layer and HIL for hole injection layer (Thejokalyani and Dhoble, 2014).

OLEDs have attracted enormous attention in the scientific community due to their potential applications for full-color flat-panel display and large area solid state lighting. Moreover, OLEDs are considered to be the next generation of flat panel displays because of their advantages, such as high brightness, high luminous efficiency, fast response time, wide viewing angle, low power consumption, light weight and easy fabrication of potentially large-area in comparison to liquid crystal displays (LCDs) and plasma display panels (PDP). A single-layer OLED consists of an emissive layer which contains organic materials that are capable of emitting light, so called organic emitting layer, sandwiched by an anode and a cathode layer. The cathode is usually made of metal with low work function (e.g. Al, Ca) while the anode is made of transparent materials such as indium tin oxide. (ITO). These layers are coated on a transparent substrate such as glass or flexible polymer as thin films. (Quirino *et al.*, 2009) as shown in Figure 1.2.

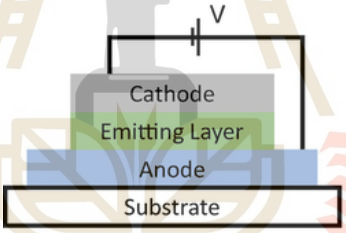

Figure 1.2 The structure of the first single layer OLED device.

When voltage is applied to the device in Figure 2, holes from anode and electrons from cathode are injected to the organic emitting layer. Excitons are generated after the combination of the holes in HOMOs and the electrons in LUMOs of the molecules in emitting layer. Upon relaxation of the excitons, the light is emitted from the emitting layer. The energy diagram of the process is depicted in Figure 1.3.

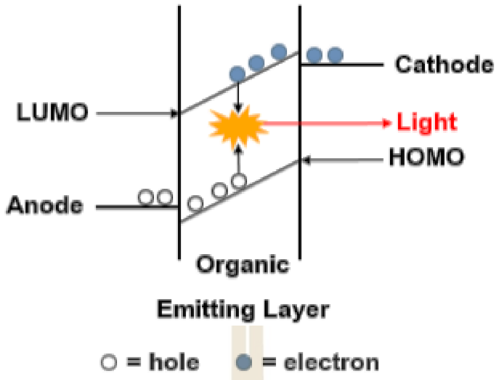

Figure 1.3 Energy diagram of a single-layer OLED.

Multilayer OLEDs, represented in Figure 1.4, consist of different layers namely an ITO glass plate, hole injection layer (HIL), emission layer (EML), electron transport layer (ETL) and anode. The materials to be used for different layers for OLEDs should meet the requirements like high luminescence efficiency, adequate conductivity, narrow spectra, correct Commission International de I’Eclairage (CIE) coordinates, good temperature stability and also good oxidative stability (to water and oxygen). Additionally, it should be mentioned that the transport layers can readily be used for increasing the efficiencies of the corresponding light-emitting devices (Thejokalyani *et al*., 2015).

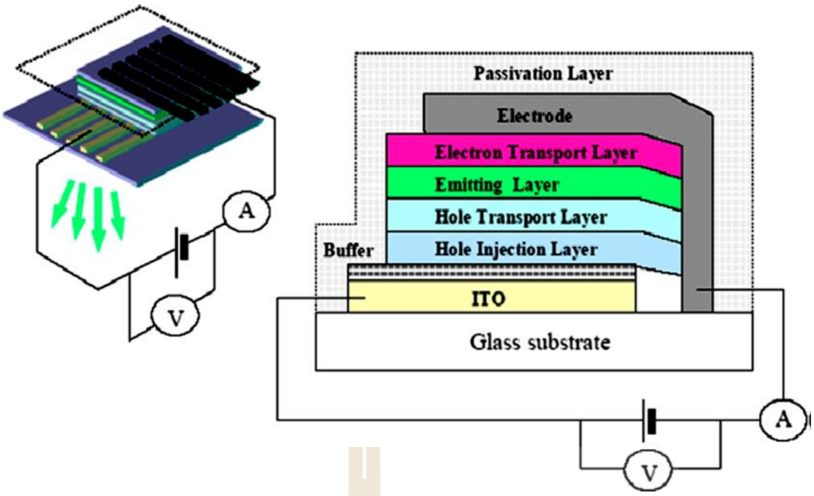

Figure 1.4 General structure of a multilayer OLED device.

Thickness of these layers can be adjusted to optimize the mobility of the carriers injected from the electrodes aiming at their recombination in the emitting layer. Another advantage of the multilayer OLED is the possibility of tuning energy levels of the materials to achieve good overlapping energy levels in each layer of the device, thus high carriers transporting efficiency is reached. A simple energy diagram of the device is shown in Figure 1.5.

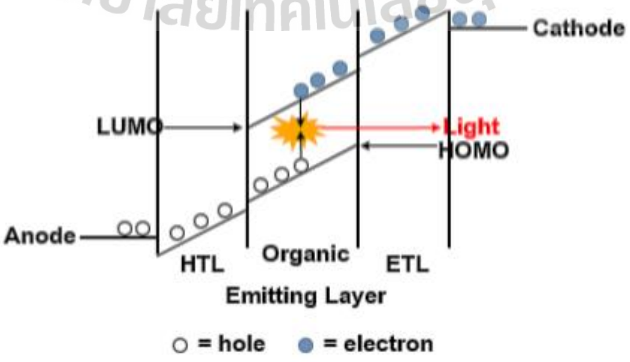

Figure 1.5 Energy diagram of a multilayer OLED.

The discovery phosphorescent organic light emitting diodes (PhOLEDs) materials containing the different transition metals, such as iridium(III), platinum(II), osmium(II), and rhenium(I) was a major breakthrough towards high performance OLEDs. According to spin statistics, 75% of triplet (T_1) and 25% of singlet (S_1) excitons are formed by the recombination of a hole and an electron under electrical excitation. In conventional fluorescent organic materials, only up to 25% of the total generated excitons from singlet (S_1) can be used for light emission.

1.3 The components of organic light emitting diodes (OLEDs)

The OLED device comprises of several organic layers in order to improve its efficiency. The organic materials used in each layer must have good thermal stability, low turn-on voltage, high conductivity, and high electroluminescence efficiency. A different layer of devices employs different materials, depending on the requirements as described below (Thejokalyani and Dhoble, 2014).

1.3.1 Anode

The anode material must be transparent in order to inject holes into organic layers and highly conductive and has high work function. In tradition, the most widely used material as an anode is ITO, because it has low roughness, good conductivity, high chemical stability, high work function (Φ_W = 4.5 to5.1 eV) and good transparency in the visible range (Schlaf *et al.*, 2001). The general requirements for an anode material are high conductivity so as to reduce contact resistance, high work function (WF) (φ >

4.1 eV) to promote efficient hole injection, good film-forming and wetting properties of applied organic materials, good thermal and chemical stability, and good transparent.

1.3.2 Hole injection layer (HIL)

The materials for the hole injection layer must have high hole mobility, high glass transition temperature and high electron blocking capacity in order to reduce the barrier for hole injection into the OLED device. Copper phthalocyanine CuPc (**1**) and 4,4′,4′′- Tris(3- methyl- phenylphenylamino) triphenylamine *m*- MTDATA (**2**) are favorably used as material for HIL because their HOMOs are comparable to the work function of ITO. Their structures can be seen in Figure 1.6.

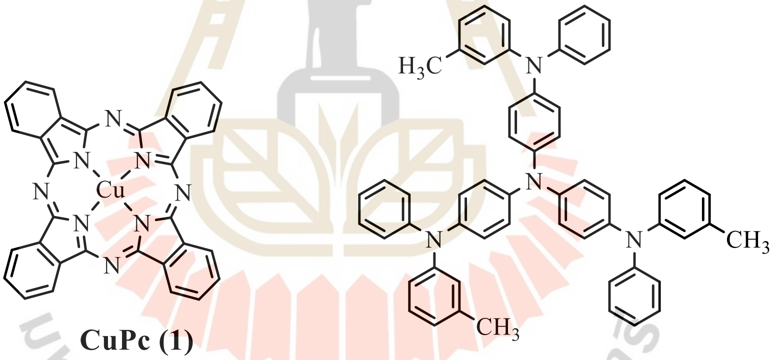

CuPc (1)

***m*-MTDATA (2)**

Figure 1.6 The structures of materials for HIL layer.

1.3.3 Hole transport layer (HTL)

The hole transporting materials must have low ionization potential with low affinities and high hole mobility in order to accept and carry a positive charge. The most widely used materials for HTL are *N*, *N′*- bis(naphthalen- 1- yl)- *N*,*N′*- bis(phenyl)-benzidine (NPB), *N*,*N′*-bis(3-methylphenyl)-*N*,*N′*-bis(phenyl)-benzidine (TPD), *N*,*N′*-

bis(naphthalen-1-yl)-*N*,*N*′-bis(phenyl)-2,2′-dimethylbenzidine (α-NPD) and Di-[4-(*N*,*N*-ditolyl-amino)-phenyl] cyclohexane (TAPC). Their structures are depicted in Figure 1.7.

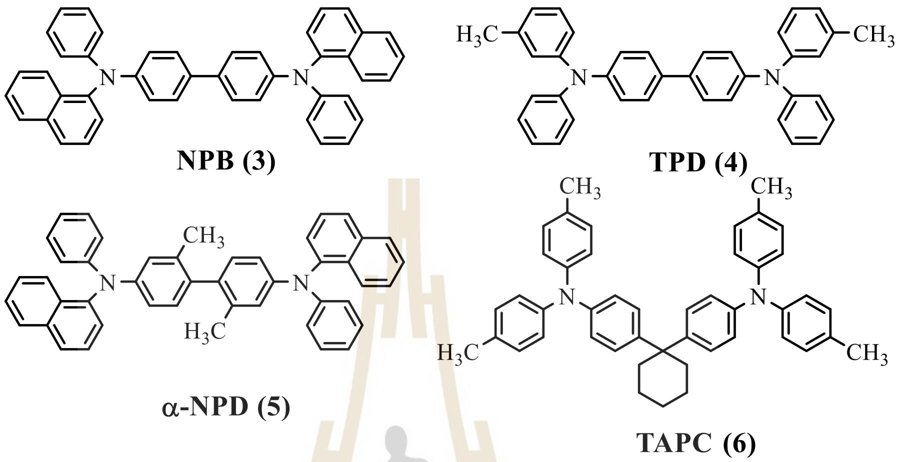

Figure 1.7 The structures of NPB (**3**), TPD (**4**), α-NPD (**5**) and TAPC (**6**).

1.3.4 Emissive layer (EML)

The material that gets most of the glory in OLEDs device is naturally the one that generates the light output. The EML is actually a mixture of two or more materials, wherein there is at least one electroluminescent emissive material in conjugation with a charge transporting host material. This layer can be a material made of organic molecules or polymer dendrimer with high efficiency, lifetime and color purity. The EML materials should have a good emission of visible photons and high glass transition temperature to obtain devices with longer lifetime. Depending on the color required, we can select materials such that the energy gap, i. e., the distance between HOMO and LUMO, will give the light released during recombination with the desired wavelength. (Chihaya *et al*., 2011). Examples are shown in Figure 1.8.

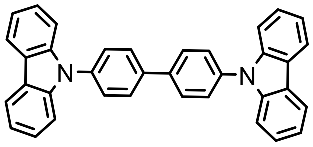

CBP (7)

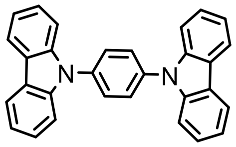

mCP (8)

Figure 1.8 The structures of materials for EML layer.

1.3.5 Electron transport layer (ETL)

ETL materials should have high electron affinities with high ionization potentials in order to transport of electrons by accepting negative charges and allowing them to move through the molecules. This layer provides an electron conductive pathway for negative charge carriers to migrate from the cathode into the emission layer. This layer functions as a conducting material to help transport electrons from the cathode and into the organic emissive layer of the device. The materials need to have a LUMO level close in energy to the WF of the cathode material to easily charge injection. Moreover, they should have good electron transporting, hole blocking property, and high electron affinity, together with high ionization potentials, since they usually function as electron transporting materials by accepting negative charges and allowing them to move through the molecules. Aluminum tris-8-hydroxyquinoline Alq3 (**9**) and 9, 10-di(2-napthyl) anthracene AND (**10**) are the most common ETL materials (Thejokalyani and Dhoble, 2014).

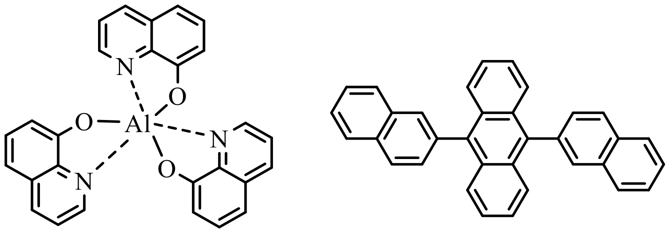

Alq$_3$ (9) **ADN molecule (10)**

Figure 1.9 The molecular structures of some ETL materials.

1.3.6 Cathode materials

The function of this layer is to inject electrons into emitting layers. The work function of cathode material should be relatively small ($\varphi_w \approx 2.9–4.0$ Ev) so as to minimize the barrier of electron injection. Moreover, this layer should have high conductivity, good film-forming ability, and good stability. Completely transparent OLEDs are needed (windshield and heads-up displays), ITO may also be used as the cathode with suitable modification. The materials such as lithium, calcium and magnesium have low work function but they are not used because of their reactive nature.

1.4 Light emitting mechanism from OLED devices

As shown in Figure 1.10, when a voltage is applied across the OLED devices, injected electrons and holes are transferred into emissive layer. An exciton is formed when electrons and holes are recombined. An exciton generates a photon whose wavelength corresponds to the energy gap after completion of its exciton lifetime. The possibility of electron-hole recombination can be increased by the use of multiple material layers as shown in Figure 1.11. The electrons and holes can be dammed by the HOMO/LUMO band energy difference, therefore the recombination position can be controlled. Then, the high efficiency OLED can be achieved (Tsujimura, 2012).

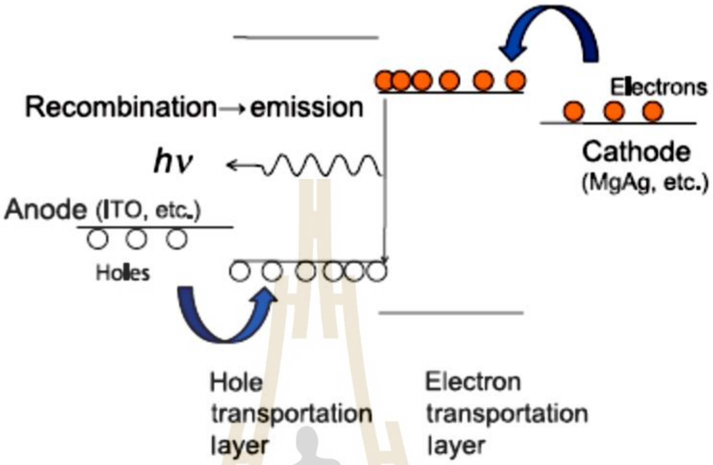

Figure 1.10 OLED band diagram for multiple organic layers (Tsujimura, 2012).

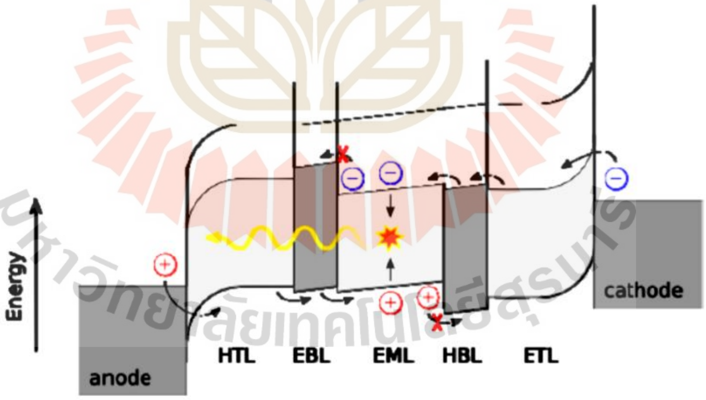

Figure 1.11 The light emitting mechanism in OLED devices (Thejokalyani *et al.*, 2015).

The emitting color of the OLED device depends on the type of organic molecules in emissive layer and the energy gap between HOMO and LUMO of the emitting material. The intensity or brightness of the light depends on the amount of electrical current applied through the device.

1.5 Luminescence in OLED devices

The light which is emitted by a substance, not the energy relaxation resulting from heat, is called luminescence. Therefore, luminescence can be found in cold body materials radiation. This radiation can be caused by a spontaneous emission, such as chemical reactions, electrical energy, subatomic motions, or stress on a crystal. The various types of luminescence are classified according to the mode of excitation, such as photoluminescence, chemiluminescence, bioluminescence, electroluminescence, cathodoluminescence, radiolu- minescence, sonoluminescence, thermoluminescence, triboluminescence (Valeur and Berberan-Santos, 2011).

1.5.1 Electroluminescence

Electroluminescence is luminescence caused by an electric current. The application of electric fields can produce luminescence in many phosphors. The well-known of electroluminescence is injection luminescence. Electrons are injected from an external supply across a semiconductor p-n junction. When applying a voltage across the junction, such as the electrons flow to the p-region, luminescence is produced by the electron-hole recombination in that region. Light-emitting diodes (LEDs) are commonly used as display devices in many instruments based on this principle. Because electroluminescence is usually performed on the finished devices, the fabrication of devices are usually time-consuming and costly, so the conventional device could not provide a fast response for material development (Valeur, 2001).

1.5.2 Photoluminescence

Photoluminescence is the process of photon excitation followed by photon emission. Electrons in a solid, which are not attached to the atom, can be hopped from one atom to another. These electrons are bound in the solid by differing amounts, so it has quite different energies. Electrons with high energies called conduction electrons, while electrons with low energies called valence electrons. There is an energy gap between the conduction and valence electron states. Under normal conditions, electrons are not allowed to have energies between the valence and conduction bands. In the process of photo excitation, when electrons are absorbed light, they can be raised from the valence band up to the conduction band. After that, the electron falls back down to the valence band and emits light. Thus, the energy of the emitted photon is a direct measure of the band gap energy (E_g). The photoluminescence process is shown in Figure 12 (Shinde *et al*., 2012). Photo luminescence should not interfere with reflection, refraction, or scattering of light, which cause most of the colors in daylight or bright artificial lighting.

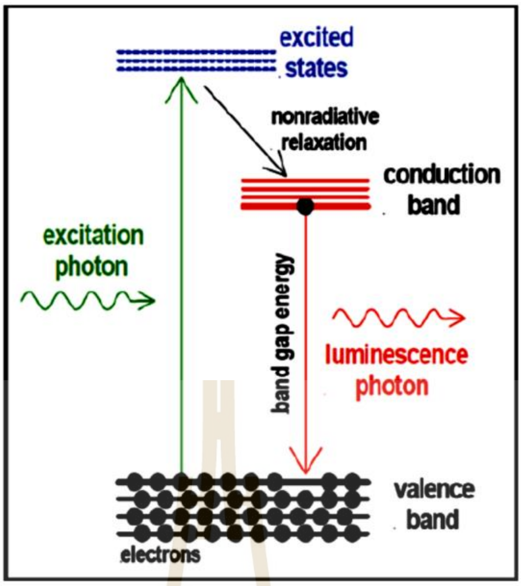

Figure 1.12 Photoluminescence process (Shinde *et al.*, 2012).

Fluorescence, phosphorescence and delayed fluorescence are well-known forms of photoluminescence.

1.5.2.1 Fluorescence

Fluorescence is the emission of light by a substance that has emitted the energy from singlet state (S_1) to ground state (S_0). When electrons in the ground states are excited by light or other electromagnetic radiation, it raises to the excited singlet states with the same spin state. The electron configurations in the ground and excited states are shown in Figure 1.13. A binding state of a pair of excited electrons and hole due to Coulomb force is called a singlet exciton. These excitons relax to ground state by emitting light, as shown in Figure 1.14.

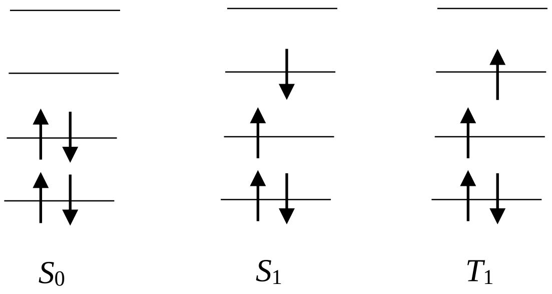

Figure 1.13 Electron configurations in the ground and excited states.

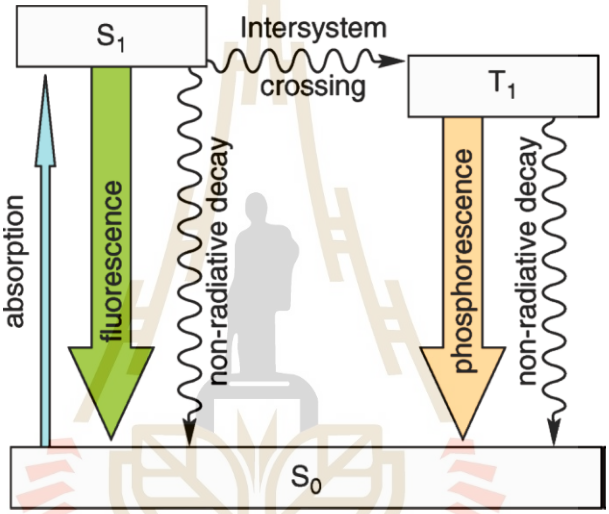

Figure 1.14 The energy diagram of fluorescence and phosphorescence processes (Valeur and Berberan-Santos, 2011).

OLED devices are based on organic fluorescent emitters whose efficiency was intrinsically capped at 25% due to only being able to recruit singlet excitons, because exciton formation results in 25% singlet excitons and 75% triplet excitons. Although these devices have achieved a high reliability practically, the external electroluminescence efficiencies (η_{EL}) are intrinsically limited to approximately 5%, due to limitations of their singlet-exciton production efficiency (η_{exciton}~25%) under electrical excitation (Adachi *et al*., 2014).

1.5.2.2 Phosphorescence

Phosphorescence is the emission of light by a substance that has emitted the energy from triplet state (T_1) to ground state (S_0). Before excitation, the electrons in the ground states are placed with both upward spin and downward spin. When excited, the electron in the upper spin state is allocated with the reversed spin via intersystem crossing (ISC) as shown in Figure 1.14. The binding states between the electrons in excited states with the reversed spin and holes called triplet exciton. Light emission from the lowest triplet state (T_1) and the ground state (S_0) is called phosphorescence. From the Pauli Exclusion Principle, when electron pairs are allocated to the same orbital, two electrons are not allowed to have the same quantum state at the same time. Therefore, when the electron is changed from the T_1 to the S_0 state, the spin direction must be reversed. This change takes a long time, so the exciton decay time of the triplet state is relatively longer than that for singlet emission. Also, the triplet state has lower energy than singlet state. Thus, the wavelength of triplet emission is longer than the long wavelength extreme of the visible spectrum (Tsujimura *et al*., 2012). In OLED devices, the phosphorescent materials revealed a η_{exciton} of almost 100% by harvesting both singlet and triplet excitons for emission due to the enhanced intersystem crossing (ISC) mediated by the large spin-orbit coupling of the heavy metals such as iridium(III) and platinum(II). The molecular structures of iridium(III) complexes are shown in Figure 1.15.

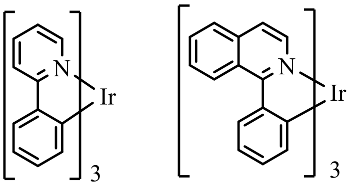

Ir(ppy)$_3$ (11) **Ir(piq)$_3$ (12)**

Figure 1.15 Example structures of phosphorescent dopant materials, Ir(ppy)$_3$ (**11**), Ir(piq)$_3$ (**12**).

1.5.2.3 Non-doped organic light emitting diodes

The doping process is the process of chemical dopants are added into the layer of OLED devices. The purpose of doping is to increase the number of free charges that can be moved by an externally applied voltage. As shown in Figure 16, the dopant has to donate electrons to the lowest unoccupied molecular orbital (LUMO) states called n-type doping, while p-type dopants extract electrons from the highest occupied molecular orbital (HOMO) states, generates holes. The dopant with n-typing doping is a donor, while the dopant with p-type doping is an acceptor (Lussem *et al.*, 2013).

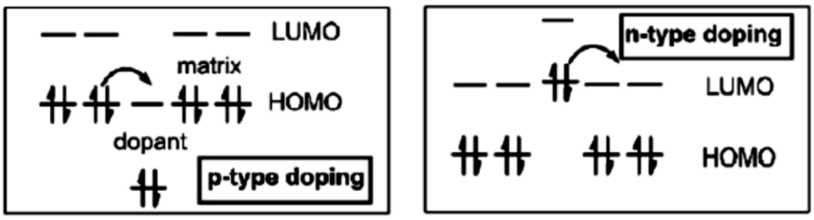

Figure 1.16 Scheme of the doping process for molecular p-type and n-type doping.

Lee *et al.* reported new twisted pyrene derivatives as a material for non-doped blue OLED. The fabricated devices exhibited an EQE of 3.69% with CIE colorcoordinates (x, y: 0.15, 0.06) (Lee *et al.*, 2016). The structures of the twisted pyrene derivatives BDPP and BDNP are shown in Figure 1.17.

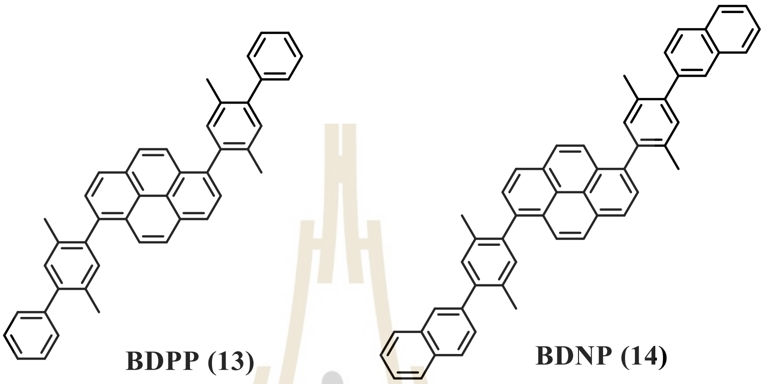

Figure 1.17 The structures of twisted pyrene derivatives.

1.6 Literature review

OLEDs displays with high performance in flexibility over a large area, low-cost fabrication and high optical and electrical properties are required in order to improve the electroluminescence efficiency of OLEDs. Various materials have been developed (Endo *et al.*, 2009). In recent years, many studies about the materials based on 1,8-naphthalimide have been reported as effectively transporting both holes and electrons. 1,8-Naphthalimide derivatives represent an interesting group of electron-deficient organic materials with promising electron-transporting properties, high photoluminescence, quantum yields (QYs) and good optical, thermal and chemical stabilities. Among those, the use of pyrene core 1,8-naphthalimide as emitting materials for OLEDs had not been studied much (Gudaika *et al.*, 2014).1 ,8 - Naphthalimide compounds are an attractive class of electron-deficient organic materials for OLEDs.

They have high electron affinities and related naphthalene tetracarboxylic diimide compounds have electron mobilities as high as 0.16 cm^2/ (Vs). 1,8-Naphthalimides can have wide energy gaps and low reduction potentials, making them good candidates for use as n-type materials in OLEDs. While many 1,8-naphthalimide derivatives have low luminescence efficiencies at room temperature, due to strong intersystem crossing to their triplet states. 1,8-Naphthalimides substituted at the 4 position with electron-donating groups can have high fluorescence quantum yields. When 1,8-naphthalimides are substituted by an electron-donating substituent at the 4-position, the fluorescence quantum yields can be increased and the emission peaks can be shifted to a longer wavelength (Gudeika *et al*., 2014).

In 2013, Mi-Seon and co-worker synthesized a new series of green dopants based on 2,2- diphenylvinyl end- capped bithiophene, as shown in Figure 1.18. The photophysical properties of 9a, 9b and 9c shown in Figure 18 were reported. The strongest PL emitting compound with the 9-phenylcarbazole moiety has been used for fabricating an OLED device with good overall performance.

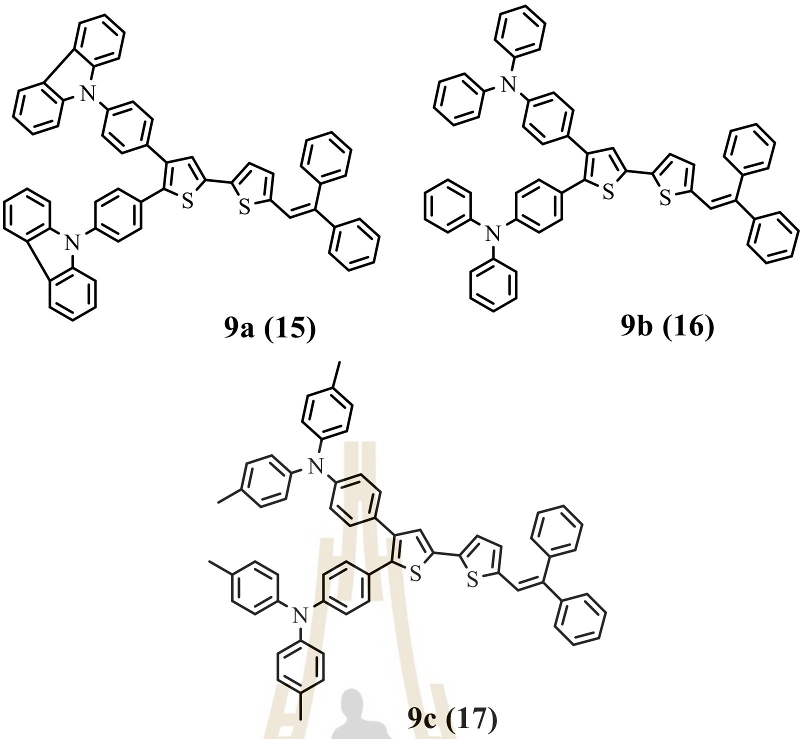

9a (15) **9b (16)**

9c (17)

Figure 1.18 The molecular structures of **9a** (**15**), **9b** (**16**), and **9c** (**17**).

In the same period, Hidayath and co-worker designed and synthesized a new series of naphthalimide derivatives by substituting with an electron donating phenoxy group at the 4th position of 1,8-naphthalimide. Their ionization potential and electron affinity were in the range of 6.30-6.36 eV and 3.31-3.43 eV, respectively, with energy band-gap in the range of 2.93-3.0 eV. The resulting energy values were relatively higher than the commonly used electron transporting compounds and hole blocking blue emitters as shown in Figure 1.19.

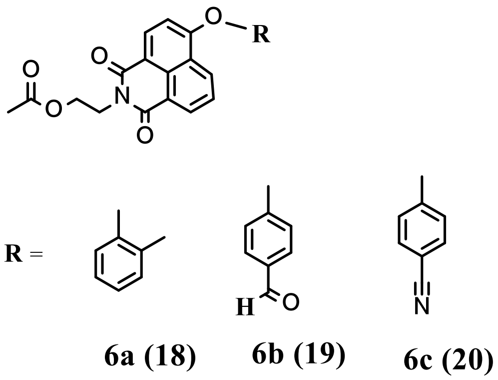

Figure 1.19 Structures of target compounds **6a** (**18**), **6b** (**19**), and **6c** (**20**).

In 2015, Arunchai and co- workers synthesized three new triphenylamino-naphthalimide (TPN1, TPN2 and TPN3 shown in Figure 20) using Suzuki cross-coupling reactions between *N*-phenyl-1,8-naphthalimide and triphenylamine precursors. The compounds in this series contain a phenyl-1,8-naphthalimide donor unit and a triphenylamine acceptor unit for a separated HOMO and LUMO with a small energy band gap 2.48, 2.52, and 2.54 eV, respectively. When TPN1-doped BCP was used as a hole-transporting material in the OLED device with ITO/PEDOT: PSS/TPN1: CBP/BCP/LiF/Al structure, a yellowish green light with a maximum brightness of 10404 cdm^{-2} at an applied voltage of 19 V was observed in Figure 21 (Arunchai *et al.*, 2015).

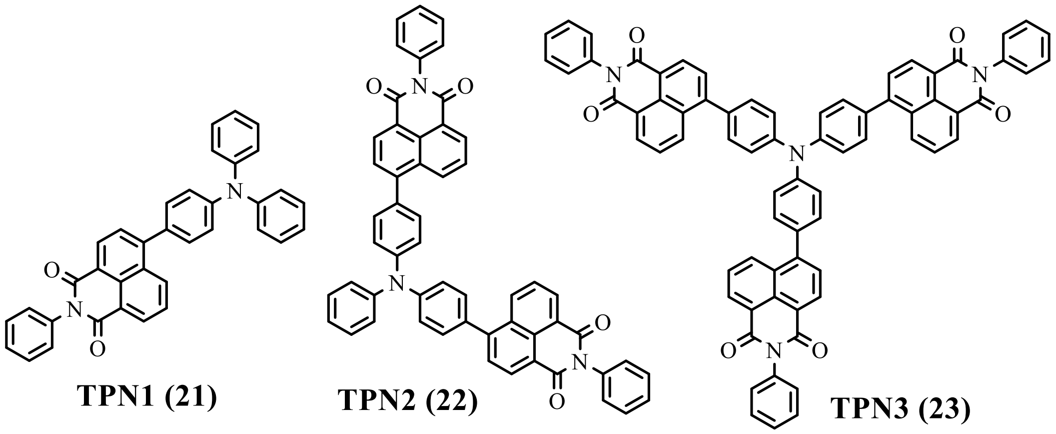

TPN1 (21) **TPN2 (22)** **TPN3 (23)**

Figure 1.20 Structures of target compounds **TPN1** (**21**), **TPN2** (**22**), and **TPN3** (**23**) (Arunchai *et al.,* 2015).

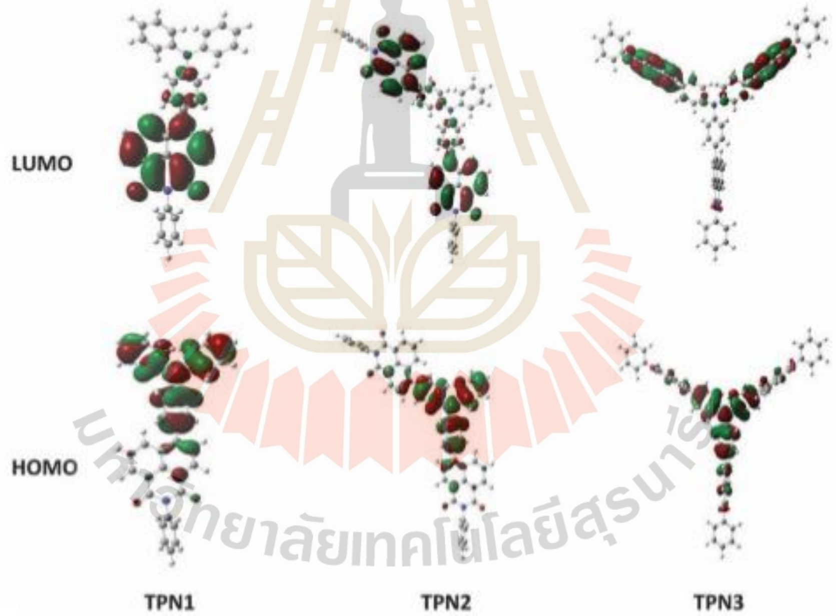

Figure 1.21 Structures of target compounds **TPN1** (**21**), **TPN2** (**22**), and **TPN3** (**23**) showing their HOMO and LUMO calculated at the B3LYP/6-31G (d) level. (Arunchai *et al.,* 2015).

In the same period, Reghu and co-workers synthesized triphenylamine core linked with the different alkoxyphenyl substituents through olefinic spacers. Their thermal, photophysical and photoelectrical properties were investigated. The synthesized compounds showed relatively good thermal stability. **24**, **25**, **26,** and **27**.

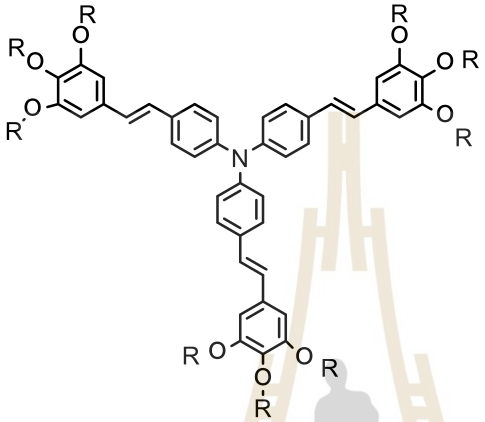

24; R = $C_{12}H_{25}$
25 ; R = $C_{10}H_{21}$
26 ; R = C_2H_5
27 ; R = CH_3

Figure 1.22 Structure of target compounds **24**, **25**, **26**, and **27**.

Shuai and co-workers synthesized donor-acceptor structures, consisting of D-π-A structures with an aromatic amine as the donor, ethene-1,2-diyl as the pi-bridge, and 1,8-naphthalimide. These compounds were used as the acceptor including **Np1** (**28**), **Np2** (**29**), and **Np3** (**30**) (Figure 1.23). With Nap3 as the guest dopant, a heavily doped standard-red OLED was achieved with CIE coordinates, EQE_{max} and CE_{max} values of (0.67, 0.32), 1.8% and 0.7 cd. A^{-1}, respectively.

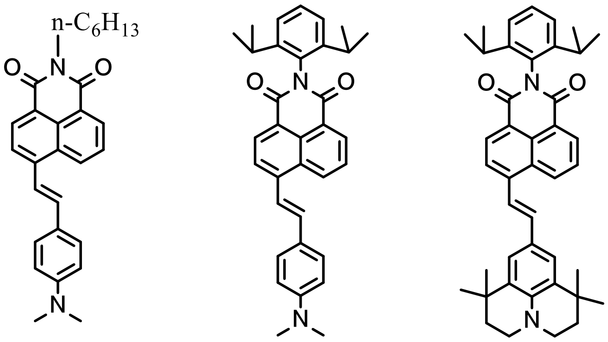

Nap1 (28) **Nap2 (29)** **Nap3 (30)**

Figure 1.23 Structures of target compounds **Np1** (**28**), **Np2** (**29**), and **Np3** (**30**).

In 2016, Gudaika and co-workers synthesized two D-π-A type organic compounds **31** and **32** (Figure 1.24) based on 1,8-naphthalimide derivatives as electron acceptor and triphenylamine as electron donor that were connected with olefinic linkages between the donor and acceptor. The obtained compounds were capable of forming molecular glasses with glass transition temperature of 56 and 75 °C recorded for mono- and di-substituted derivatives of triphenylamine, respectively. They exhibited high thermal stabilities with 5% weight loss at 350-363 °C. Fluorescence quantum yields of the dilute solution of the synthesized compounds range from 0.065 to 0.72, while of the solid films are 0.028 and 0.034, respectively. The compound **31** is indicated as good hole transporting material.

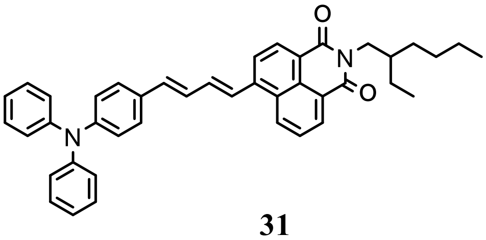

31

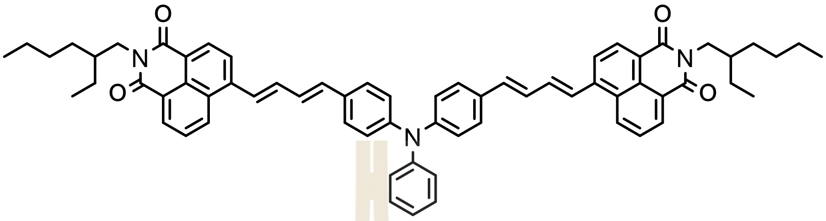

32

Figure 1.24 Structures of target compounds **31** and **32** (Gudaika *et al*., 2016).

In 2017, Shuai and co-workers designed and synthesized two molecules of chiral 1,8-naphthalimide-based enantiomers incorporating D/L-alanine and pyrene fluorophore moieties. The obtained compounds showed fluorescence emission gradually changing from bright-yellow to red when the fraction of the poor solvent methanol increased from 0 to 99 vol %. The molecular structure of structure **D/L-1** (**33**) and **D/L-2** (**34**) are shown in Figure 1.25. Organic light-emitting diodes (OLEDs) displaying with high performance, flexibility over a large area, low-cost fabrication and good optical and electrical properties are required. In order to improve the electroluminescence efficiency of OLEDs, various materials have been developed (Endo *et al*., 2009).

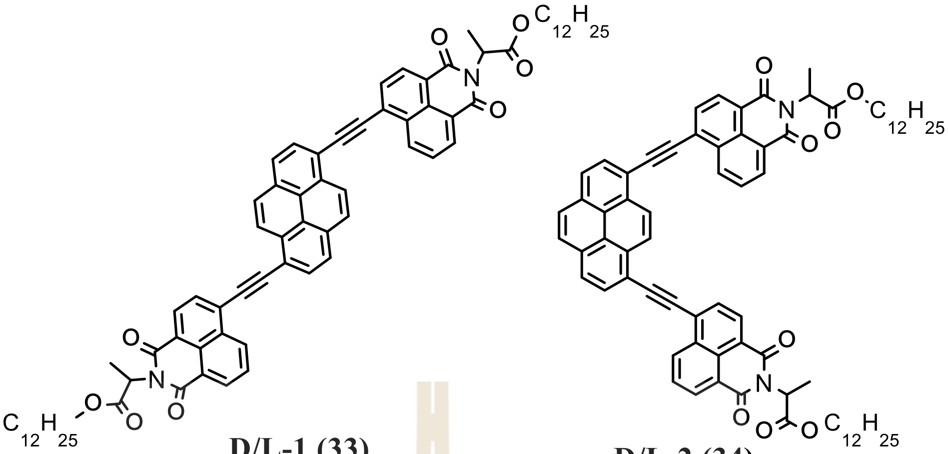

D/L-1 (33) **D/L-2 (34)**

Figure 1.25 The molecular structures of **D/L-1** (**33**) and **D/L-2** (**34**).

Tetrasubstituted-pyrene containing peripheral diarylamine (**35-38**) or fluorenes (**39-40**) are non-doped blue-emitting devices (Rossatorn *et al*., 2014). Their compounds are highly fluorescent and possess high morphological stability and thermal stability. The compounds of arylamines (**35-37** in Figure 1.26) can be used as the hole-transport and green-emitting materials and fluorenes (**39-40**) are efficient blue emitters, ambipolar carrier-transport characteristics with high electron mobilities (10^{-3}- 10^{-2} $cm^2/Vs.$) and high hole mobilities (> 10^{-3} $cm^2/Vs.$).

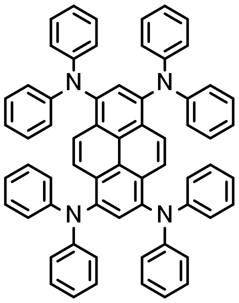

35

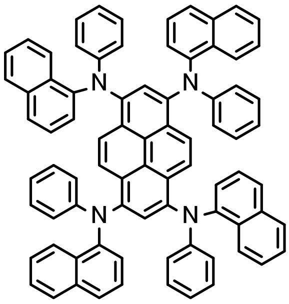

36

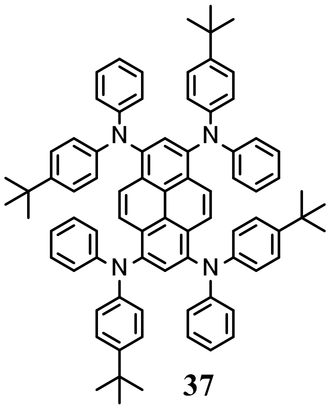

37

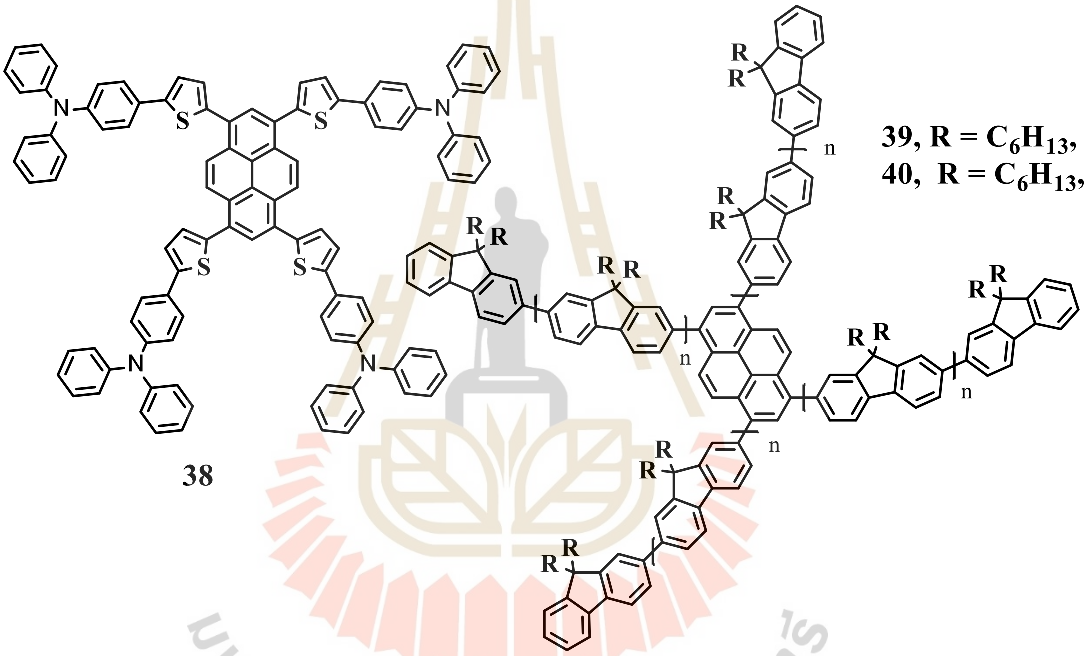

38

39, R = C_6H_{13}, n = 0
40, R = C_6H_{13}, n = 1

Figure 1.26 The structures of arylamine and fluorene compounds **35-40**.

In 2014, Gudaika and co-workers synthesized four targeted molecules of triphenylamine containing different numbers of naphthalimide derivative moieties. The compounds (**4**, **5**, **6,** and **7** in Figure 1.27) obtained are capable of forming molecular glasses with glass transition temperatures ranging from 429 to 483 °C. Fluorescence quantum yields of the dilute solution in nonpolar solvents of the synthesized materials range from 0.63 to 0.78, while emission yield of the neat films are in the range of 0.10 – 0.23. Compound 41, with a polar methoxy group in the donor triphenylamino moieties, showed the strongest solvatochromic effect, with electron mobilities of 7.5 × 10^{-4} cm^2 $V^{-1}s^{-1}$ and hole mobilities of 1.1 × 10^{-4} cm^2 V^{-1} s^{-1}.

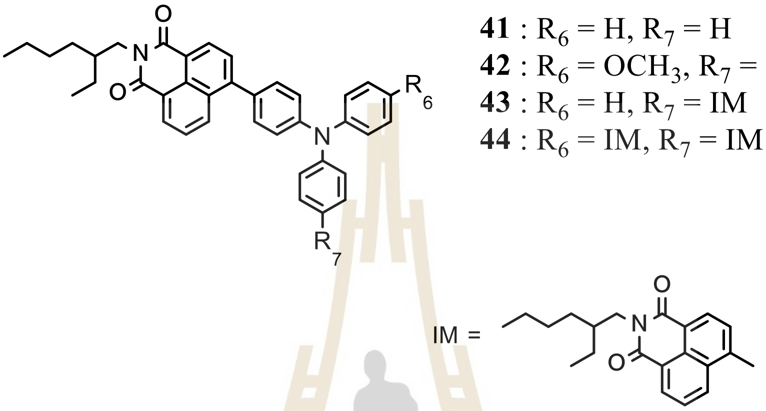

41 : R_6 = H, R_7 = H
42 : R_6 = OCH_3, R_7 = OCH_3
43 : R_6 = H, R_7 = IM
44 : R_6 = IM, R_7 = IM

Figure 1.27 The structures of triphenylamine compounds **41, 42, 43,** and **44**.

1,8-Naphthalimide compounds are an attractive class of electron-deficient organic materials for OLEDs. They have high electron affinities, and related naphthalene tetracarboxylic diimide compounds have electron mobilities as high as 0.16 cm^2/(Vs). 1,8-Naphthalimides can have wide energy gaps and low reduction potentials, making them good candidates for use as n-type materials in OLEDs. While many 1,8-naphthalimide derivatives have low luminescent efficiencies at room temperature, due to strong intersystem crossing to their triplet states, 1,8-naphthalimides substituted at the 4 position with electron-donating groups can have high fluorescent quantum yield (Lee *et al.*, 2016a). Naphthalimides have been utilized in both small molecule and polymer-based OLEDs. The small molecule based devices, utilizing 4-amino-1,8-naphthalimides as light-emitting material, showed performance inferior to that of Alq3-

based OLEDs. Emission from intramolecular charge-transfer states contribute greatly to electroluminescence of these devices. Doping an orange/red fluorescent dye (DCM) into a 4-amino- 1,8-naphthalimide matrix shifted the EL spectra to correspond exactly to the PL spectrum of DCM, but did not noticeably improved performance of the devices. The authors concluded that there was no energy transfer from the naphthalimide matrix to DCM, but the dye molecules could efficiently trap charge carriers in the devices, leading to electron-hole recombination at the DCM dopants followed by DCM emission. OLEDs utilizing side-chain naphthalimide polymers showed that these materials affect the device charge transport properties significantly and, in particular, reduce the bias necessary for electroluminescence.

1.7 Scope and limitations

1. The designed pyrene cored 1,8- naphthalimides **49**, **50,** and **51** will be synthesized, and characterized as electroluminescent materials. Their structures are shown in Figure 1.28.

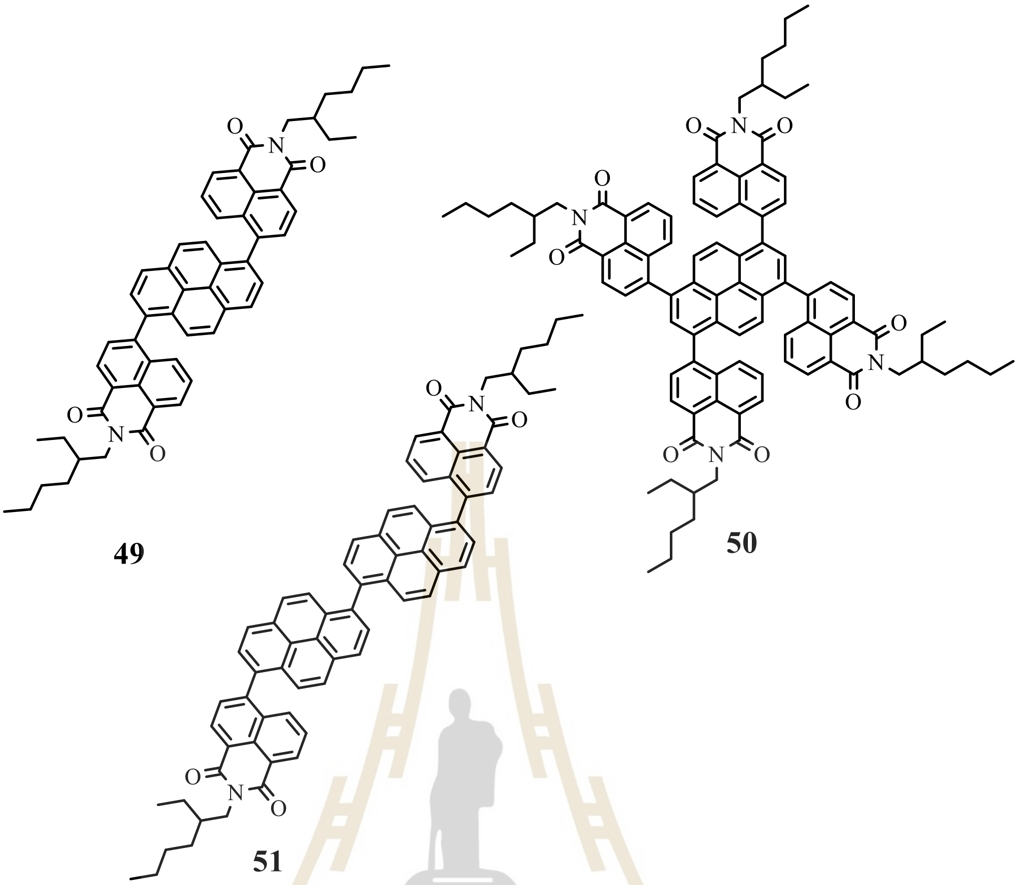

49

50

51

Figure 1.28 The structures of compounds **49**, **50**, and **51**.

2. A new series of triphenylamine cored 1,8-naphthalimide **53**, **54**, **55**, and **56** will be synthesized and characterized as hole transporting materials. Their structures are shown in Figure 1.29.

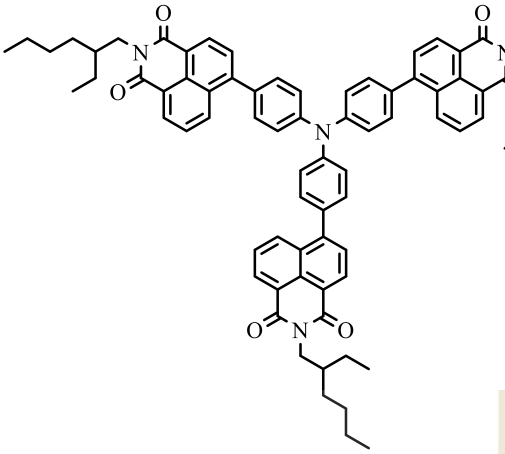

53

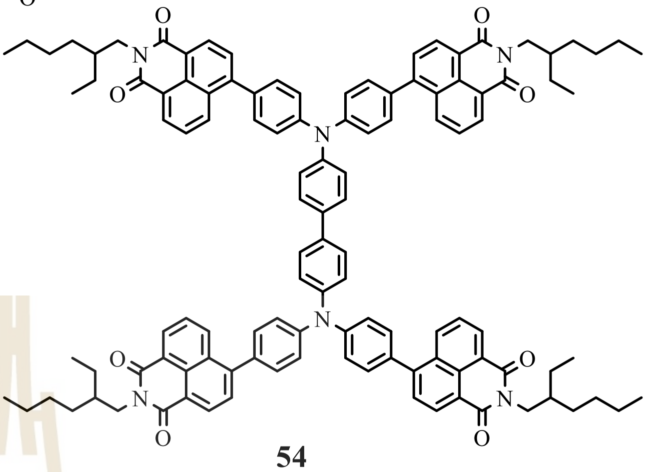

54

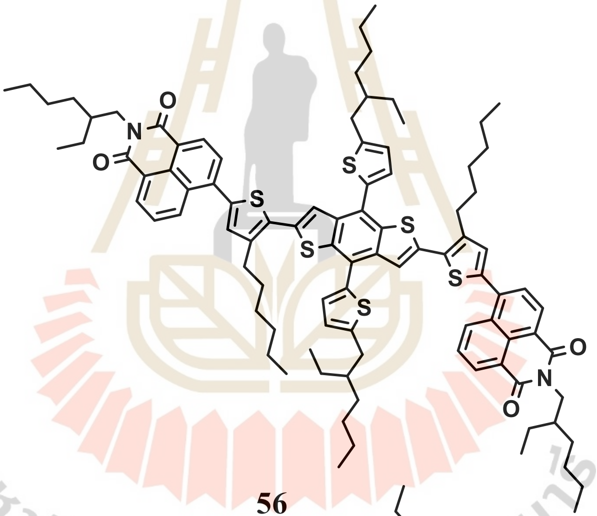

56

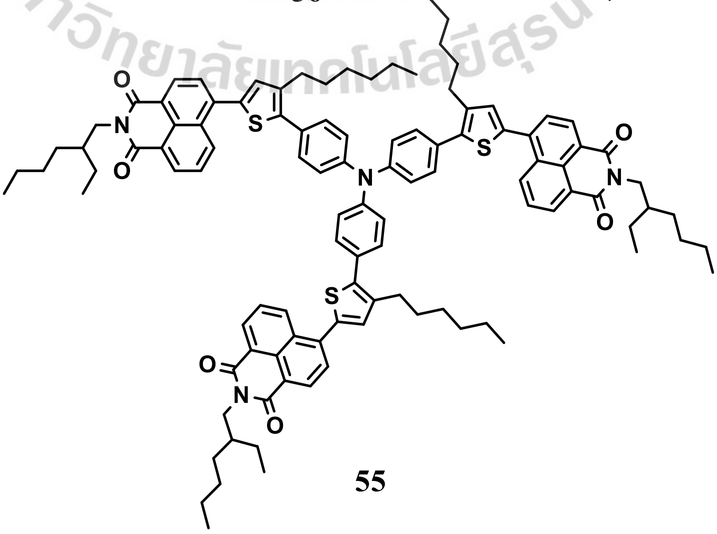

55

Figure 1.29 The structures of compounds **53**, **54**, **55**, and **56**.

3. A new series of the designed D-π-A-π-D based on pyridinthiadiazole acceptor of **63**, **64**, **65**, and **66** will be synthesized and characterized as hole-transporting deep red emitters. Their structures are shown in Figure 1.30.

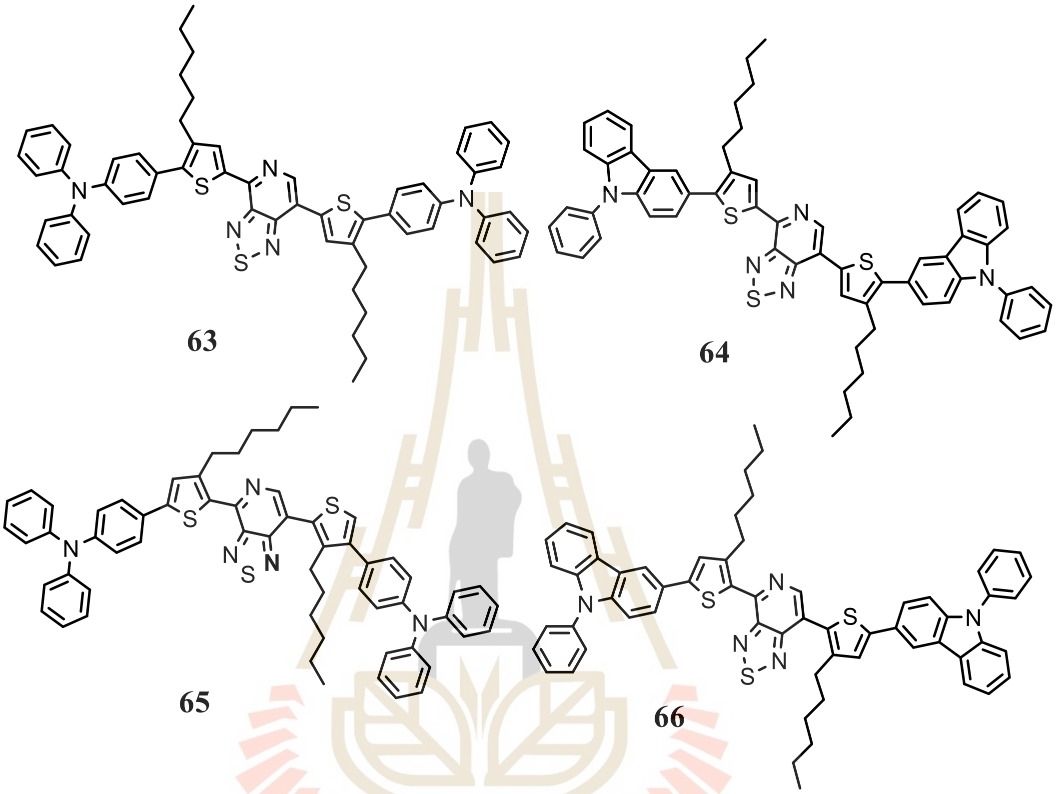

Figure 1.30 The structures of compounds **63**, **64**, **65**, and **66**.

4. To synthesize new series of designed triphenylamine cored 1,8-naphthalimide **67** and **68**. Their structure are shown in Figure 1.31.

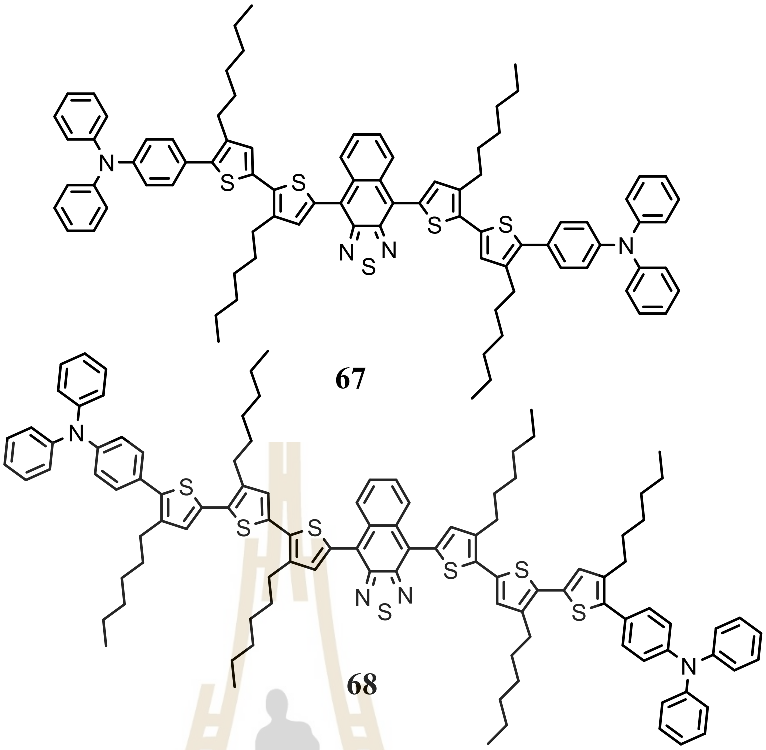

67

68

Figure 1.31 The structures of compounds **67** and **68**.

5. The photophysical, electrochemical and thermal properties of the target molecules were studied by UV-visible spectroscopy, fluorescence spectroscopy, cyclic voltammetry, and DSC-TGA techniques.

6. The OLEDs properties will be obtained with the fabrication device processing the desired molecules as non-doped emitters. The structure of the devices will consist of ITO/PEDOT: PSS/novel non-doped emitters/LiF/Al. The OLEDs devices were fabricated by The Smart Organic Materials and Semiconductor Devices Laboratory, VISTEC, Rayong, Thailand.

CHAPTER II

SYNTHESIS AND CHARACTERIZATION OF PYRENE-CORE NAPHTHALIMIDE DERIVATIVES AS LIGHT-EMITTING MATERIALS FOR ORGANIC LIGHT-EMITTING DIODES

2.1 Introduction

In the past, much attention has been paid to the design and synthesis of new 1,8-naphthalimide architectures for optoelectronic applications. The optical, photophysical, photoelectrical, electrochemical properties of 1,8-naphthalimide derivatives are determined by the nature of the substituents. Linking of electron donating groups at C-4 position of the naphthalic ring gives a “push–pull” electronic configuration and generate ICT excited states. This ICT character leads to a large excited-state dipole moment and broad absorption and emission bands at longer wavelengths. ICT transition is highly solvent dependent, and the photophysical properties of the compounds with ICT character, such as the wavelengths of the maxima of absorption and emission spectra, the fluorescence lifetimes as well as the fluorescence quantum yields, are all affected by the properties of solvents. In this part, we interest to use the concept of A–D system based on 1,8-naphthalimide derivatives composing of pyrene as donor and 1,8-naphthalimide derivatives as acceptor for designing new materials for OLED applications.

2.2 Aims of the study

1 To design, synthesize and characterize new A–D system based on 1,8-naphthalimide derivatives (Figure 2.1) using pyrene as a core substituted with 1,8-naphthalimide moiety for using as electroluminescent materials for OLEDs.

2 To study the photophysical, electrochemical, and thermal properties by UV-visible spectroscopy, fluorescence spectroscopy, cyclic voltammetry, and DSC-TGA techniques and investigate their performance in OLEDs.

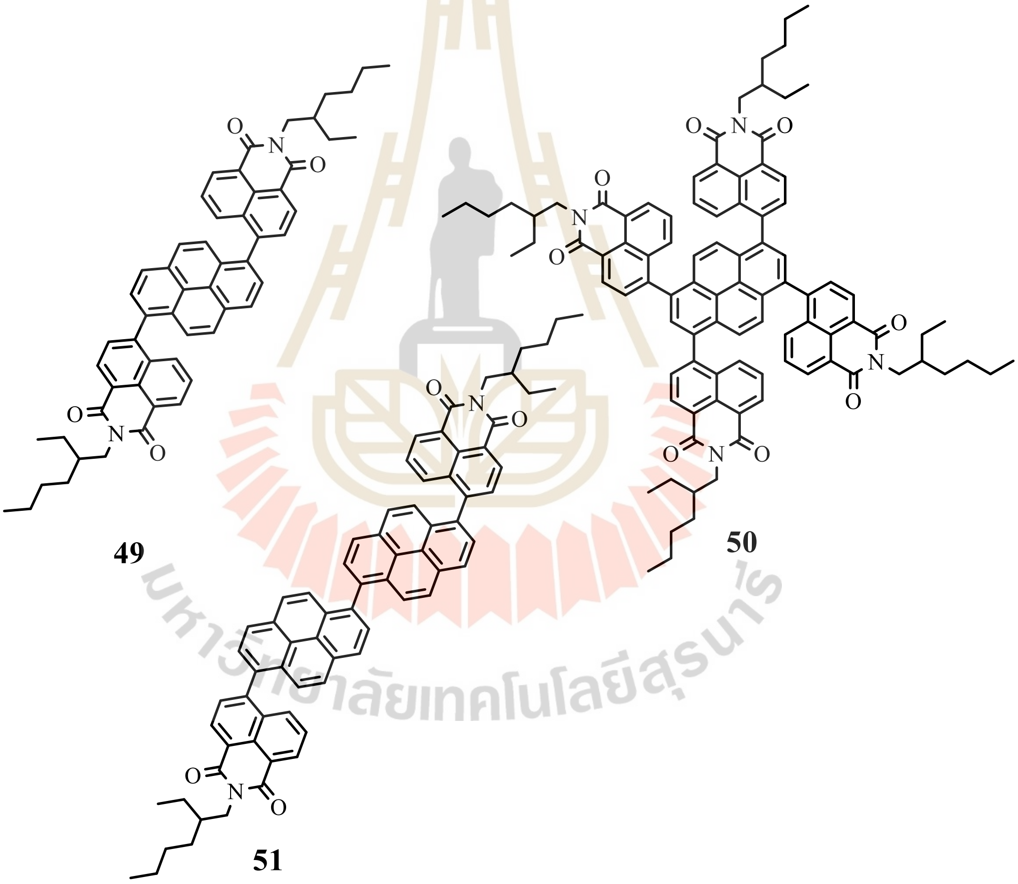

Figure 2.1 The structures of pyrene-core naphthalimide derivatives **49**, **50,** and **51**.

2.3 Results and discussion

2.3.1 The synthesis of pyrene-core naphthalimide derivatives 49, 50, and 51.

2.3.1.1 The synthesis of 1,8-naphthalimide derivatives 49.

As described in Figure 2.2, pyrene derivatives **49** could be synthesized by Suzuki cross coupling reaction of 4-bromo-*N*-(2-ethylhexyl)-1,8-naphthalimide dioxaborolane (**46**) and 1, 6-dibromopyrene (**47**). The intermediate **46** could be obtained from 4-bromo-*N*-(2-ethylhexyl)-1,8-naphthalimide (**45**) which could be synthesized by condensation reaction of 2-ethylhexylamine with 4-bromo-1,8-naphthalimide anhydride (**44**).

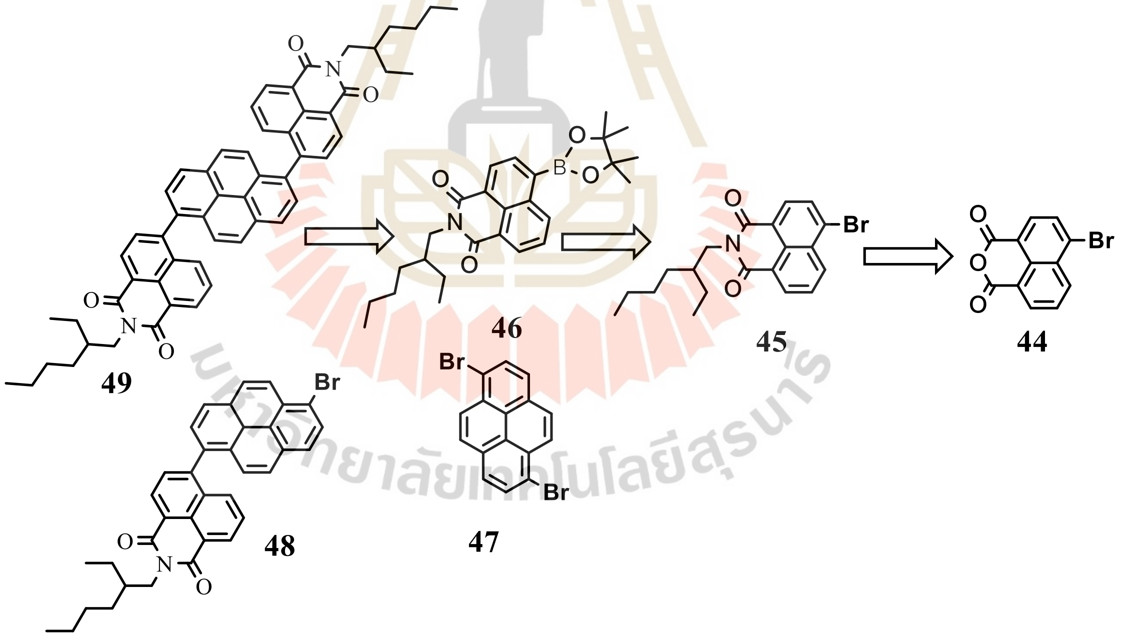

Figure 2.2 Retrosynthesis of 1,8-naphthalimide derivatives **49**.

First step, 4-bromo-*N*-(2-ethylhexyl)-1,8-naphthalimide (**45**) was synthesized from 4-bromo-1,8-naphthalimide anhydride (**44**) and 2-ethylhexylamine by condensation reaction. The intermediate **46** was then synthesized from borylation of compound **45** with bis(pinacolato)diboron in the presence of $Pd(PPh)_3Cl_2$ as catalyst and potassium acetate (KOAc) as base in toluene as solvent (Figure 2.3).

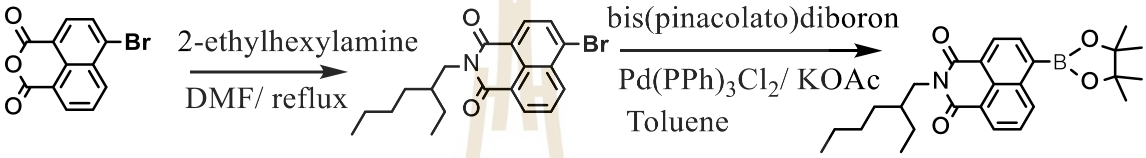

44 **45, 71%** **46, 72%**

Figure 2.3 Synthesis of compound **46**.

The structure of **45** was confirmed by ^{1}H-NMR spectroscopy (Figure 2.4). For synthesis, **45** was using condensation reaction between **44** and 2-ethylhexylamine in the presence DMF as solvent to give **45** in 71% yield. The chemical structure of compound **45** was confirmed by ^{1}H-NMR spectrum, ^{13}C-NMR as well as MALDI-TOF MS. The ^{1}H-NMR spectrum collected in $CDCl_3$ show a triplet signal at 0.95-0.98 ppm (3H), 1.01-1.03 ppm (3H) assigned to methyl groups, the multiplet signal at 1.99-2.03 ppm (1H) assigned to CH proton and the multiplet signal at 4.19-4.22 ppm (2H) assigned to CH_2 proton. Furthermore, the proton signal at aromatic regions were found at chemical shift at 7.93-7.95 ppm (1H), 8.13-8.15 ppm (1H), 8.50-8.52 ppm (1H), 8.67-8.69 ppm (1H), and 8.74-8.76 ppm (1H) assigned to aromatic proton of naphthalimide. The number of proton aromatic regions are (5H) corresponding to ^{1}H-NMR spectrum. In addition, MALDI-TOF MS spectrum was used to confirm the structure and found to be 388.1105 m/z, agreeing with the calculated mass of $C_{20}H_{22}BrNO_2$: 389.08.

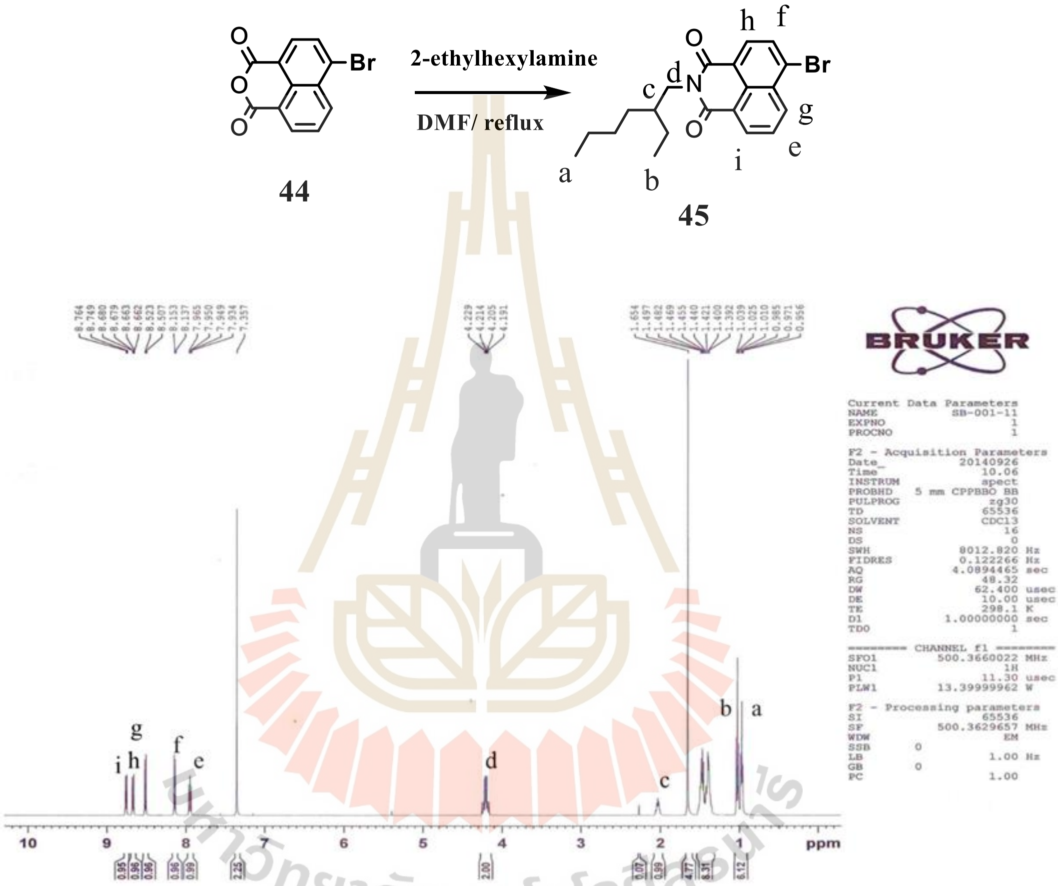

Figure 2.4 The ^{1}H-NMR spectrum in $CDCl_3$ of compound **45**.

The reaction mechanism involves firstly a nucleophilic attack on the fairly positive carbon atom by the lone pair on the nitrogen atom in the amine (2-ethylhexylamine) (Figure 2.5). Secondly, the carbon-oxygen double bond reforms and oxygen is pushed off, follow hydrogen transfer, remove hydrogen and water one atom.

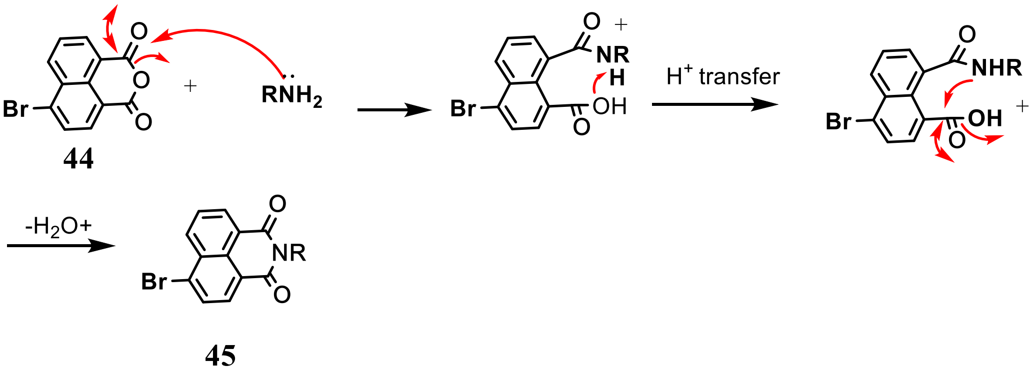

Figure 2.5 Mechanism of condensation reaction of **45**.

For synthesis of **46,** Miyaura borylation reaction between **45** and bis (pinacolato)diboron in the presence of, Pd(PPh)$_3$Cl$_2$, potassium acetate (KOAc) as base in toluene as solvent gave **46** in 72% yield. The chemical structure of compound **46** was confirmed by ^{1}H-NMR spectrum (Figure 2.6), ^{13}C-NMR as well as MALDI-TOF MS. The ^{1}H-NMR spectrum collected in CDCl$_3$ show a triplet signal at 0.85-0.87 ppm (3H), 0.91-0.93 ppm (3H) assigned to methyl groups, the singlet at 1.44 ppm (12H) of methyl groups, the multiplet 1.92-1.95 ppm (1H) assigned to CH proton and the multiplet signal at 4.07-4.15 ppm (2H) assigned to CH$_2$ proton. Furthermore, the proton signal at aromatic regions were found at chemical shift at 7.75-7.78 ppm (1H), 8.28-8.30 ppm (1H), 8.55-8.59 ppm (1H), and 9.09-9.11 ppm (1H) assigned to aromatic proton of naphthalimide. The number of proton aromatic regions are (5H) corresponding to ^{1}H-NMR spectrum. In addition, MALDI-TOF MS spectrum was used to confirm the structure and found to be 434.2339 m/z, agreeing with the calculated mass of $C_{26}H_{34}BNO_4$: 435.26.

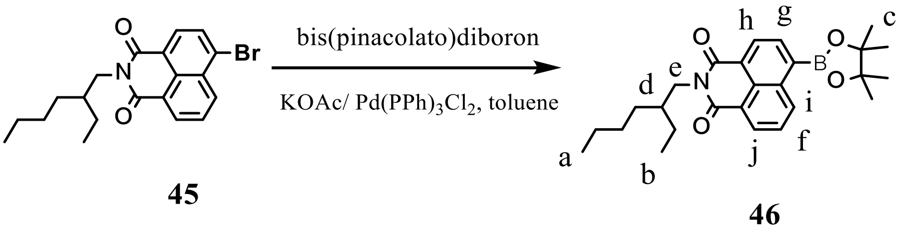

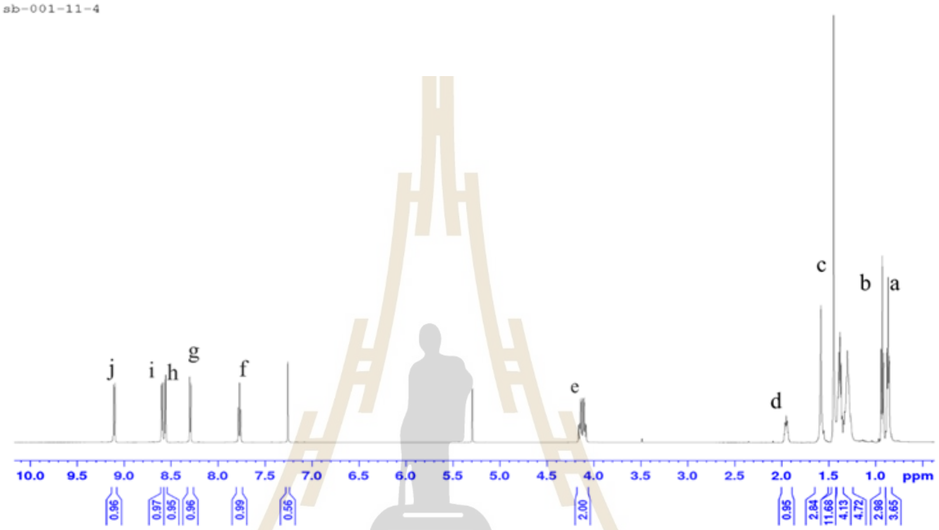

Figure 2.6 The ^{1}H-NMR spectrum in $CDCl_3$ of compound **46**.

Miyaura borylation reaction mechanism of aryl halide and boronate ester involves firstly the oxidation of Pd(0) and alkyl halide number 2 to from complex number 3 (organopalladium species). Secondly organopalladium species number 3 reacts with base give intermediate number 4. Third step intermediate number 4 react with boronate number 6 via transmetalation reaction and follow with transcis isomerization to produce organopalladium species number 8. Finally step, organopalladium species number 8 is elimination by reduction reaction to from product number 9 and original palladium catalyst number 1 see in (Figure 2.7).

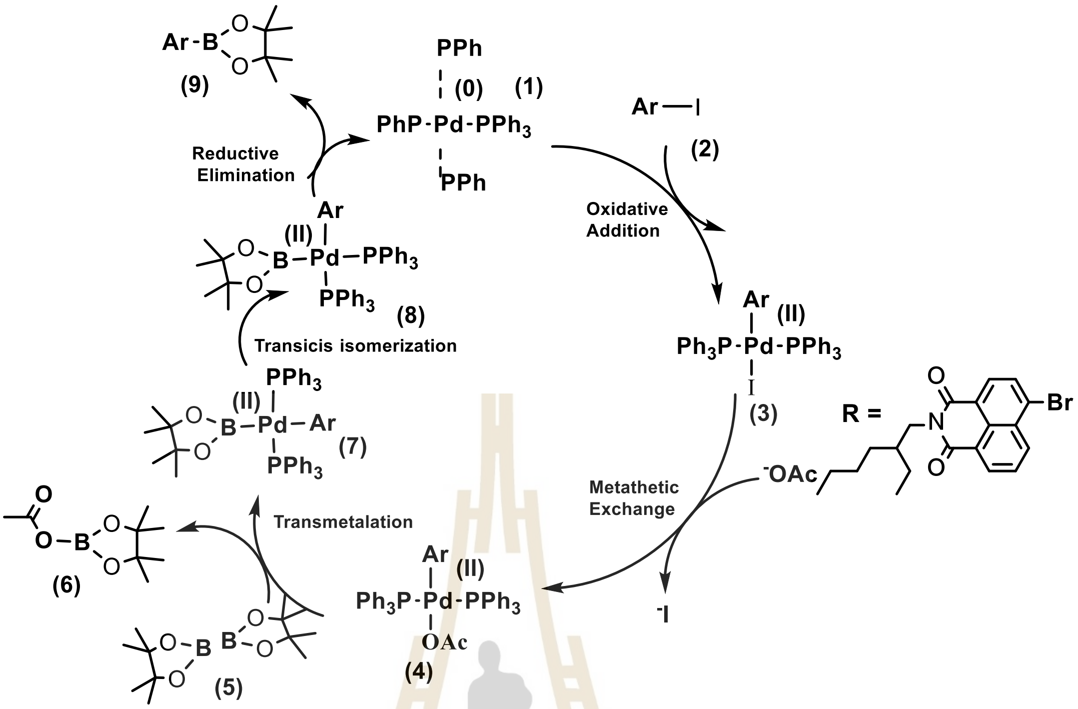

Figure 2.7 Mechanism of Miyaura borylation reaction of **46**.

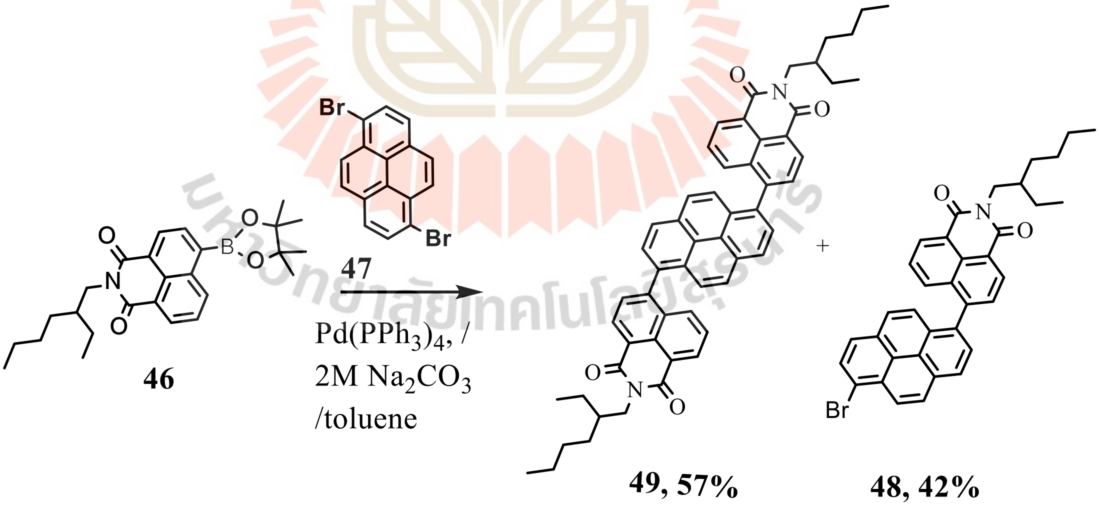

Figure 2.8 Synthesis of compound **49** and **48**.

Finally, (Figure 2.8) Suzuki cross coupling reaction between 4-bromo-*N*-(2-ethylhexyl)-1,8-naphthalimide dioxaborolane (**46**) and 1, 6-dibromopyrene (**47**) in the presence of $Pd(PPh_3)_4$ as catalyst in 2M Na_2CO_3 as base in toluene as solvent afforded **49** in 57% yield and 6-(6-bromopyren-1-yl)-2-(2-ethylhexyl)-1H-benzo[de]isoquinoline-1,3(2H)-dione (**48**).

The chemical structure of compound **49** was confirmed by ^{1}H-NMR spectrum, ^{13}C-NMR as well as MALDI-TOF MS. The ^{1}H-NMR spectrum collected in $CDCl_3$ show a triplet signal at 0.88-0.91 ppm (6H), 0.94-0.95 ppm (6H) assigned to two side of methyl groups and the multiplet signal at 1.99-2.03 ppm (2H) assigned to CH proton. Furthermore, the proton signal at aromatic regions were found at chemical shift at 7.66-7.68 ppm (2H) and 7.75-7.76 ppm (2H) assigned to aromatic proton of pyrene. The number of proton aromatic regions are (18H) corresponding to ^{1}H-NMR spectrum. In addition, MALDI-TOF MS spectrum was used to confirm the structure and found to be 817.4456 m/z, agreeing with the calculated mass of $C_{56}H_{52}N_2O_4$: 818.04. (see in Figure 2.6).

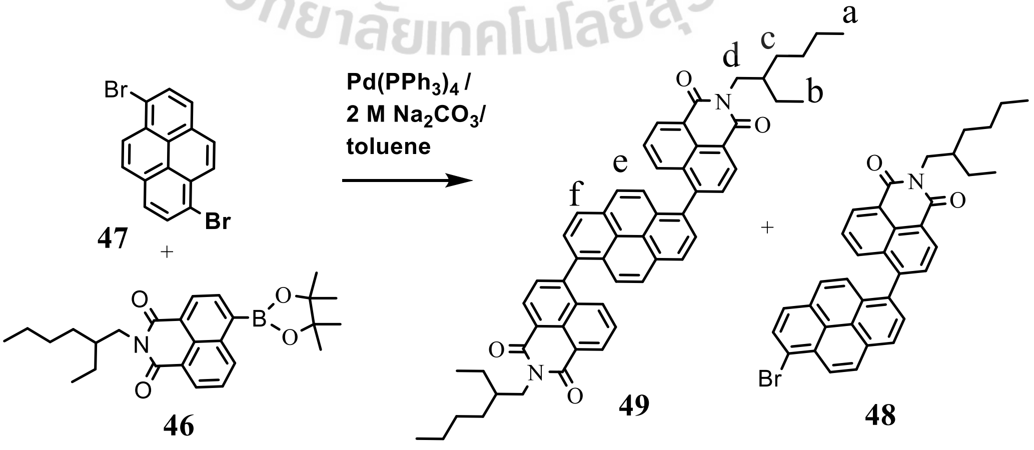

Figure 2.9 The ^{1}H-NMR spectrum in $CDCl_3$ of compound **49**.

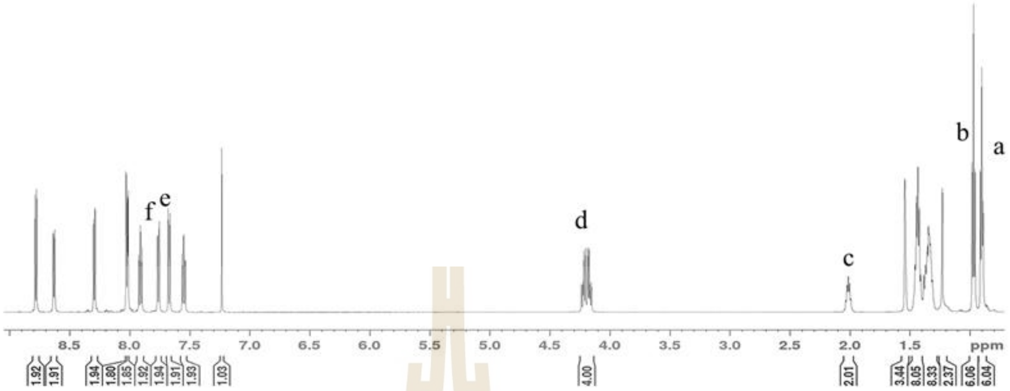

Figure 2.9 The ^{1}H-NMR spectrum in $CDCl_3$ of compound **49** (Continued).

The reaction mechanism of palladium-catalyzed Suzuki cross-coupling reaction of organoboranes with organic halides (Miyaura, 1981, Ishiyama, 1991 and Suzuki 2004) are proposed in (Figure 2.10). The first step was the oxidative addition of palladium 0 (**1**) to the pyrene halide starting meterial (**2**) to form the organopalladium species (**3**). The second step was metalthetic exchange with base to give intermediate (**4**), which via transmetalation with the boron-ate complex (**5**) forms the oganopalladium species (**6**). Reductive elimination of the desired pyrene product (**7**) restores the original palladium catalyst 0.

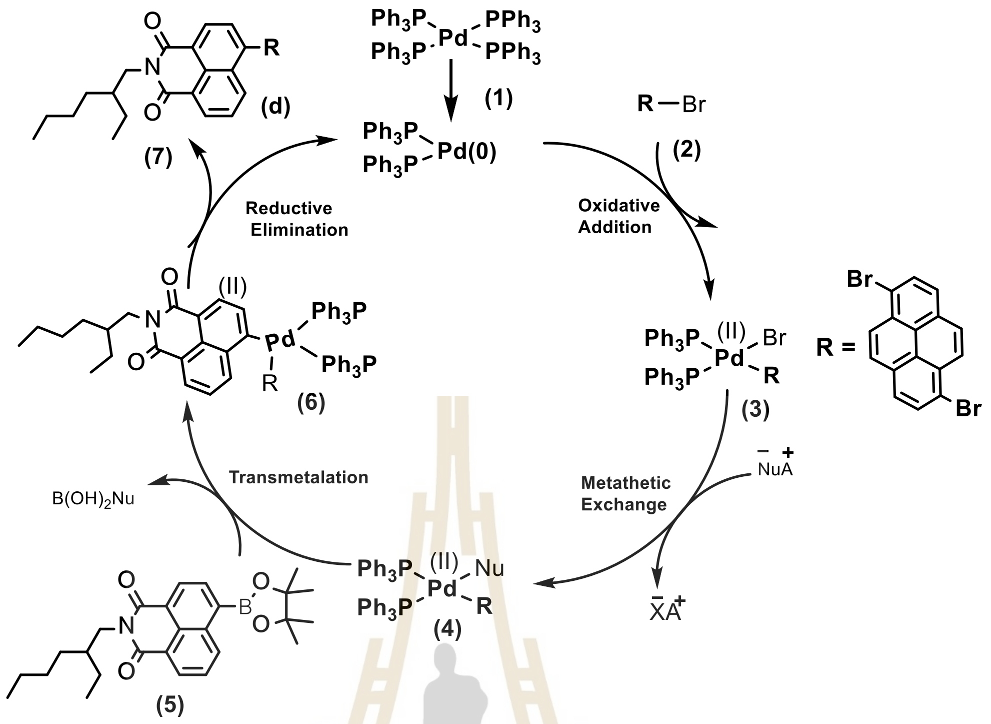

Figure 2.10 Mechanism of Suzuki cross coupling reaction of **49**.

2.3.1.2 The synthesis of 1,8-naphthalimide derivatives **50**.

A described in Figure 2.11, **50** could be formed by the reaction of 1,3,6,8-tetrabromopyrene (**52**) and **46** using Suzuki cross coupling reaction.

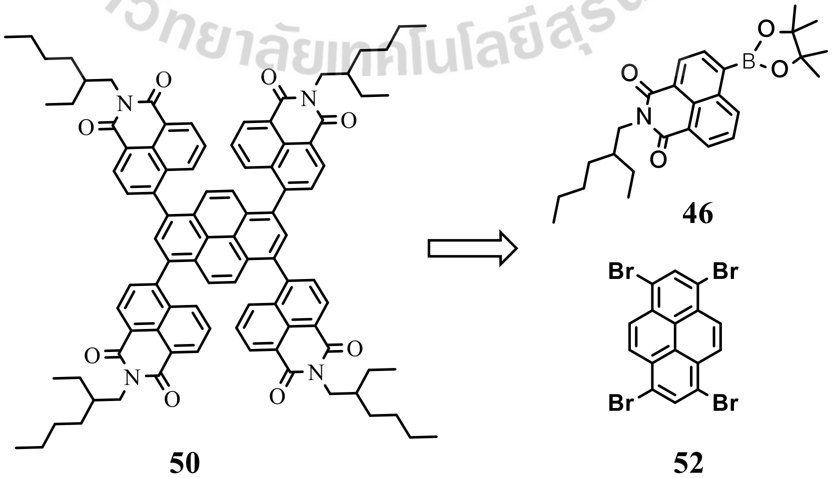

50

46

52

Figure 2.11 Retrosynthesis of 1,8-naphthalimide derivatives **50**.

The synthesis of 50 and ^{1}H-NMR are show in (Figure 2.12). The synthesis of **50** was used the similar conditions with **49**. The target molecule **50** was formed from C-C coupling reaction between **52** and **46** to give **50** in 77% yield. The chemical structure of compound **50** was confirmed by ^{1}H-NMR spectrum, ^{13}C-NMR as well as MALDI-TOF MS. The ^{1}H-NMR spectrum collected in $CDCl_3$ show a triplet signal at 0.86-0.88 ppm (12H), 0.93-0.95 ppm (12H) assigned to four side of methyl groups and the multiplet signal at 1.95-1.99 ppm (4H) assigned to CH proton. Furthermore, the proton signal at aromatic regions were found at chemical shift at 7.82-7.84 ppm (1H) and 7.90-7.92 ppm (1H) assigned to aromatic proton of pyrene. The number of proton aromatic regions were (26H) corresponding to ^{1}H-NMR spectrum. In addition, MALDI-TOF MS spectrum was used to confirm the structure and found to be 1432.0879 m/z, agreeing with the calculated mass of $C_{96}H_{94}N_4O_8$: 1433.71.

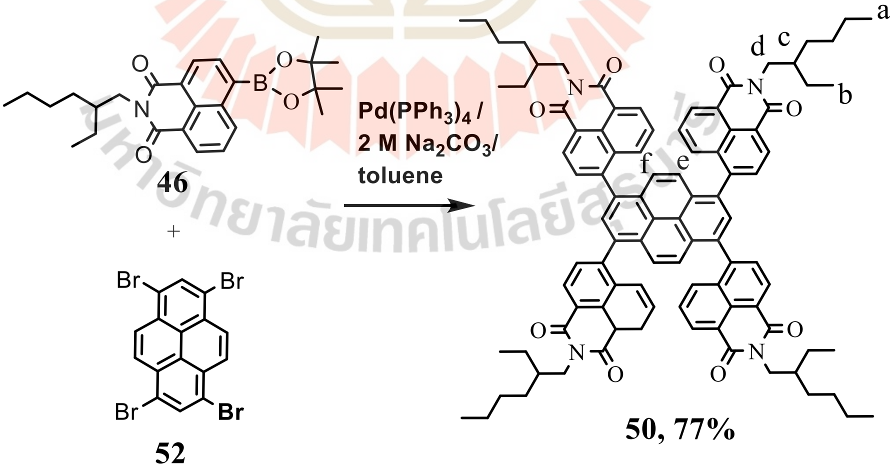

Figure 2.12 The ^{1}H-NMR spectrum in $CDCl_3$ of compound **50**.

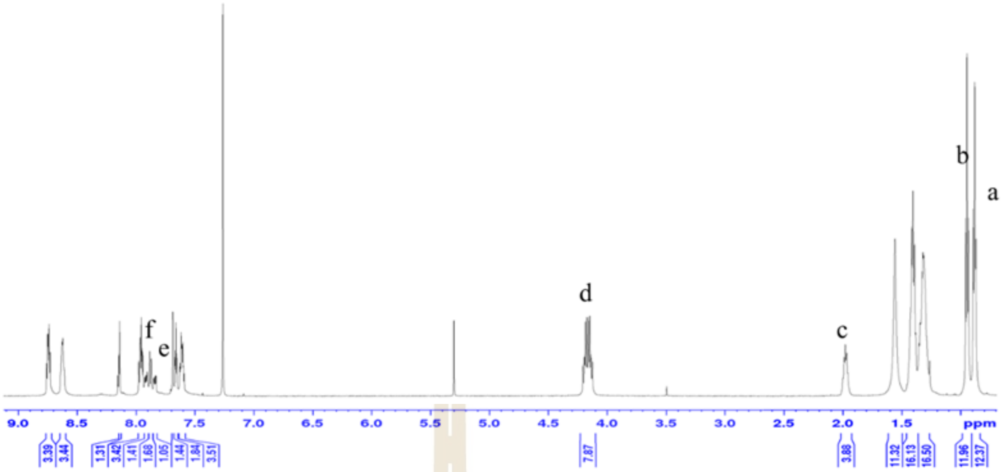

Figure 2.12 The ^{1}H-NMR spectrum in $CDCl_3$ of compound **50** (Continued).

2.3.1.3 The synthesis of 1,8-naphthalimide derivatives 51.

Compound **51** could be prepared from the intermediate **48**. These structures was characterized by ^{1}H-NMR, ^{13}C-NMR and mass spectrometry are shown in (Figure 2.13).

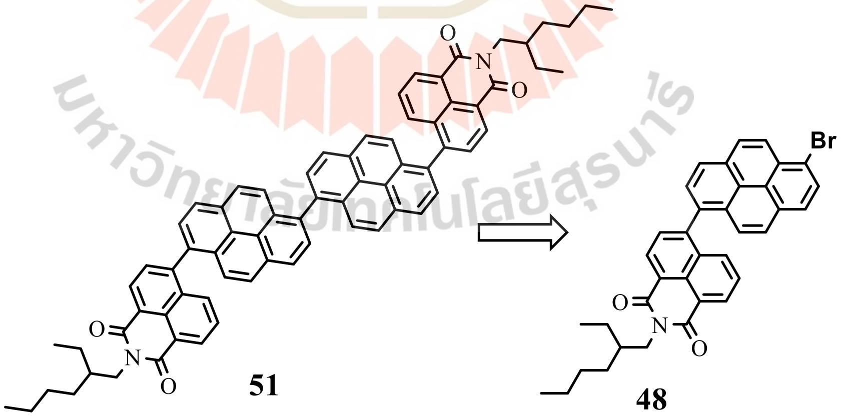

Figure 2.13 Retrosynthesis of 1,8-naphthalimide derivatives **51**.

The synthesis of **51** and ^{1}H-NMR are show in (Figure 2.14). The synthesis of **51** was formed from C-C coupling reaction of **48** in the presence of Pd(PPh)$_3$Cl$_2$ as catalyst in KOAc as base in toluene as solvent to give **51** in 11% yield. The chemical structure of compound **51** was confirmed by ^{1}H-NMR spectrum, ^{13}C-NMR as well as MALDI-TOF MS. The ^{1}H-NMR spectrum collected in CDCl$_3$ show a triplet signal at 0.90-0.92 ppm (6H), 0.96-0.99 ppm (6H) assigned to four side of methyl groups, the multiplet signal at 2.01-2.03 ppm (2H) assigned to CH proton and the multiplet signal at 4.16-4.25 ppm assigned to CH$_2$ proton. Furthermore, the proton signal at aromatic regions were found at chemical shift at 8.18-8.21 ppm (1H) and 8.63-8.65 ppm (1H) assigned to aromatic proton of pyrene. The number of proton aromatic regions are (21H) corresponding to ^{1}H-NMR spectrum. In addition, MALDI-TOF MS spectrum was used to confirm the structure and found to be 1017.4105 m/z, agreeing with the calculated mass of $C_{72}H_{60}N_2O_4$: 1018.28.

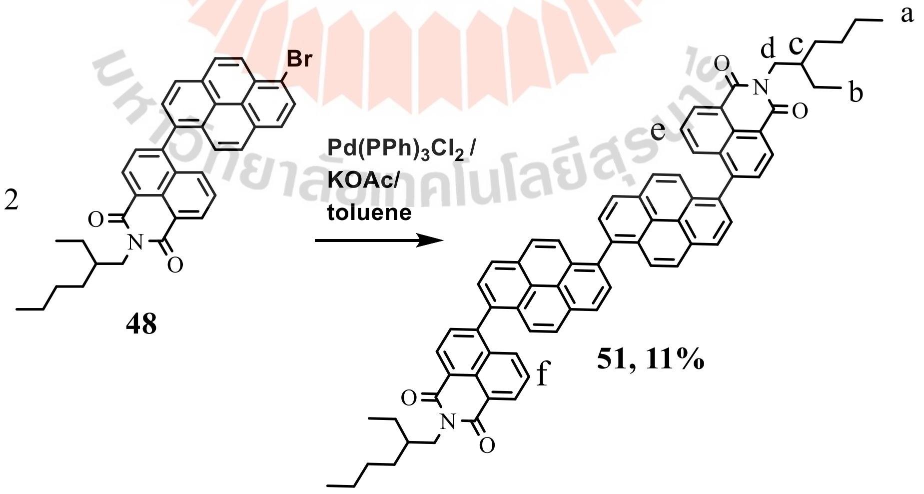

Figure 2.14 The ^{1}H-NMR spectrum in CDCl$_3$ of compound **51**.

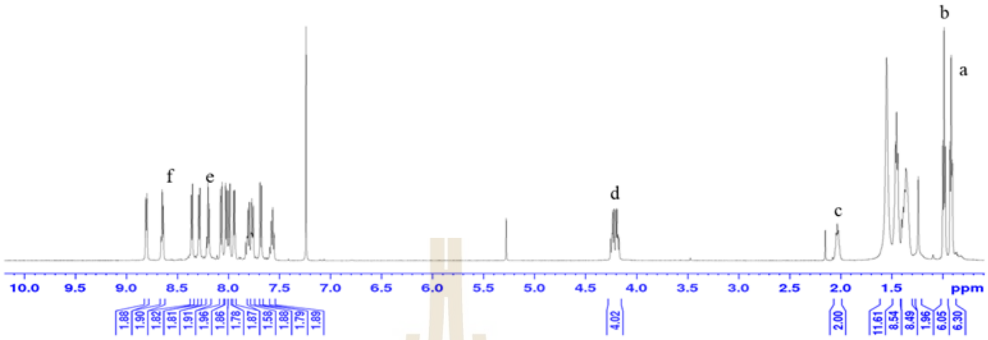

Figure 2.14 The ^{1}H-NMR spectrum in $CDCl_3$ of compound **51** (Continued).

2.4. Photophysical properties.

UV-vis absorption spectra and photoluminescence of the compounds **49**, **50**, and **51** were recorded in DCM. Representative absorption and emission spectra in solution are shown in (Figure 2.15a). In the solution phase, each compound exhibited a characteristic π–π* transition, as observed by the absorption peak around 258-284 nm along with a charge transfer between the naphthalimide(s) and pyrene group evidenced by the absorption peak around 351-353 nm (Figure 2.15b). The compound **51** showed an absorption peak longer than other molecules because it has structure that has the mostly π-conjugated. Therefore, the molar extinction coefficient of the latter peak increases with the number of conjugates between naphthalimide and pyrene group.

The absorption spectra of neat films of compounds **49**, **50**, and **51** are broader and slightly red shifted. It is presumed that the red shifts of the absorption spectra of films as compared to those of solutions may be due to smaller dihedral angles in solid state, thus giving rise to more efficient π-conjugation and decreased HOMO-LUMO gap, but can also be due to more efficient π-stacking and stronger intramolecular interactions in the films than in dilute solutions. In the solid state, the absorption spectra of these compounds also have the same pattern as in the solution phase (Figure 2.15b). However, the maximum absorption wavelengths appear at longer wavelengths (285-289 and 356-361 nm) because of stacking effect.

The normalized fluorescence spectra in the solution phase and neat films are also shown in (Figure 2.15a). **49**, **50**, and **51** exhibited a maximum emission wavelength at 521 - 574, and 508 - 526 nm, respectively. The emission spectra showed deceased, which increase the number of naphthalimide unite. The fluorescence spectra in thin film showed emission peaks gradually blue-shifted because of solvent effect.

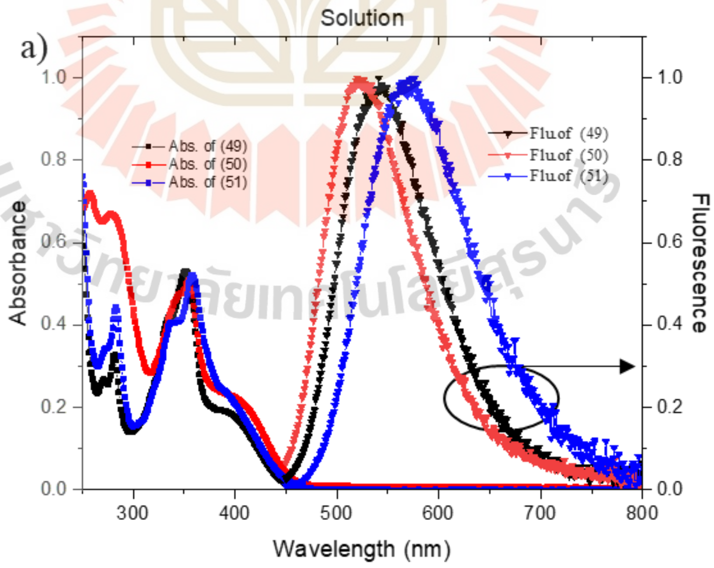

Figure 2.15 a) UV-Vis and fluorescence in DCM b) thin film state.

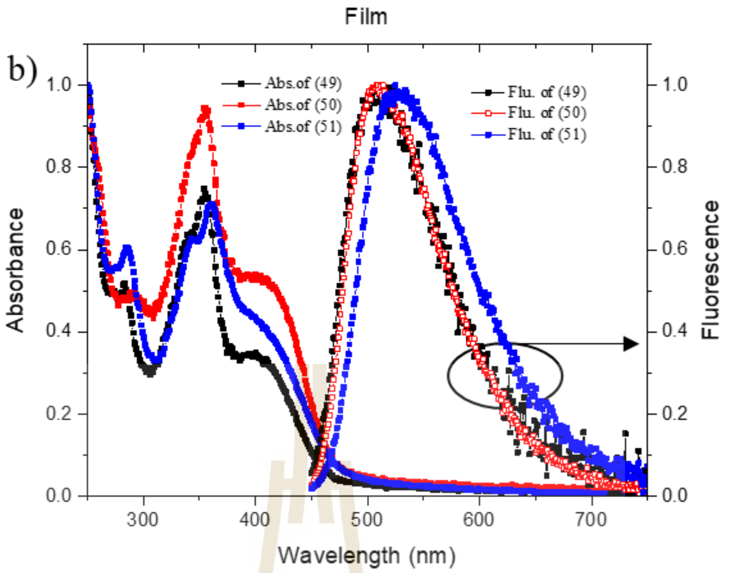

Figure 2.15 a) UV-Vis and fluorescence in DCM b) thin film state (Continued).

The lifetimes of the materials in the solution increased dramatically to 3.6, 3.7, and 4.8 ns (Figure 2.16) with increasing the number of π-conjugate. However, the lifetimes of thin film show decay decrease to 2.2, 2.2, and 2.1 ns, respectively. The data are summarized in Table 2.1.

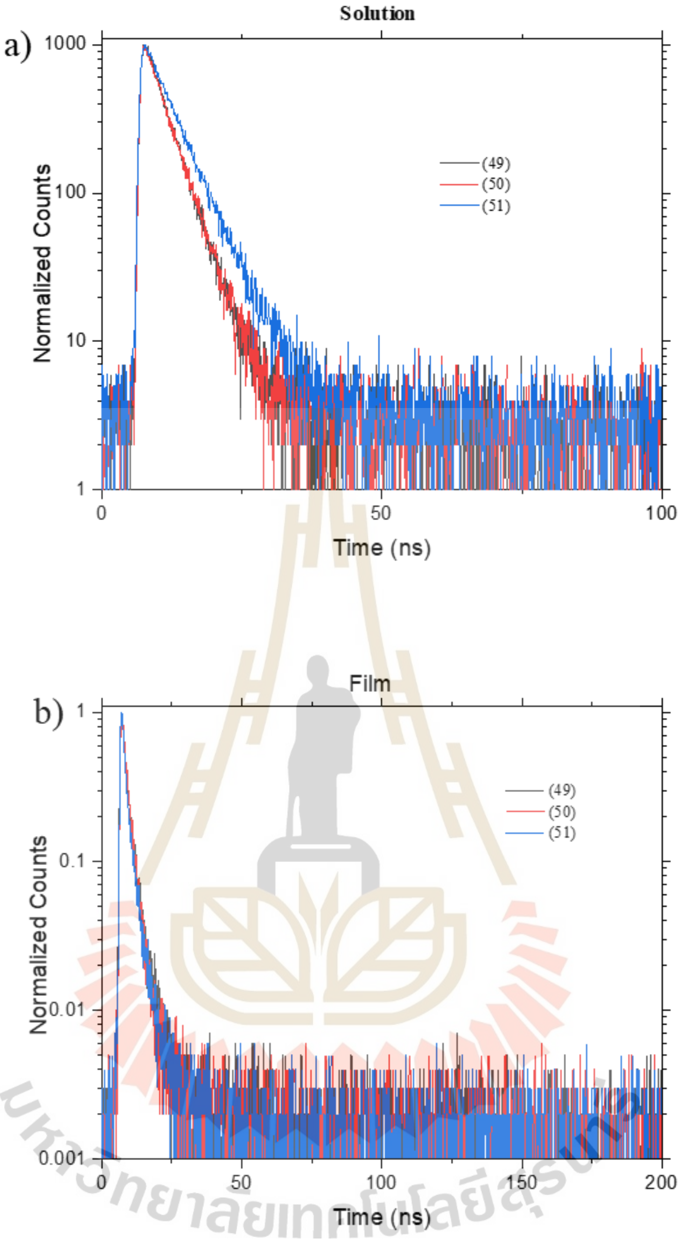

Figure 2.16 a) Fluorescene lifetime in DCM b) thin film state.

Table 2.1 Photophysical properties of **49**, **50**, and **51**.

Comp.	λ^{sol} abs /λ^{film} abs (nm)[a]	λ^{sol} em /λ^{film} em (nm)[b]	τ_P (ns)[c]		QY	
			sol	film	sol	film
49	281,351/ 284,360	544/ 510	3.6	2.2	39.7	29.6
50	258,352/ 289,356	521/ 508	3.7	2.2	52.4	34.0
51	284,353/ 285,361	574/ 526	4.8	2.1	38.3	7.8

[a] Measured in DCM (10^{-5}M) and thin film at 298 K.
[b,c] Measured in DCM (10^{-6}M) and thin film at 298 K.

The quantum yields of these compounds increases, which the number of naphthalimide units. The compound **50** has the highest quantum yield of 52.4% in solution because an increasing number of naphthalimide units made more steric effect leading to the decrease in π-stacking and electron quenching. Compound **49** and **51** have the same number of naphthalimide but compound **51** has 2 pyrene function make decrease value of quantum yield because the energy band gap of compound **51** has lower than compound **49** suggesting that it is more planar and higher π stacking.

2.5 Thermal properties

The thermal properties of all the compounds were determined by thermogravimetric analysis (TGA) and differential scanning calorimetry (DSC) with a heating rate of 10 °C min^{-1} under nitrogen atmosphere. The TGA curves (Figure 2.17) revealed that **49**, **50,** and **51** were thermally stable with high 10% weight loss temperatures (T_d^{10}) at 499, 465 and 384 °C, respectively. The melting temperature of **49**, **50**, and **51** were at 251

°C, 280 °C, and 290 °C, respectively. These abilities of forming molecular glasses with high thermal stability are highly desirable for optoelectronic materials. (Table 2.2)

The thermal properties of **49**, **50**, and **5** were examined by DSC and TGA under a nitrogen atmosphere. The values of glass transition temperatures (T_g), melting point (Tm) and 10% weight loss temperatures (T_d^{10}) are summarized in (Table 2.2). TGA revealed that all the target compounds exhibit excellent thermal stabilities. Their (T_d^{10}) range from 499, 465, and 384 °C, respectively. The high glass transition temperature (Tg) is usually preferred for OLED materials. From the DSC experiment on **49** (Table 2.2), one sharp endothermic peak at 336.48 °C due to melting temperature (Tm) and no glass transition temperature suggested that **49** is a crystalline material. For both **50** and **51** there were endothermic baseline shifts, which indicated a glass transition temperature at 346 °C and 387 °C.

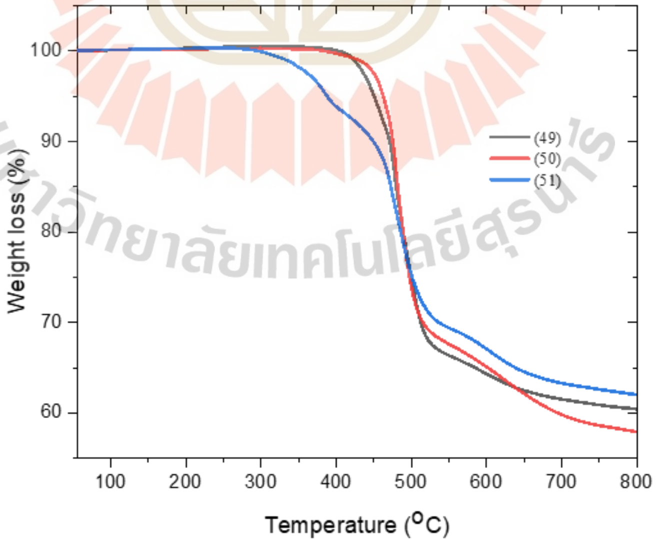

Figure 2.17 TGA curves of **49**, **50**, and **51**.

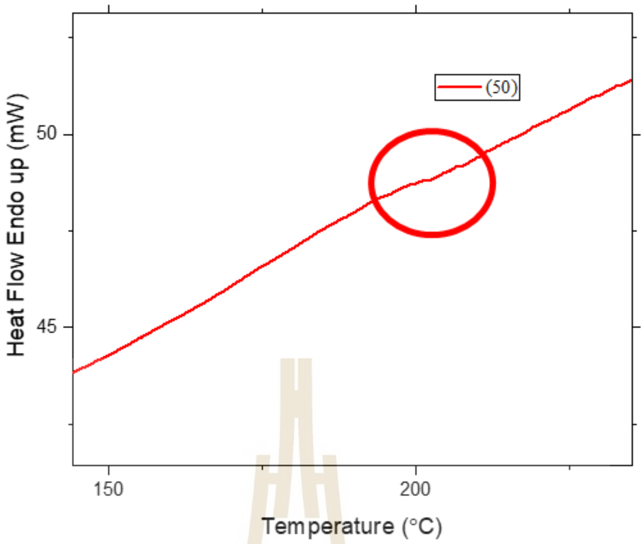

Figure 2.18 DSC analysis of compound **50**.

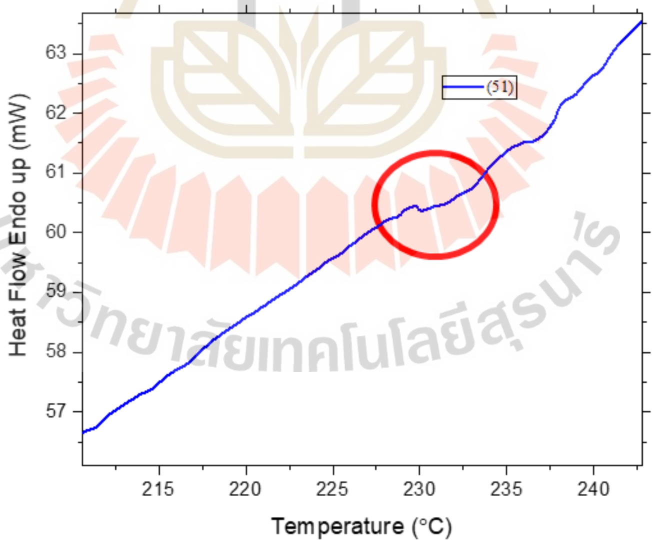

Figure 2.19 DSC analysis of compound **51**.

Table 2.2 Thermal properties of **49**, **50**, and **51**.

Comp.	T_g^a (°C)	T_m^a (°C)	T_d^b (°C)
49	-	260	499
50	206	280	465
51	229	290	384

[a] Obtained from DSC measurements during the second heating cycle with a heating rate of 10 °C min^{-}1 under N_2 atmosphere. [b] 10% weight loss temperature obtained from TGA measurement with a heating rate of 10 °C min^{-}1 under N_2.

2.6 Electrochemical properties

The electrochemical properties of compounds **49**, **50**, and **51** were investigated by CV. As it is shown in (Figure 2.20) compounds **49**, **50**, and **51** showed ambipolar redox behavior with only one reversible oxidation and reduction couple waves around -1.6 and 1.8 eV respectively (vs. Ag/$AgNO_3$). The results of the electrochemical measurements are listed in (Table 2.**3**). The reduction peak is predetermined by withdrawing nature of 1.8-naphthalimide moieties, while one reversible oxidation peak is predetermined by the electron donating nature of pyrene. (Figure 2.20) displays the oxidation behavior in the CV curves of **49**, **50**, and **51**, (Table 2.3) lists the electrochemical properties of these molecules. The result of cyclic voltammograms showed related to structures of final products such as donor of pyrene at the position of oxidation. The compound 51 has 2 pyrene function related to cyclic voltammograms which has 2 lope. The oxidation potentials (E^{ox}_{on}) of **49**, **50**, and **51**, were 1.14, 0.88, and 0.86 V, respectively. The value of E^{ox}_{on} of **50** was lower than those of **49** and **51** because the former possesses electron-donating end groups of 1,8-naphthalimide moieties. The HOMO energy levels for **49**,

50, and **51** are -5.58, -5.32, and -5.30 eV, respectively. The HOMO energy levels of **49**, **50** are lower than that of **51**, consistent with the 1,8-naphthalimide units being strongly electron-withdrawing end groups. Our calculated LUMO energy levels for **49**, **50,** and **51** were -2.81, -2.59, and -2.55 eV, respectively.

The calculated LUMO levels of **49**, **50**, and **51** are -2.55, -2.85 and -2.47 eV, respectively, while the HOMO levels are -5.72, -5.97, and -5.48 eV accordingly (Figure 2.21).

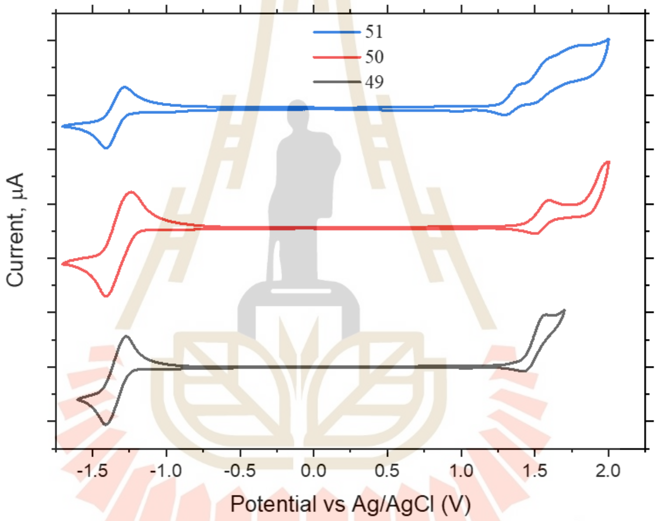

Figure 2.20 CV curves of **49**, **50**, and **51** (10^{-5} M solutions in DCM with 0.1 M n-Bu_4NPF_6).

The incorporation of the peripheral electron-withdrawing group of 1,8-naphthalimide onto molecules results in the decrease of LUMO levels. The trend of the calculation results does match that of the experimental data.

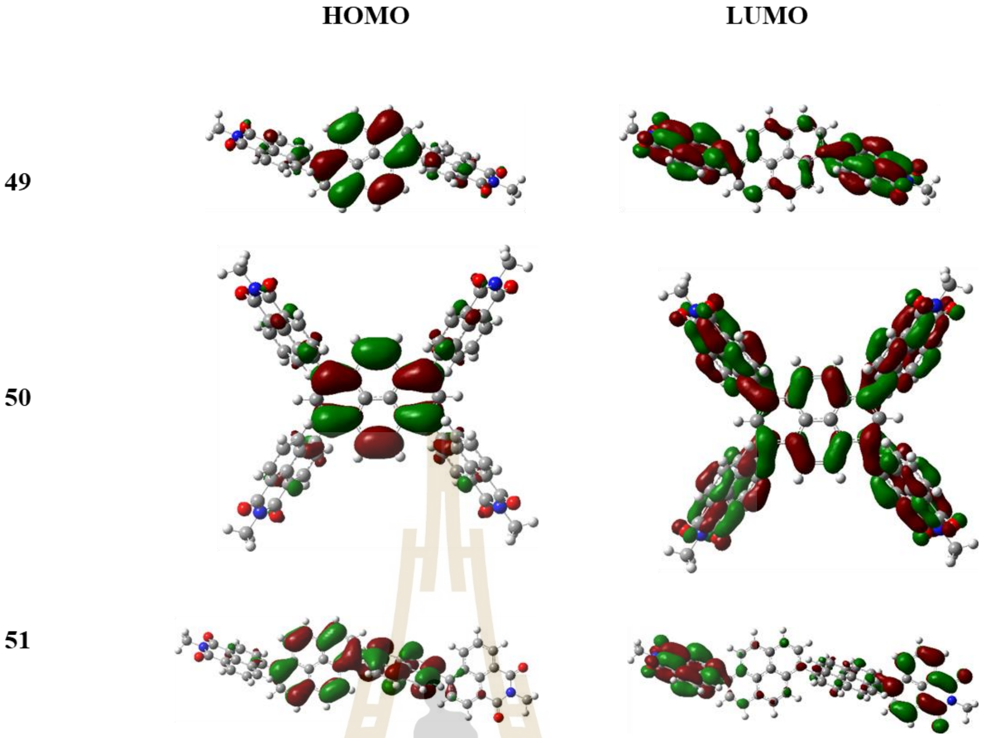

Figure 2.21 Optimized structures obtained from B3LYP/6-31G d, p) in gas phase.

Table 2.3 Electrochemical and theoretical electronic characteristics of **49**, **50**, and **51**.

Comp.	E_{on}^{ox} (eV)a	E_g^{opt} (eV)b	HOMO (eV)c	LUMO (eV)d	HOMO (eV)e	LUMO (eV)e	E_g (eV)e
49	1.14	2.77	-5.58	-2.81	-5.72	-2.55	3.17
50	0.88	2.73	-5.32	-2.59	-5.97	-2.85	3.11
51	0.86	2.75	-5.30	-2.55	-5.48	-2.47	3.01

[a] Measured by CV in DCM vs Ag/Ag^+ at scan rate of 50 mV/s.
[b] Calculated from $\lambda^{abs}{}_{onset}$, $E_g = 1240/\lambda^{abs}{}_{onset}$
[c] Calculated from onset oxidation potential HOMO = -($E^{ox}{}_{on}$ + 4.44) eV
[d] Calculated from LUMO = HOMO + E_g
[e] Calculated from DFT B3LYP/6-31G(d, p)

2.7 OLED device fabrication

For the preliminary investigations on material performance and their electro luminescence, five non-optimized OLED devices were fabricated between the ITO and LiF/Al electrodes using PEDOT-PSS as the hole-injection layer (Figure 2.22). The attempt to fabricate a multi-layer device using **50** as the emissive layer led to poor device performance (Table 2.4), which might result from an improper barrier for electron migration at the interface between the emissive layer and the LiF/Al electrode and a poor film forming ability of **50**. When a layer of hole-blocking material, 4,4'-Bis(*N*-carbazolyl)-1,1,-biphenyl (CBP), 1,3,5-tri(m-pyrid-3-yl-phenyl)benzene (TmPyPb) as electron transport and exiton blocking layer were incorporated, these devices showed blue wish green and yellow green region luminescence with featureless patterns, emission peaks around 490 nm (Figure 2.23a).

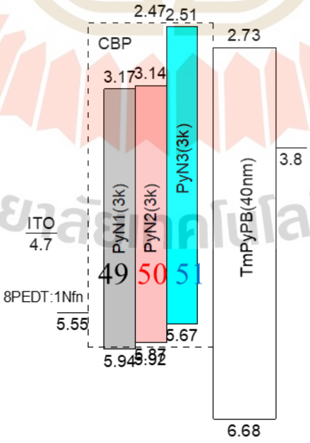

Figure 2.22 Band diagrams for ITO, PEDOT: PSS, **49**, **50**, and **51**, BCP, TmPyPb, and LiF/Al.

We therefore fabricated multilayered devices of **49**, **50**, and **51** using of these materials doped in 4, 4′-bis(*N*-carbazolyl)-1,10-biphenyl (CBP) as the emissive layer (EML). Under the applied voltages, all the fabricated OLEDs Devices of **49**, **50**, and **51** emit a bright yellowish green emission with featureless patterns, emission peaks around 481-493 nm (Figure 2.23a and Table 2.4). The EL spectra of devices of **49**, **50**, and **51** were identical to their thin-film PL spectra, indicating that the EL purely originates from their corresponding EML. The emission of the host BCP showed slightly shoulder of emission peak the host BCP to **49**, **50**, and **51**. Among these diodes, Device **49**, which has 5% **49** doped 4,40-bis(*N*-carbazolyl)-1,10-biphenyl (CBP) as the emissive layer, offers the best performance with a maximum luminance of 1,200 (cd/m^2), % EQE$_{max}$/V of 1.42/6.8% and a turn-on voltage of 4.4 V in Figure 2.22. This device also showed a current density of 194 (mA/cm^2) and emitted a yellowish green light with the CIE coordinates at (0.186, 0.335). Device **51**, using 5% **51-**doped CBP as the EML, showed a slightly lower device performance with a maximum luminance of 1,200 (cd/m^2), %EQE$_{max}$/V of 1.36/8.8% and emitted a yellowish green light with the CIE coordinates at (0.233, 0.438). For device **50** was using 5% **50** doped CBP as the EML, exhibited a poor device performance performance with a maximum luminance of 1,109 (cd/m^2), %EQE$_{max}$/V of 1.15/5.0% and emitted a yellowish green light with the CIE coordinates at (0.208, 0.385).

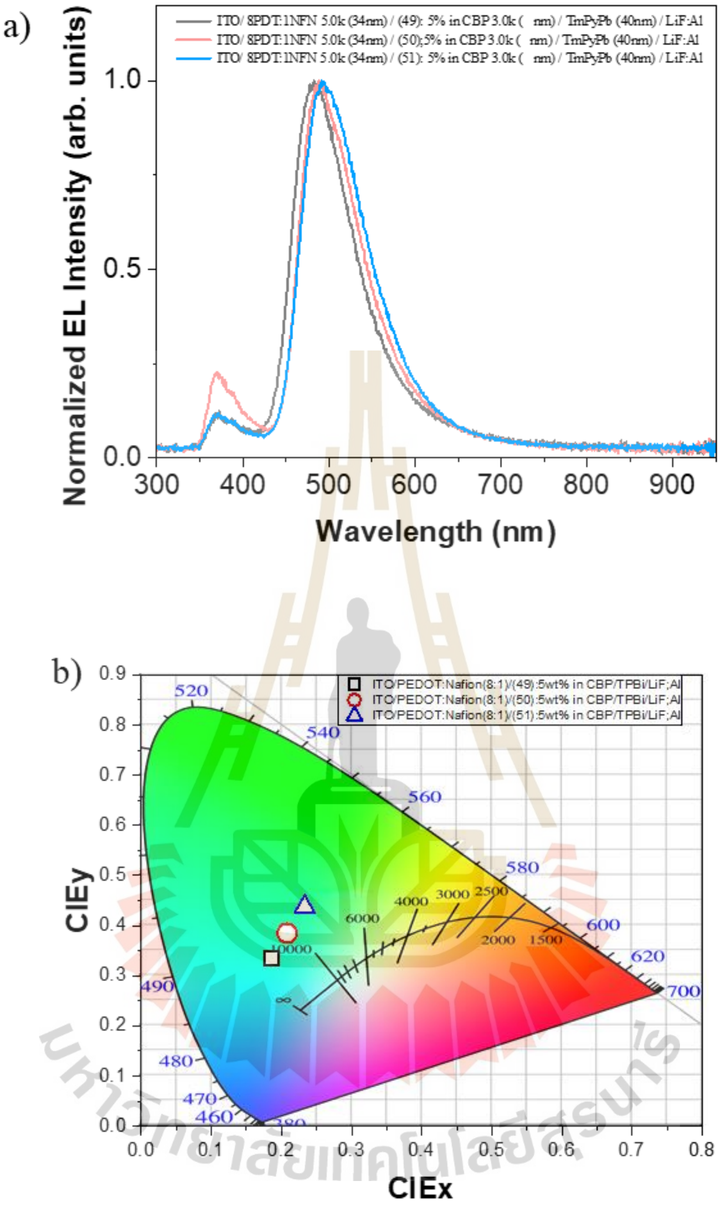

□ : ITO/PEDOT: Nafion(8:1)/**49** :5 wt% in CBP:TmPyPb/LiF/Al
○ : ITO/PEDOT: Nafion(8:1)/**50** :5 wt% in CBP: TmPyPb /LiF/Al
△ : ITO/PEDOT: Nafion(8:1)/**51** :5 wt% in CBP: TmPyPb /LiF/Al

Figure 2.23 a) Normalized electroluminescence spectra at high brightness b) International Commission on Illumination (CIE).

The surface morphologies of the **49**, **50**, and **51** films of were examined by atomic force microscopy (AFM), with corresponding images shown in (Figure 2.23). One can clearly observe that the device film based on **50** and **51** exhibited relatively smooth surface topographic morphology with a root-mean-square (rms) value of 2 μm. **49** showed slightly rougher morphology.

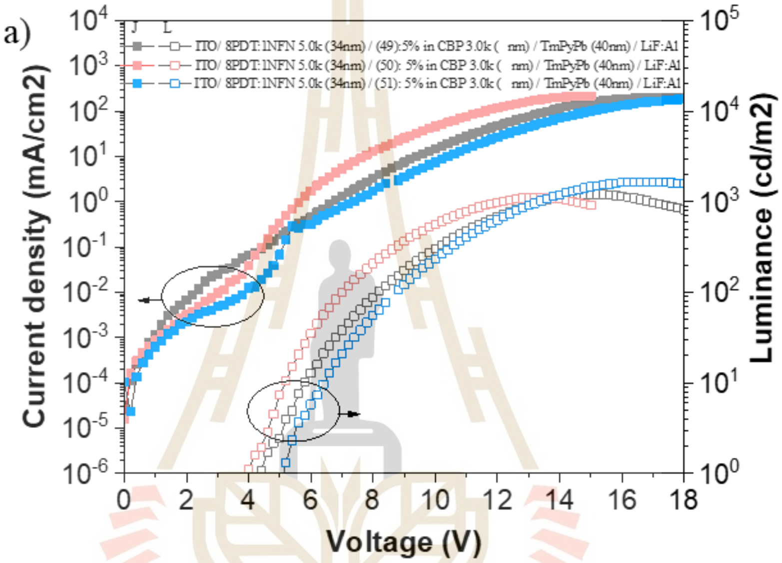

Figure 2.24 (a) Current density-voltage-luminance characteristics (b) External quantum efficiency-current density characteristics.

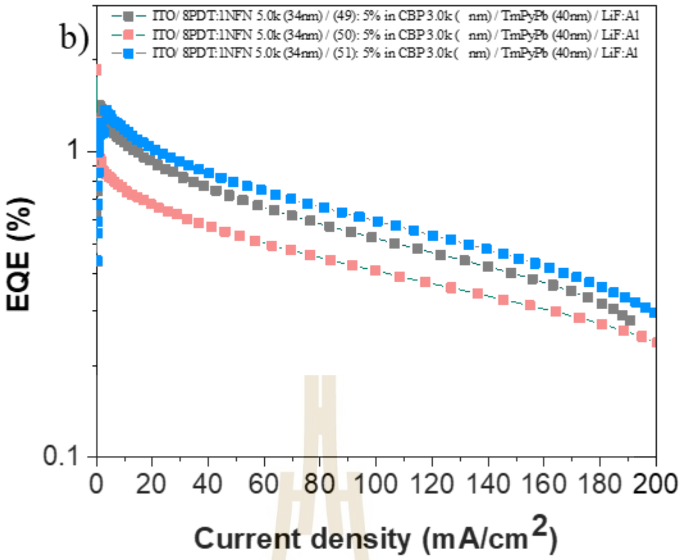

Figure 2.24 (a) Current density-voltage-luminance characteristics (b) External quantum efficiency-current density characteristics (Continued).

(49) (50) (51)

Figure 2.25 AFM images of the thin films of **49**, **50**, and **51**.

Table 2.4 Photophysical property of OLEDs based on **49**, **50**, and **51** series fluorescent materials dope 5 wt% in CBP by using TmPyPb as electron transport layer.

Comp.	CIE$_{xy}$	V$_{on}$ (V)	L_{max} (cd/m^2)	J_{max} (mA/cm^2)	%EQE$_{max}$ /V	ELmax (nm)
49	(0.186, 0.335)	4.4	1,200	194	1.42/6.8	483
50	(0.208, 0.385)	4.0	1,109	216	1.15/5.0	489
51	(0.233, 0.438)	5.1	1,659	202	1.36/8.8	492

2.8 Conclusion

A series of ambipolar materials containing electron accepting 1,8-naphthalimide moieties and electron-donating pyrene groups were obtained via Suzuki cross-coupling reaction. The synthesized compounds exhibit high thermal stability. Their 10% weight loss temperatures range from 384 to 499 °C. The dilute solutions of the compounds in DCM solvents and thin film show fluorescence quantum yields from 38.3 to 52.4, while emission yields of the neat films are in the range of 7.8 to 34.0. Due to pronounced electron donor acceptor characterization. All compounds **49**, **50**, and **51** were employed as the emitters as well as the hole-transporting materials in EL devices based on ITO/PEDOT-PSS/ **49**, **50**, and **51** doped in CBP/ TmPyPb and LiF/Al, in which TmPyPb was used as an electron-transporting layer. We found that the device **49** exhibited good performance with a low turn-on voltage of 4.4 V, a high maximum luminance of 1,200 cd/m^2 at 6.8 V, a high current maximum of 194 mA/cm^2, and a high power efficiency of 1.42. It suggested the luminogens of pyrene functionalized 1,8-

naphthalimide may be used as promising materials for the emissive layer materials on OLEDs.

CHAPTER III

SYNTHESIS AND CHARACTERIZATION OF TRIPHENYLAMINE-CORE NAPHTHALIMIDE DERIVATIVES AS LIGHT-EMITTING MATERIALS FOR ORGANIC LIGHT-EMITTING DIODES

3.1 Introduction

A new series of triphenylamine-core naphthalimide derivatives **53** and **54** were designed using the concept of (A-D-A) system contained 1,8-naphthalimide derivatives as acceptor (A) and triphenylamine as donor (D). For **55** and **56** were designed using the concept of (A-π-D) system contained 1,8-naphthalimide derivatives as acceptor (A) combine with thiophene as π-conjugated and triphenylamine as donor (D). The incorporation of the strong electron acceptor 1,8-naphthalimide was expected to enhance the ICT effect and decrease the band gap energy, resulting in OLEDs exhibiting improved %EQE$_{max}$. These (A-D-A) and (A-π-D-π-A)-structured were exhibited different absorption behaviors in the visible region, electrochemical properties and hole-transporting capacities.

3.2 Aims of the study

1 To design, synthesize and characterize new triphenylamine -core with 1,8-naphthalimide derivatives based electroluminescent materials for OLEDs.

2 To study the photophysical, electrochemical, and thermal properties by UV-visible spectroscopy, fluorescence spectroscopy, cyclic voltammetry and DSC-TGA techniques.

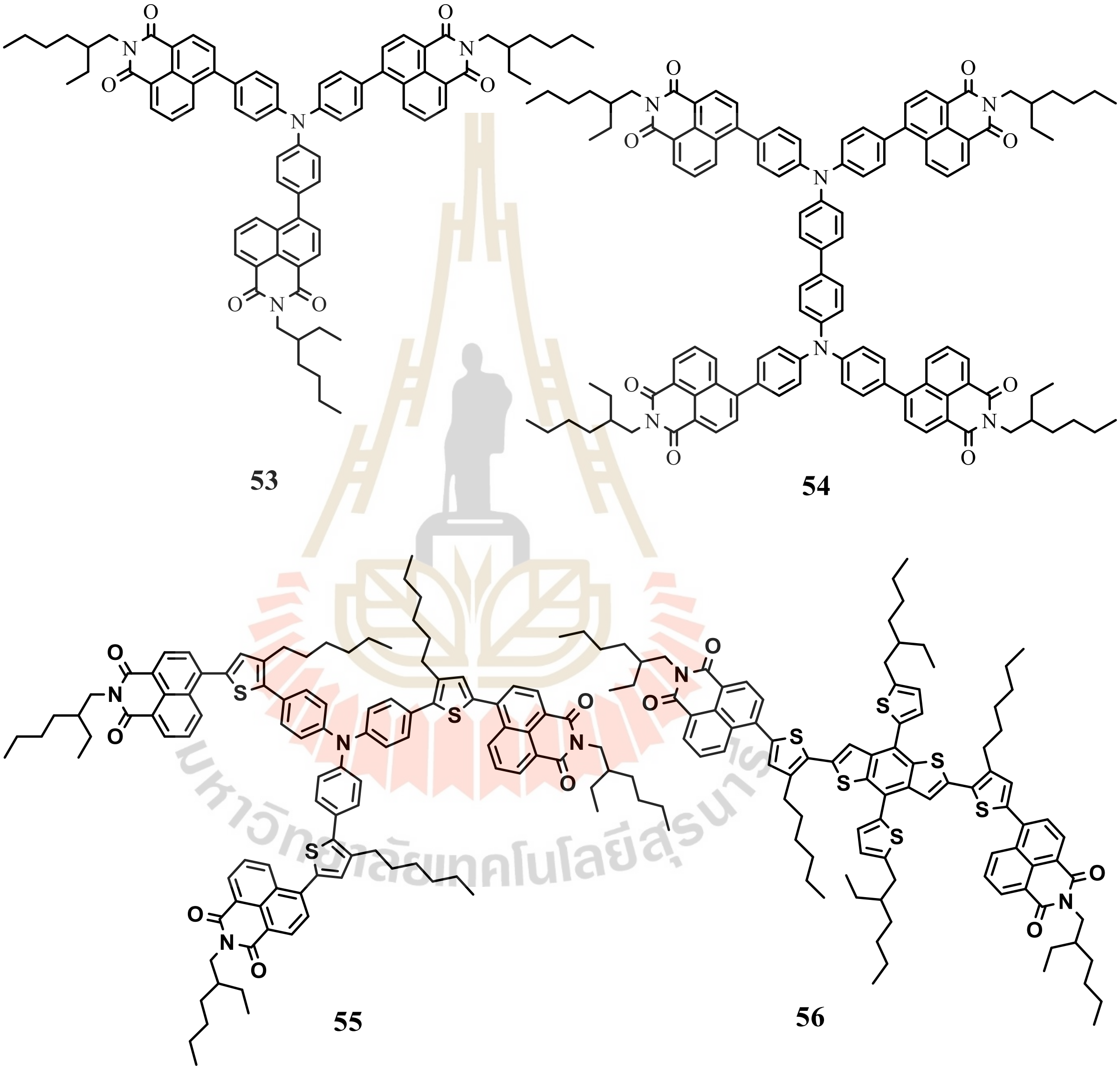

53 **54**

55 **56**

Figure 3.1 The structures of compounds **53**, **54**, **55**, and **56**.

3.3 Results and discussion

3.3.1 The synthesis routes of TPA-core derivatives 53, 54, 55, and 56.

The synthetic routes of the designed **53**, **54**, **55**, and **56** are outlined in (Figure 3.2). Firstly, the key intermediate tris(4-bromophenyl)amine (**58**) will be synthesized by bromination reaction of triphenylamine (**57**) (1 equiv) with *N*-bromosuccinimide (3.2 equiv) in THF. Secondly, generation of triboran triphenylamine using borylation reaction of (**58**) (1 equiv) with bis(pinacolato)diboron (3.2 equiv) in the present of potassium acetate (KOAc), Pd(PPh)$_3$Cl$_2$ in toluene to yield tris(4-(4,4,5,5-tetramethyl-1,3,2-dioxaborolan-2-yl) phenyl) amine **59**. Thirdly, Suzuki cross coupling reaction of **46** (3.2 equiv) with **58** to afford 6,6',6''-(nitrilotris(benzene-4,1-diyl))tris(2-(2-ethylhexyl)-1H-benzo[de]isoquinoline-1,3(2H)-dione) (**53**) and 6,6'-(((4-bromo phenyl)azanediyl) bis(4,1-phenylene))bis(2-(2-ethylhexyl)-1H-benzo[de] isoquinoline-1,3 (2H)-dione) (**60**). Fourthly, borylation reaction of **60** (2 equiv) with bis (pinacolato) diboron (1.2 equiv) catalyzed by potassium acetate (KOAc), Pd(PPh)$_3$Cl$_2$ in toluene to yield 6,6',6'',6'''-(([1,1'-biphenyl]-4,4'-diylbis (azanetriyl)) tetrakis (benzene-4,1-diyl))tetrakis(2-(2-ethylhexyl)-1Hbenzo [de]isoquinoline-1,3(2H)-dione) (**54**). Fifthly, Suzuki cross coupling reaction of 4-bromo-*N*-(2-ethylhexyl)-1,8-naphthalimide (**46)** with 4-hexylthiophene-2-boronic acid pinacol ester (1.2 equiv) catalysed by Pd(PPh$_3$)$_4$, 2M Na$_2$CO$_3$ in toluene to produce 2-(2-ethylhexyl)-6-(4-hexylthiophen-2-yl)-1H-benzo[de]isoquinoline-1,3(2H)-dione (**61**). Sixthly, bromination reaction of **61** followed by Suzuki cross coupling reaction of the resultant with compound **46** (1 equiv), **62** using Pd(PPh$_3$)$_4$, 2M Na$_2$CO$_3$ in toluene to give 6,6',6''-((nitrilotris(benzene-4,1-diyl))tris(4-hexylthiophene-5,2-diyl))tris(2-(2-ethylhexyl)-1H-benzo [de]isoquinoline-1,3(2H) -dione) (**55**). While Stille reaction of compound **62** with 2,6-bis(trimethyltin)-4,8-bis(5-(2-ethylhexyl)thiophene-2-yl)benzo

[1,2-b,4,-5-b′]thiophene (**76**) catalyzed by Pd(PPh$_3$)$_4$ in toluene will produce 6,6'-((4,8-bis(5-(2-ethylhexyl)thiophen-2-yl) benzo[1,2-b:4,5-b']dithiophene-2,6-diyl)bis(4-hexylthiophene-5,2-diyl))bis(2-(2-ethylhexyl)-1H-benzo[de]isoquinoline-1,3(2H)-dione) (**56**).

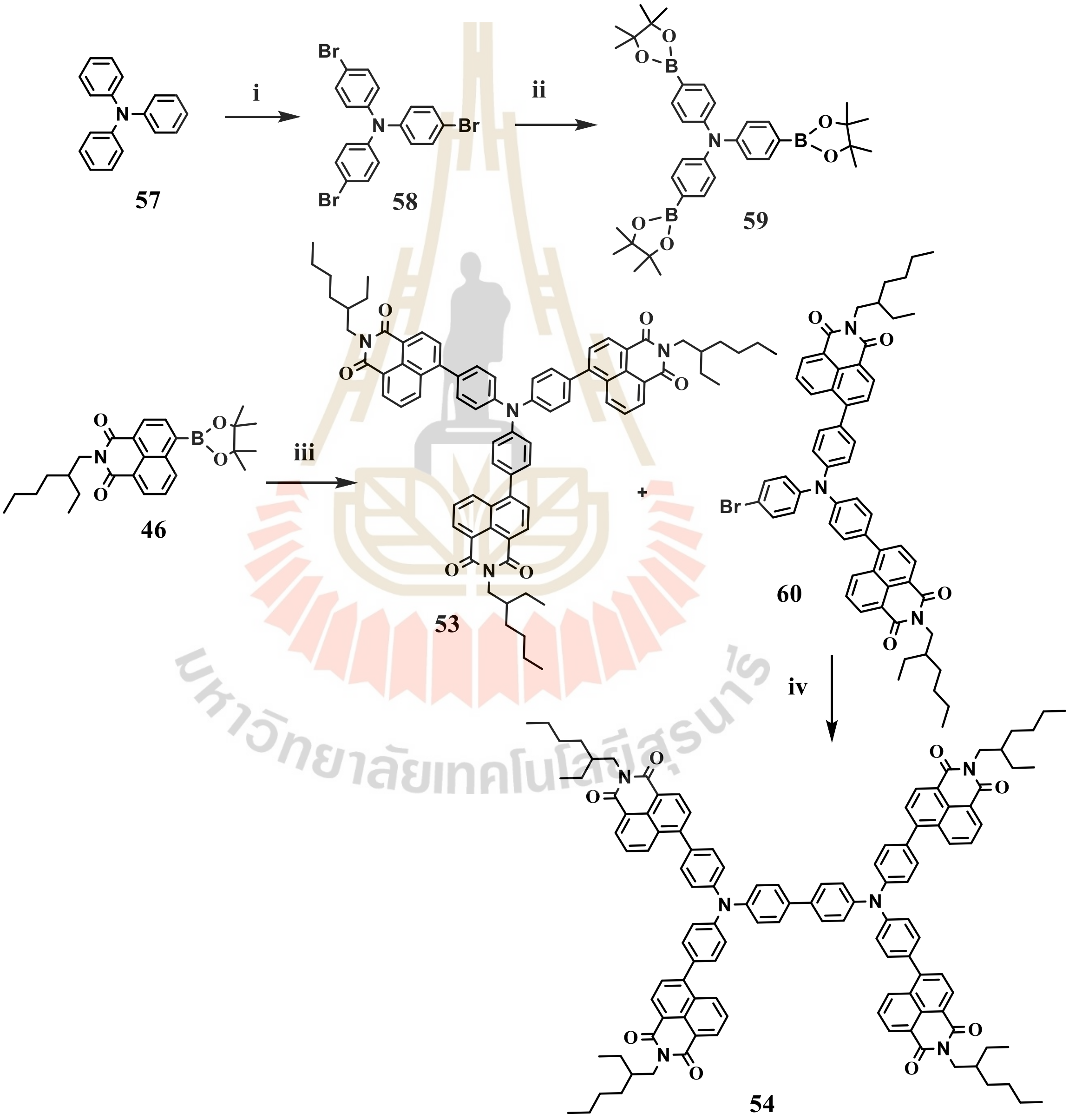

Figure 3.2 The synthetic routes of **53**, **54**, **55**, and **56** molecules.

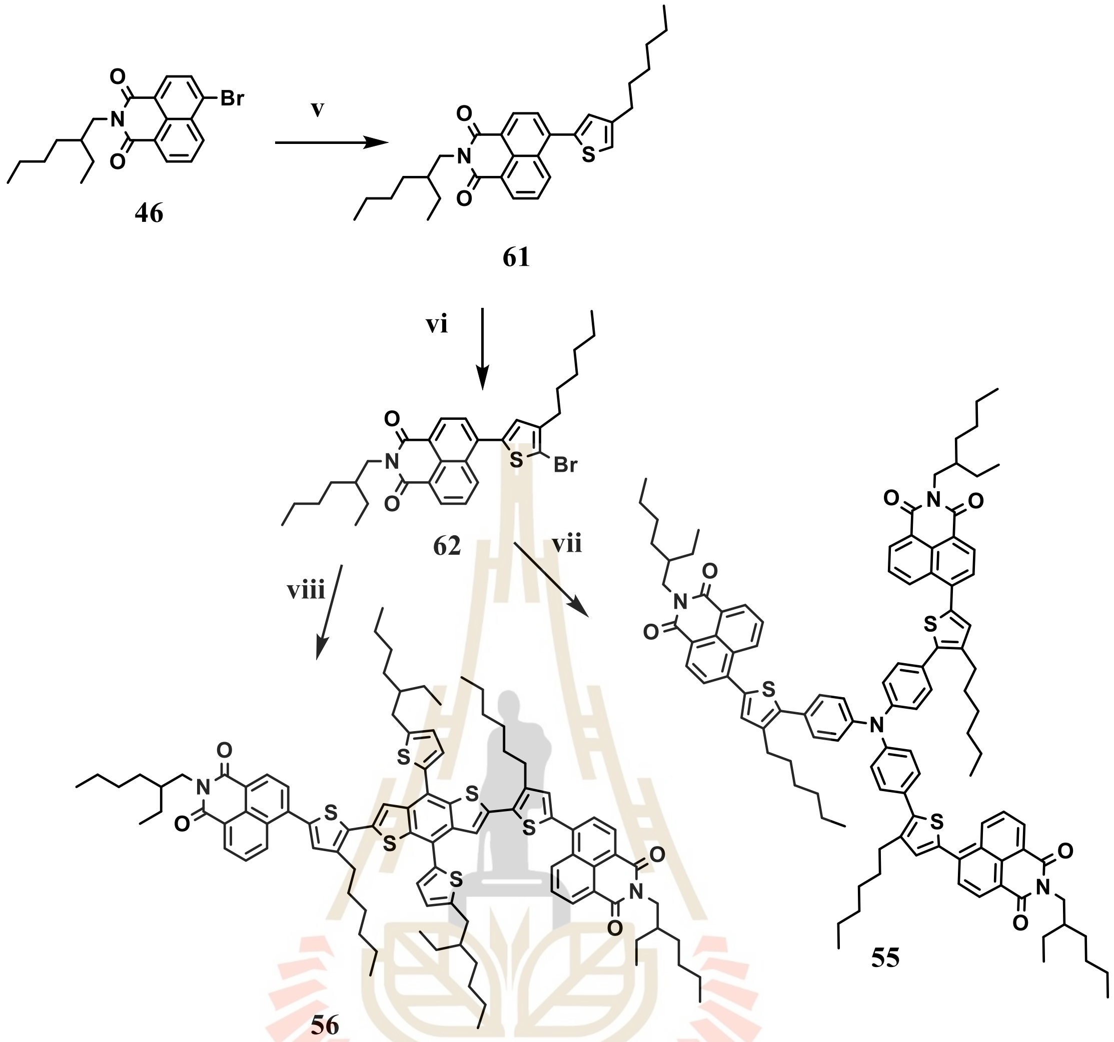

Figure 3.2 The synthetic routes of **53**, **54**, 55, and **56** molecules (Continued).

i, vi = bromination reaction, *N*-bromosuccinimide, THF.
ii = borylation reactionbis, (pinacolato)diboron, (KOAc), $Pd(PPh)_3Cl_2$, toluene.
iii = Suzuki cross coupling reaction, **58**, $Pd(PPh_3)_4$, 2M Na_2CO_3, toluene.
iv = borylation reactionbis, **60,** (pinacolato)diboron, (KOAc), $Pd(PPh)_3Cl_2$, toluene.
v = Suzuki cross coupling reaction, **46**, 4-Hexyl-2-(4,4,5,5-tetrametyl-1,3,2-dioxaborolan-2-yl)thiophene (2.2 equiv, 7.53mmol, $Pd(PPh_3)_4$, 2M Na_2CO_3, toluene.
vii = Suzuki cross coupling reaction, **62**, **46**, $Pd(PPh_3)_4$, 2M Na_2CO_3, toluene.
viii = Stille reaction, **62**, 2,6-Bis(trimethyltin)-4,8-bis(5-(2-ethylhexyl)thiophene-2-yl) benzo[1,2-b,4,-5-b′]thiophene, $Pd(PPh_3)_4$, toluene.

First step involves the synthesis of **58** from triphenylamine (**57**) by using bromination reaction with NBS. The resultant was then proceeded to borylation reaction of $Pd(PPh)_3Cl_2$ to give starting material **59** (Figure 3.3).

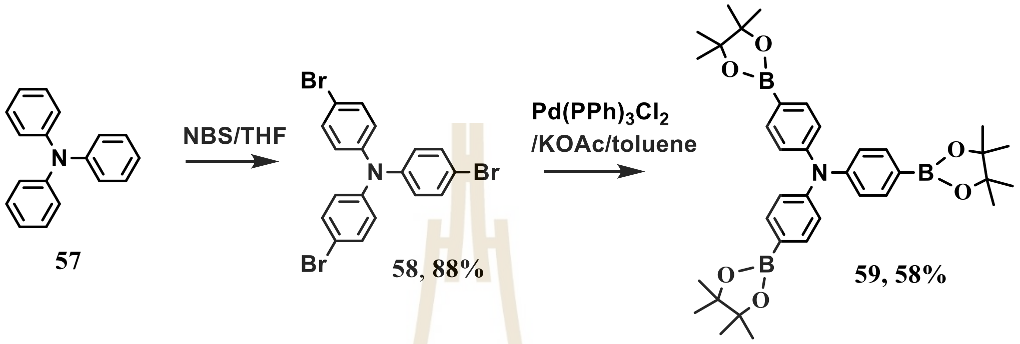

Figure 3.3 Synthesis of compound **59**.

The reaction mechanism for NBS bromination involves firstly cleavage of the N-Br bond forms two bromine. Second step is electrophilic aromatic substituted at the position para direct to give product and hydrogen bromide (Figure 3.4).

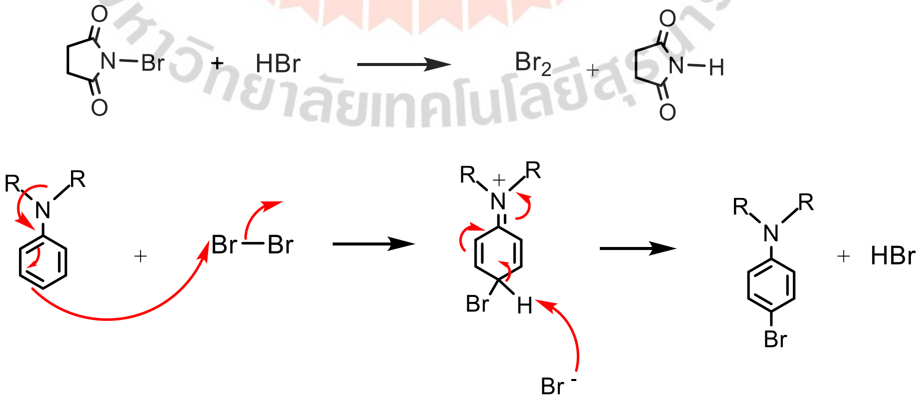

Figure 3.4 Mechanism of Brominated reaction **59**.

The structure of **58** was confirmed by ^{1}H-NMR spectroscopy. The aromatic proton of linker resonates show two doublet at δ = 6.90-6.92 ppm (6H) *J* = 8.70 Hz, H_{Ar} doublet and δ = 7.34-7.35 ppm (6H) *J* = 8.70 Hz, $H_{Ar.}$ In addition, the ^{13}C NMR (600 MHz, $CDCl_3$) show signals of aromatic carbons at δ 144.08, 132.34, 128.63 and 124.09.

The structure of **59** was confirmed by ^{1}H-NMR spectroscopy. The proton signal of aromatic regions were found at δ = 7.67-7.69 (d, 6H, *J* = 8.40 Hz, H_{Ar}), 7.06-7.08 (d, 6H, *J* = 8.40 Hz, H_{Ar}). In addition, the proton signal of aliphatic regions was found at δ = 1.33 (s, 36H, $H_{Aliphatic}$) (Figure 3.5).

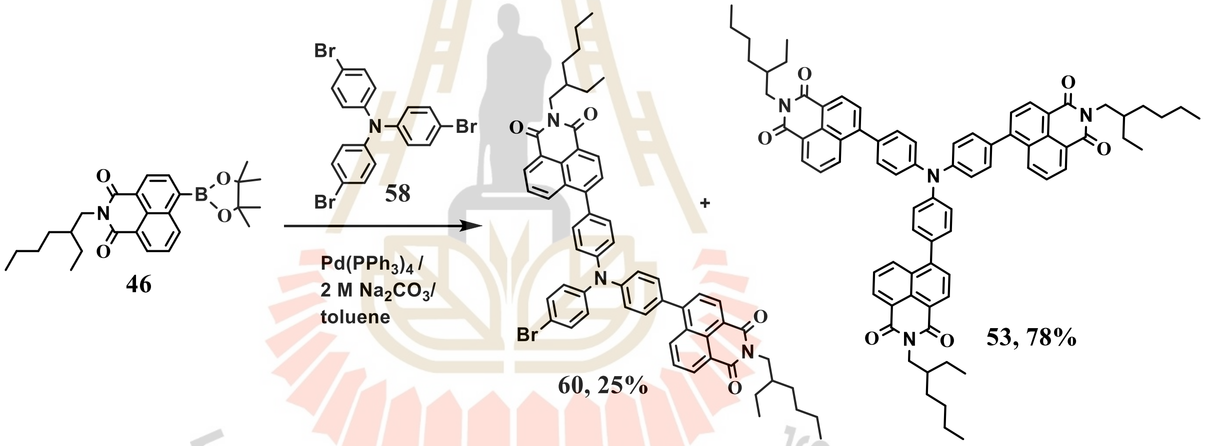

Figure 3.5 Synthesis of compound **53**.

Figure 3.6 shows the synthesis of **53** and ^{1}H-NMR spectrum. For synthesis, **53** was formed using C-C coupling reaction between **46** and **58** in the presence of $Pd(PPh_3)_4$ as catalyst in 2M Na_2CO_3 as base in toluene as solvent to give **53** in 78% yield. The chemical structure of compound **53** was confirmed by ^{1}H-NMR spectrum, ^{13}C-NMR as well as MALDI-TOF MS. The ^{1}H-NMR spectrum collected in $CDCl_3$ show pattern of a triplet signal at 0.87-0.90 ppm (9H), 0.93-0.96 ppm (9H) assigned to two side of methyl groups, the multiplet signal at 1.95-2.00 ppm (3H) assigned to CH proton and the multiplet signal at 4.12-4.20 ppm (6H) assigned to CH_2 proton. Furthermore, the proton signal at aromatic regions were found at chemical shift at 7.46-7.48 ppm (6H) and 7.53-7.54 ppm (6H) assigned to aromatic proton of triphenylamine. The number of proton aromatic regions are (27H) corresponding to ^{1}H-NMR spectrum. In addition, MALDI-TOF MS spectrum was used to confirm the structure and found to be 1167.4825 m/z, agreeing with the calculated mass of $C_{78}H_{78}N_4O_6$: 1167.50.

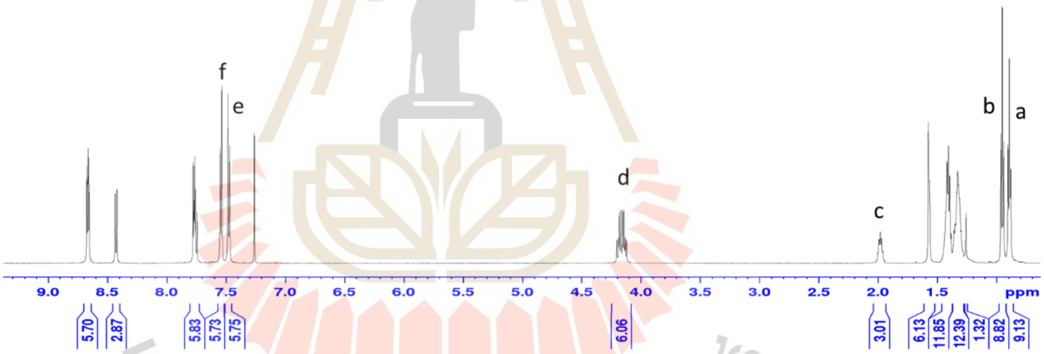

Figure 3.6 The synthesis and ^{1}H-NMR spectrum in $CDCl_3$ of **53**.

Figure 3.7 shows the synthesis of **54** and ^{1}H-NMR spectrum. **54** was formed from C-C coupling borylation reaction between **60** and bis(pinacolato) diboron in the presence of $Pd(PPh)_3Cl_2$ as catalyst in KOAc as base in toluene as solvent to give **54** in 28% yield. The chemical structure of compound **54** was confirmed by ^{1}H-NMR spectrum, ^{13}C-NMR as well as MALDI-TOF MS. The ^{1}H-NMR spectrum collected in $CDCl_3$ show pattern of a triplet signal at 0.87-0.90 ppm (12H), 0.93-0.96 ppm (12H) assigned to two side of methyl groups, the multiplet signal at 1.97-1.99 ppm (4H) assigned to CH proton and the multiplet signal at 4.12-4.20 ppm (8H) assigned to CH_2 proton. Furthermore, the proton signal at aromatic regions were found at chemical shift at 7.46-7.48 ppm (6H) and 7.53-7.54 ppm (6H) assigned to aromatic proton of triphenylamine. The number of proton aromatic regions are (27H) corresponding to ^{1}H-NMR spectrum. In addition, MALDI-TOF MS spectrum was used to confirm the structure and found to be 1167.4825 m/z, agreeing with the calculated mass of $C_{78}H_{78}N_4O_6$: 1167.50.

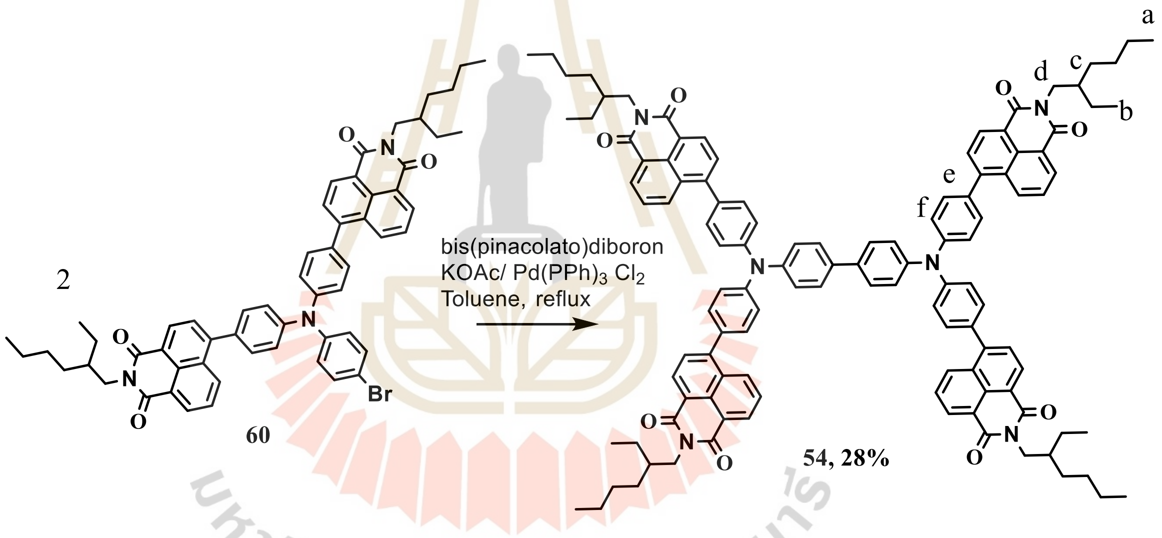

Figure 3.7 The synthesis and ^{1}H-NMR spectrum in $CDCl_3$ of **54**.

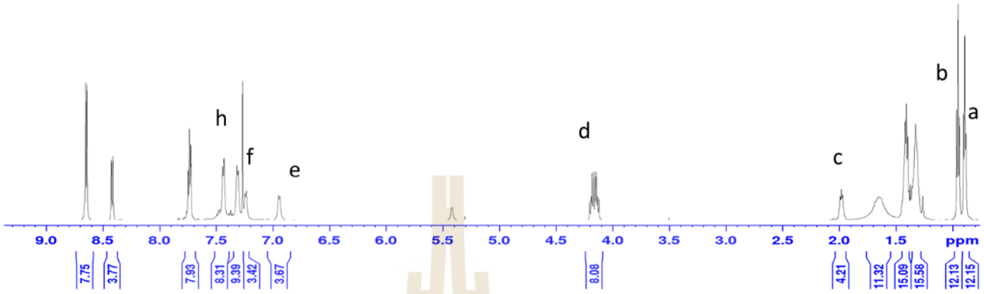

Figure 3.7 The synthesis and ^{1}H-NMR spectrum in $CDCl_3$ of **54** (Continued).

Figure 3.8 shows the synthesis of **55** and ^{1}H-NMR spectrum. For synthesis, **55** was formed from C-C coupling reaction between **46** and **62** in the presence of $Pd(PPh_3)_4$ as catalyst in 2M Na_2CO_3 as base in toluene as solvent to give **55** in 28% yield. The chemical structure of compound **55** was confirmed by ^{1}H-NMR spectrum, ^{13}C-NMR as well as MALDI-TOF MS. The ^{1}H-NMR spectrum collected in $CDCl_3$ show pattern of a triplet signal at 0.86ppm (18H), 0.94 ppm (9H) assigned to two side of methyl groups, the multiplet signal at 1.73 ppm (6H) assigned to CH_2 proton, the multiplet signal at 1.97 ppm (3H) assigned to CH proton and the multiplet signal at 2.80 ppm (6H) assigned to CH_2. Furthermore, the proton signal at aromatic regions were found at chemical shift at 7.29-7.30 ppm (6H) and 7.53-7.54 ppm (6H) assigned to aromatic proton of thiophene derivatives. The number of proton aromatic regions are (40H) corresponding to ^{1}H-NMR spectrum. In addition, MALDI-TOF MS spectrum was used to confirm the structure and found to be 1658.9320 m/z, agreeing with the calculated mass of $C_{108}H_{120}N_4O_6S_3$: 1664.84.

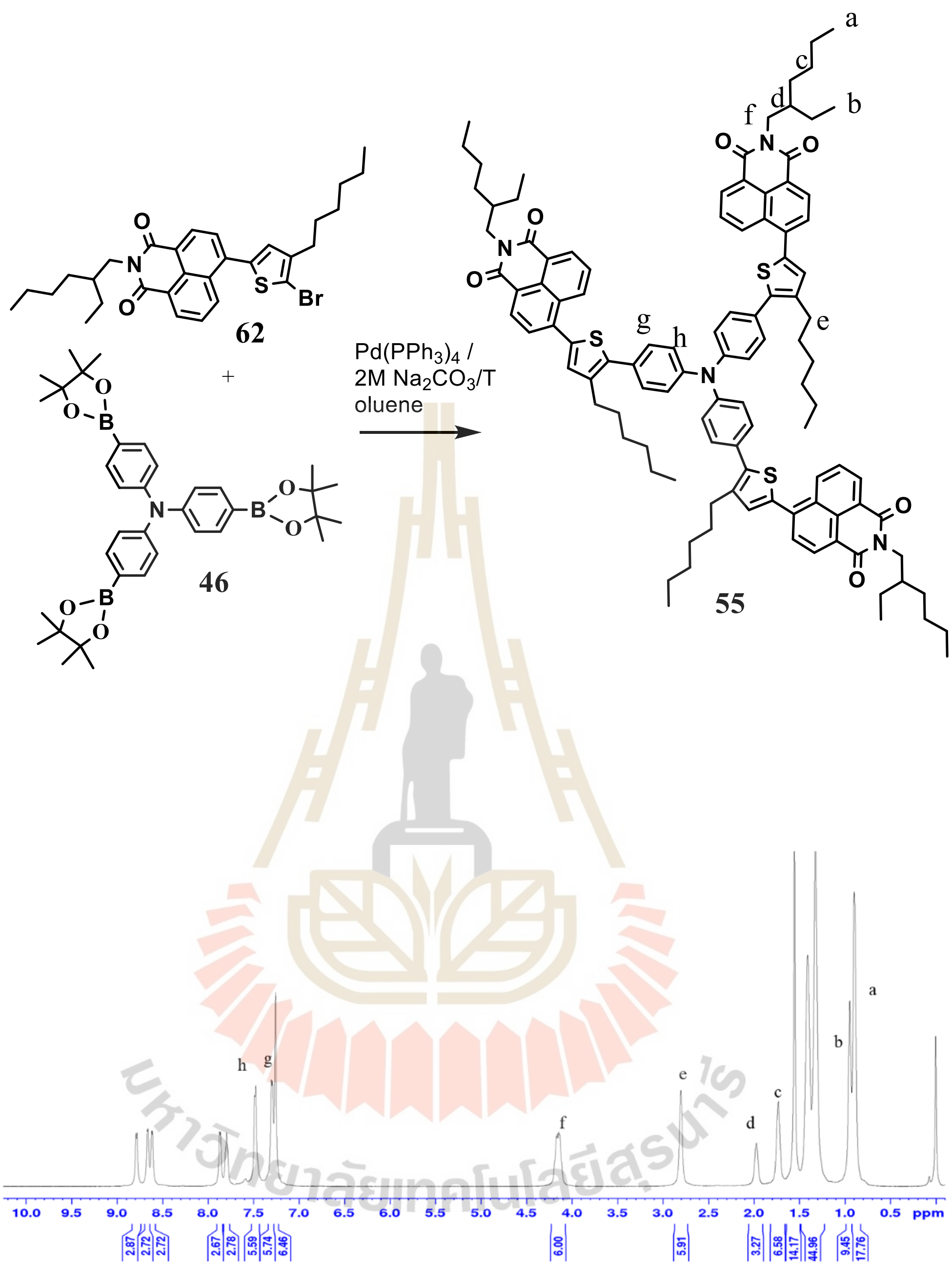

Figure 3.8 The synthesis and ^{1}H-NMR spectrum in $CDCl_3$ of **55**.

Figure 3.9 shows the synthesis of **56** and ^{1}H-NMR spectrum. For synthesis, **56** was formed from C-C coupling of Stille reaction between **62** and 2,6-bis(trimethyltin)-4,8-bis(5-(2-ethylhexyl)thiophene-2-yl)benzo[1,2-b,4,-5-b′]thiophene (**76**) in the presence of $Pd(PPh_3)_4$ as catalyst and toluene as solvent to give **56** in 62% yield. The chemical structure of compound **56** was confirmed by ^{1}H-NMR spectrum, ^{13}C-NMR as well as MALDI-TOF MS. The ^{1}H-NMR spectrum collected in $CDCl_3$ show pattern of a triplet signal at 0.90-0.91 ppm (18 H), 0.95-0.98 ppm (12H) assigned to two sides of methyl groups, the multiplet signal at 1.98-1.99 ppm (2H) assigned to CH proton and the multiplet signal at 4.12-4.20 ppm (4H) assigned to CH_2 proton. Furthermore, the proton signal at aromatic regions were found at chemical shift at 6.95 ppm (2H), the singlet at 7.24 ppm assigned to two side (2H) proton of SH, the doublet at 8.67-8.678 ppm (2H) and 8.73-8.74 ppm (2H) assigned to two side of 1,8-naphthalimide.. The number of proton aromatic regions are (18H) corresponding to ^{1}H-NMR spectrum. In addition, MALDI-TOF MS spectrum was used to confirm the structure and found to be 1525.2544 m/z, agreeing with the calculated mass of $C_{94}H_{112}N_2O_4S_6$: 1524.69.

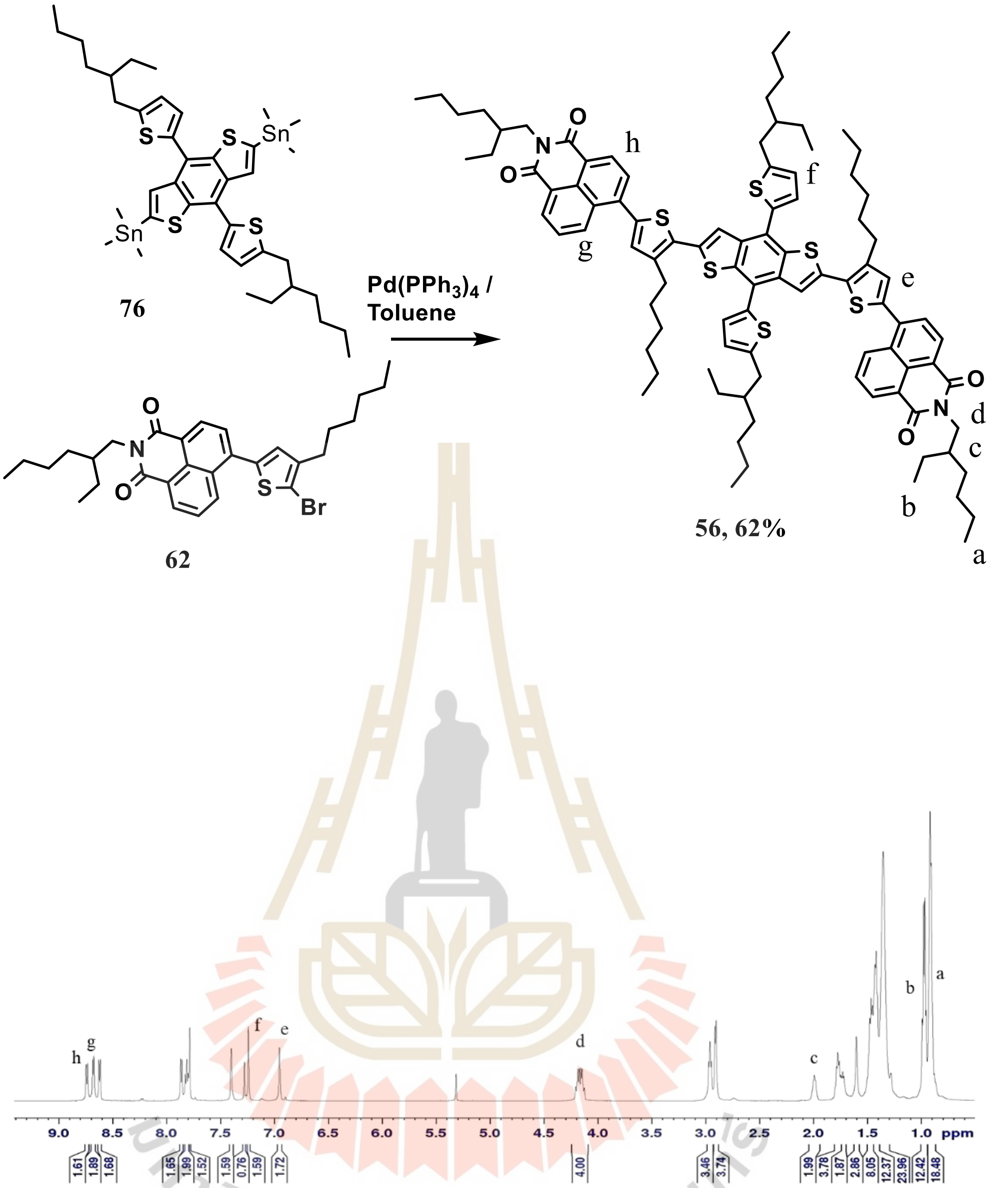

Figure 3.9 The synthesis and ^{1}H-NMR spectrum in CDCl$_3$ of **56**.

3.4 Optical properties

The absorption and emission properties of **53**, **54**, **55**, and **56** in both DCM solution and as a spin-casted thin film were investigated and summarized in Table 2.1. In the solution phase, each compound exhibited a characteristic π–π* transition, as observed by the maximum absorption peak around (325-347 nm) and (462-489 nm) showed in Figure

3.10a. Therefore, the molar extinction coefficient of the latter peak increases with the number of naphthalimide units. In the solid state, the absorption spectra of these compounds also have the same pattern as in the solution phase Figure 3.10b. However, the maximum absorption wavelengths appear at longer wavelengths (320-351 and 430-449 nm) due to more efficient π-conjugation between the 1,8-naphthalimide and triphenylamine groups in the solid state, which may be caused by the restricted molecular vibration and rotation. The normalized fluorescence spectra in DCM solution and in the solid phase are also shown in Figure 3.11. The maxima PL wavelength in DCM solution exhibited orange emission spectra (λ_{em} = 665-718 nm). The maxima PL wavelength in thin film of **53** showed a bathochromic shifted around 33 nm, compounds **54**, **55**, and **56** showed blue shift. suggesting that increase in the number of 1,8-naphthalimide groups, the fluorescence emission peaks are gradually blue-shifted due to a decrease in the electron delocalization between the donor and the acceptor.

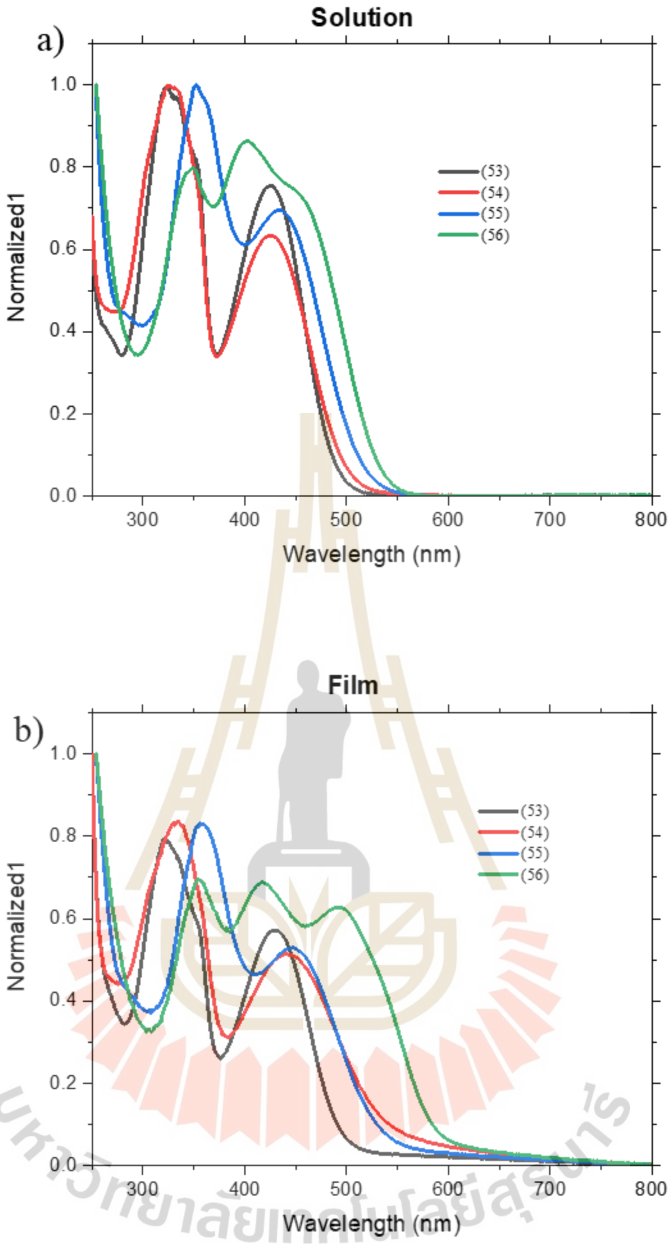

Figure 3.10 a) UV- Vis absorption spectra of **53**, **54**, **55**, and **56** in DCM solution and b) thin film.

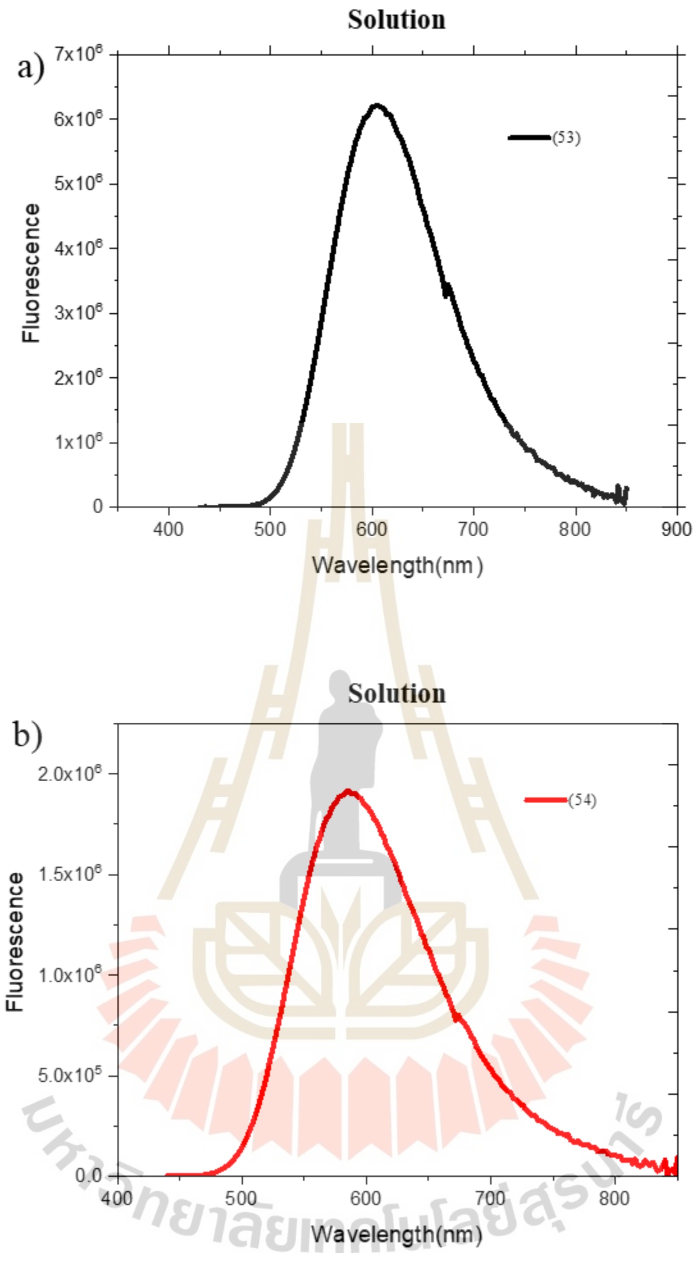

Figure 3.11 a), b) fluorescence spectra of **53** and **54** in DCM solution.

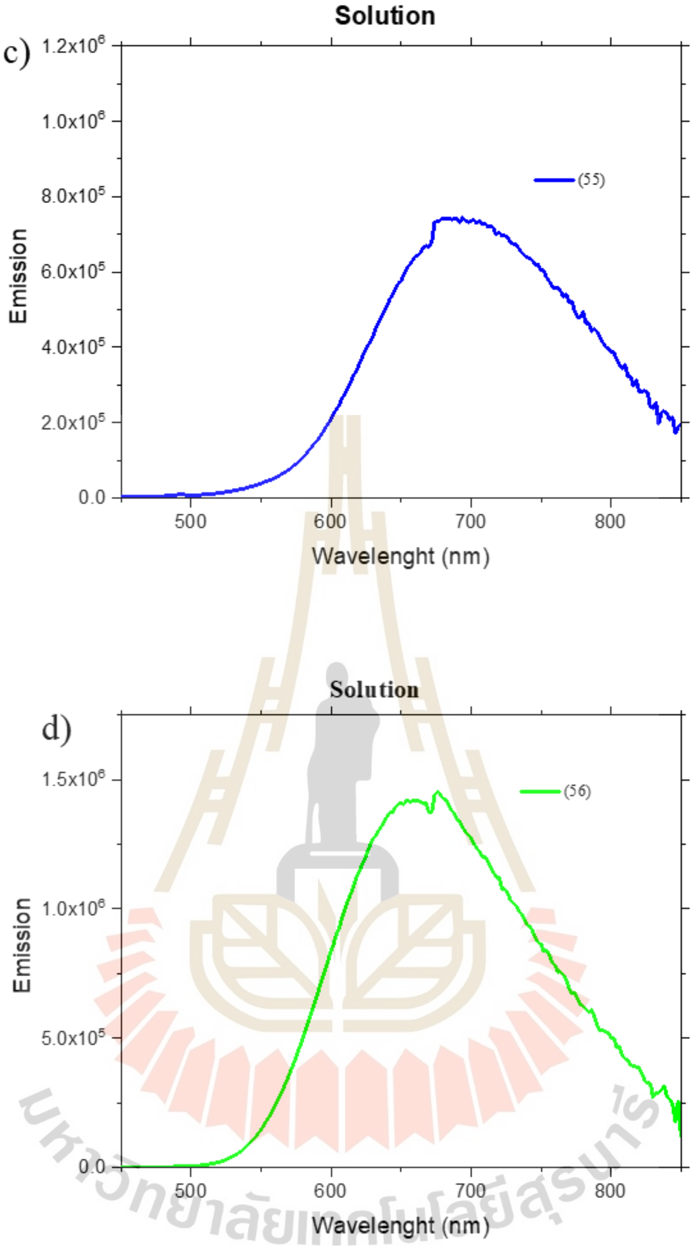

Figure 3.11 c), d) fluorescence spectra of **55** and **56** in DCM solution (Continued).

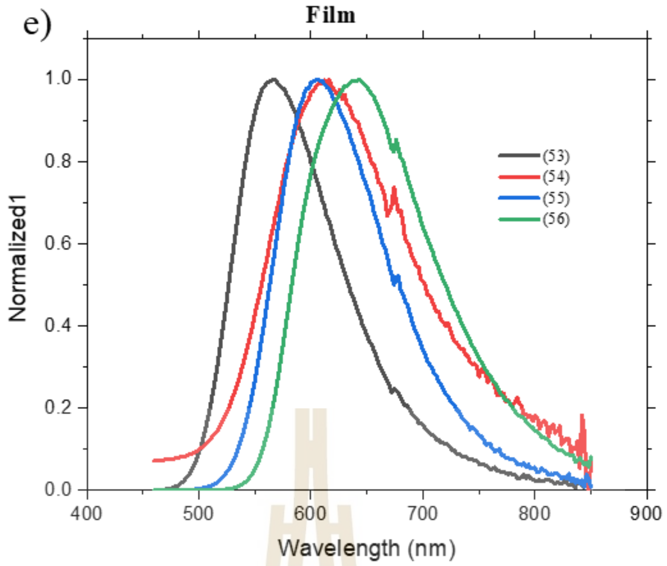

Figure 3.11 (e) thin film state (Continued).

3.4.1 Time-resolved fluorescence decay

The lifetimes of the slow decay in the solution decrease to 7.83, 7.23, 1.44, and 1.34 ns of **53**, **54**, **55**, and **56**, respectively (Figure 3.12). The thin film phase showed value at 16.25, 0.78, 4.66, and 0.84 ns. The quantum yields of these compounds has the high quantum yield 74.65%, 33.24%, 11.5% and 18.37% of **53**, **54**, **55**, and **56**, respectively (Table 3.1). The thin film phase showed decrease value to 41.92%, 0.14%, 5.31%, and 3.96%.

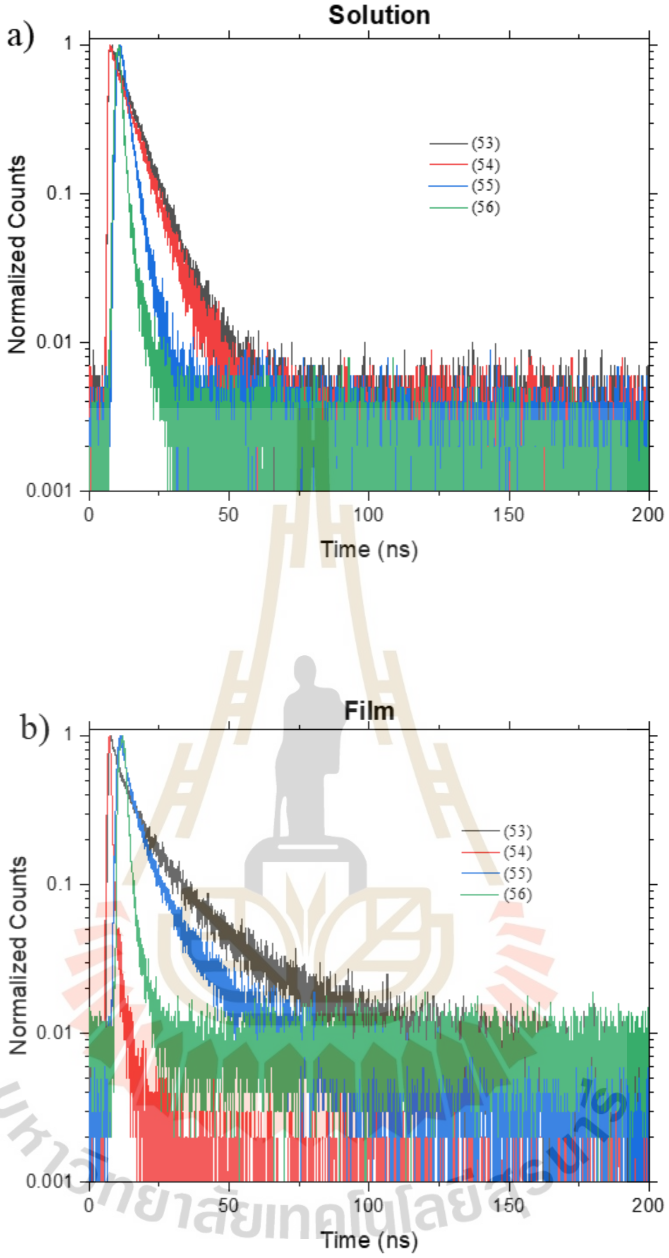

Figure 3.12 Time-resolved fluorescence decay of **53**, **54**, **55**, and **56** emitter in a) DCM solution and b) thin film.

Table 3.1 Photophysical properties and emission lifetimes of **53**, **54**, **55**, and **56**

Comp.	λ^{sol} abs /λ^{film} abs (nm)[a]	λ^{sol} em /λ^{film} em (nm)[b]	τ_P (ns)[c]		QY	
			sol	film	sol	film
53	325,426/ 320,430	704/ 737	7.83	16.25	74.65	41.92
54	327,425/ 332,446	718/ 715	7.23	0.78	33.24	0.14
55	346,431/ 351,443	682/ 626	1.44	4.66	11.58	5.31
56	347,489/ 344,449	665/ 640	1.34	0.84	18.37	3.96

[a] Measured in DCM (10^{-5}M) and thin film at 298 K.
[b, c, d] Measured in DCM (10^{-6}M) and thin film at 298 K.

3.5 Electrochemical properties

The experimental and computationally calculated electrochemical properties are summarized in Table 3.2. The cyclic voltammograms acquired by the anodic scans at room temperature exhibit one reversible oxidation peak for each compound, which might be attributed to the electron-donating ability. The HOMO energy levels were obtained from the onset oxidation potential (E_{onset}) observed on the cyclic voltammograms, and the LUMO energy levels were estimated from the Eg and HOMO data. All compounds displayed an irreversible redox process with onset oxidation peaks at +0.62, +0.18, +0.12, and +0.44 V, respectively. On the basis of the first oxidation potential, the highest occupied molecular orbital (HOMO) energy levels can be estimated as -5.06 eV for **53**, -4.62 eV for **54**, -4.56 eV for **55** and -4.88 eV for **56**. The lowest unoccupied molecular orbital (LUMO) energy level of these compounds could be estimated from the HOMO energy level and energy band gap (Eg) using the following equation: LUMO = HOMO + Eg. The LUMO energy levels are -2.59 eV, -2.32 eV, -2.18 eV, and -2.18 eV of **53**, **54**, **55**, and **56**, respectively (see Figure 3.13).

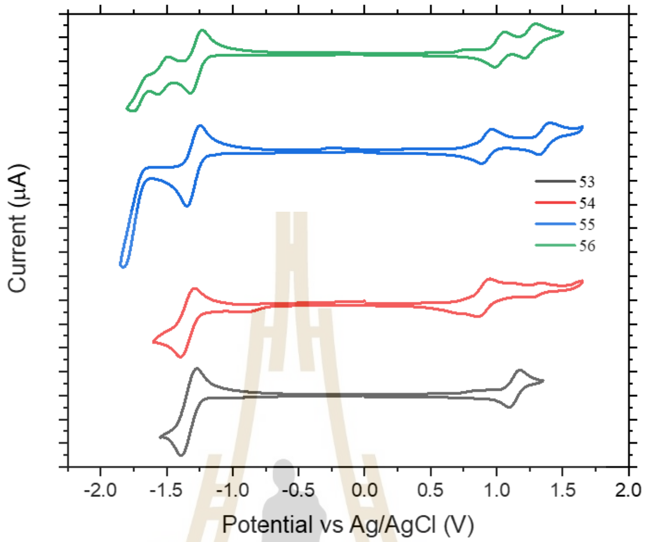

Figure 3.13 a) Cyclic voltammograms of **53**, **54**, **55**, and **56** (10^{-5} M) in $CHCl_3$ solutions using 0.1 M Bu_4NPF_6 at a scan rate of 50 mV/s.

3.5.1 Quantum chemical calculation

The calculation results revealed that the (Figure 3.14). Their geometries and energies were optimized by density functional theory (DFT) calculation using DFT B3LYP/6-31G(d, p) method were investigated and summarized in Table 3.2. The frontier orbitals for the **53**, **54**, **55**, and **56** look very similar for all compounds, being localized almost entirely on the triphenylamine core or 2,6-Bis(trimethyltin)-4,8-bis(5-(2-ethylhexyl)thiophene-2-yl) benzo [1,2-b,4,-5-b′]thiophene for the HOMO or 1.8-naphthalimide moiety for the LUMO. Whereas the LUMO were mainly localized on the electron withdrawing at the 1,8-napthalimide units.

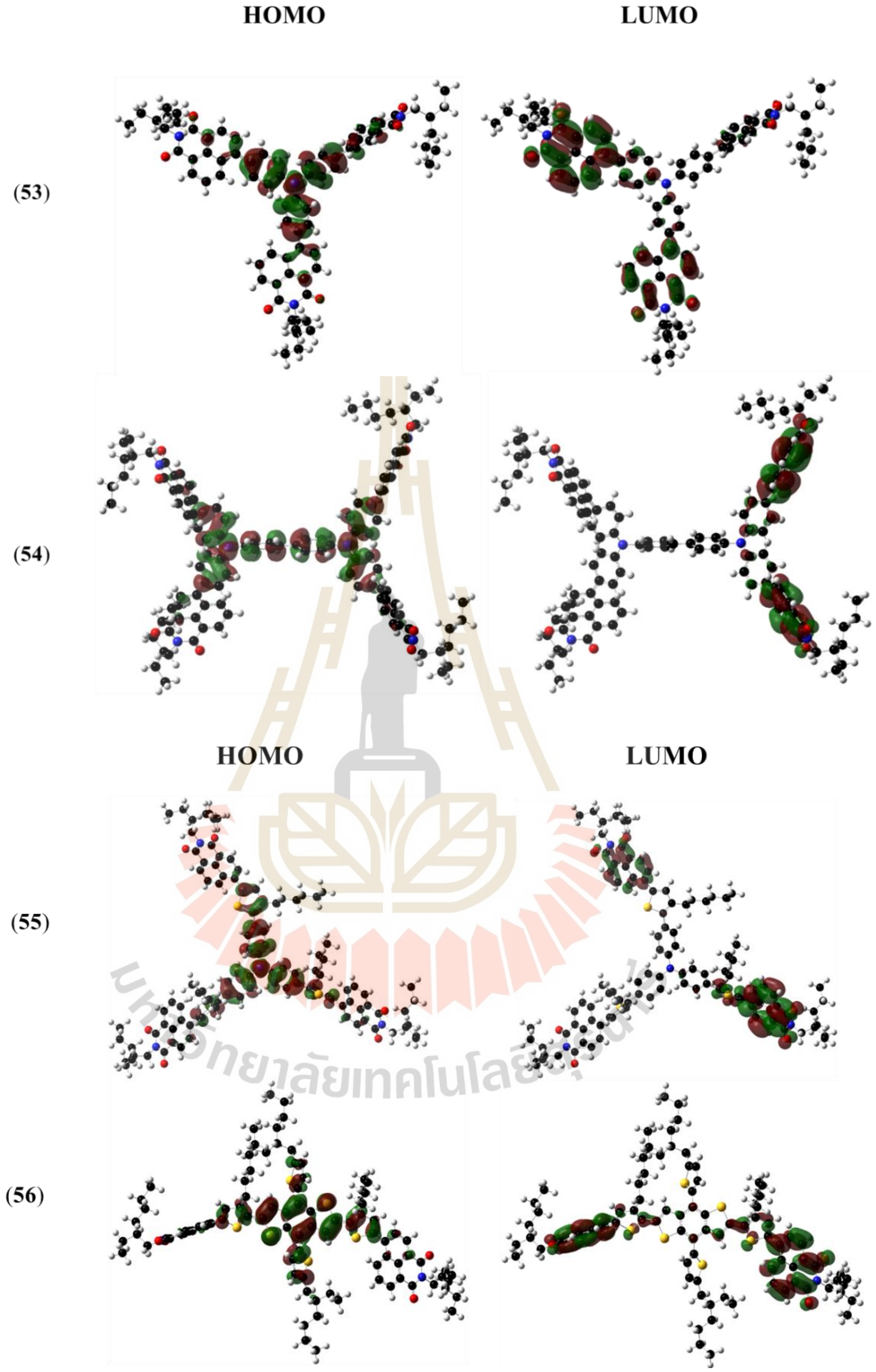

Figure 3.14 The spatial distribution of HOMO (left) and LUMO (right) energies densities of **53**, **54**, **55**, and **56** by DFT B3LYP/6-31G (d, p) calculation.

Table 3.2 Electrochemical and theoretical electronic characteristics of **53**, **54**, **55**, and **56**.

Comp.	$E^{ox}{}_{on}$ (eV) [a]	$E_g{}^{opt}$ (eV) [b]	HOMO (eV) [c]	LUMO (eV) [d]	HOMO (eV) [e]	LUMO (eV) [e]	E_g (eV) [e]
53	0.62	2.47	-5.06	-2.59	-5.53	-2.55	2.98
54	0.18	2.30	-4.62	-2.32	-5.29	-2.51	2.78
55	0.12	2.38	-4.56	-2.18	-5.25	-2.51	2.74
56	0.44	2.07	-4.88	-2.18	-5.25	-2.51	2.74

[a] Measured by CV in DCM vs Ag/Ag$^+$ at scan rate of 50 mV/s.
[b] Calculated from $\lambda^{abs}{}_{onset}$, $E_g = 1240/\lambda^{abs}{}_{onset}$
[c] Calculated from onset oxidation potential HOMO = $-(E^{ox}{}_{on} + 4.44)$ eV
[d] Calculated from LUMO = HOMO + E_g
[e] Calculated from DFT B3LYP/6-31G(d, p)

3.6 Conclusion

Four new derivatives of triphenylamine containing electron accepting 1,8-naphthalimide moieties and electron-donating triphenylamino groups, 2,6-bis(trimethyltin)-4,8-bis(5-(2-ethylhexyl)thiophene-2-yl)benzo[1,2-b,4,-5-b′]thiophene were obtained via Suzuki cross-coupling reaction, Stille reaction. The fluorescence quantum yields from 74.65 and 11.58, while emission yields of the neat films are 41.92 and 0.14 due to pronounced electron donor-acceptor character. These compounds exhibited absorption maxima around 425-489 nm and emission maxima around 704-718 nm in DCM solution. The Stoke’s shifts were narrower for the spectra of these compounds in the solid state as a result of solid packing expect **53**. The electrochemical properties were examined using cyclic voltammetry and the data were in good agreement with those obtained from the computational calculations obtained using the

Gaussian 09 program. The ionization potential values of the synthesized compounds measured by the cyclic voltammetry are -5.06 eV, -4.62 eV, -4.56 eV, -4.88 eV, and electron affinities -2.59 eV, -2.32 eV,-2.18 eV, and -2.18 eV of **53**, **54**, **55**, and **56**, respectively.

CHAPTER IV

SYNTHESIS AND CHARACTERIZATION OF THIADIAZOLE DERIVATIVES AS LIGHT-EMITTING MATERIALS FOR ORGANIC LIGHT-EMITTING DIODES

4.1 Introduction

A new series of D-π-A type thiadiazole derivatives containing triphenylamine or phenylcarbazole as donor, thiophene derivatives as π-conjugated and 4,7-dibromo-(1,2,5) thiadiazole as acceptor investigated as near IR emitting materials for solution processed OLEDs. These-compounds were synthesized through Suzuki cross coupling reaction. Their skeleton, which exhibits an intramolecular charge-transfer (ICT) transition from the donor to the acceptor upon photo irradiation. In order to broaden the absorption spectra of the sensitizers in the visible and near-IR region, an additional electron-accepting group in the conjugated spacer is an efficient approach for red shifting the absorption spectra.

4.2 Aims of the study

1. To design, synthesize and characterize D-π-A-π-D type thiadiazole derivatives **63**, **64**, **65**, and **66** as near IR emitting materials for solution processed OLEDs.

2. The photophysical, electrochemical and thermal properties of the target molecules were studied by UV-visible spectroscopy, fluorescence spectroscopy, cyclic voltammetry and DSC-TGA techniques.

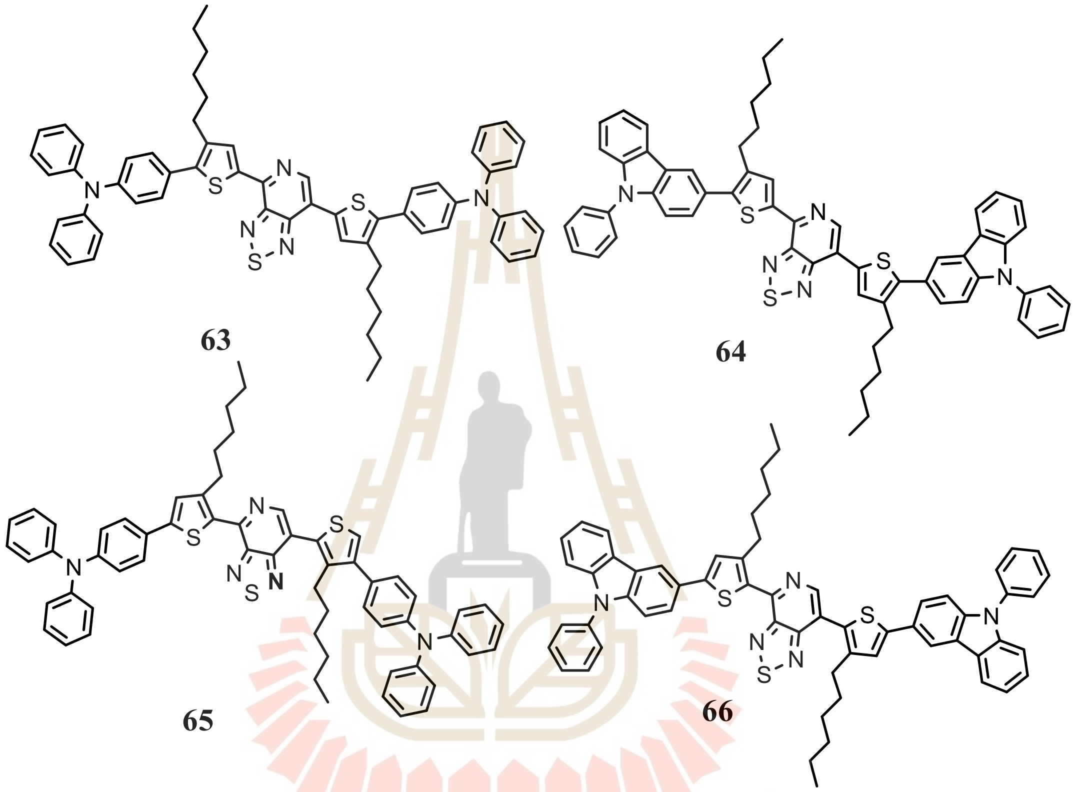

Figure 4.1 The structures of compounds **63**, **64**, **65**, and **66**.

4.3 Results and discussion

4.3.1 The synthesis routes of thiadiazole derivatives.

The synthetic routes of the designed D-π-A type thiadiazole derivatives **63**, **64**, **65**, and **66** are outlined in (Figure 4.2). Firstly, the key intermediate **68** and **70** were synthesized by Suzuki cross coupling reaction of 4,7-dibromo-(1,2,5)thiadiazole (**67**) (1.0 equiv) connecting with 4-hexyl-2-(4,4,5,5-tetra metyl-1,3,2-dioxaborolan-2-

yl)thiophene (**72**) (2.2 equiv) or 3-hexyl-2-(4,4,5,5-tetra metyl-1,3,2-dioxaborolan-2-yl)thiophene (**73**) (2.2 equiv). The second step involved bromination reaction of **68** or **70** with *N*-bromosuccinimide and THF to produce **69** or **71**. Final step employed Suzuki cross coupling reaction of 4-(diphenylamino)Phenyl boronic acid (**74**) or 9-pheny lcarbazole-3-broronic acid (**75**) to afford the designed **63**, **64**, **65**, and **66**.

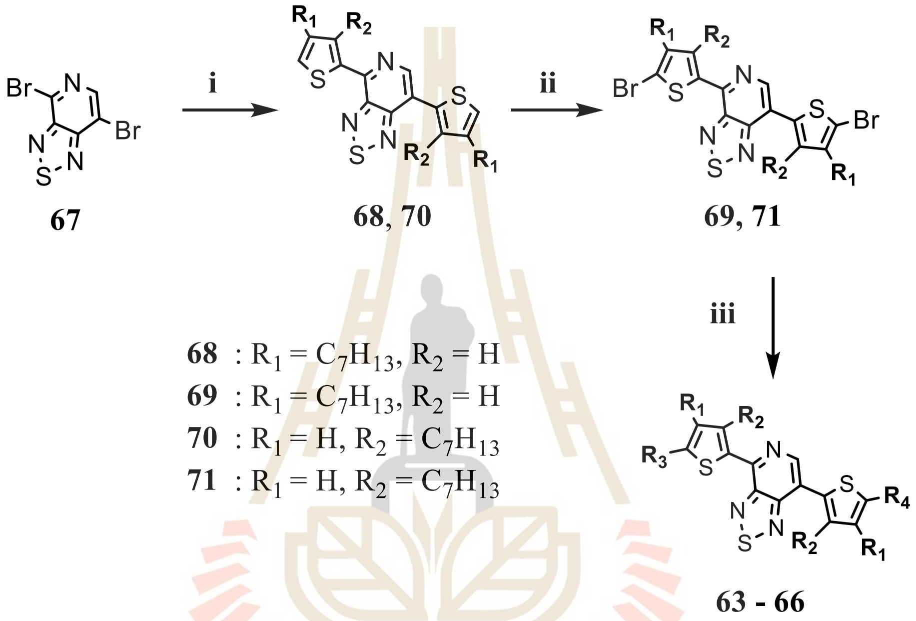

67

68, **70**

69, **71**

63 - 66

68 : $R_1 = C_7H_{13}$, $R_2 = H$
69 : $R_1 = C_7H_{13}$, $R_2 = H$
70 : $R_1 = H$, $R_2 = C_7H_{13}$
71 : $R_1 = H$, $R_2 = C_7H_{13}$

63 : $R_1 = C_7H_{13}$, $R_2 = H$, R_3, R_4 = triphenylamine
64 : $R_1 = C_7H_{13}$, $R_2 = H$, R_3, R_4 = 9-phenylcarbazole
65 : $R_1 = H$, $R_2 = C_7H_{13}$, R_3, R_4 = triphenylamine
66 : $R_1 = C_7H_{13}$, $R_2 = H$, R_3, R_4 = 9-phenylcarbazole

Figure 4.2 The synthetic routes of **63**, **64**, **65**, and **66** molecules.

i = Suzuki cross coupling reaction with 4-Hexyl-2-(4,4,5,5-tetrametyl-1,3,2-dioxaborolan-2-yl)thiophene (**72**) (2.2 equiv) or 3-Hexyl-2-(4,4,5,5-tetrametyl-1,3,2-dioxaborolan-2-yl)thiophene (**73**), $Pd(PPh_3)_4$, 2M Na_2CO_3, toluene.
ii = bromination reaction, *N*-bromosuccinimide, THF.
iii = Suzuki cross coupling reaction with 4-(diphenylamino)phenylboronic (**74**) acid or 9-phenylcarbazole-3-broronic acid (**75**), $Pd(PPh_3)_4$, 2M Na_2CO_3, toluene.

4.3.1.1 The synthesis of thiadiazole derivatives 63 and 64

In the first step, compound **68** was synthesized from **67** and **72** by using Suzuki cross coupling reaction and followed by bromination reaction of the resultant with BNS to give starting material **69** (Figure 4.3).

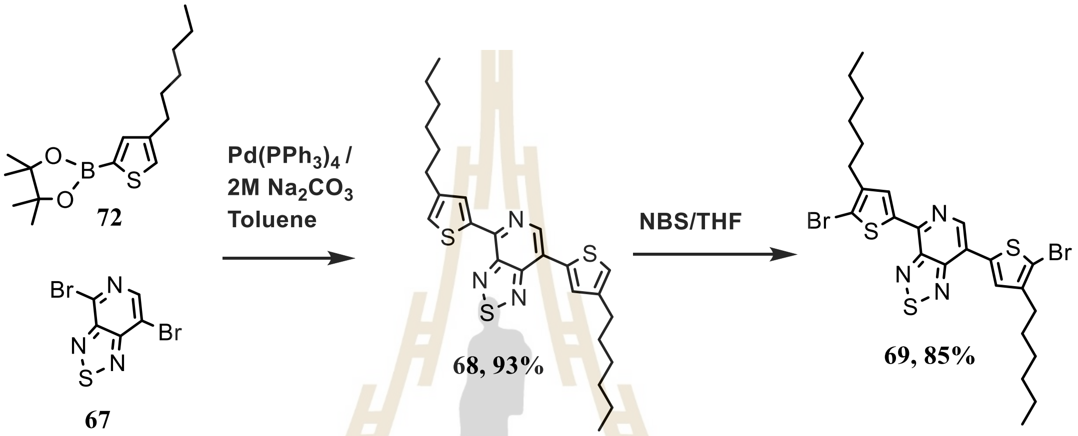

Figure 4.3 Synthesis of thiadiazole derivatives **69**.

The structure of **68** was confirmed by ^{1}H-NMR spectroscopy (Figure 4.4). The proton signal of aromatic was found pattern of thiadiazoloe at δ = 8.80 ppm as singlet (1H). The thiophene proton show singlet at δ = 8.51 ppm (1H), 7.95 ppm (1H), 7.20 ppm (1H), 7.06 ppm (1H). In addition, the proton signal of aliphatic regions was found at δ = 0.98 ppm as triplet 2 × CH_3 (methyl proton) of chain alkyl (see in chapter 6 experimental). MALDI-TOF (m/z) calcd for $C_{25}H_{31}N_3S_3$: 469.17, found 470.2969 (M^+). The structure of **69** was confirmed by ^{1}H-NMR spectroscopy. The proton signal of aromatic was found pattern of thiadiazoloe at δ = 8.70 ppm as singlet (1H). The thiophene proton show singlet at δ = 8.32 ppm (1H), 7.75 ppm (1H). High resolution mass spectrometry confirmed the identity of the compound with m/z: (HRMS) = 624.7553 (required m/z = 624.99) (Figure 4.5).

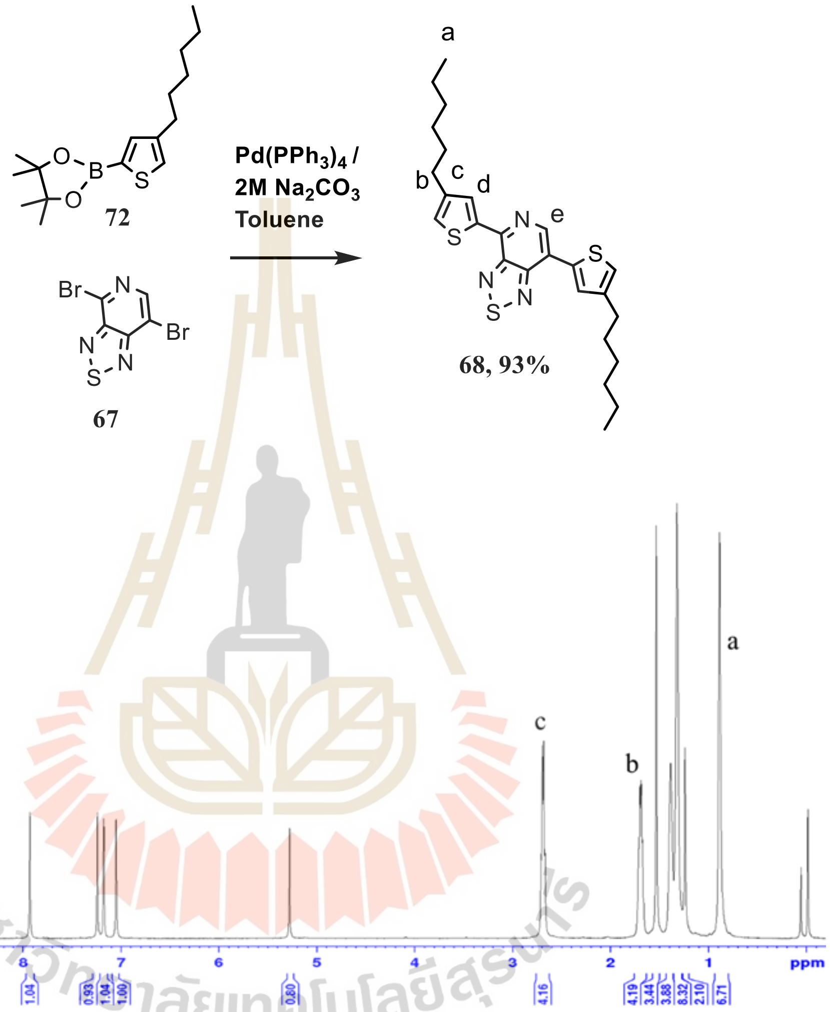

Figure 4.4 The synthesis and ^{1}H-NMR spectrum in CDCl$_3$ of **68**.

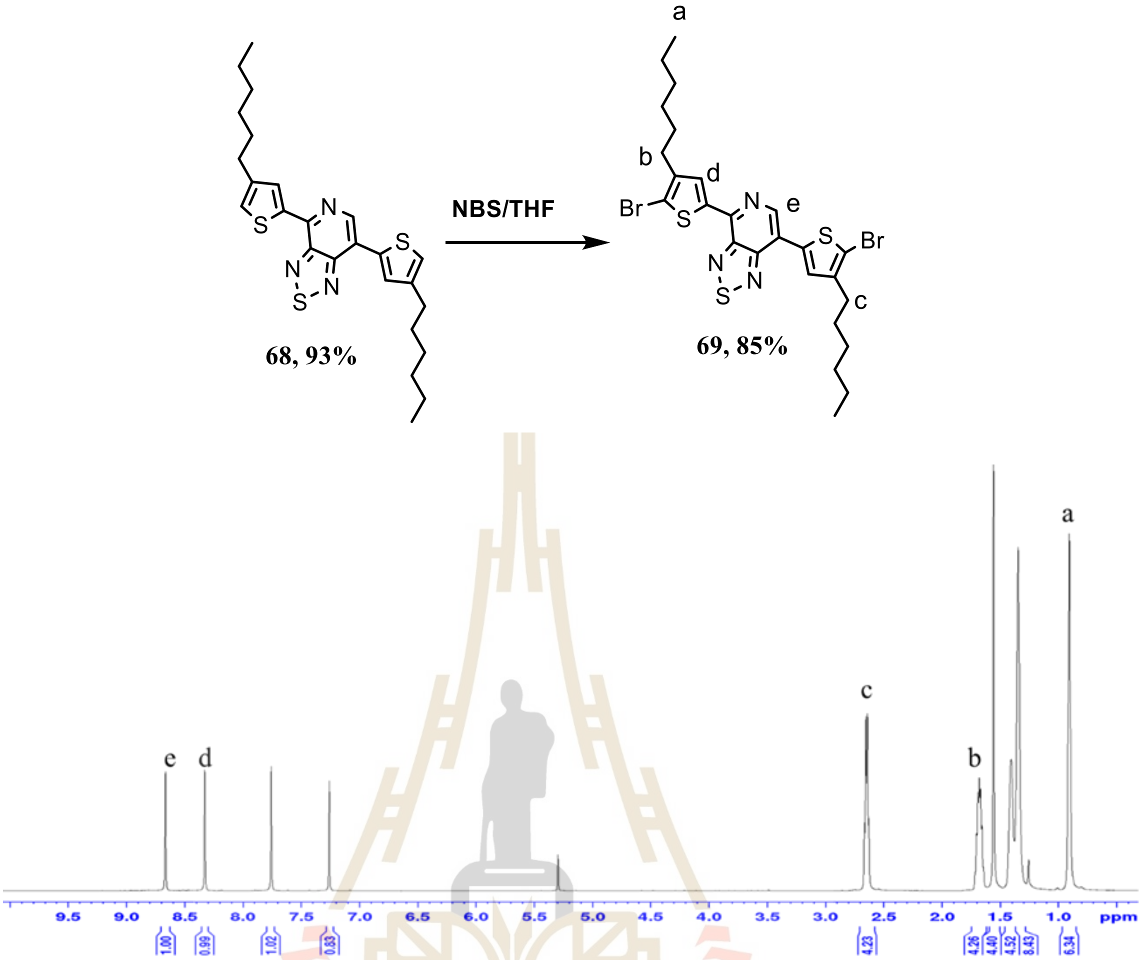

Figure 4.5 The synthesis and ^{1}H-NMR spectrum in $CDCl_3$ of **69**.

The target molecule **63** was synthesized from **69** and 4-(diphenylamino) phenylboronic acid (**74**) using Suzuki cross coupling reaction and obtained in a good yield 73% (Figure 4.6).

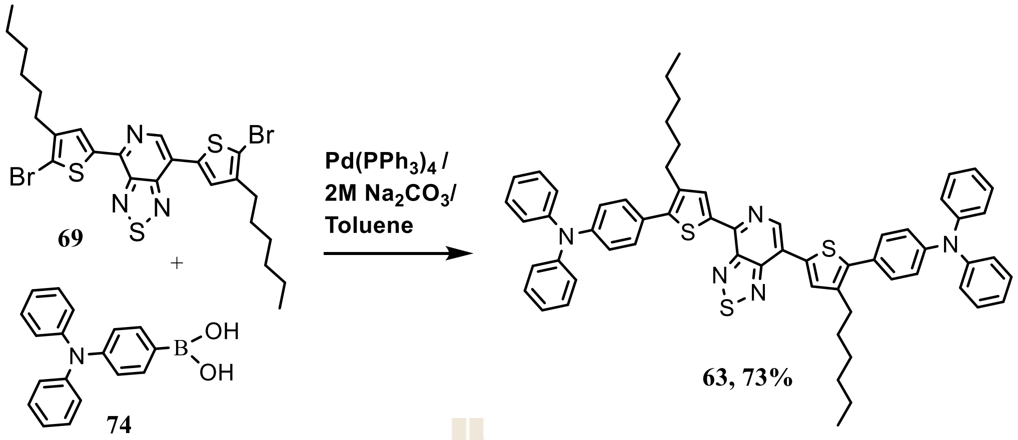

Figure 4.6 Synthesis of compound **63**.

The structure of compound **63** was confirmed by ^{1}H-NMR spectrum, ^{13}C-NMR as well as MALDI-TOF MS. The ^{1}H-NMR spectrum collected in $CDCl_3$ show pattern of a triplet signal at 0.87-0.89 ppm (6H) assigned to two side of methyl groups, the multiplet signal at 1.68-1.76 ppm (4H), 2.73-2.78 ppm (4H) assigned to two side of CH_2 proton of alkyl thiophene. Furthermore, the proton signal at aromatic regions were found pattern of thiadiazoloe the singlet at 8.00 ppm (1H), 8.53 ppm (1H) and 8.79 ppm (1H) assigned to aromatic proton of thiadiazoloe (Figure 4.7). The number of proton aromatic regions are (31H) corresponding to ^{1}H-NMR spectrum. In addition, MALDI-TOF MS spectrum was used to confirm the structure and found to be 955.7325 m/z, agreeing with the calculated mass of $C_{61}H_{57}N_5S_3$: 955.38.

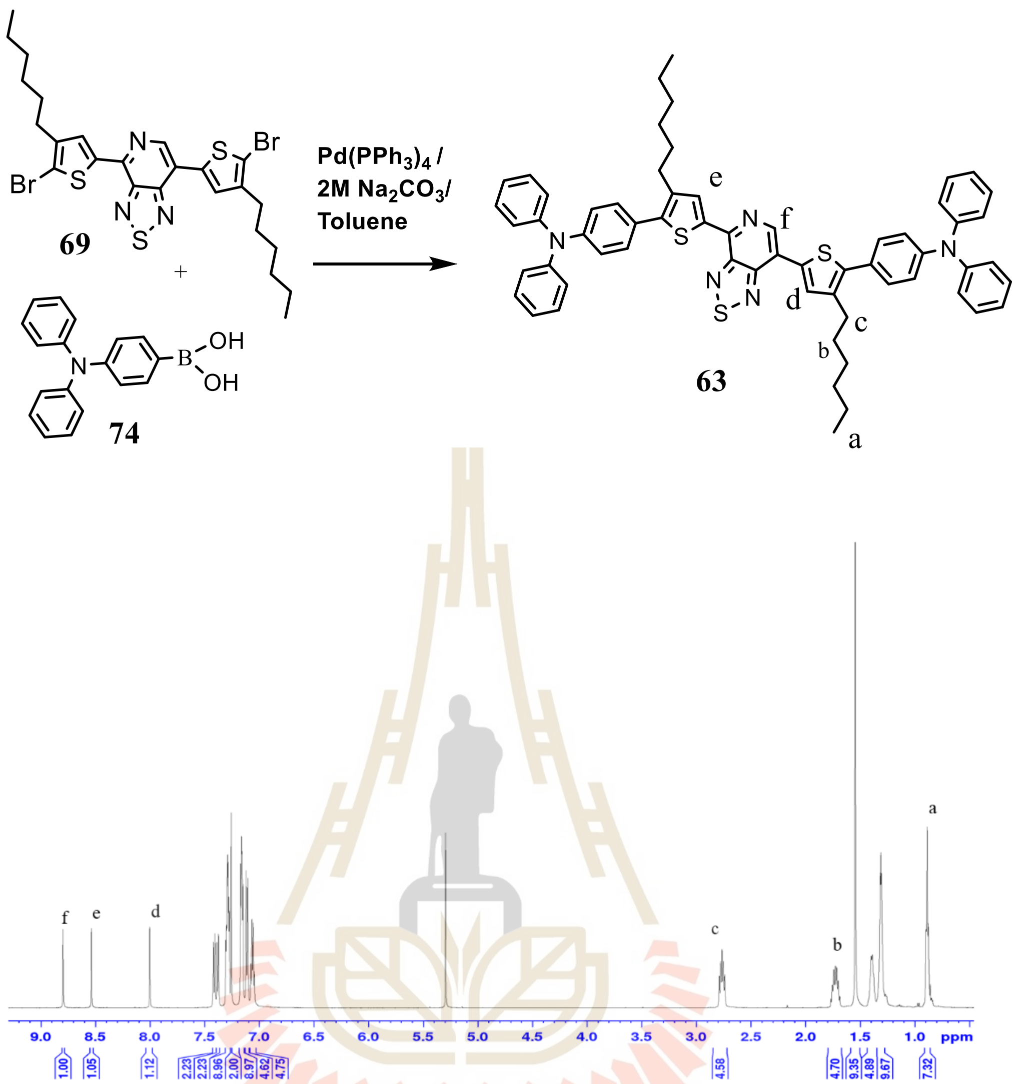

Figure 4.7 The synthesis and ^{1}H-NMR spectrum in $CDCl_3$ of **63**.

The compound **64** was synthesized from **69** and **75** by using Suzuki cross coupling reaction (Figure 4.8).

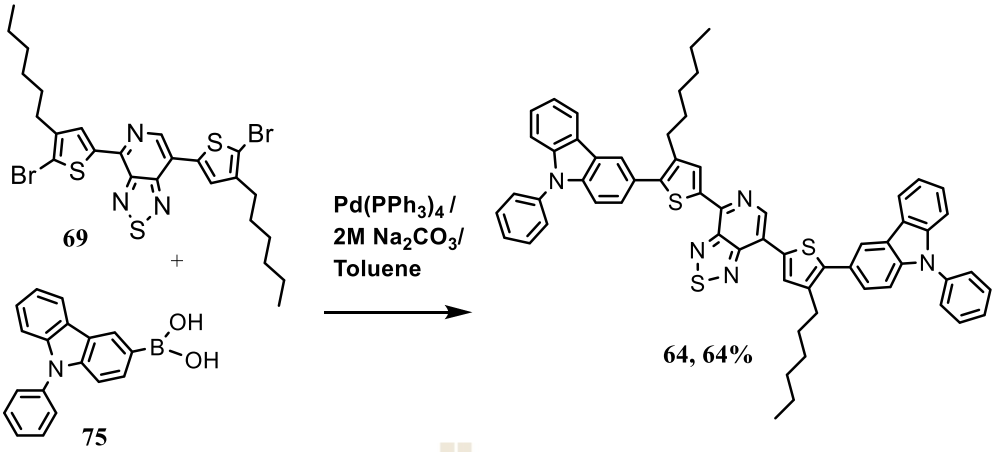

Figure 4.8 Synthesis of compound **64**.

The structure of compound **64** was confirmed by ^{1}H-NMR spectrum, ^{13}C-NMR as well as MALDI-TOF MS (Figure 4.9). The ^{1}H-NMR spectrum collected in $CDCl_3$ show pattern of a triplet signal at 0.86 ppm (6H) assigned to two side of methyl groups, the multiplet signal at 1.67-1.74 ppm (4H), 2.71-2.76 ppm (4H) assigned to two side of CH_2 proton of alkyl thiophene. Furthermore, the proton signal at aromatic regions were found pattern of thiadiazoloe the singlet at 7.98 ppm (1H), 8.51 ppm (1H) and 8.77 ppm (1H) assigned to aromatic proton of thiadiazoloe. The number of proton aromatic regions are (27H) corresponding to ^{1}H-NMR spectrum. In addition, MALDI-TOF MS spectrum was used to confirm the structure and found to 952.6076 m/z, agreeing with the calculated mass of $C_{61}H_{53}N_5S_3$: 951.35.

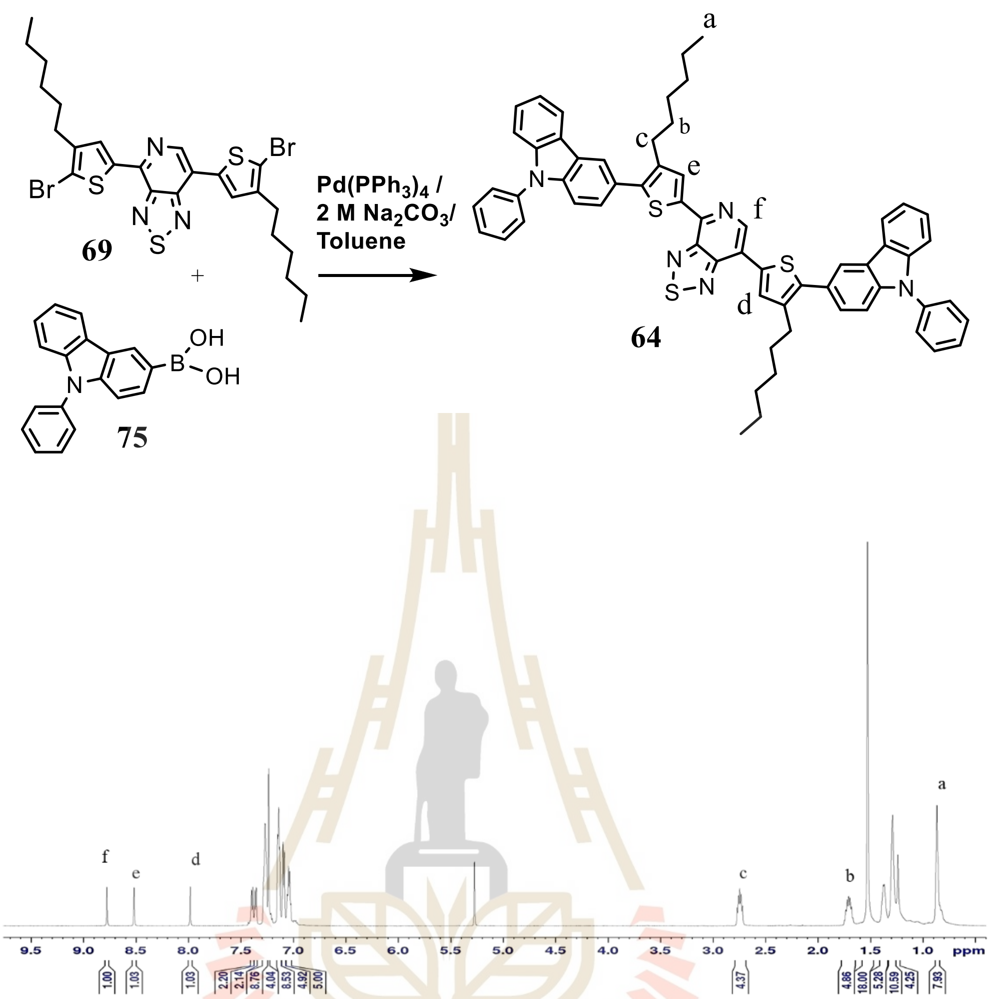

Figure 4.9 The synthesis and ^{1}H-NMR spectrum in $CDCl_3$ of **64**.

4.3.1.2 The synthesis of thiadiazole derivatives 65 and 66

In the first step, **70** was synthesized from **67** and **73** by using Suzuki cross coupling reaction and followed by bromination reaction of the resultant with BNS to give starting material **71** (Figure 4.10).

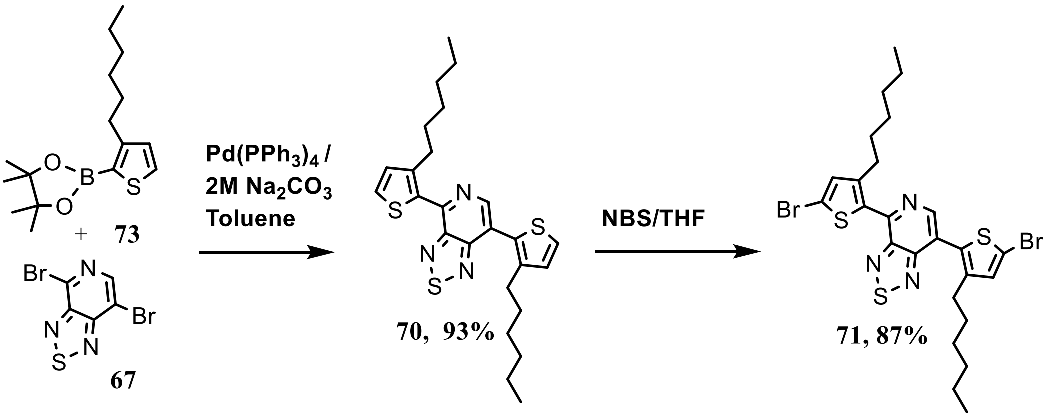

Figure 4.10 Synthesis of compound **71**.

The structure of **70** was confirmed by ^{1}H-NMR spectroscopy. The proton signal of aromatic was found pattern of thiadiazoloe at δ = 8.63 ppm as singlet (1H). The thiophene proton show doublet at δ = 7.57-7.56 ppm (1H), 7.46 ppm (1H), 7.13-7.11 ppm (2H). In addition, the proton signal of aliphatic regions was found at δ = 0.86-0.80 ppm as triplet 2 × CH_3 (methyl proton) of chain alkyl (see in chapter 6 experimental). MALDI-TOF (m/z) calcd for $C_{25}H_{31}N_3S_3$:469.17, found 470.2969 (M^+) (Figure 4.11).

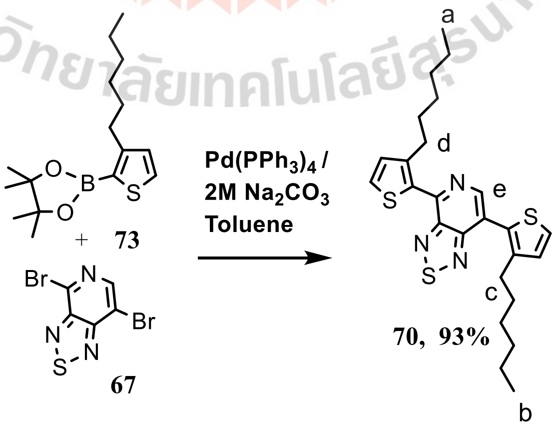

Figure 4.11 The synthesis and ^{1}H-NMR spectrum in $CDCl_3$ of **70**.

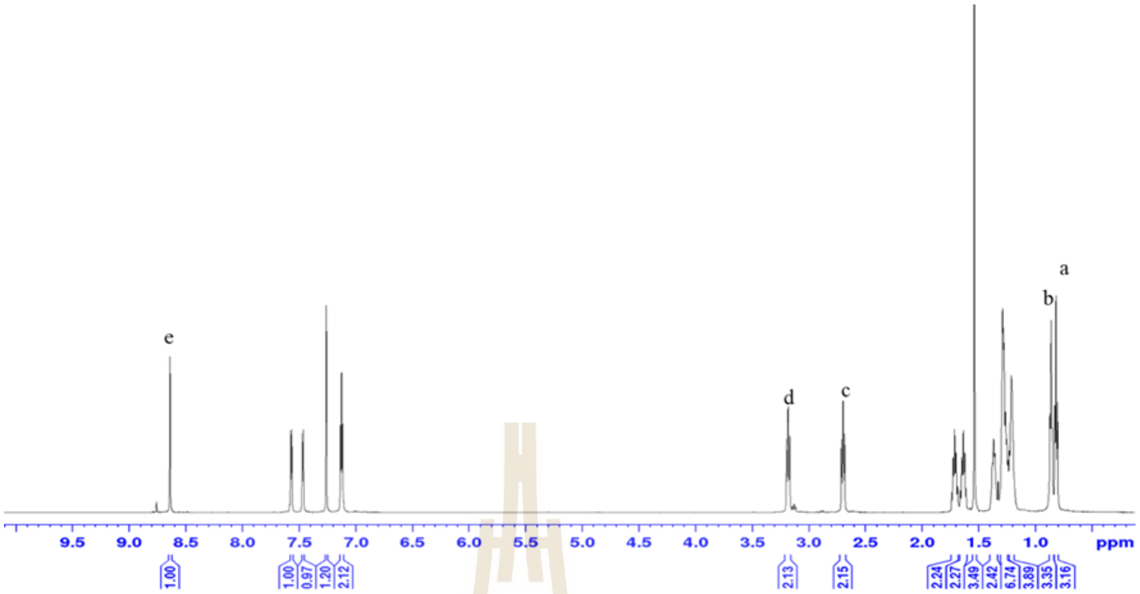

Figure 4.11 The synthesis and ^{1}H-NMR spectrum in $CDCl_3$ of **70** (Continued).

The structure of **71** was confirmed by ^{1}H-NMR spectroscopy. The proton signal of aromatic was found pattern of thiadiazoloe at $\delta = 8.70$ ppm as singlet (1H). The thiophene proton show singlet at $\delta = 8.32$ ppm (1H), 7.75 ppm (1H). High resolution mass spectrometry confirmed the identity of the compound with m/z: (HRMS) = 624.7553 (required m/z = 624.99) (Figure 4.12).

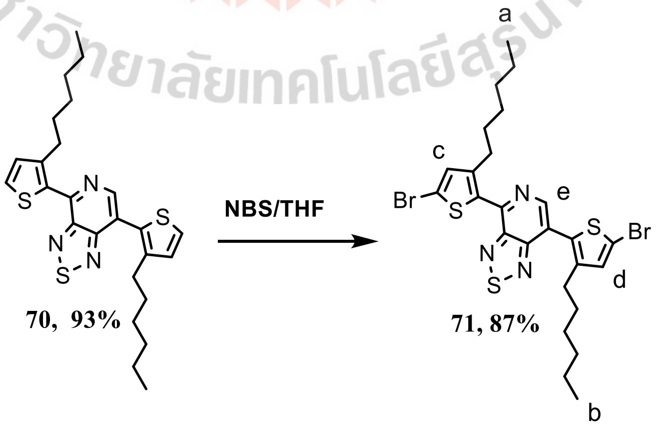

70, 93%

71, 87%

Figure 4.12 The synthesis and ^{1}H-NMR spectrum in $CDCl_3$ of **71**.

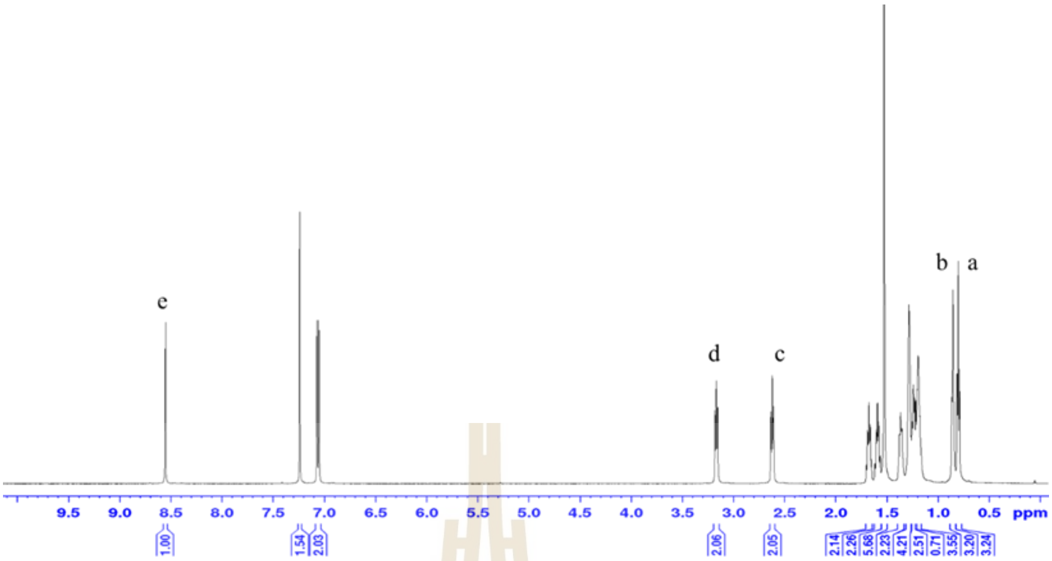

Figure 4.12 The synthesis and ^{1}H-NMR spectrum in $CDCl_3$ of **71** (Continued).

In second step, **71** was reacted with 4-(diphenylamino) phenylboronic acid (**74**) to give the **65** in well yield 84% (Figure 4.13).

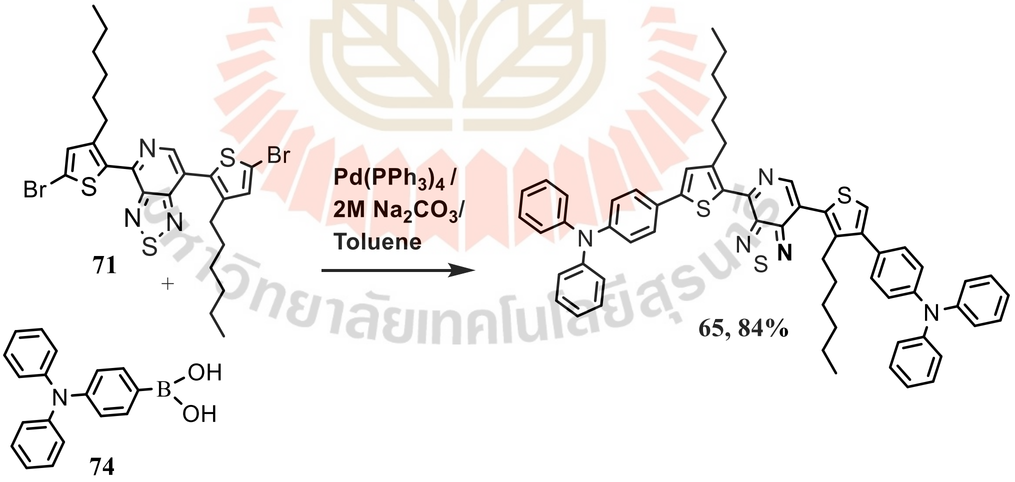

Figure 4.13 Synthesis of compound **65**.

The structure of **65** shows synthesis and ^{1}H-NMR spectrum. The proton signal of aromatic was found pattern of was formed from C-C coupling reaction between **71** and **74** in the presence of Pd(PPh$_3$)$_4$ as catalyst in 2M Na$_2$CO$_3$ as base in toluene as solvent to give **65** in 84% yield (Figure 4.14). The chemical structure of compound **65** was confirmed by ^{1}H-NMR spectrum, ^{13}C-NMR as well as MALDI-TOF MS. The ^{1}H-NMR spectrum collected in CDCl$_3$ show pattern of a triplet signal at 0.82-0.84 ppm (3H) and 0.87-0.89 ppm (3H) assigned to two side of methyl groups, the multiplet signal at 2.67-2.79 ppm (2H), 3.27-3.30 ppm (2H) assigned to two side of CH$_2$ proton of alkyl thiophene. Furthermore, the proton signal at aromatic regions were found pattern of thiadiazoloe the singlet at 8.42 ppm (1H), 8.51 ppm (1H) and 8.70 ppm (1H) assigned to aromatic proton of thiadiazoloe. The number of proton aromatic regions are (31H) corresponding to ^{1}H-NMR spectrum. In addition, MALDI-TOF MS spectrum was used to confirm the structure and found to 955.7352 m/z, agreeing with the calculated mass of C$_{61}$H$_{57}$N$_5$S$_3$: 955.38.

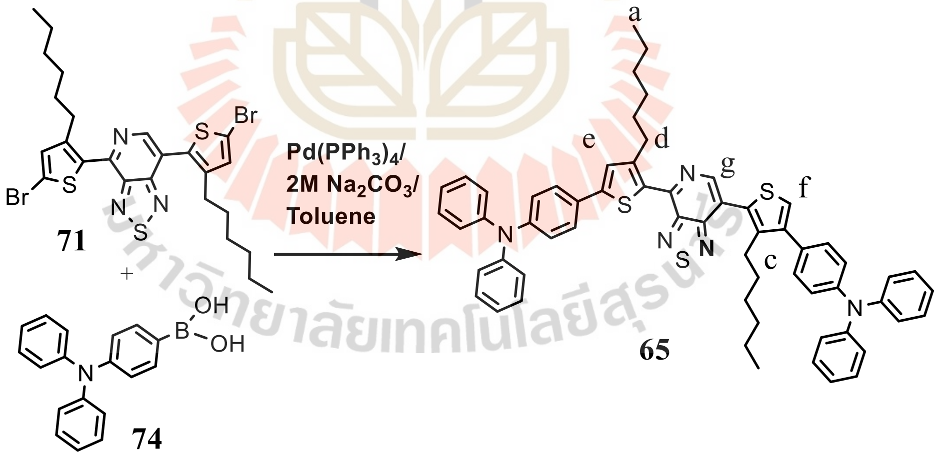

Figure 4.14 The synthesis and ^{1}H-NMR spectrum in CDCl$_3$ of **65**.

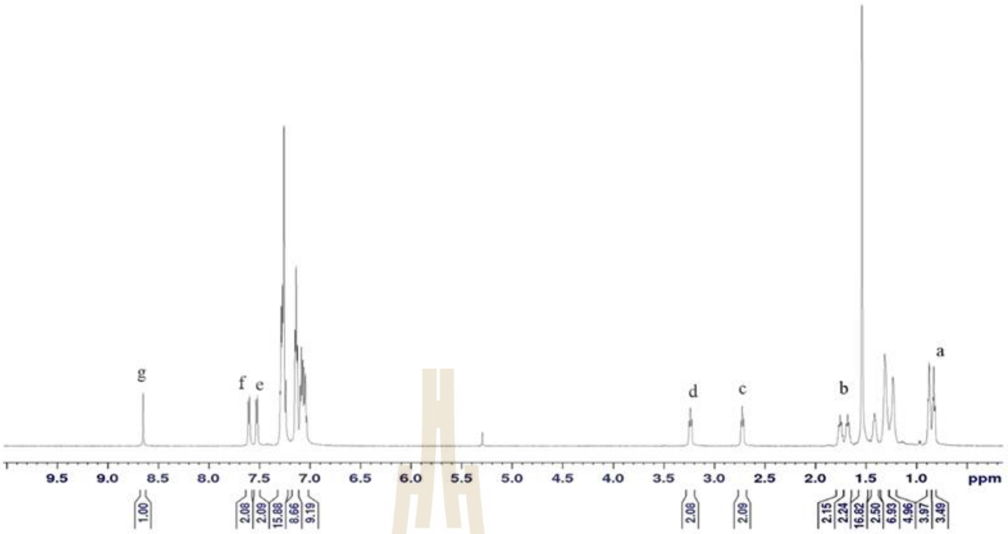

Figure 4.14 The synthesis and ^{1}H-NMR spectrum in $CDCl_3$ of **65** (Continued).

In second step, **71** was reacted with 9-phenylcarbazole-3-broronic acid (**75**) to give the **66** in well yield 70% (Figure 4.15).

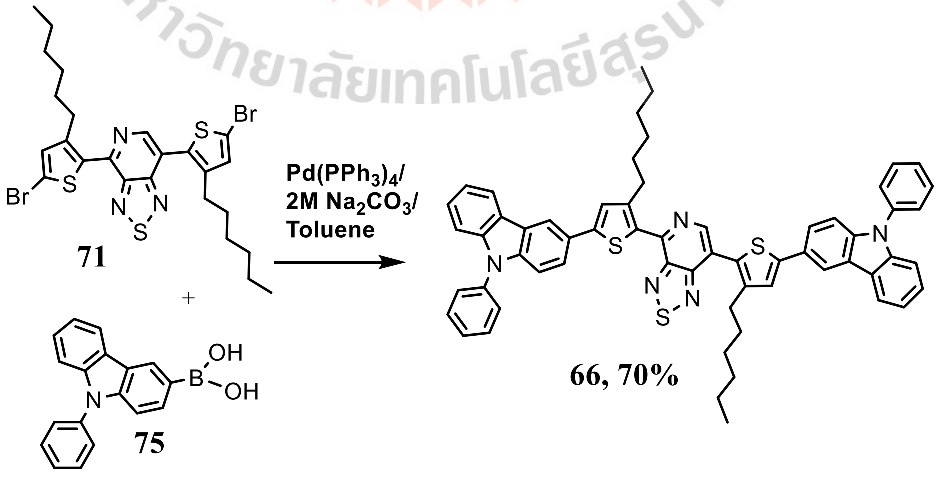

Figure 4.15 Synthesis of compound **66**.

The structure of **66** shows synthesis and ^{1}H-NMR spectrum. The synthesis, **66** was formed from C-C coupling reaction between **71** and 9-phenylcarbazole-3-broronic acid (**75**) in the presence of $Pd(PPh_3)_4$ as catalyst in 2M Na_2CO_3 as base in toluene as solvent to give **66** in 70% yield (Figure 4.16). The chemical structure of compound **66** was confirmed by ^{1}H-NMR spectrum, ^{13}C-NMR as well as MALDI-TOF MS. The ^{1}H-NMR spectrum collected in $CDCl_3$ show pattern of a triplet signal at 0.82-0.84 ppm (3H), 0.87-0.89 ppm (3H) assigned to two side of methyl groups, the multiplet signal at 2.76-2.79 ppm (2H), 3.27-3.30 ppm (2H) assigned to two side of CH_2 proton of alkyl thiophene. Furthermore, the proton signal at aromatic regions were found pattern of thiadiazoloe the singlet at 8.24 ppm (1H), 8.51 ppm (1H) and 8.70 ppm (1H) assigned to aromatic proton of thiadiazoloe. The number of proton aromatic regions are (27H) corresponding to ^{1}H-NMR spectrum. In addition, MALDI-TOF MS spectrum was used to confirm the structure and found to 952.6076 m/z, agreeing with the calculated mass of $C_{61}H_{53}N_5S_3$: 951.35.

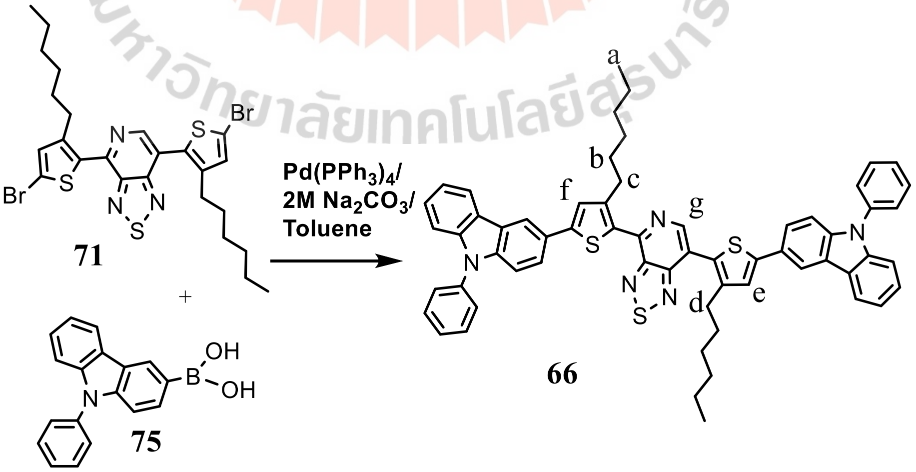

Figure 4.16 The synthesis and ^{1}H-NMR spectrum in $CDCl_3$ of **66**.

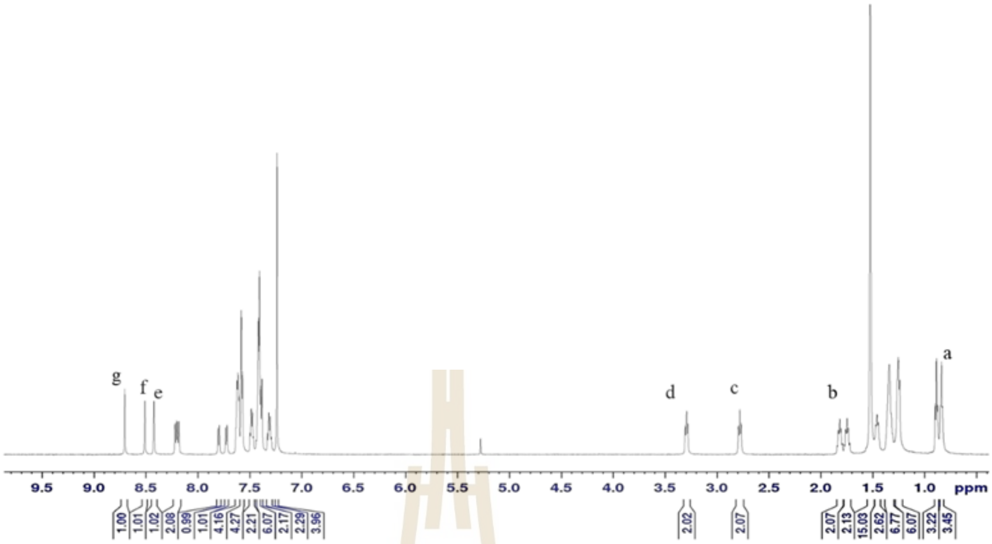

Figure 4.16 The synthesis and ^{1}H-NMR spectrum in $CDCl_3$ of **66** (Continued).

4.4 Optical properties

The UV-vis absorption spectra of compounds in chloroform solution (1 ×10^{-5} mol L^{-1}) and as thin films are shown in (Figure 4.17). These molecules exhibit dual absorbance comprised with π-π* transition and ICT bands, which differ with the electron-withdrawing abilities of the compounds. The maximal absorption peaks of **63**, **64**, **65**, and **66** were located at 547, 542, 540 and 522 nm, respectively. For solids film state showed red shift absorption and much broader than in solution phase, as can be attributed to the effects of molecular packing. In addition, **66** emitted intense purple fluorescence with a maximum at 768 nm when excited at 570 nm (Figure 4.18). The compound **64** showed blue shift at 729 nm due to donor of phenylcarbazole.

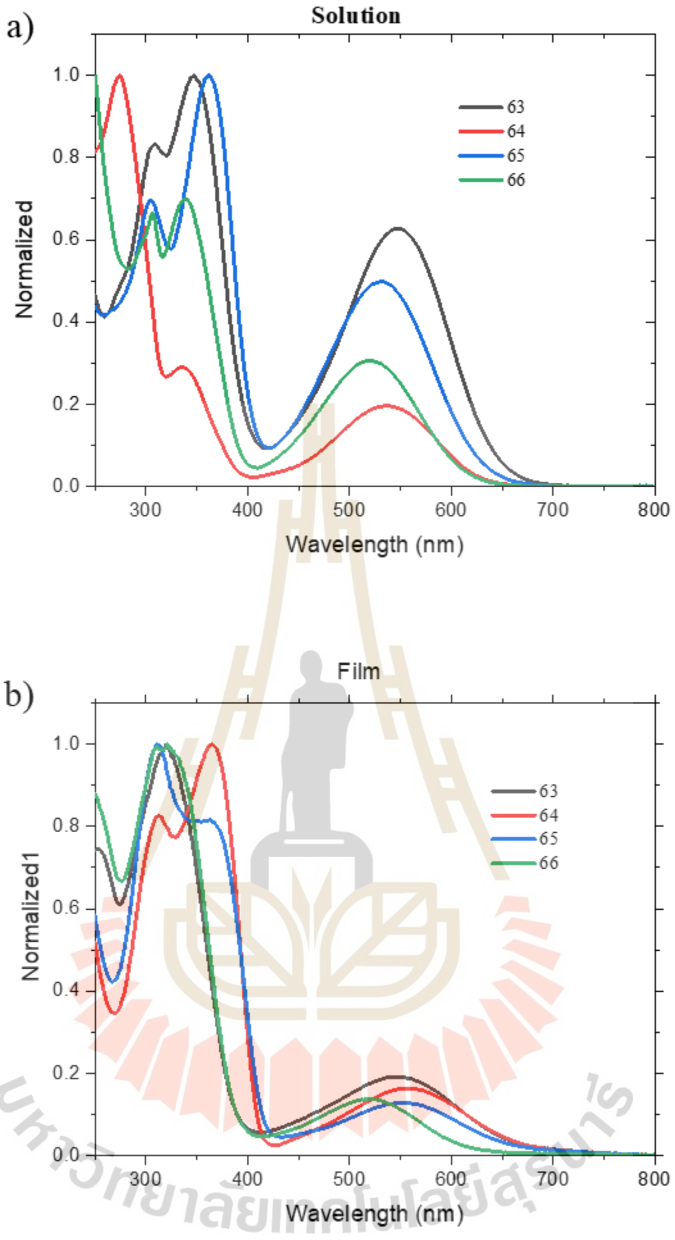

Figure 4.17 a) UV-Vis absorption spectra of **63**, **64**, **65**, and **66** in DCM solution b) thin film state.

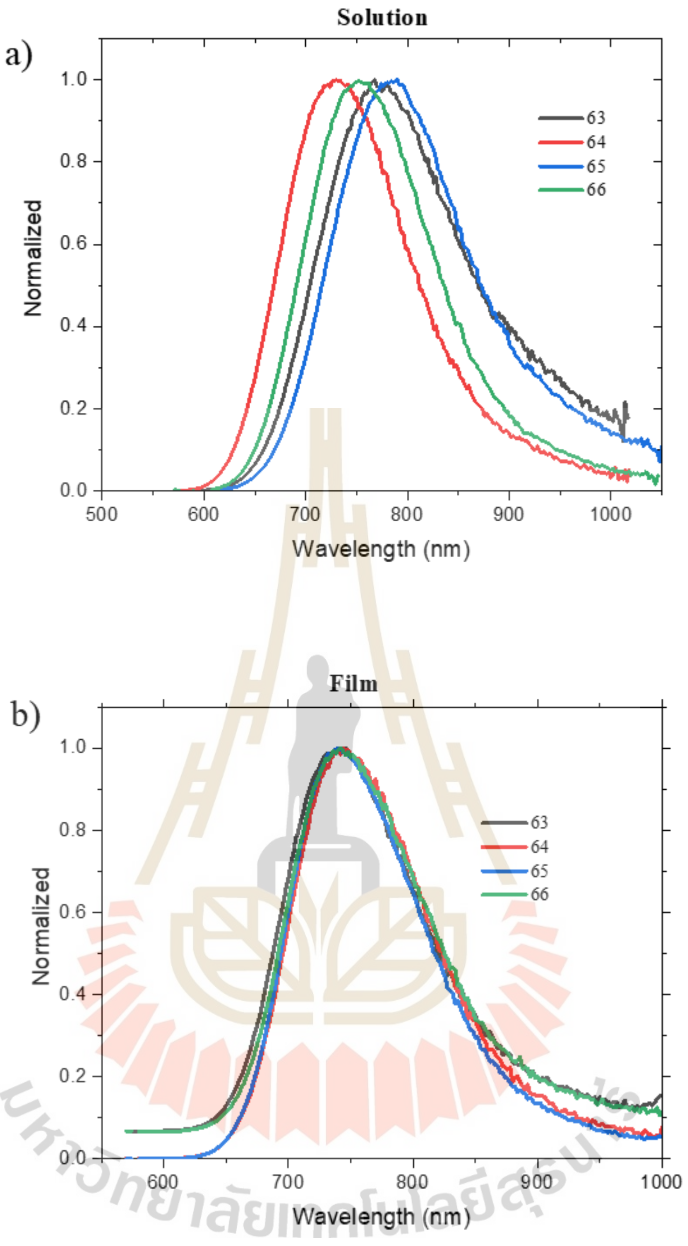

Figure 4.18 a) PL spectra of **63**, **64**, **65**, and **66** in DCM solution b) thin film state.

4.4.1 Time-resolved fluorescence decay

The lifetimes of the slow decay in the solution phase exhibited to 2.4, 2.4, 0.7, and 2.4 ns of **63**, **64**, **65**, and **66**, respectively (Figure 4.19). For the thin film state showed value to 1.8, 3.1, 2.5, and 1.9 ns. The quantum yields of these compounds of **64** has the highest quantum yield 18.37%. All the compounds are strongly emissive in dichloromethane, with the PL quantum yields (Φ_f) ranging from 13.4%, 23.71%, 4.45%, and 17.2% in solution and 4.96%, 14.92%, 11.48%, and 19.76% in thin film.

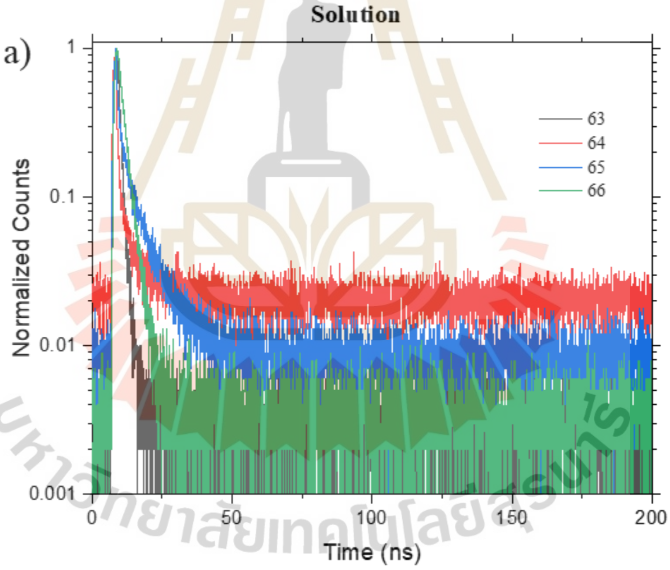

Figure 4.19 a) Time-resolved fluorescence decay of **63**, **64**, **65**, and **66** emitter in DCM solution.

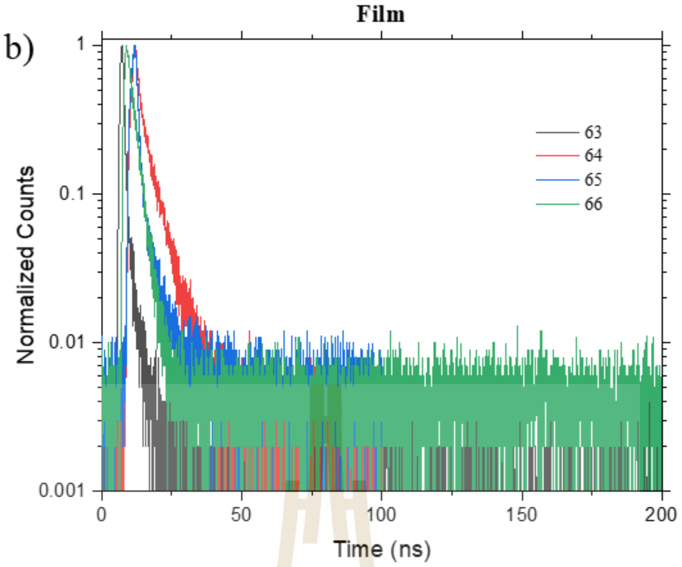

Figure 4.19 a) Time-resolved fluorescence decay of **63**, **64**, **65**, and **66** emitter in DCM solution (Continued).

Table 4.1 Photophysical properties and emission lifetimes of of **63**, **64**, **65**, and **66**.

Comp.	λ^{sol} abs /λ^{film} abs (nm)^a	λ^{sol} em /λ^{film} em (nm)^b	τ (ns)^c		QY	
			sol	film	sol	film
63	347,547/ 320,549	768/ 745	2.4	1.8	13.4	4.96
64	275,542/ 366,562	729/734	2.4	3.1	23.71	14.92
65	362,540/313,560	787/ 732	0.7	2.5	4.45	11.48
66	338,522/320,528	724/729	2.4	1.9	17.2	19.76

^{a} Measured in DCM (10^{-5}M) and thin film at 298 K.
^{b,c,d} Measured in DCM (10^{-6}M) and thin film at 298 K.

4.5 Electrochemical properties

The experimental and computationally calculated electrochemical properties are summarized in (Table 4.2). The cyclic voltammograms acquired by the anodic scans at room temperature exhibit one reversible oxidation peak for each compound, which might be attributed to the electron-donating ability of triphenylamine for **63**, **65** or phenylcarbazole for **64**, **66**. The HOMO energy levels were obtained from the onset oxidation potential (E_{onset}) observed on the cyclic voltammograms, and the LUMO energy levels were estimated from the E_g and HOMO data. These data indicated the stabilization of the HOMO level due to the electron-withdrawing characteristics of the thidiazole group. The HOMO energy levels of **63**, **65** exhibit high energy levels than **64**, **66** due to electron-donating ability of triphenylamine from -5.11 eV, -5.13, and -5.18 and-5.20 for **63**, **65**. These cause a wider band gap, which increases in the order 1.90 eV **63**, 1.94 eV **64**, 1.98 eV **64**, and 2.00 eV **66** (Figure 4.20).

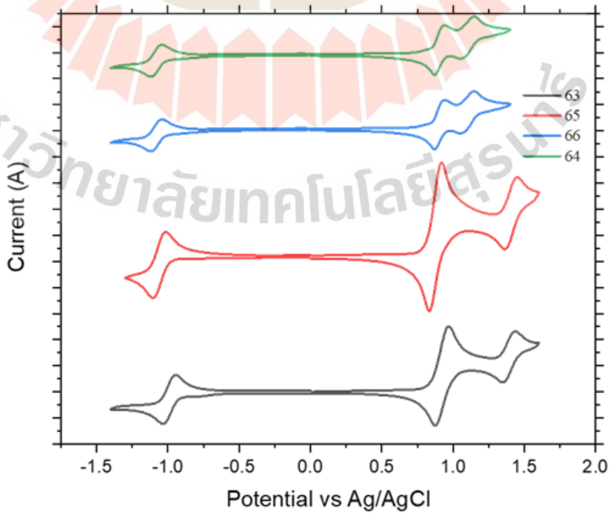

Figure 4.20 CV curves of **63**, **64**, **65**, and **66** (10^{-5} M solutions in DCM with 0.1 M n-Bu_4NPF_6).

4.5.1 Quantum chemical calculation

The tendencies of the experimental Eg, HOMO, and LUMO were gave same result with the calculated values, as shown in Table 4.2. The calculation results revealed that the (Figure 4.21). Their geometries and energies were optimized by density functional theory (DFT) calculation using DFT B3LYP/6-31G(d, p) method were investigated and summarized in Table 4.2. The frontier orbitals for the **63**, **64**, **65**, and **66** look very similar for all compounds, being localized almost entirely on the thiadiazole core for the HOMO or of triphenylamine, phenylcarbazole for the LUMO. Whereas the LUMO were mainly localized on the electron withdrawing at the triphenylamine, phenylcarbazole units.

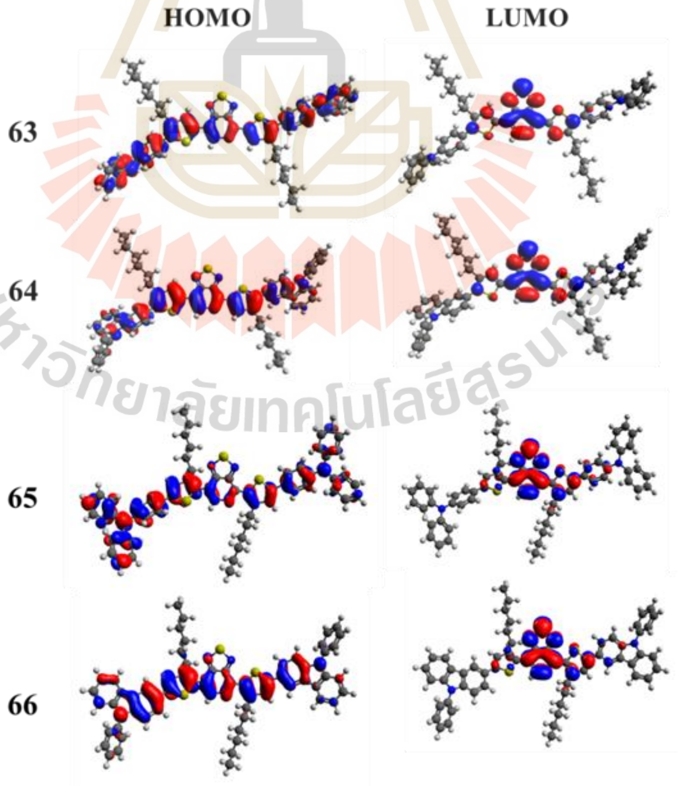

Figure 4.21 Optimized structures obtained from B3LYP/6-31G d, p) in gas phase.

Table 4.2 Electrochemical and theoretical electronic characteristics of **63**, **64**, **65**, and **66**.

Comp.	E_{on}^{ox} (eV)a	E_g^{opt} (eV)b	HOMO (eV)c	LUMO (eV)d	HOMO (eV)e	LUMO (eV)e	E_g (eV)e
63	0.67	1.90	-5.11	-3.21	-4.80	-2.73	2.07
64	0.74	1.98	-5.18	-3.20	-4.89	-2.66	2.23
65	0.69	1.94	-5.13	-3.19	-4.78	-2.70	2.08
66	0.76	2.00	-5.20	-3.20	-4.89	-2.64	2.24

[a] Measured by CV in DCM vs Ag/Ag^+ at scan rate of 50 mV/s.
[b] Calculated from $\lambda^{abs}{}_{onset}$, $E_g = 1240/\lambda^{abs}{}_{onset}$
[c] Calculated from onset oxidation potential HOMO = $-(E^{ox}{}_{on} + 4.44)$ eV
[d] Calculated from LUMO = HOMO + E_g
[e] Calculated from DFT B3LYP/6-31G(d, p)

4.6 Conclusion

Using electron-rich triphenylamine, phenylcarbazole as the donor constructive units, four purple-emissive thiadiazole derivatives were designed and synthesized, and correlations between the molecular structures and photophysical properties of these compounds have been investigated. For solution-processable derivatives of triphenylamine, phenylcarbazole and thiadiazole with the olefnic linkages between chromophores were synthesized by Suzuki cross coupling reaction. Their optical and electrochemical properties were studied and discussed in terms of the correlation with the chemical structures and compared with those of the earlier reported derivatives of triphenylamine, phenylcarbazole and thiadiazole with the single bonds between chromophores. The solution of the emission quantum yield of 13.4, 23.71, 4.45, 17.20, respectively. Due to pronounced electron donor–acceptor character. This series, we focus on hole transport layer and emissive layer material. The structure of all target molecules can be combine hole transport layer and emissive layer materials in one molecules because of the HOMO level showed around -5.11, -5.18, -5.13, and -5.20 eV, which have value close to indium tin oxide.

CHAPTER V

SYTHESIS AND CHARACTERISZATION OF NAPHTHO[2,3-C] [1,2,5]THIADIAZOLE DERIVATIVES FOR ORGANIC LIGHT-EMITTING DIODES

5.1 Introduction

The synthesis and properties of organic semiconductors D-π-A-π-D type naphtho[2,3-c] [1,2,5]thiadiazole derivatives consisting of naphtho[2,3-c][1,2,5]thiadiazole as core acceptor (A) and triphenylamine as terminal donor (D) linked with bithiophene and terthiophene as π-conjugated spacer (π), respectively. In this work, a series of naphtho[2,3-c][1,2,5]thiadiazole, namely (**77**) and (**78**), were designed and investigated. A typical organic OLEDs has a donor−π bridge−acceptor (D-π-A-π-D) skeleton, which exhibits an intermolecular charge-transfer (ICT) transition from the donor to the acceptor upon photo irradiation. In order to broaden the absorption spectra of the sensitizers in the visible and near-IR region, D-π-A-π-D type organic with an additional electron-accepting group in the conjugated spacer is an efficient approach for red shifting the absorption spectra.

5.2 Aims of the study

1. To synthesize new series of designed D-π-A-π-D type naphtho[2,3-c] [1,2,5] thiadiazole derivatives as near IR electroluminescent materials for solution processed OLEDs.

2. To study the photophysical, electrochemical, and thermal properties by UV-visible spectroscopy, fluorescence spectroscopy, cyclic voltammetry and DSC-TGA techniques.

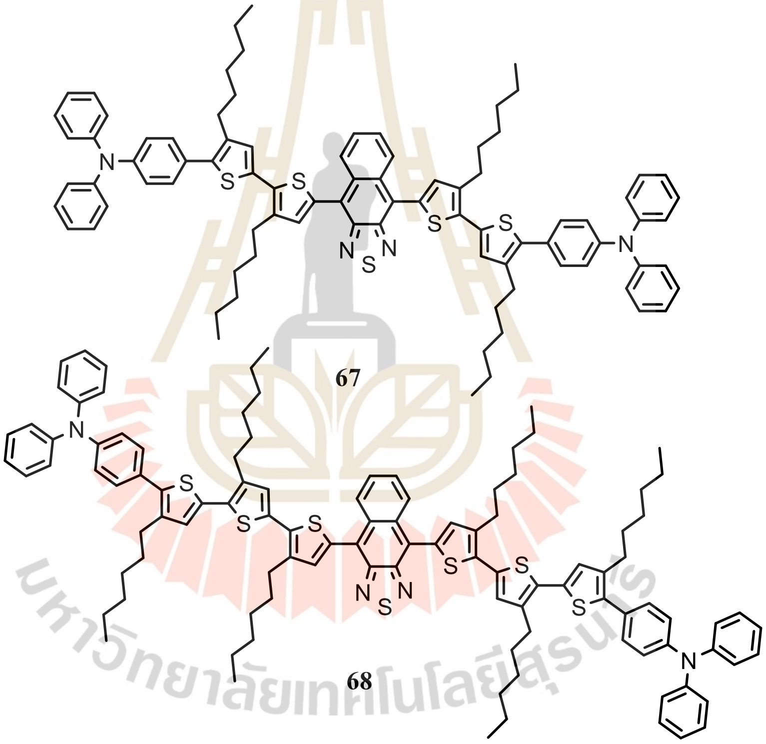

Figure 5.1 The structures of compounds **67** and **68**.

5.3 Results and discussion

5.3.1 The synthesis routes of naphtho thiadiazole derivatives of 67 and 68

The synthetic routes of the designed **67** and **68** are outlined in (Figure 5.2). Firstly, the synthesis of the key intermediates **79**, **81**, and **83** involves an iterative reaction of Suzuki cross coupling reaction and bromination. The Suzuki cross coupling reaction of 4-hexyl-2-(4,4,5,5-tetrametyl-1,3,2-dioxaborolan-2-yl)thiophene (**72**) (2.2 equiv) with the aryldibro- mide catalyzed by Pd(PPh$_3$)$_4$ and 2M Na$_2$CO$_3$ in THF was employed to introduce 4-hexyl thiophene ring to the molecule. While the bromination reaction of with *N*-bromosuccinimide in THF will arrow to introduce the dibromide functional group to the terminal end of thiophene rings. The final step was achieved by a Suzuki cross coupling reaction between intermediates **79**, **81**, and **83** and 4-(diphenylamino)phenylboronic acid (**72**) to afford **67** catalyzed by Pd(PPh$_3$)$_4$ and 2M Na$_2$CO$_3$ in toluene to form the designed target molecules.

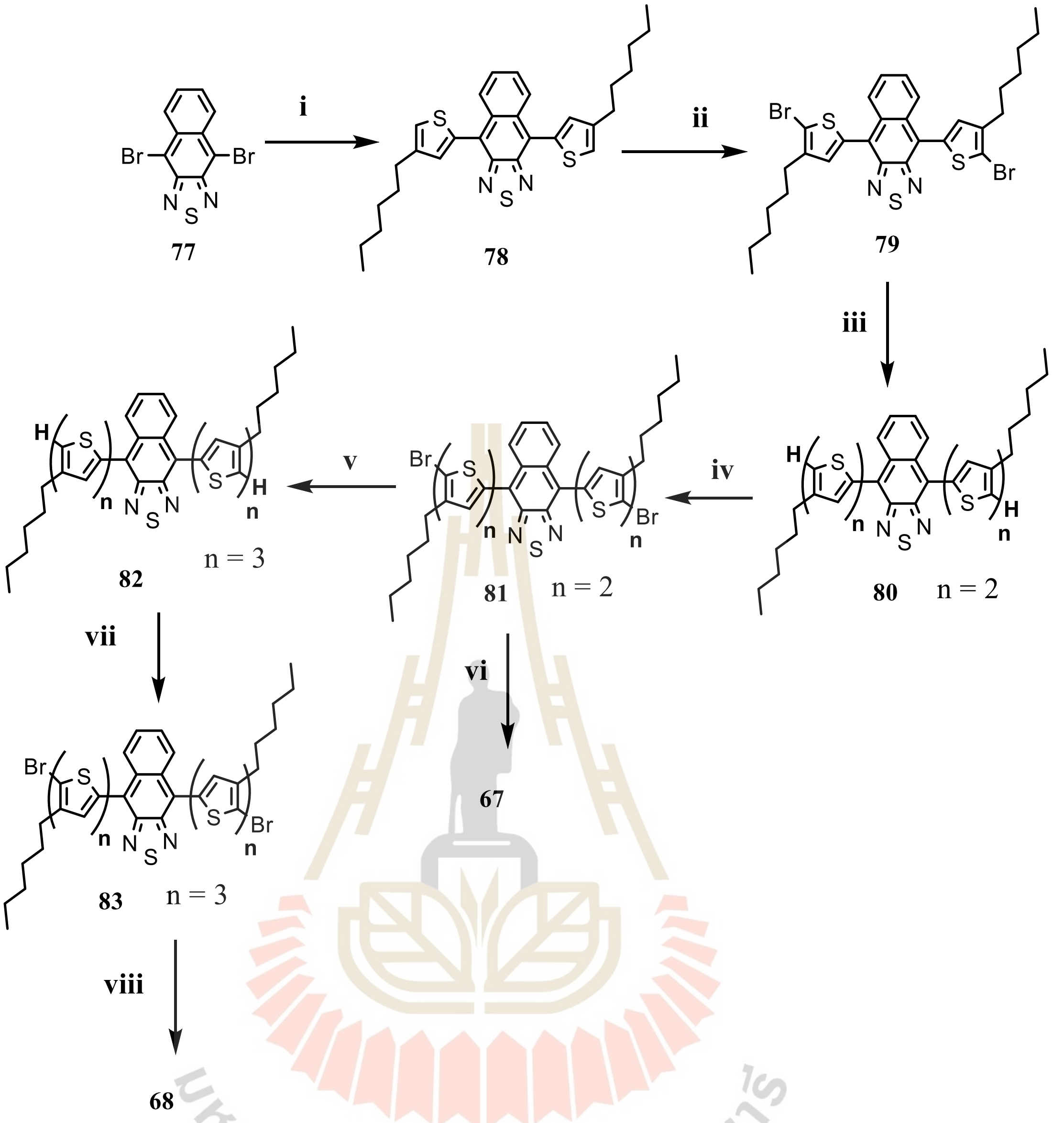

Figure 5.2 The synthetic routes of **67** and **68** molecules.

i, iii, v = Suzuki cross coupling reaction, 4-Hexyl-2-(4,4,5,5-tetrametyl-1,3,2-dioxaborolan-2-yl)thiophene (**72**), Pd(PPh$_3$)$_4$, 2M Na$_2$CO$_3$, toluene.
ii. iv, vii = Bromination reaction, *N*-bromosuccinimide, THF.
vi, viii = Suzuki cross coupling reaction, 4-(diphenylamino)phenylboronic acid (**74**), Pd(PPh$_3$)$_4$, 2M Na$_2$CO$_3$, toluene.

5.3.1.1 The synthesis of naphtho thiadiazole derivative 67

In the first step, **78** was synthesized from **72** and 4,7-dibromo-(1,2,5) thidiazole (**77**) by using Suzuki cross coupling reaction and followed with NBS to give starting material **79** (Figure 5.3).

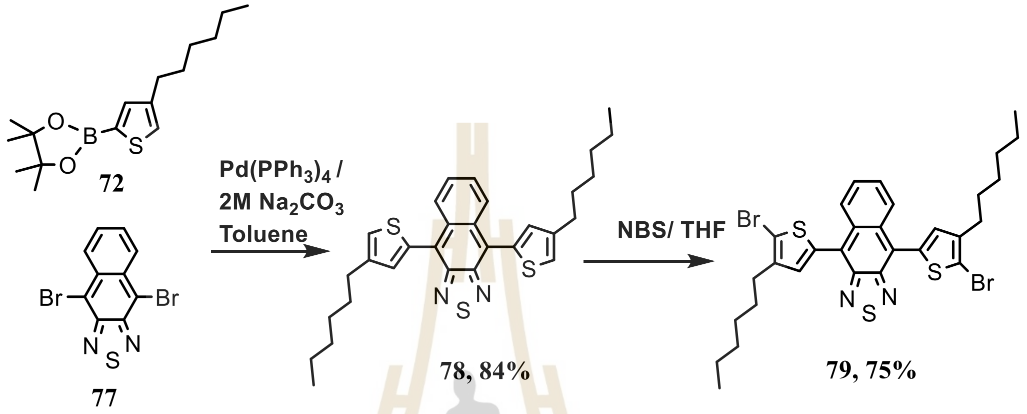

Figure 5.3 The synthesis of naphtho thiadiazole derivative **79**.

The structure of **78** was confirmed by ^{1}H-NMR spectroscopy. The characteristic peak of naphtho thiadiazole position is visible at $\delta = \delta$ 8.31 - 8.32 ppm (q, 2H, J = 1.26Hz, H_{Ar}), 7.40-7.42 ppm (q, 2H, J = 1.26Hz, H_{Ar}). The thiophene proton show at δ = 7.28 (s, 2H, H_{Ar}), 7.25 (s, 2H, H_{Ar}), and found that methyl proton of side chain show at δ = 0.91 (t, 6H, 2 × CH_3,- $H_{aliphatic}$). In addition, MALDI-TOF MS spectrum was used to confirm the structure and found to 518.7352 m/z, agreeing with the calculated mass of $C_{30}H_{34}N_2S_3$: 518.19. The structure of **79** was confirmed by ^{1}H-NMR spectroscopy. The characteristic peak of naphtho thiadiazole position is visible at δ = 8.32 - 8.31 ppm (q, 2H, J = 1.26Hz, H_{Ar}), and 7.42 - 7.40 (q, 2H, J = 1.26Hz, H_{Ar}). The thiophene proton show at δ = 7.28 (s, 2H, H_{Ar}) and 7.25 (s, 2H, H_{Ar}). The methyl proton of side chain show at δ = 0.91 ppm (t, 6H, 2 × CH_3, $H_{aliphatic}$). (The mechanism was proposed in Figure 2.9).

The intermediate of **80** was synthesized from **79** and **72** by using Suzuki cross coupling reaction and followed with NBS to give intermediate number **81** (Figure 5.4).

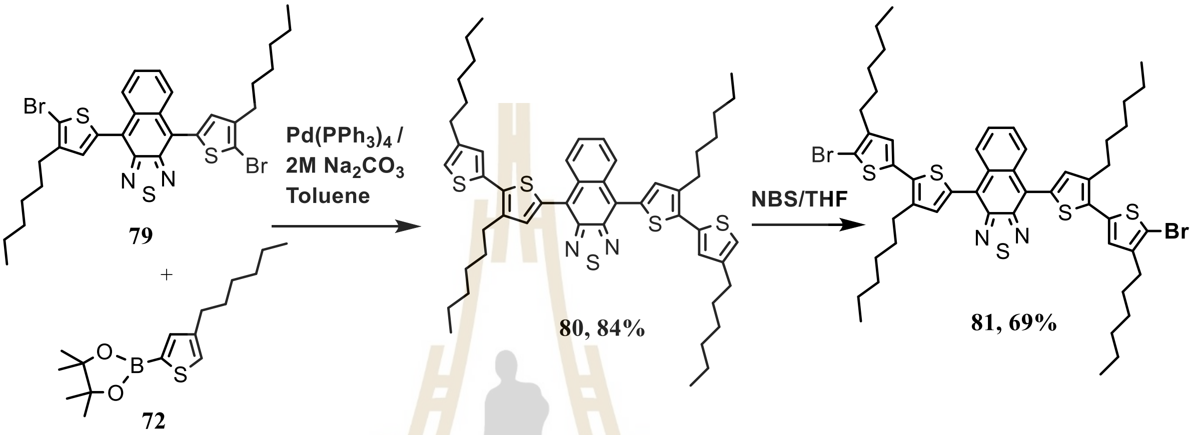

Figure 5.4 The synthesis of naphtho thiadiazole derivative **81**.

The structure of **80** was confirmed by ^{1}H-NMR spectroscopy. The characteristic peak of naphtho thiadiazole position is visible at $\delta = 8.32 - 8.31$ ppm (q, 2H, $J = 1.26$ Hz, H_{Ar}), and 7.42 - 7.40 (q, 2H, $J = 1.26$ Hz, H_{Ar}). The structure of **81** was confirmed by MALDI- TOF (m/z) calcd for $C_{50}H_{60}Br_2N_2S_5$: 1,006.17 and found 1,006.3066 (M^+).

In the final step, **67** was formed by using Suzuki cross coupling reaction between **81** and **74** as shown in (Figure 5.5)

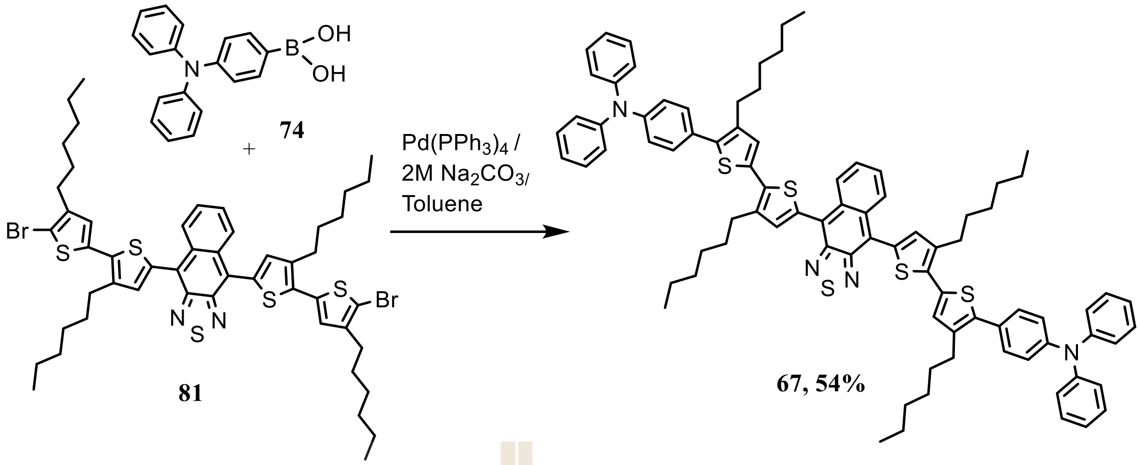

Figure 5.5 The synthesis of compound **67**.

Figure 5.6 shows the synthesis of **67** and ^{1}H-NMR spectrum. For synthesis, **67** was formed from C-C coupling reaction between **81** and 4-(diphenylamino) phenylboronic acid (**74**) in the presence of $Pd(PPh_3)_4$ as catalyst in 2M Na_2CO_3 as base in toluene as solvent to give **67** in 54% yield. The chemical structure of compound **67** was confirmed by ^{1}H-NMR spectrum, ^{13}C-NMR as well as MALDI-TOF MS. The ^{1}H-NMR spectrum collected in $CDCl_3$ show pattern of a triplet signal at 0.87-0.89 ppm (12H) assigned to two side of methyl groups, the multiplet signal at 2.68-2.70 ppm (4H), 2.93-2.96 ppm (4H) assigned to two side of CH_2 proton of alkyl thiophene. Furthermore, the proton signal at aromatic regions were found pattern of naphtha thiadiazole the singlet at 7.45-7.47 ppm (2H) and 8.47-8.48 ppm (2H) assigned to aromatic proton of naphtha thiadiazole. The number of proton aromatic regions are (36H) corresponding to ^{1}H-NMR spectrum. In addition, MALDI-TOF MS spectrum was used to confirm the structure and found to 1348.4917 m/z, agreeing with the calculated mass of $C_{86}H_{88}N_4S_5$: 1336.56.

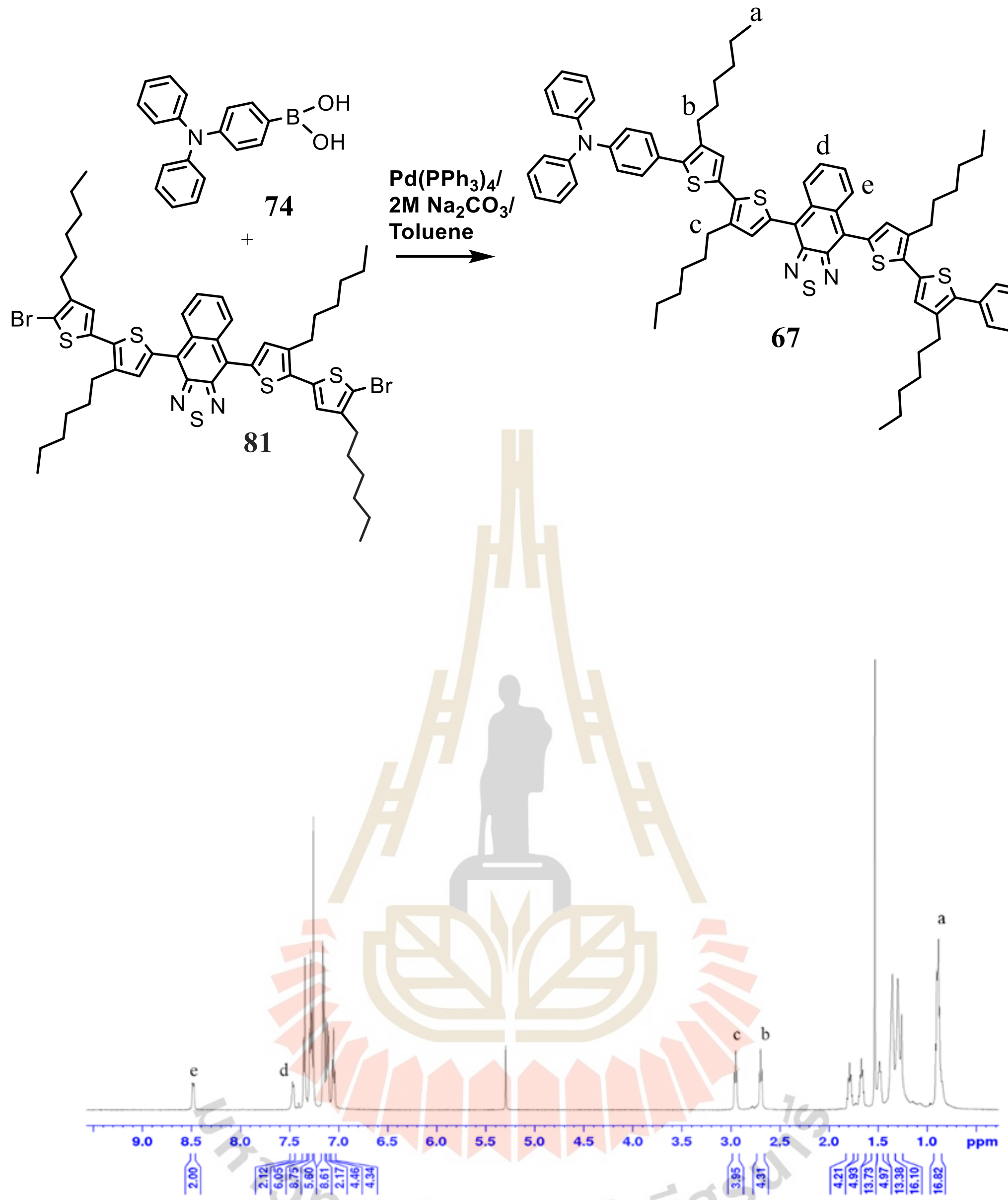

Figure 5.6 The synthesis and ^{1}H-NMR spectrum in CDCl$_3$ of **67**.

5.3.1.2 The synthesis of naphtho thiadiazole derivative 68

The first step involved the synthesis of **82** from **72** and 4,9-bis(5'-bromo-3,4'-dihexyl-[2,2'-bithiophen]-5-yl)naphtho[2,3-c][1,2,5]thiadiazole (**81**) by using Suzuki cross coupling reaction (Figure 5.7) and followed with NBS to give intermediate number **83** (Figure 5.8).

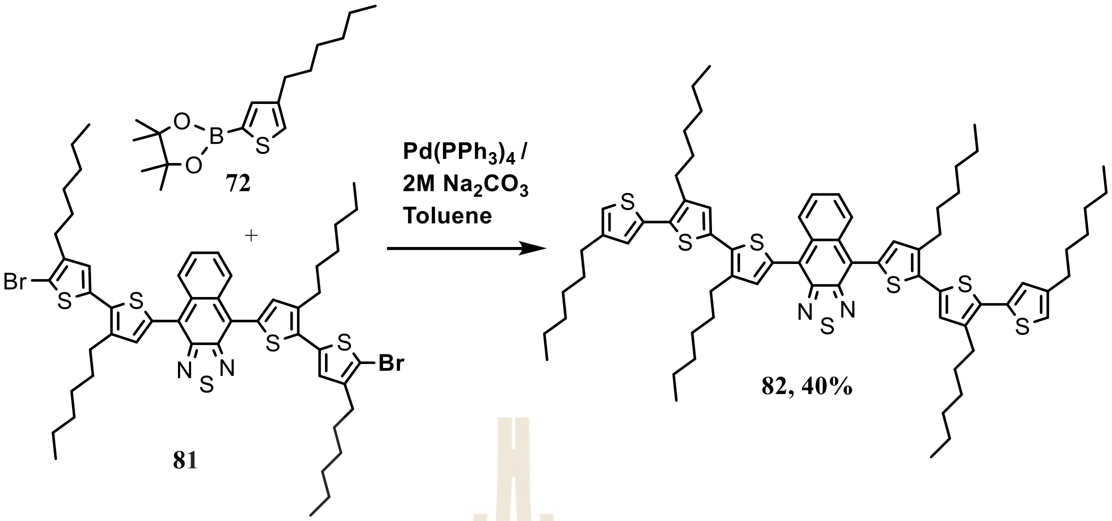

Figure 5.7 The synthesis of naphtho thiadiazole derivative **82**.

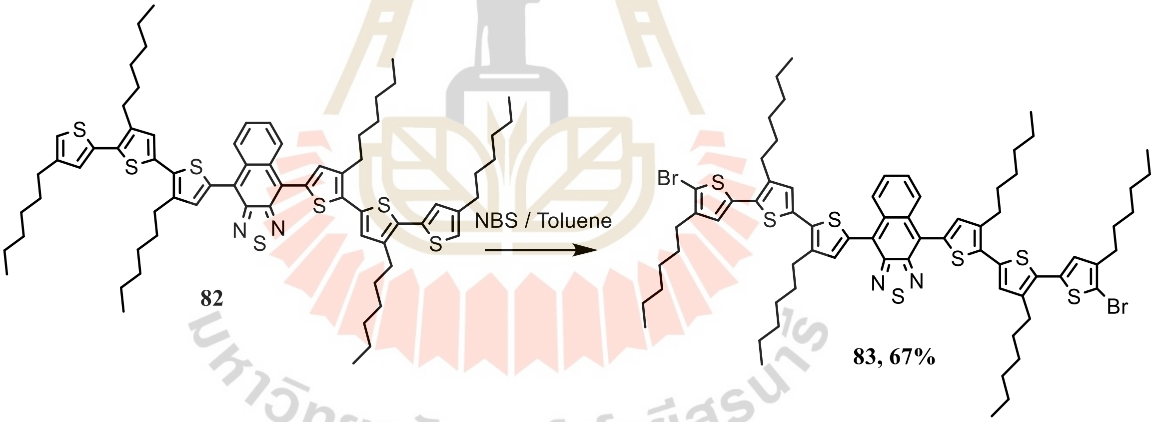

Figure 5.8 The synthesis of naphtho thiadiazole derivative **83**.

In the final step, **68** was formed using Suzuki cross coupling reaction between **83** and **74** as shown in (Figure 5.9).

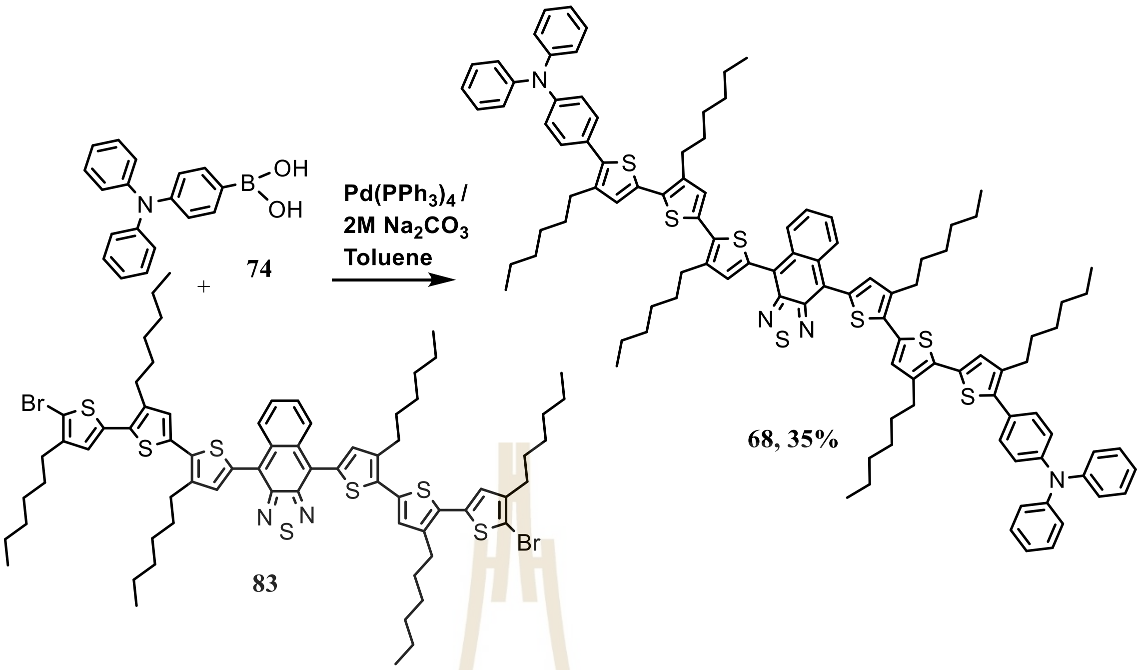

Figure 5.9 The synthesis of compound **68**.

Figure 5.10 shows the synthesis of **68** and ^{1}H-NMR spectrum. For synthesis, **68** was formed from C-C coupling reaction between **83** and 4-(diphenylamino)phenylboronic acid (**74**) in the presence of Pd(PPh$_3$)$_4$ as catalyst in 2M Na$_2$CO$_3$ as base in toluene as solvent to give **68** in 35% yield. The chemical structure of compound **68** was confirmed by ^{1}H-NMR spectrum, ^{13}C-NMR as well as MALDI-TOF MS. The ^{1}H-NMR spectrum collected in CDCl$_3$ show pattern of a triplet signal at 0.87-0.89 ppm (9H), 1.29-1.32 ppm (9H) assigned to two side of methyl groups, the multiplet signal at 1.71-1.76 ppm (4H), 2.81-2.83 ppm (4H) assigned to two side of CH$_2$ proton of alkyl thiophene. Furthermore, the proton signal at aromatic regions were found pattern of naphtha thiadiazole the singlet at 7.36 ppm (2H) and 8.48-8.49 ppm (2H) assigned to aromatic proton of naphtha thiadiazole. The number of proton aromatic regions are (38H) corresponding to ^{1}H-NMR spectrum. In addition, MALDI-TOF MS spectrum was used to confirm the structure and found to 1665.7152 m/z, agreeing with the calculated mass of $C_{106}H_{116}N_4S_7$: 1664.72.

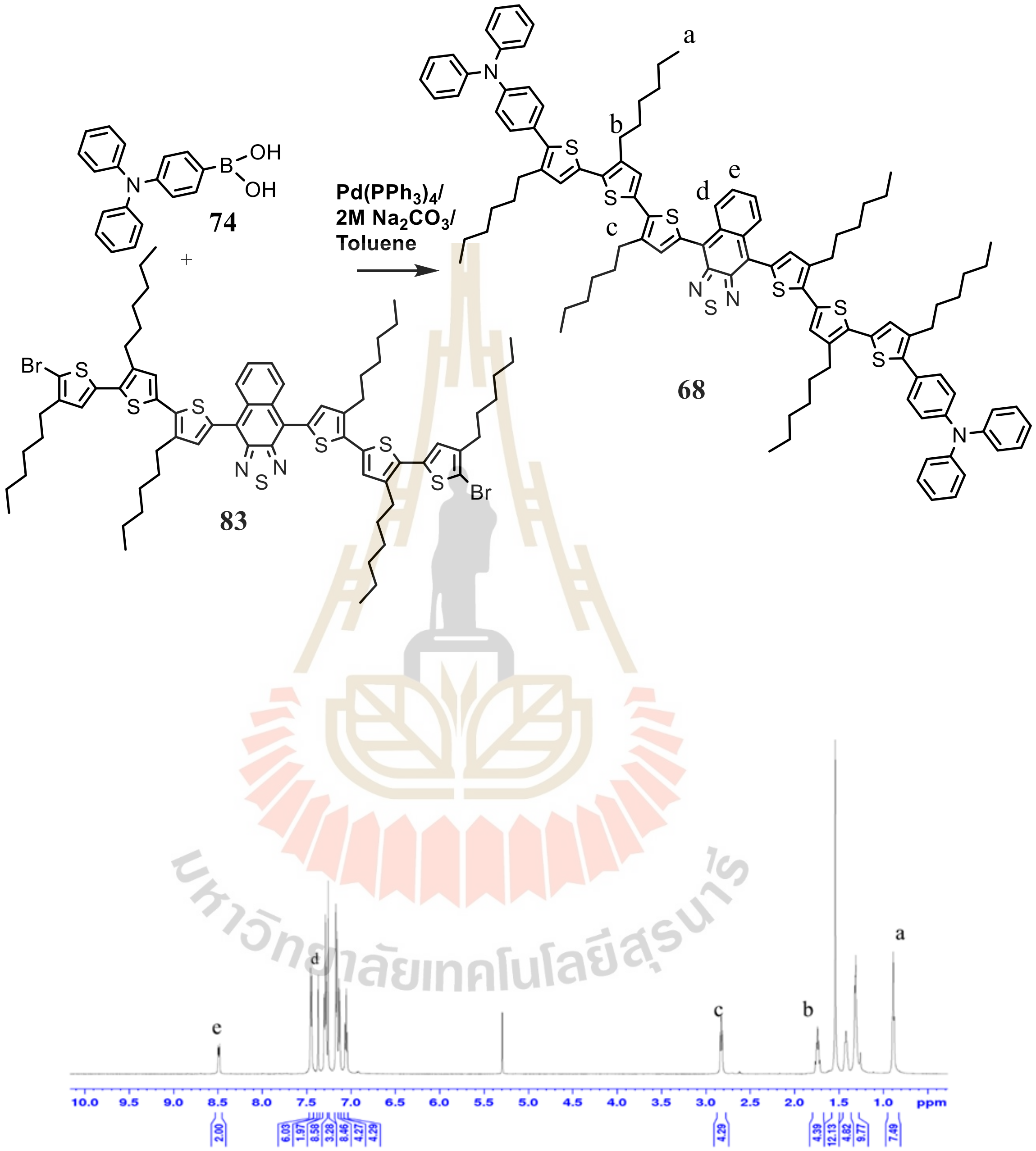

Figure 5.10 The synthesis and ^{1}H-NMR spectrum in $CDCl_3$ of **68**.

5.4 Optical properties

The absorption and emission properties of **67** and **68** in both DCM solution and as a spin-casted thin film were investigated and summarized in Table 5.1. In the solution phase, each compound exhibited a characteristic π–π* transition, as observed by the absorption peak around 347-368 nm along with a charge transfer between the naphtho[2,3-c] [1,2,5] thiadiazole and triphenylamine group evidenced by the absorption peak around 553-593 nm (Figure 5.11). The UV-visible spectra of compounds 67 and 68 showed bands below 400 nm can be attributed to localized π−π* transition, while the band between 400−700 nm are the intramolecular charge transfer transition (ICT) from the triphenylamine donor to the napthothaidiazole acceptor transfer electron. The compound 67 showed a maximum absorption peak at 553 nm and thin film showed red shift because of stacking effect. The compound 68 showed red shift than molecule 67 related to structure because of compound 68 has more π-conjugate.

The normalized fluorescence spectra in the solution phase are also shown in (Figure 5.11). The fluorescence spectra showed emission peak in the range of IR region. The emission peak in thin film showed slightly red shift because of more planar structure.

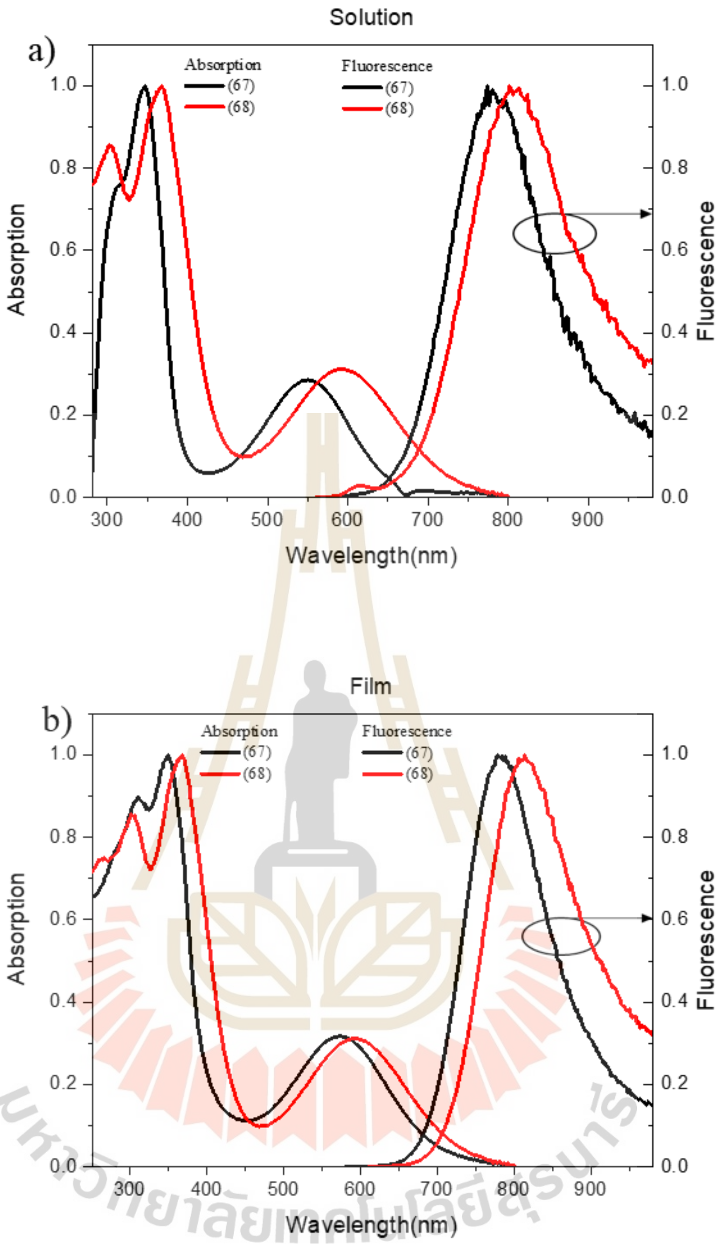

Figure 5.11 a) UV-Vis and fluorescence in DCM b) thin film state (right), excitation wavelength 570 nm.

Table 5.2 Photophysical properties and emission of **67** and **68**.

Comp.	λ^{sol} abs /λ^{film} abs (nm)[a]	λ^{sol} em /λ^{film} em (nm)[b]
67	347,553/ 350,571	780/ 781
68	368,593/ 367,591	808/ 814

[a] Measured in DCM (10^{-5}M) and thin film at 298 K.
[b,c,d] Measured in DCM (10^{-6}M) and thin film at 298 K.

5.5 Theoretical calculation and electrochemical properties

The theoretical calculations in this study were carried out in the frame of density functional methods (DFT). B3LYP (Kohn. and Sham. 1965) functional was used for the calculation of molecular properties, whereas the DFT B3LYP/6-31G**functional was used during the geometry optimizations of dimers constituted from like molecules. The geometry of all molecules in their neutral and cationic states were optimized without symmetry constraints by using the 6-31G(d, p) basis set. The vertical ionization potentials (Ip) were calculated at the neutral state geometry as energy difference between neutral and cation species. All calculations were performed by using the Gaussian 09 program. HOMO and LUMO of model compounds **67** and **68** are given in Figure 5.12. Both HOMOs are basically localized on the naphtho[2,3-c][1,2,5]thiadiazole as core acceptor (A) and bithiophene and terthiophene as π-conjugated spacer (π), with the dominant contribution coming from the TPA. Similarly, the naphtho[2,3-c][1,2,5]thiadiazole was found to contribute to the LUMOs, with practically no contribution from the TPA terminal donor (D). The data of DFT calculation for HOMO level the electrons are homogeneously distributed all over the molecules. However, the

LUMO showed electron localization at acceptor. The compound **68** has the lowest energy band gap due to more π spacers.

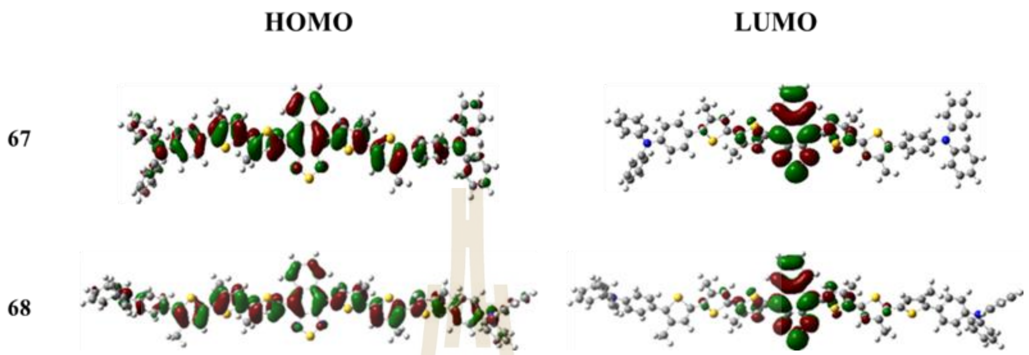

Figure 5.12 HOMO and LUMO electronic density states of **67** and **68** obtained by density functional theory (DFT) calculations using GAUSSIAN09 TD-DFT B3LYP/6-31G**.

The cyclic voltammograms acquired by the anodic scans at room temperature exhibit one reversible oxidation peak for each compound, which might be attributed to the electron-donating ability of triphenylamine. The HOMO energy levels were obtained from the onset oxidation potential (E_{onset}) observed on the cyclic voltammograms, and the LUMO energy levels were estimated from the E_g and HOMO data. The E_{onset} were influenced and shifted toward more positive potentials with an increase in the number of thiophene units. This data indicated the stabilization of the HOMO level due to the electron-withdrawing characteristics of the naphtho[2,3-c][1,2,5]thiadiazole group. It is noted that when the number of thiophene is increased, the measured HOMO is stabilized from -5.17 eV and -5.31 eV whereas the LUMO is increased from -3.48 eV and -3.55 for **67** and **68**. These cause a wider band gap, which increases in the order 1.80 eV and 1.90 eV for **68** and **67** as shown in Table 5.2 and (Figure 5.13).

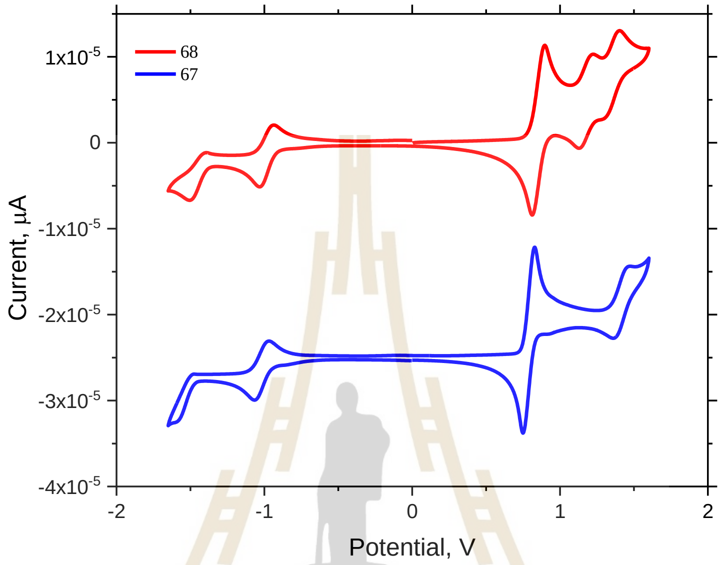

Figure 5.13 Cyclic voltammetry of compounds **67** and **68** in DCM solution. Experiments were

Performed with three electrode system and sample concentration of ca. 10^{-4} M in 0.1 M n-Bu4NPF6 under Ar-saturated at room temperature.

Table 5.2 Electrochemical and theoretical electronic characteristics of **67** and **68**.

Comp.	E_{on}^{ox} (eV)a	E_g^{opt} (eV)b	HOMO (eV)c	LUMO (eV)d	HOMO (eV)e	LUMO (eV)e	E_g (eV)e
67	0.59	1.76	-5.31	-3.55	-4.64	-2.74	1.90
68	0.68	1.69	-5.17	-3.48	-4.58	-2.79	1.79

[a] Measured by CV in DCM vs Ag/Ag$^+$ at scan rate of 50 mV/s.

[b] Calculated from λ^{abs}_{onset} , $E_g = 1240/\lambda^{abs}_{onset}$

[c] Calculated from onset oxidation potential HOMO = $-(E^{ox}_{on} + 4.44)$ eV

[d] Calculated from LUMO = HOMO + E_g

[e] Calculated from DFT B3LYP/6-31G(d

5.5 Conclusion

Two new naphtho[2,3-c][1,2,5]thiadiazole derivatives with different numbers of π -conjugated units were successfully synthesized using Suzuki coupling reaction in good to moderate yields. These compounds exhibited absorption maxima around 553-593 nm for DCM solution and 517-591 nm for thin film, emission maxima around 780-808 nm in DCM solution and 781-814 in thin film. This series, we focus on hole transport layer and emissive layer material. The structure of all target molecules can be combine hole transport layer and emissive layer materials in one molecules because of the HOMO level showed around -531 eV and -5.17 eV, which have value close to indium tin oxide.

CHAPTER VI

EXPERIMENTAL

6.1 General procedures and instruments

^{1}H-NMR spectra were recorded on Bruker AVANCE (600 MHZ) spectrometer. 13C NMR spectra were recorded on Bruker AVANCE spectrometer and were fully decoupled.

Chemical shifts (d) are reported relative to the residual solvent peak in part per million (ppm). Coupling constants (*J*) are given in Hertz (Hz). Multiplicities are quoted as singlet (s), broad (br), doublet (d), triplet (t), quartet (q), AA′BB′ quartet system (AA′BB′), AB quartet (ABq) and multiplet (m).

UV-visible spectra were measured in spectrometric grade dichloromethane on a Perkin-Elmer UV Lambda 25 spectrometer. The absorption peaks are reported as in wavelength (nm) (log e/dm^{3}mol^{-1}cm^{-1}) and reference to the shoulder. Fluorescence spectra were recorded as dilute solution in spectroscopic grade dichloromethane on a Perkin-Elmer LS 50B Luminescence Spectrometer. UV-visible and fluorescence spectra were recorded on Perkin-Elmer UV-visible spectrophotometer LAMDA 35 and fluorescence spectrophotometer LS-45. The absorption and emission in solution were measured in distilled dichloromethane.

The absorption and emission in thin film were measured compounds coated on glass substrates by spin coating technique.Analytical thin-layer chromatography (TLC) was performed with Merck aluminium plates coated with silica gel 60 F254. Column chromatography was carried out using gravity feed chromatograph with Merck silica gel mesh, 60 Å. Where solvent mixtures are used, the portions are given by volume.The electrochemistry was performed using an AUTOLAB spectrometer. All measurements were made at room temperature on sample dissolved in freshly distilled dichloromethane, 0.1 M tetra n-butylammoniuum hexafluorophosphate as electrolyte. Dichloromethane was washed with concentrated sulfuric acid and distilled from calcium hydride. A glassy carbon work in electrode, and a Ag/AgCl/NaCl (Sat.) reference electrode were used. The ferrocenium/ferrocene couple was used 74 as standard, and the ferrocene was purified by recrystallization from ethanol and then dried under high vacuum and stored over P_2O_5.

Melting point was measured by BIBBY Stuart Scientific melting point apparatus SMP3 in open capillary method and are uncorrected and reported in degree Celsius.

6.2 Synthesis

6.2.1 Synthesis for Chapter II

4-Bromo-*N*-(2-ethylhexyl)-1,8-naphthalimide (**45**)

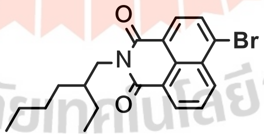

A solution of 4-bromo-1,8-naphthalimide anhydride (**44**) (5.00 g, 1.80 mmol) in 50 ml of dimethylformamyde (DMF) was added to a 100 ml three neck round bottom flask equipped with a reflux condenser and magnetic stirrer. Then 2-ethylhexylamine (2.50 g, 1.98 mmol) was added drop-wise and the reaction mixture was heated up to 110 °C and stirrer under nitrogen for 1.5 hr. The end of reaction was detected by TLC (eluent: hexane/DCM, 2:1). The reaction mixture was concentrated using rotary evaporator. The product was precipitated out into 1 N HCl, filtered off and washed with 1 N HCl. The crude product was purified by silica gel column chromatography using hexane and DCM mixture (vol. ratio 60:40) as an eluent. Then the mixture was sonicated for 1 h, the mixture was filtered, washed with hexane to obtain the product as white solid (7.8 g) in a yield of 71 %;^{1}H NMR spectrum (600MHz, $CDCl_3$, δ, ppm): 8.80 (dd, 1H, J =1.13 Hz, J = 7.31 Hz, H_{Ar}), 8.61 (dd, 1H, J = 1.17 Hz, J = 8.56 Hz,-H_{Ar}), 8.55 (d, 1H, J = 7.88 Hz, H_{Ar}), 8.25 (d, 1H, J = 7.87 Hz, H_{Ar}), 7.95 (t, 1H, J = 7.32 Hz, J = 8.52 Hz, H_{Ar}), 4.25–4.15 (m, 2H, –CH_2, $H_{aliphatic}$), 2.10-2.00 (m, 1H, -CH, $H_{aliphatic}$) 1.55–1.35 (m, 8H, 4×CH_2, $H_{aliphatic}$), 1.05-0.95 (t, 3H, CH_3, $H_{aliphatic}$). 0.95-0.90 (t, 3H, -CH_3, $H_{aliphatic}$); ^{13}C. NMR spectrum (150 MHz, $CDCl_3$, δ, ppm): 164.73, 164.72, 135.79, 135.29, 134.85, 130.90, 129.80, 127.94, 127.08, 124.81, 122.69, 84.57, 44.20, 37.93, 30.79, 28.74, 24. 97, 24.12, 23.06, 14.06, 10. 66; MALDI-TOF (m/z) calcd for $C_{20}H_{22}BrNO_2$ 389.08, found 388.1105 (M^+).

2-(2-ethylhexyl)-6-(4,4,5,5-tetramethyl-1,3,2-dioxaborolan-2-yl)-1H-benzo[de] isoquinoline-1,3(2H)-dione (**46**)

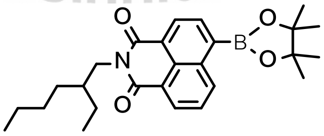

A mixture of bis(pinacolato)diboron (**45**) (5 mmol), potassium acetate (7.5 mmol), $Pd(PPh_3)_4$ (0.2 mmol) and toluene (25 mL) were added into a 50 mL branch-pipe round bottom flask. The mixture was degassed by gently bubbling nitrogen for 30 min and then heated in an oil bath at 85 °C until completion (72 h). After cooling, the product was extracted with CH_2Cl_2, washed with water, dried over Na_2SO_4, filtered, concentrated and further purified by column chromatography (silica gel, hexane/ethyl acetate, 50/1, v/v). After the reaction mixture was refluxed for 24 h, the solvent was removed and the residue was extracted with CH_2Cl_2 / brine. The organic layer was dried over sodium sulphate anhydrous, then filtered and dried to give crude product. The crude product was further purified by column chromatography. Then the mixture was sonicated for 1 h, the mixture was filtered, washed with hexane to obtain the product as white solid (12.0 g) in a yield of 72%; ^{1}H NMR (600 MHz, $CDCl_3$) δ 9.12 (d, 1H, *J* = 8.40 Hz, H_{Ar}), 8.60 (d, 1H, *J* = 7.20 Hz, H_{Ar}), 8.55 (d, 1H, *J* = 7.80 Hz, H_{Ar}), 8.20 (d, 1H, *J* = 7.20 Hz, H_{Ar}), 7.75-7.80 (m, 1H, H_{Ar}), 4.05-4.15 (m, 2H, $-CH_2$, $H_{aliphatic}$), 2.00-1.90 (m, 1H, -CH, $H_{aliphatic}$), 1.40 (s, 4×CH_3, H_{methyl}), 1.05-0.95 (t, 3H, $-CH_3$, $H_{aliphatic}$). 0.95-0.90 (t, 3H, $-CH_3$, $H_{aliphatic}$) ppm; ^{13}C. NMR spectrum (150 MHz, $CDCl_3$, *δ*, ppm): 164.26, 133.41, 132.32, 131.52, 131.35, 130.89, 130.38, 129.31, 128.34, 123.43, 122.57, 44.54, 38.17, 31.0, 28.95, 24.32, 23.32, 14.34, 10.90 ppm; MALDI-TOF (m/z) calcd for $C_{26}H_{34}BNO_4$ 435.26, found 434.2339 (M^+).

6,6'-(pyrene-1,6-diyl)bis(2-(2-ethylhexyl)-1H-benzo[de]isoquinoline-1,3(2H)-dione) (**49**)

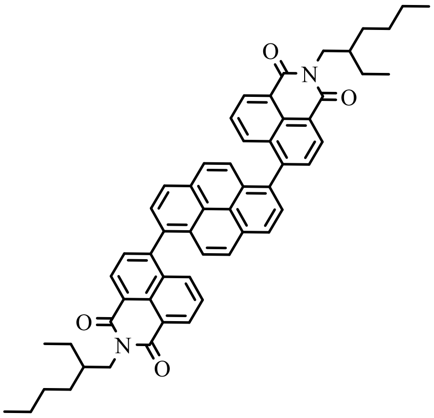

To the flask containing a mixture of 4-Bromo-*N*-(2-ethylhexyl)-1,8-naphthalimide dioxaborolane (**46**) (7.93 g, 21.0 mmol), 1,6 dibromopyrene (2.11 g, 4.04 mmol), To Na_2CO_3 (2 M in H_2O, 9.0 mL, 8.9 mmol), and $Pd(PPh_3)_4$ (0.49 g, 0.42 mmol) was added 70 mL of dry toluene. After the reaction mixture was refluxed for 24 h, the solvent was removed and the residue was extracted with CH_2Cl_2 and brine. The organic layer was dried over magnesium sulfate, then filtered and dried. The crude product was further purified by column chromatography using CH_2Cl_2 /hexane (1:5 v/v) as eluent to give the **49** as a pale yellow powder (350 mg, 57%); mp = 251 °C; ^{1}H NMR (600 MHz, $CDCl_3$): δ 8.80 (d, 1H, *J*= 7.80 Hz, H_{Ar}), 8.65 (d, 1H, *J*= 7.20 Hz, H_{Ar}), 8.30 (d, 1H, *J* = 7.80 Hz, H_{Ar}), 8.05 (q 1H, *J*= 2.40 Hz, H_{Ar}), 7.90 (t, 1H, *J* = 1.20 Hz, H_{Ar}), 7.50 (d, 1H, *J* = 8.40 Hz, H_{Ar}), 7.65 (d, 1H, *J* = 9.00 Hz, H_{AR}), 7.55 (t, 1H, *J* = 1.20 Hz, H_{Ar}), 4.25-4.15 (m, 2H, CH_2, $H_{aliphatic}$), 2.00-2.10 (m, 1H, CH, $H_{aliphatic}$), 1.50-1.40 (m, 2×CH_2, $H_{ethylene}$), 1.40-1.30 (m, 2×CH_2, $H_{ethylene}$), 1.05-0.95 (t, 2×CH_3, H_{methyl}) 0.95-0.90 (t, 2×CH_3, H_{methyl}) ppm; ^{13}C ; NMR spectrum (150 MHz, $CDCl_3$, δ, ppm): 178.72, 165.44, 162.52, 161.52, 161.35, 155.79, 150.90, 149.31, 148.34, 133.63, 132.67, 45.55, 39.16, 31.0, 28.95, 24.32, 23.32, 14.34, 10.90 ppm; MALDI-TOF (m/z) calcd for $C_{56}H_{52}N_2O_4$: 818.04 found 817.4456 (M^+).

6-(6-bromopyren-1-yl)-2-(2-ethylhexyl)-1H-benzo[de]isoquinoline-1,3(2H)-dione (**48**)

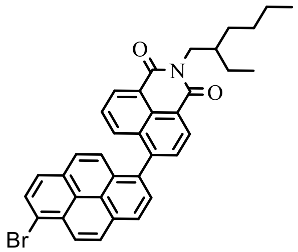

To the flask containing a mixture of 4-Bromo-*N*-(2-ethylhexyl)-1,8-naphthalimide dioxaborolane (**46**) (7.93 g, 21.0 mmol), 1,6 dibromopyrene (2.11 g, 4.04 mmol), To Na_2CO_3 (2 M in H_2O, 9.0 mL, 8.9 mmol), and $Pd(PPh_3)_4$ (0.49 g, 0.42 mmol) was added 70 mL of dry toluene. After the reaction mixture was refluxed for 24 h, the solvent was removed and the residue was extracted with CH_2Cl_2 and brine. The organic layer was dried over magnesium sulfate, then filtered and dried. The crude product was further purified by column chromatography using CH_2Cl_2 /hexane (1:5 v/v) as eluent to give the 6-(6-bromopyren-1-yl)-2-(2-ethylhexyl)-1H-benzo[de]isoquinoline-1,3(2H)-dione (**48**) as a pale yellow powder (450 mg, 42 %);^{1}H NMR (150 MHz, $CDCl_3$): δ 8.78-8.79 (d, 2H, *J*= 7.32 Hz, H_{Ar}), 8.63-8.64 (d, 2H, *J* = 7.08 Hz, H_{Ar}), 8.32-8.34 (d, 1H, *J* = 7.68 Hz, H_{Ar}), 8.27-8.28 (d, 1H, *J* = 7.56 Hz, H_{Ar}), 8.18-8.20 (d, 1H, H_{Ar}), 8.07-8.05 (t, 1H, H_{Ar}), 8.00-8.01 (d, 1H, *J* = 7.68 Hz, H_{Ar}), 7.94-7.95 (d, 1H, *J* = 9.24 Hz, H_{Ar}), 7.91-7.92 (d, 2H, *J* = 7.32 Hz, H_{Ar}), 7.78-7.79 (d, *J* = 8.46 Hz, H_{Ar}), 7.58-7.60 (d, 1H, *J* = 9.18 Hz, H_{Ar}), 7.54-7.56 (t, 1H, H_{Ar}), 4.17-4.26 (m, 1×CH_2, $H_{Aliphatic}$), 2.01-2.04 (m, 1×CH, $H_{ethylene}$), 1.57 (s, 4×CH_2, $H_{ethylene}$), 1.44-1.47 (m, 2×CH_2, H_{methyl}), 1.37 (m, 4H, $H_{ethylene}$) 0.98-1.00 (t, 1×CH_3, H_{methyl}), 0.91-0.94 (t, 1×CH_3, H_{methyl}), ppm; ^{13}C NMR spectrum (150 MHz, $CDCl_3$, δ, ppm) 144.85, 132.45, 131.95, 130.55, 130.45, 130.42, 130.33, 129.31, 129.75, 128.60, 128.44, 127.53, 127.31, 127.15, 126.89, 126.33, 125.98, 125.38, 124.74, 124.47, 123.84, 123.61, 123.54, 122.01, 121.36, 43.26, 37.04, 30.91, 29.83, 28.68, 27.76, 23.12, 22.12, 21.67, 13.12, 13.09, 9.71 ppm; MALDI-TOF (m/z) calcd for $C_{36}H_{30}BrNO_2$: 587.15 found 590.1384 (M^+).

6,6',6"-(8-(2-(2-ethylhexyl)-1,3-dioxo-2,3,9,9a-tetrahydro-1H-benzo[de]isoquinolin-6-yl) pyrene-1,3,6-triyl)tris(2-(2-ethylhexyl)-1H-benzo[de]isoquinoline-1,3(2H)-dione) (**50**)

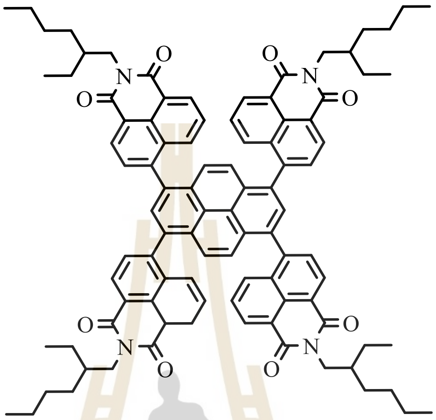

To the flask containing a mixture of 4-Bromo-*N*-(2-ethylhexyl)-1,8-naphthalimide dioxaborolane (**46**) (0.60 g, 21.0 mmol), 1,3,6,8-tetrabromopyrene (0.10 g, 4.04 mmol). To Na_2CO_3 (2 M in H_2O, 9.0 mL, 8.9 mmol), and $Pd(PPh_3)_4$)0.49 g, 0.42 mmol) was added 70 mL of dry toluene. After the reaction mixture was refluxed for 24 h, the solvent was removed and the residue was extracted with CH_2Cl_2 /brine. The organic layer was dried over magnesium sulfate, then filtered and dried. The crude product was further purified by column chromatography using CH_2Cl_2 /hexane (1:5 v/v) as eluent to give the (**50**) as a pale yellow powder (180 mg, 77%); mp = 280-281 ^{o}C; ^{1}H NMR (150 MHz, $CDCl_3$): δ 8.70 (q, 2H, *J*= 1.20 Hz, H_{Ar}), 8.65 (d, 2H, *J* = 4.80 Hz, H_{Ar}), 8.15 (d, 1H, *J* = 4.20 Hz, H_{Ar}), 7.90 (m 2H, H_{Ar}), 7.85 (m, 1H, H_{Ar}), 7.80 (t, 1H, H_{Ar}), 7.20 (d, 1H, *J* = 9.00 Hz, H_{Ar}), 7.15 (t, 1H, *J* = 1.20 Hz, H_{Ar}), 7.05 (m, 2H, H_{Ar}), 4.20-4.10 (m, 4×CH_2, $H_{Aliphatic}$), 2.05-1.95 (m, 4×CH, $H_{Aliphatic}$), 1.45-1.35 (m, 4×CH_2,

$H_{ethylene}$), 1.35-1.25 (m, 4×CH_2, $H_{ethylene}$), 1.05-0.95 (t, 4×CH_3, H_{methyl}) 0.95-0.90 (t, 4×CH_3, H_{methyl}), ppm; ^{13}C NMR spectrum (150 MHz, $CDCl_3$, δ, ppm) 164.43, 164.30, 144.24, 144.22, 134.67, 134.61, 134.56, 134.45, 132.35, 132.17, 131.49, 131.46, 131.30, 130.62, 130.48, 130.04, 130.00, 129.64, 129.56, 128.52, 128.48, 127.40, 127.35, 127.32, 126.41, 125.12, 125.07, 123.24, 122.88, 44.31, 37.98, 30.79, 28.72, 24.11, 23.07, 14.07, 10.68 ppm; MALDI-TOF (m/z) calcd for $C_{96}H_{94}N_4O_8$: 1433.71 found 1432.0879 (M^+).

6,6'-([1,1'-bipyrene]-6,6'-diyl)bis(2-(2-ethylhexyl)-1H-benzo[de]isoquinoline-1,3(2H)-dione) (**51**)

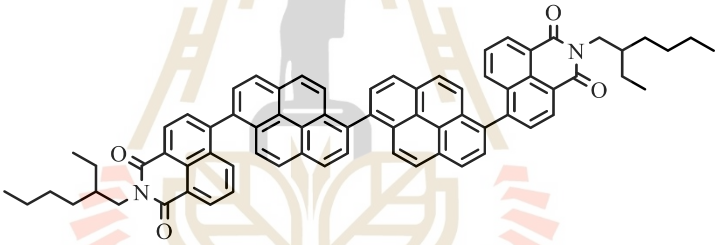

A mixture of **48** (400 mg, 5. mmol), bis(pinacolato) diboron (0.81 mg, 0.65 mmol), (KOAc), Pd(PPh)$_3$Cl$_2$, toluene (40 mL) was purged with nitrogen.. The reaction mixture was stirred at 110 °C for 24 hr. After the reaction mixture was refluxed for 24 h, the solvent was removed and the residue was extracted with CH_2Cl_2 and brine. The organic layer was dried over sodium sulfate anhydrouse, then filtered and dried. The crude product was further purified by column chromatography using CH_2Cl_2 /hexane (1:5 v/v) as eluent to give the **51** as a pale yellow powder (90 mg, 11%); mp = 290-291 ^{o}C; ^{1}H NMR (600 MHz, $CDCl_3$): δ 8.80 (d, 2H, *J*= 7.20 Hz, H_{Ar}), 8.60 (d, 2H, *J* = 6.60 Hz, H_{Ar}), 8.35 (d, 2H, *J* = 7.80 Hz, H_{Ar}), 8.25 (d, 2H, *J* = 7.80 Hz, H_{Ar}), 8.20 (d, *J* = 7.20 Hz, H_{Ar}), 8.03 (d, *J* = 9.00 Hz, H_{Ar}), 8.05 (d, *J* = 9.00 Hz, H_{Ar}), 8.00 (d, *J* = 7.20

Hz, H_{Ar}), 7.98(d, *J* = 9.60 Hz, H_{Ar}), 7.95 (d, *J* = 7.20 Hz, H_{Ar}), 7.81 (d, *J* = 8.40 Hz, H_{Ar}), 7.79 (d, *J* = 9.60 Hz, H_{Ar}), 6.84 (d, *J* = 9.00 Hz, H_{Ar}), 6.78 (t, H_{Ar}), 4.20-4.10 (m, 2×CH_2, $H_{Aliphatic}$), 2.05-1.95 (m, 2×CH, $H_{Aliphatic}$), 1.45-1.35 (m, 2×CH_2, $H_{ethylene}$), 1.35-1.25 (m, 2×CH_2, $H_{ethylene}$), 1.05-0.95 (t, 2×CH_3, H_{methyl}) 0.95-0.90 (t, 2×CH_3, H_{methyl}) ppm; ^{13}C NMR spectrum (150 MHz, $CDCl_3$, δ, ppm) 163.73, 163.60, 144.83, 135.91, 132.88, 131.96, 130.39, 129.79,129.38, 128.99, 128.48, 128.31, 127.58, 127.31, 127.21, 126.67, 126.06, 125.45, 124.18, 124.07, 123.92, 123.82, 123.74, 122.07, 121.46, 52.39, 43.30, 37.06, 30.91, 29.85, 28.68, 28.64, 28.34, 27.77, 23.14, 22.14, 21.67, 13.13, 9.72 ppm; MALDI-TOF (m/z) calcd for $C_{72}H_{60}N_2O_4$:1018.28 found 1017.4105 (M^+).

6.2.2 Synthesis for Chapter III

Tris(4-bromophenyl)amine (**58**)

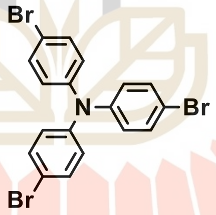

The solution of triphenylamine (1.0 g, 4.0 mmol), tris(4-bromophenyl)amine (5 mmol), (0.5 g, 1.29 mmol), THF (25 mL) were added *N*-bromosuccinimide (2.3 g, 1.30 mmol). mmol) and toluene (20 mL) was purged with nitrogen. The reaction mixture was stirred at room temperature for 3 hr. After that, the product was extracted with CH_2Cl_2, washed with water, dried over Na_2SO_4. The solvent was evaporated to afford a crude product. The crude product was purified by crystallized to obtain **58** as white powder with the yield of (2.50 g, 0.52 mmol) (88%); ^1H NMR (600 MHz, $CDCl_3$) : δ 7.34 -7.35 (d 6H, *J* = 8.70

Hz, H_{Ar}), 6.90 – 6.92 (d, 6H, *J* = 8.70 Hz, H_{Ar})); ^{13}C NMR (600 MHz, $CDCl_3$) δ 144.08, 132.34, 128.63, 124.09.

Tris(4-(4,4,5,5-tetramethyl-1,3,2-dioxaborolan-2-yl)phenyl)amine (**59**)

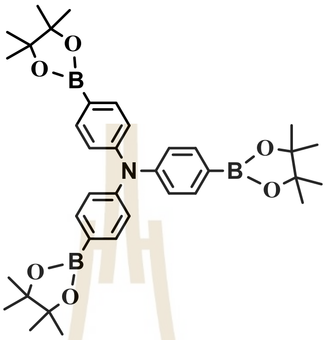

The solution of tris(4-bromophenyl)amine (**58**) (2.0 g, 0.32 mmol) , bis(pinacolato) diboron (0.81 mg, 0.65 mmol), (KOAc), $Pd(PPh)_3Cl_2$, toluene (40 mL) was purged with nitrogen. The reaction mixture was stirred at 110 °C for 24 hr. After cooling, the product was extracted with CH_2Cl_2, washed with water, dried over Na_2SO_4. The solvent was evaporated to afford a crude product. The crude product was purified by silica gel column chromatography using the eluent mixture of hexane/CH_2Cl_2, 6:4, v/v) to obtain **59** as white powder with the yield of (1.80 mg, 0.14 mmol) (58%). ^{1}H NMR (600 MHz, $CDCl_3$) : δ 7.67-7.69 (d, 6H, *J* = 8.40 Hz, H_{Ar}), 7.06-7.08 (d, 6H, *J* = 8.40 Hz, H_{Ar}), 1.33 (s, 36H, H_{Ar}).

4 ,4′,4′′-(Tris(*N*-(2-etylhexyl)-1,8-naphthalimide-4-yl) phenyl) benzenamine (**53**)

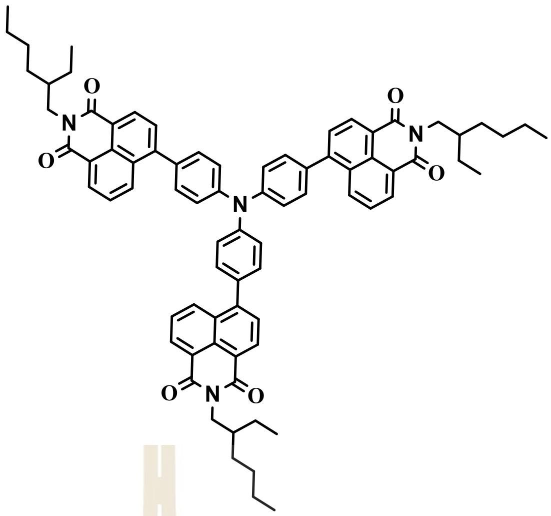

The solution of 4-bromo-*N*-(2-ethylhexyl)-1,8-naphthalimide dioxaborolane (**46**) (0.5 g,1.29 mmol), tris(4-bromophenyl)amine (**58**) (0.5 g,1.29 mmol), Pd(PPh$_3$)$_4$ (0.49 g, 0.42 mmol), Na_2CO_3 (2 M in H_2O, 9.0 mL, 8.9 mmol) and toluene (20 mL) was purged with nitrogen. The reaction mixture was stirred at 110 °C for 24 hr. After cooling, the product was extracted with CH_2Cl_2, washed with water, dried over Na_2SO_4. The solvent was evaporated to afford a crude product. The crude product was purified by silica gel column chromatography using the eluent mixture of hexane/CH_2Cl_2, 8:2, v/v) to obtain **53** as orange powder with the yield of (350 mg, 0.14 mmol) (78%); M.p. 133-134 ^{o}C. ^{1}H NMR (600 MHz, $CDCl_3$) : δ 8.65 (q, 6H, J = 2.76 Hz, H_{Ar}), 8.40 (d, 3H, J = 2.51 Hz, H_{Ar}), 7.75 (q, 6H, J_1 = 8.64 Hz, H_{Ar}), 7.56 (d, 6H, J = 7.70 Hz, H_{Ar}), 7.45 (d, H, J = 8.68 Hz, H_{Ar}), 4.18-4.12 (m, 6H, $H_{aliphatic}$), 2.05-1.90, (m, 3H, 3.× CH, $H_{aliphatic}$), 1.48-1.32 (t, 9H, 3 × CH_3,- $H_{aliphatic}$), 1.00-0.91 (t, 9H, 3 × CH_3,- $H_{aliphatic}$); ^{13}C NMR (600 MHz, $CDCl_3$) δ 163.66, 163.48, 146.48, 132.94, 131.39, 130.27, 130.23, 129.92, 128.99, 127.90, 126.82, 125.84, 125.78, 123.40, 122.12, 120.75, 43.22, 36.98, 29.80, 27.73, 23.11, 22.08, 13.08, 9.0; MALDI-TOF (m/z) calcd for $C_{78}H_{78}N_4O_6$:1167.50, found 1167.4825 (M^+).

6,6'-(((4-bromophenyl)azanediyl)bis(4,1-phenylene))bis(2-(2-ethylhexyl)-1H-benzo [de]isoquinoline-1,3(2H)-dione) (**60**)

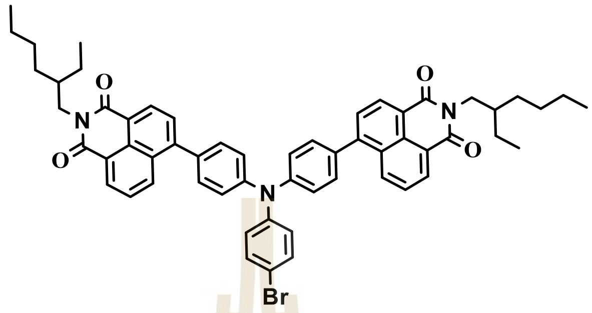

The solution of 4-bromo-*N*-(2-ethylhexyl)-1,8-naphthalimide dioxaborolane (**46**) (0.5 g, 1.29 mmol), tris(4-bromophenyl)amine (**58**) (0.5 g,1.29 mmol), $Pd(PPh_3)_4$ (0.49 g, 0.42 mmol), Na_2CO_3 (2 M in H_2O, 9.0 mL, 8.9 mmol) and toluene (20 mL) was purged with nitrogen. The reaction mixture was stirred at 110 °C for 24 hr. After cooling, the product was extracted with CH_2Cl_2, washed with water, dried over Na_2SO_4. The solvent was evaporated to afford a crude product. The crude product was purified by silica gel column chromatography using the eluent mixture of hexane/CH_2Cl_2, 8:2, v/v) to obtain 6,6'-(((4-bromophenyl)azanediyl)bis(4,1-phenylene))bis(2-(2-ethylhexyl)-1H-benzo[de]isoquinoline-1,3(2H)-dione) (**60**) as orange powder with the yield of (350 mg, 0.14 mmol) (78%); ^{1}H NMR (600 MHz, $CDCl_3$) : δ 8.65-8.64 (d, 2H, *J* = 7.80 Hz, H_{Ar}), 8.38-8.39 (d, 2H, *J* = 8.40 Hz, H_{Ar}), 7.54-7.73 (t, 4H, H_{Ar}), 7.49-7.50 (d, 4H, *J* = 9.00 Hz, H_{Ar}), 7.47-7.49 (d,4 H, *J* = 6.60 Hz, H_{Ar}), 7.33-7.34 (d, 4H, *J* = 8.40 Hz, H_{Ar}), 7.18-7.20 (d, 2H, *J* = 8.40 Hz, H_{Ar}), 4.11-4.19 (m, 4H, 2.× CH_2, $H_{aliphatic}$), 1.96-1.99, (m, 2H, 2.× CH, $H_{aliphatic}$), 1.42-1.36 (m, 8H, 4 × CH_2,- $H_{aliphatic}$), 1.00-0.91 (t, 3H, 1 × CH_3,- $H_{aliphatic}$), 0.94-0.96 (t, 3H, 1 × CH_3,- $H_{aliphatic}$).

6,6',6'',6'''-(([1,1'-biphenyl]-4,4'-diylbis(azanetriyl))tetrakis(benzene-4,1-diyl)) tetrakis(2-(2-ethylhexyl)-1H-benzo[de]isoquinoline-1,3(2H)-dione) (**54**)

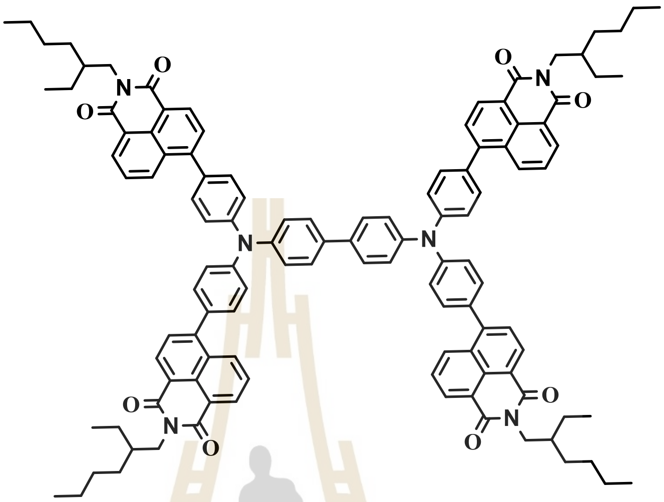

A mixture of 6,6'-(((4-(4,4,5,5-tetramethyl-1,3,2-dioxaborolan-2-yl) phenyl)azanediyl) bis(4,1-phenylene))bis(2-(2-ethylhexyl)-1H-benzo[de]isoquinoline -1,3 (2H)-dione) (**60**) (0.7 mmol), Na_2CO_3 (2 M in H_2O, 9.0 mL, 8.9 mmol), $Pd(PPh_3)_4$ (0.2 mmol) and toluene (25 mL) was purged with nitrogen. The reaction mixture was stirred at 110 °C for 24 hr. After cooling, the product was extracted with CH_2Cl_2, washed with water, dried over Na_2SO_4, filtered, concentrated and further purified by column chromatography (silica gel, hexane/dichloromethane, (50/1, v/v). to obtain **54** as orange powder with the yield of (70 mg, 0.14 mmol) (28%); of 22%. ^1H NMR (600 MHz, $CDCl_3$) δ 8.65 - 8.64 (d, 8H, J =7.44 Hz, H_{Ar}), 8.42 - 8.41 (d, 4H, J = 8.40 Hz, H_{Ar}), 7.74 - 7.72 (q, 8H, J = 3.96 Hz, H_{Ar}), 7.44 - 7.43(d, 6H, J = 7.62 Hz, H_{Ar}), 7.31 -7.30 (d, 6H, J = 7.62 Hz, H_{Ar}), 7.24 – 7.23 (d, 2H, J = 7.68 Hz, H_{Ar}), 6.95 – 6.93 (d, 2H, J = 8.94 Hz, H_{Ar}), 4.20-4.12 (m, 8H, 4×CH_2 $H_{Aliphatic}$), 1.99 -1.97 (m, 4H, 4 × CH, $H_{Aliphatic}$), 1.41 – 1.39 (m, 14H, 7×CH_2 $H_{aliphatic}$), 1.34 – 1.32 (m, 14H, 7×CH_2, $H_{aliphatic}$), 0.96 – 0.93 (t, 12H, 4× CH_3, $H_{aliphatic}$), 0.92 – 0.87 (t, 12H, 4× CH_3, $H_{aliphatic}$); ^{13}C NMR (600 MHz, $CDCl_3$) δ 164.39, 147.60, 146.74, 146.30, 140.17, 139.59, 139.18, 137.57, 133.45, 132.50, 132.36, 131.58, 131.28, 131.10, 130.96, 130.81, 130.33, 130.02, 129.81, 129.16, 129.04, 128.93, 128.26, 127.80, 127.13, 126.81, 124.52, 124.00, 123.10, 121.77, 121.65, 44.26, 37.98, 31.04, 30.82, 29.71, 29.23, 28.98, 28.76, 24.13, 23.10, 22.63, 14.10, 10.70; MALDI-TOF (m/z) calcd for $C_{116}H_{112}N_6O_8$: 1716.85, found 1718.7435 (M^+).

2-(2-ethylhexyl)-6-(4-hexylthiophen-2-yl)-1H-benzo [de]isoquinoline -1,3(2H)-dione (**61**)

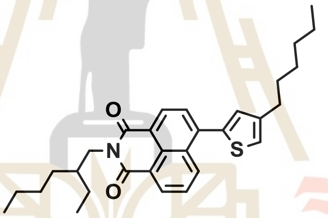

A solution of 4-Bromo-*N*-(2-ethylhexyl)-1,8-naphthalimide (**46**) (300 mg, 0.78 mmol), 4-Hexyl-2-(4,4,5,5-tetrametyl-1,3,2-dioxaborolan-2-yl)thiophene (1.2 equiv, 1.4 mmol) $Pd(PPh_3)_4$ (0.2 mmol), Na_2CO_3 (2 M in H_2O, 9.0 mL, 8.9 mmol) and toluene (25 mL) was purged with nitrogen. The reaction mixture was stirred at 110 °C for 24 hr. After cooling, the product was extracted with CH_2Cl_2, washed with water, dried over Na_2SO_4, filtered, concentrated and further purified by column chromatography (silica gel, hexane/ethyl acetate, (50/1, v/v). Then the mixture was sonicated for 1 h, the mixture was filtered, washed with hexane to obtain the product as yellow oil with in a yield of 70%. ^{1}H NMR (600 MHz, $CDCl_3$) δ 8.65-8.62, (q, 2H, H_{Ar}), 8.58 - 8.56, (d, H, J = 7.56 Hz, H_{Ar}), 7.80 - 7.79, (d, J = 7.56 Hz), 7.76 - 7.73, (t, H, H_{Ar}), 4.17 - 4.09 (m, 2H,

$H_{aliphatic}$), 2.71-2.69 (t, 2H, $H_{aliphatic}$), 1.98 - 1.94 (m, H, $H_{aliphatic}$), 1.72 -1.76 (m, 2H, $H_{aliphatic}$), 1.42 – 1.37 (m, 6H, 3× CH_2, $H_{aliphatic}$), 1.35 - 1.32 (m, 8H, 4× CH_2, $H_{aliphatic}$), 1.35 – 1.32 (m, 8H, 4× CH_2, $H_{aliphatic}$), 0.95 -0.92 (t, 3H, 1× CH_3, $H_{aliphatic}$), 0.91 -0.89 (t, 3H, 1× CH_3, $H_{aliphatic}$), 0.89 -0.86 (t, 3H, 1× CH_3, $H_{aliphatic}$), ^{13}C NMR (600 MHz, $CDCl_3$) δ MALDI-TOF (m/z) calcd for $C_{30}H_{37}NO_2S$: 475.25, found 475.3197 (M^+).

Tris[4-(4,4,5,5-tetramethyl-1,3,2-dioxaborolan-2-yl) phenyl] amine (**62**)

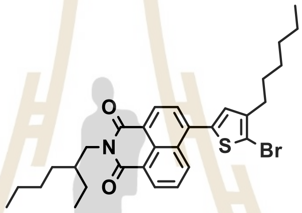

A mixture of (2-ethylhexyl)-6-(4-hexylthiophen-2-yl)-1H-benzo [de] isoquinoline-1,3 (2H)-dione (**61**) (425 mg, 0.89 mmol), THF (15 mL) were added *N*-bromosuccinimide (191 mg, 1.07 mmol). The mixture was stirred at the room temperature for 4 hr. Then the mixture was poured in water 100 mL the aqueous layer was extracted with DCM dry over Na_2SO_4. The solvent was removed and the residue was extracted with CH_2Cl_2/ brine. The residue was purified through column chromatography (silica gel, hexane/dichloromethane, (100/20, v/v) afforded compound **62** as yellow oil with the yield of 82%, ^1H NMR (600 MHz, $CDCl_3$) : δ 8.64-8.62 (d, 1H, *J* = 7.14 Hz, H_{Ar}), 8.60-8.59(d, 1H, *J* = 8.34 Hz, H_{Ar}), 8.58-8.56 (d, H, *J* = 7.56 Hz, H_{Ar}), 7.77-7.75, (t, H, H_{Ar}), 7.03(s, H, H_{Ar}), 4.17-4.09 (m, 2H, $H_{aliphatic}$), 2.67-2.64 (t, 2H, $H_{aliphatic}$), 1.97-1.93 (m, H, $H_{aliphatic}$), 1.69-1.65 (m, 2H, $H_{aliphatic}$), 1.59 (s, H, $H_{aliphatic}$), 1.41-1.28 (m, 14H, $H_{aliphatic}$) 0.98-0.91 (t, 3H, 1 × CH_3,- $H_{aliphatic}$), 0.88-0.86 (t, 6H, 2 ×

$CH_{3,-}$ $H_{aliphatic}$), ^{13}C NMR (600 MHz, $CDCl_3$) δ 163.66, 163.48, 146.48, 145.12, 132.94, 131.39, 130.27, 130.23, 129.92, 128.99, 127.90, 126.82, 125.84, 125.78, 123.40, 122.12, 120.75, 43.22, 36.98, 29.80, 27.73, 23.11, 22.08, 13.08, 9.68, MALDI-TOF (m/z) calcd for $C_{30}H_{36}BrNO_2S$: 553.17, found (M^+).

6,6',6"-((nitrilotris(benzene-4,1-diyl))tris(4-hexylthiophene-5,2-diyl))tris(2-(2-ethyl hexyl)-1H-benzo[de]isoquinoline-1,3(2H)-dione) (**55**)

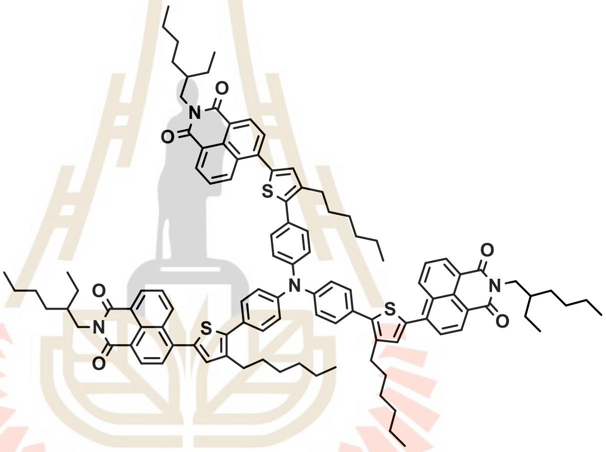

A solution of Tris[4-(4,4,5,5-tetramethyl-1,3,2-dioxaborolan-2-yl) phenyl] amine (**59**) (122 mg, 0.16 mmol), 2,6-Bis(trimethyltin)-4,8-bis(5-(2-ethylhexyl)thiophene-2-yl)benzo[1,2-b,4,-5-b′]thiophene (**62**) (70 mg, 0.07 mmol), Pd(PPh_3)$_4$ (0.2 mmol) and toluene (25 mL) was purged with nitrogen. The reaction mixture was stirred at 110 °C for 24 hr. After cooling, the product was extracted with CH_2Cl_2, washed with water, dried over Na_2SO_4, filtered, concentrated and further purified by column chromatography (silica gel, hexane/ethyl acetate, (50/1, v/v). Then the mixture was sonicated for 1 h, the mixture was filtered, washed with hexane to obtain the product **55** as yellow oil with in a yield of 34%; ^{1}H NMR (600 MHz, $CDCl_3$) δ 8.79-8.77 (d, 2H, J = 7.32 Hz, H_{Ar}), 8.66-8.65, (d, 2H, J = 5.40 Hz, H_{Ar}), 8.61-8.60, (d, 2H, J = 6.12 Hz, H_{Ar}), 7.87-7.86, (d, 2H, J = 6.12 Hz, H_{Ar}), 7.79 (s, 2H, H_{Ar}), 7.48-7.47 (d, 4H, H_{Ar}), 7.30-7.29 (d, 4H, H_{Ar}), 4.16-4.13 (q, 6H, $H_{aliphatic}$), 2.80 (s, 2H $H_{aliphatic}$), 1.97 (s, 3, $H_{aliphatic}$), 1.73 (s, 6H, $H_{aliphatic}$), 1.55 (s, 12H, H_{Ar}), 1.40 (s, 16H, $H_{aliphatic}$), 1.32 (m, 22H, $H_{aliphatic}$), 0.94 (t, 9H, $3 \times CH_{3}$,- $H_{aliphatic}$), 0.89 (t, 9H, $3 \times CH_{3}$,- $H_{aliphatic}$); ^{13}C NMR (600 MHz, $CDCl_3$) δ 164.63, 164.38, 146.79, 140.25, 139.53, 139.21, 137.49, 132.37, 131.57, 131.41, 130.23, 130.15, 129.80, 129.03, 128.90, 128.24, 127.11, 124.31, 123.90, 123.08, 121.73, 44.25, 37.98, 31.65, 30.81, 29.22, 28.98, 24.13, 23.09, 22.62, 14.10, 10.69; MALDI-TOF (m/z) calcd for $C_{108}H_{120}N_{4}O_{6}S_{3}$: 1664.84, found 1664.9880 (M^{+}).

6,6'-((4,8-bis(5-(2-ethylhexyl)thiophen-2-yl)benzo[1,2-b:4,5-b']dithiophene-2,6-diyl)bis(4-hexylthiophene-5,2-diyl))bis(2-(2-ethylhexyl)-1H-benzo[de]isoquinoline-1,3(2H)-dione) (**56**)

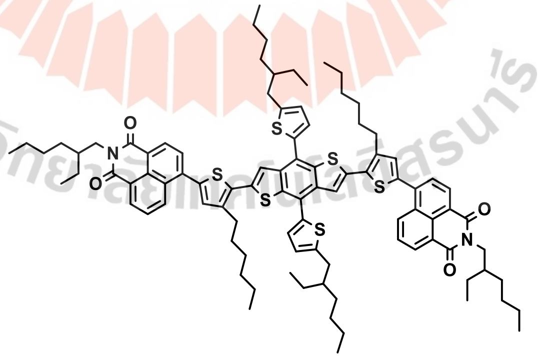

A solution of Tris[4-(4,4,5,5-tetramethyl-1,3,2-dioxaborolan-2-yl) phenyl] amine (**62**) (252 mg, 0.45 mmol), 2,6-Bis(trimethyltin)-4,8-bis(5-(2-ethylhexyl)thiophene-2-yl)benzo[1,2-b,4,-5-b′]thiophene (**76**) (70 mg, 0.07 mmol), $Pd(PPh_3)_4$ (0.2 mmol) and toluene (25 mL) was purged with nitrogen. The reaction mixture was stirred at 110 °C for 24 hr. After cooling, the product was extracted with CH_2Cl_2, washed with water, dried over Na_2SO_4, filtered, concentrated and further purified by column chromatography (silica gel, hexane/ethyl acetate, (50/1, v/v). Then the mixture was sonicated for 1 h, the mixture was filtered, washed with hexane to obtain the product **56** as yellow oil with in a yield of 62%. ^1H NMR (600 MHz, $CDCl_3$) δ 8.74-8.73 (d, 2H, $J = 8.34$ Hz, H_{Ar}), 8.68-8.67, (d, 2H, $J = 6.96$ Hz, H_{Ar}), 8.62-8.61, (d, 2H, $J = 7.38$ Hz, H_{Ar}), 7.86-7.85, (d, 2H, $J = 7.44$ Hz, H_{Ar}), 7.82-7.80 (t, 2H, H_{Ar}), 7.78 (s, 2H, H_{Ar}), 7.40 (s, 2H, H_{Ar}), 7.24 (s, 2H, H_{Ar}), 6.95 (s, 2H, H_{Ar}), 4.20-4.12 (m, 4H, $H_{aliphatic}$), 2.97-2.94 (t, 3H, $H_{aliphatic}$), 2.91-2.90 (d, 2H, H_{Ar}), 1.99-1.98 (t, 2H, $H_{aliphatic}$), 1.78- 1.76 (t, 4H, $H_{aliphatic}$), 1.75-1.71 (t, 2H, $H_{aliphatic}$), 1.60 (s, 3H, $H_{aliphatic}$), 1.48-1.46 (m, 8H, $H_{aliphatic}$), 1.45-1.40 (m, 12H, $H_{aliphatic}$), 1.35 (s, 24H, $H_{aliphatic}$), 0.98-0.96 (t, 12H, $1 \times CH_3$,- $H_{aliphatic}$), 0.92-0.90 (t, 3H, $1 \times CH_3$,- $H_{aliphatic}$); ^{13}C NMR (600 MHz, $CDCl_3$) δ 164.56, 164.29, 146.11, 141.88, 139.23, 138.94, 138.55, 136.98, 136.81, 136.61, 133.47, 132.12, 131.45, 130.71, 129.74, 128.69, 128.32, 127.87, 127.26, 125.52, 123.61, 123.10, 122.10, 122.04, 44.26, 41.53, 37.97, 34.33, 32.56, 31.65, 30.81, 30.72, 29.71, 29.30, 28.95, 28.75, 25.77, 24.13, 23.08, 22.65, 14.14, 14.08, 10.93, 10.68; MALDI-TOF (m/z) calcd for $C_{94}H_{112}N_2O_4S_6$: 1524.69, found 1525.2544 (M^+).

6.2.3 Synthesis for Chapter IV

4,7-bis(4-hexylthiophen-2-yl)-[1,2,5]thiadiazolo[3,4-c] pyridine (**68**)

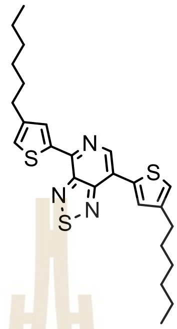

A mixture of 4,7-dibromo-(1,2,5)thidiazole (**67**) (100 mg, 3.40 mmol), 4-Hexyl-2-(4,4,5,5-tetrametyl-1,3,2-dioxaborolan-2-yl)thiophene (**72**) (2.2 equiv, 7.53mmol.), $Pd(PPh_3)_4$ (0.2 mmol), 2M Na_2CO_3 and THF (25 mL) was purged with nitrogen. The reaction mixture was reflux for 24 hr. After cooling, the product was extracted with CH_2Cl_2, washed with water, dried over Na_2SO_4, filtered, concentrated and further purified by column chromatography (silica gel, hexane/ ethyl acetate, (50/ 1, v/ v). Then the mixture was sonicated for 1 h, the mixture was filtered, washed with hexane to obtain the product as **68** as orange powder with the yield of (93 mg, 0.14 mmol) (93%). ^{1}H NMR (600 MHz, $CDCl_3$) : δ 8.80 (s, 1H, H_{Ar}), 8.51 (s, 1H, H_{Ar}), 7.95 (s, 1H, H_{Ar}), 7.20 (s, 1H, H_{Ar}), 7.06 (s, H, H_{Ar}), 2.72-2.68 (q, 4H, Hz, $H_{aliphatic}$), 1.70 (s, 4H, $H_{aliphatic}$), 1.60 (s, 4H, $H_{aliphatic}$), 1.50 (s, 4H, $H_{aliphatic}$), 1.30 (bs, H, $H_{aliphatic}$), 0.98 (t, 6H, $H_{aliphatic}$); ^{13}C NMR (600 MHz, $CDCl_3$) δ 154.94, 149.08, 146.40, 145.25, 144.53, 140.70, 136.23, 133.07, 129.35, 125.68, 120.53, 31.69, 30.68, 30.47, 30.46, 29.69, 29.02, 29.00, 22.62, 14.08; MALDI-TOF (m/z) calcd for $C_{25}H_{31}N_3S_3$:469.17, found 470.2969 (M^+).

4,7-bis(5-bromo-4-hexylthiophen-2-yl)-[1,2,5]thiadiazolo[3,4-c]pyridine (**69**)

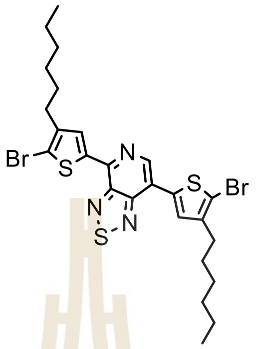

A mixture of 4,7-bis(4-hexylthiophen-2-yl)-[1,2,5]thiadiazole[3,4-c] pyridine (**68**) (1.0 equiv, 7.53mmol.), were added *N*-bromosuccinimide (0.11 mg, 0.63 mmol), THF (15 mL). The mixture was stirred at the room temperature for 4 hr. Then the mixture was poured in water 100 mL the aqueous layer was extracted with DCM dry over Na_2SO_4. The solvent was removed and the residue was extracted with CH_2Cl_2/brine. The residue was purified through column chromatography (silica gel, hexane/dichloromethane, (100/20, v/v). afforded compound **69** with the yield of (80 mg, 0.14 mmol). ^{1}H NMR (600 MHz, $CDCl_3$) : δ 8.70 (s, 1H, H_{Ar}), 8.32 (s, 1H, H_{Ar}), 7.75 (s, 1H, H_{Ar}), 2.64 (d, 4H, $H_{aliphatic}$),1.70 (s, 4H, $H_{aliphatic}$), 1.60 (s, 4H, $H_{aliphatic}$), 1.50 (s, 4H, $H_{aliphatic}$), 1.30 (bs, H, $H_{aliphatic}$), 0.98 (t, 6H, $H_{aliphatic}$); ^{13}C NMR (600 MHz, $CDCl_3$) δ 154.59, 147.70, 145.48, 144.27, 143.34, 140.98, 140.16, 135.94, 132.54, 128.53, 119.86, 116.47, 111.92, 31.62, 29.82, 29.70, 29.65, 28.93, 22.60; 14.08, MALDI-TOF (m/z) calcd for $C_{25}H_{29}Br_2N_3O_3$:624.99, found 624.7553.(M^+).

4,4'-([1,2,5]thiadiazolo[3,4-c]pyridine-4,7-diylbis(3-hexylthiophene-5,2-diyl))bis (N,N-diphenylaniline) (**63**)

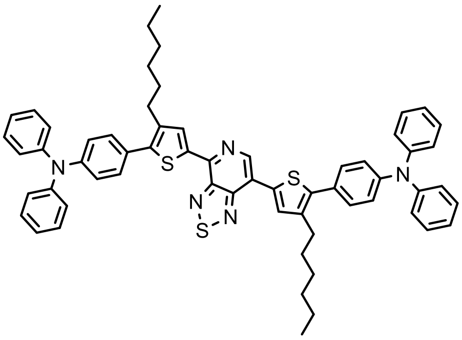

A mixture of 4,7-bis(5-bromo-4-hexylthiophen-2-yl)-[1,2,5] thiadiazolo [3,4-c]pyridine (**69**) (150 mg, 0.52 mmol), 4-(diphenylamino)phenylboronic acid (**72**) (330 mg, 1.44 mmol.), $Pd(PPh_3)_4$ (0.2 mmol), 2M Na_2CO_3 and toluene (25 mL) was purged with nitrogen. The reaction mixture was stirred at 110 °C for 24 hr. After cooling, the product was extracted with CH_2Cl_2, washed with water, dried over Na_2SO_4. The solvent was evaporated to afford a crude product. The crude product was purified by silica gel column chromatography using the eluent mixture of hexane/CH_2Cl_2, (8:2, v/v) to obtain **63** as purple black solid with the yield of (150 mg, 0.64 mmol) (73%), M.p. 187-188 °C. ^{1}H NMR (600 MHz, $CDCl_3$) : δ 8.79 (s, 1H, H_{Ar}), 8.53 (s, 1H, H_{Ar}), 8.00 (s, 1H, H_{Ar}), 7.40-7.42 (m, 2H, J = 8.52 Hz, H_{Ar}), 7.37-7.38 (m, 2H, J = 8.52 Hz, H_{Ar}), 7.28-7.30 (m, 8H, H_{Ar}), 7.14-7.17 (m, 8H, H_{Ar}), 7.12-7.10 (d, 4H, J = 8.46 Hz, H_{Ar}), 7.04-7.07 (q, 4H, H_{Ar}), 2.76-2.71 (m, 4H, $H_{aliphatic}$), 1.74-1.66, (m, 4H, $H_{aliphatic}$), 1.52, (s, 8H, $H_{aliphatic}$), 1.37-1.36 (d, 4H, $H_{aliphatic}$), 1.29-1.28 (t, 9H, 3 × CH_3,- $H_{aliphatic}$), 0.87- 0.85 (t, 9H, 3 × CH_3,- $H_{aliphatic}$); ^{13}C NMR (600 MHz, $CDCl_3$) δ 154.92 148.22, 147.66, 147.51, 147.44, 145.95, 143.72, 140.55, 140.34, 139.96, 139.56, 138.69, 134.54, 134.02, 130.69, 129.90, 129.80,129.38, 129.35, 127.88, 124.90, 124.76, 123.37, 123.25, 122.99, 122.74, 120,10, 31.66, 30.98, 30.93, 29.22, 29.15, 28.95, 22.62, 14.10; MALDI-TOF (m/z) calcd for $C_{61}H_{57}N_5S_3$: 955.38, found 955.7352 (M^+).

4,7-bis(4-hexyl-5-(9-phenyl-9H-carbazol-3-yl)thiophen-2-yl)-[1,2,5]thiadiazolo [3,4-c]pyridine (**64**)

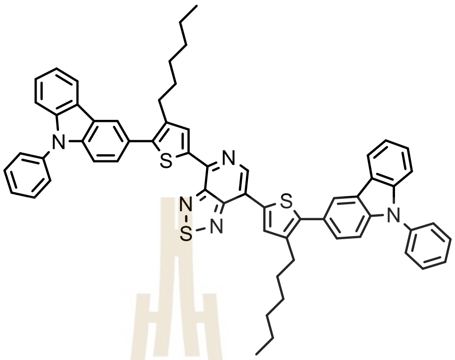

A mixture of 4,7-bis(5-bromo-4-hexylthiophen-2-yl)-[1,2,5] thiadiazolo [3,4-c]pyridine (**69**) (150 mg, 0.23 mmol), 9-phenylcarbazole-3-broronic acid (**75**) (150 mg, 0.52 mmol.), $Pd(PPh_3)_4$ (0.2 mmol), 2M Na_2CO_3 and toluene (25 mL) was purged with nitrogen. The reaction mixture was stirred at 110 °C for 24 hr. After cooling, the product was extracted with CH_2Cl_2, washed with water, dried over Na_2SO_4. The solvent was evaporated to afford a crude product. The crude product was purified by silica gel column chromatography using the eluent mixture of hexane/CH_2Cl_2, (8:2, v/v) to obtain **64** as purple black solid with the yield of (110 mg, 0.28 mmol) (64%), M.p. 147-148 °C. ^1H NMR (600 MHz, $CDCl_3$) : δ 8.79 (s, 1H, H_{Ar}), 8.53 (s, 1H, H_{Ar}), 8.00 (s, 1H, H_{Ar}), 7.41-7.37 (m, 2H, H_{Ar}), 7.28-7.25 (d, 2H, H_{Ar}), 7.16 (d, 8H, H_{Ar}), 7.15-7.14 (d, 4H, H_{Ar}), 7.11-7.10 (d, 8H, H_{Ar}), 7.07 (t, 4H, H_{Ar}), 7.05-7.04 (t, 4H, H_{Ar}), 2.78-2.73 (q, 4H, $H_{aliphatic}$), 1.75-1.69, (q, 4H, $H_{aliphatic}$), 1.54, (s, 17H, $H_{aliphatic}$), 1.39-1.38 (d, 4H, $H_{aliphatic}$), 1.30-1.25 (d, 9H, 3 × CH_3,- $H_{aliphatic}$), 0.87 - 0.85 (t, 9H, 3 × CH_3,- $H_{aliphatic}$); ^{13}C NMR (600 MHz, $CDCl_3$) δ 155.01, 148.27, 146.03, 144.85, 141.41, 141.40, 141.11, 140.59, 140.45, 140.37, 139.60, 138.93, 137.56, 137.52, 134.42, 134.19, 129.97, 127.68, 127.66, 127.50, 127.33, 127.12, 126.16, 126.04, 123.66, 123.63, 121.18, 121.10, 120.48, 120.45,120.31, 120.25, 120.23, 110.02, 109.99, 109.89, 109.82, 31.69, 31.09, 31.05, 29.27, 29.13, 28.95, 22.65, 14.08; MALDI-TOF (m/z) calcd for $C_{61}H_{53}N_5S_3$: 951.35, found 952.6076 (M^+).

4,7-bis(3-hexylthiophen-2-yl)-[1,2,5]thiadiazolo[3,4-c]pyridine (**70**)

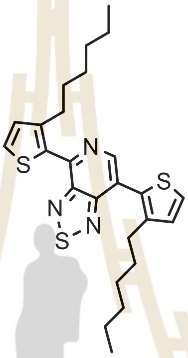

A mixture of 4,7-dibromo-(1,2,5)thidiazole (**67**) (100 mg, 3.40 mmol), 3-Hexyl-2-(4,4,5,5-tetrametyl-1,3,2-dioxaborolan-2-yl)thiophene (**73**) (2.2 equiv, 7.53mmol.), $Pd(PPh_3)_4$ (0.2 mmol), 2M Na_2CO_3 and THF (25 mL) was purged with nitrogen. The reaction mixture was reflux for 24 hr. After cooling, the product was extracted with CH_2Cl_2, washed with water, dried over Na_2SO_4. The solvent was evaporated to afford a crude product. The crude product was purified by silica gel column chromatography using the eluent mixture of hexane/CH_2Cl_2, (8:2, v/v) to obtain **70** as orange powder with the yield of (93 mg, 0.14 mmol) (93%). ^{1}H NMR (600 MHz, $CDCl_3$) : δ 8.80 (s, 1H, H_{Ar}), 8.51 (s, 1H, H_{Ar}), 7.95 (s, 1H, H_{Ar}), 7.20 (s, 1H, H_{Ar}), 7.06 (s, H, $_{Ar}$), 2.72-2.68 (q, 4H, Hz, $H_{aliphatic}$), 1.70 (s, 4H, $H_{aliphatic}$), 1.60 (s, 4H, $H_{aliphatic}$), 1.50 (s, 4H, $H_{aliphatic}$), 1.30 (bs, H, $H_{aliphatic}$), 0.98 (t, 6H, $H_{aliphatic}$); ^{13}C NMR (600 MHz, $CDCl_3$) δ 154.94, 149.08, 146.40, 145.25, 144.53, 140.70, 136.23, 133.07, 129.35, 125.68, 120.53, 31.69, 30.68, 30.47, 30.46, 29.69, 29.02, 29.00, 22.62, 14.08; MALDI-TOF (m/z) calcd for $C_{25}H_{31}N_3S_3$: 469.17, found 470.2969 (M^+).

4,7-bis(5-bromo-3-hexylthiophen-2-yl)-[1,2,5]thiadiazolo[3,4-c] pyridine (**71**)

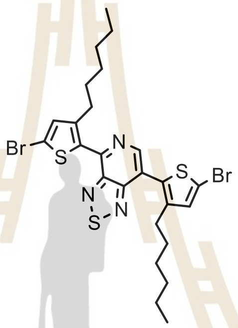

A mixture of 4,7-bis(3-hexylthiophen-2-yl)-[1,2,5] thiadiazolo [3,4-c] pyridine (**70**) (200 mg, 1.02 mmol) were added *N*-bromosuccinimide (0.11 mg, 0.63 mmol), THF (15 mL). The mixture was stirred at the room temperature for 4 hr. Then the mixture was poured in water 100 mL the aqueous layer was extracted with DCM dry over Na_2SO_4. The solvent was removed and the residue was extracted with CH_2Cl_2/brine. The residue was purified through column chromatography (silica gel, hexane/dichloromethane, (100/20, v/v). afforded compound **71** with the yield of (93 mg, 0.14 mmol). ^1H NMR (600 MHz, $CDCl_3$) : δ 8.55 (s, 1H, H_{Ar}), 7.07-7.05 (d, 2H, *J* = 8.80 Hz, H_{Ar}), 3.17-3.15 (t, 2H, $H_{aliphatic}$), 2.63-2.60 (t, 2H, $H_{aliphatic}$), 1.68-1.66 (t, 2H, $H_{aliphatic}$), 1.59-1.57 (t, 2H, $H_{aliphatic}$), 1.37 (s, 5H, $H_{aliphatic}$), 1.35 (s, 2H, $H_{aliphatic}$), 1.28-1.25 (t, 4H, $H_{aliphatic}$), 1.24-1.22 (m, 2H, $H_{aliphatic}$), 0.98 (t, 3 × CH_3,- $H_{aliphatic}$), 0.77 (t, 3 × CH_3,- $H_{aliphatic}$); ^{13}C NMR (600 MHz, $CDCl_3$) δ 156.39, 148.76, 148.35, 144.28, 143.07, 133.22, 132.17, 119.39, 114.26, 113.65, 31.62, 31.51, 30.57, 30.17, 29.46, 29.27, 29.02, 22.55, 22.49, 14.06,13.97; MALDI-TOF (m/z) calcd for $C_{25}H_{29}Br_2N_3O_3$:624.99, found 624.6076 (M^+).

4-(5-(7-(4-(4-(diphenylamino)phenyl)-3-hexylthiophen-2-yl)-[1,2,5]thiadiazolo [3,4-c]pyridin-4-yl)-4-hexylthiophen-2-yl)-N,N-diphenylaniline (**65**)

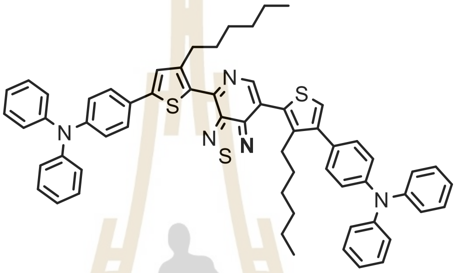

A mixture of 4,7-bis(5-bromo-3-hexylthiophen-2-yl)-[1,2,5] thiadiazolo[3,4-c]pyridine (**71**) (150 mg, 0.52 mmol), 4-(diphenylamino)phenylboronic acid (**72**) (330 mg, 1.44 mmol.), Pd(PPh_3)$_4$ (0.2 mmol), 2M Na_2CO_3 and toluene (25 mL) was purged with nitrogen. The reaction mixture was stirred at 110 °C for 24 hr. After cooling, the product was extracted with CH_2Cl_2, washed with water, dried over Na_2SO_4. The solvent was evaporated to afford a crude product. The crude product was purified by silica gel column chromatography using the eluent mixture of hexane/CH_2Cl_2, (8:2, v/v) to obtain **65** as purple black solid with the yield of (110 mg, 0.56 mmol) (84%), M.p. 130-131 °C. ^1H NMR (600 MHz, $CDCl_3$) : 8.65 (s, 1H, H_{Ar}), 7.61-7.59 (d, 2H, J = 8.22 Hz, H_{Ar}), 7.53-7.52 (d, 2H, J = 8.22 Hz, H_{Ar}), 7.29-7.28 (t, 15H, H_{Ar}), 7.14-7.13 (M, 8H, H_{Ar}), 7.07-7.03 (m, 9H, H_{Ar}), 3.25-3.23. (t, 2H, $H_{aliphatic}$), 2.73-2.71 (t, 2H, $H_{aliphatic}$), 1.76-1.57 (d, 2H, $H_{aliphatic}$), 1.68-1.67 (d, 2H, $H_{aliphatic}$), 1.53, (s, 16H, $H_{aliphatic}$), 1.42-1.41, (d, 2H, $H_{aliphatic}$), 1.31-1.23 (d, 6H, $H_{aliphatic}$), 1.29-1.28 (t, 9H, 3 × CH_3,- $H_{aliphatic}$), 0.87- 0.85 (t, 9H, 3 × CH_3,- $H_{aliphatic}$);

^{13}C NMR (600 MHz, $CDCl_3$) δ 156.63, 149.10, 148.75, 148.16, 147.97, 147.49, 147.38, 144.31, 143.37, 130.86, 129.36, 129.32, 128.35, 127.86, 126.75, 126.60, 126.33, 124.79, 124.73, 124.58, 123.33, 123.15, 119.86, 31.70, 31.61, 31.19, 30.78, 30.36, 29.77, 29.40, 29.18, 22.61, 22.55, 14.11, 14.03; MALDI-TOF (m/z) calcd for $C_{61}H_{57}N_5S_3$: 955.38, found 955.7352 (M^+).

4,7-bis(3-hexyl-5-(9-phenyl-9H-carbazol-3-yl)thiophen-2-yl)-[1,2,5]thiadiazolo [3,4-c]pyridine (**66**)

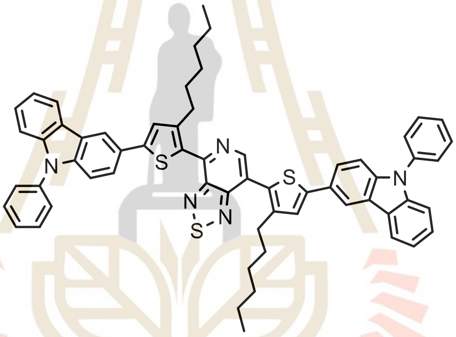

A mixture of 4,7-bis(5-bromo-3-hexylthiophen-2-yl)-[1,2,5]thiadiazolo[3,4-c]pyridine (**71**) (150 mg, 0.52 mmol), 9-phenylcarbazole-3-broronic acid (**75**) (150 mg, 0.52 mmol.), $Pd(PPh_3)_4$ (0.2 mmol), 2M Na_2CO_3 and toluene (25 mL) was purged with nitrogen. The reaction mixture was stirred at 110 °C for 24 hr. After cooling, the product was extracted with CH_2Cl_2, washed with water, dried over Na_2SO_4. The solvent was evaporated to afford a crude product. The crude product was purified by silica gel column chromatography using the eluent mixture of hexane/CH_2Cl_2, (8:2, v/v) to obtain **66** as purple black solid with the yield of (150 mg, 0.14 mmol) (70%). M.p. 121-122°C. ^{1}H NMR (600 MHz, $CDCl_3$) : 8.70 (s, 1H, H_{Ar}), 8.51 (s, 1H, H_{Ar}), 8.42 (s, 1H, H_{Ar}), 8.20-8.22 (d, 1H, *J* =

7.68 Hz, H_{Ar}), 8.18-8.19 (d, 1H, *J* = 7.68 Hz, H_{Ar}), 7.79-7.80 (d, 1H, *J* = 8.34 Hz, H_{Ar}), 7.71-7.73 (d, 1H, *J* = 8.40 Hz, H_{Ar}), 7.60-7.63. (m, 4H, H_{Ar}), 7.57-7.58 (d, 2H, H_{Ar}), 7.47-7. 49 (m, 2H, H_{Ar}), 7.40-7.41 (d, 6H, H_{Ar}), 7.38- 7.39 (d, 2H, *J* = 6.72 Hz, H_{Ar}), 7.30-7.33, (m, 2H, H_{Ar}), 3.30-3.28 (t, 2H, $H_{aliphatic}$), 2.79-2.77 (t, 2H, $H_{aliphatic}$), 1.84-1.83 (d, 2H, $H_{aliphatic}$), 1.80-1.79 (d, 15H, $H_{aliphatic}$), 1.77-1.76 (m, 2H, $H_{aliphatic}$), 1.34-1.41, (d, 2H, $H_{aliphatic}$), 1.29-1.28 (t, 9H, 3 × CH_3,- $H_{aliphatic}$), 0.87- 0.85 (t, 9H, 3 × CH_3,- $H_{aliphatic}$); ^{13}C NMR (600 MHz, $CDCl_3$) δ 156.75, 149.53, 149. 18, 149.03, 148.81, 146.30, 144.38, 143.45, 141.50, 140.62, 137.53, 137.46, 130.77, 129.99, 129.96, 128.19, 127.64, 127.10, 126.47, 126.41, 126.32, 124.84, 124.43, 124.40, 123.94, 123.88, 123.32, 120.59, 120.35, 120.24, 117.91, 117.71, 110.19, 110.13, 110.05, 110.00, 77.22, 77.00, 76.79, 76.79, 31.74, 31.65, 31.31, 30.88, 30.45, 29.87, 29.70, 29.50, 22.65, 22.59, 14.13, 14.05; MALDI-TOF (m/z) calcd for $C_{61}H_{53}N_5S_3$: 951.35, found 952.6076 (M^+).

6.2.4 Synthesis for Chapter V

4, 9-bis(4-hexylthiophen-2-yl)naphtho[2,3-c][1,2,5]thiadiazole (**78**)

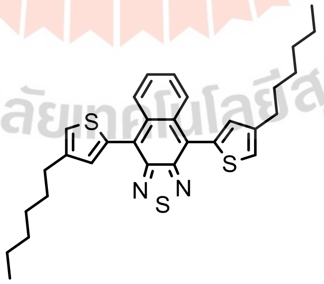

A mixture of 4,9-dibromonaphtho[2,3-c][1,2,5]thiadiazole (**77**) (1.0 g, 2.9 mmol), 4-Hexyl-2-(4,4,5,5-tetrametyl-1,3,2-dioxaborolan-2-yl)thiophene (**72**) (2.5 equiv, 7.40 mmol.), $Pd(PPh_3)_4$ (0.2 mmol), 2M Na_2CO_3 and THF (25 mL) was purged with nitrogen. The reaction mixture was stirred and reflux for 24 hr. After cooling, the product was extracted with CH_2Cl_2, washed with water, dried over Na_2SO_4. The solvent was evaporated to afford a crude product. The crude product was purified by silica gel column chromatography using the eluent mixture of hexane/CH_2Cl_2, (8:2, v/v) to obtain **78** as orang solid with the yield of (1.50 g, 0.14 mmol) (84%). ^{1}H NMR (600 MHz, $CDCl_3$) : δ 8.31 - 8.32 (q, 2H, J = 1.26Hz, H_{Ar}), 7.40-7.42(q, 2H, J = 1.26Hz, H_{Ar}), 7.28 (s, 2H, H_{Ar}), 7.25 (s, 2H, H_{Ar}), 1.35 (s, 10H, , $H_{aliphatic}$), 0.91 (t, 6H, 2 × CH_3,- $H_{aliphatic}$), ^{13}C NMR (600 MHz, $CDCl_3$) δ 154.34, 148.08, 146.40, 145.25, 144.53, 140.70, 136.23, 133.07, 129.35, 125.68, 126.82, 120.53, 31.69, 30.68, 30.58, 30.45, 30.46, 29.69, 29.02, 29.00, 22.62, 14.06, MALDI-TOF (m/z) calcd for $C_{30}H_{34}N_2S_3$: 518.19, found 518.7352 (M^+).

4, 9-bis(5-bromo-4-hexylthiophen-2-yl)naphtho[2,3-c][1,2,5] thiadiazole (**79**)

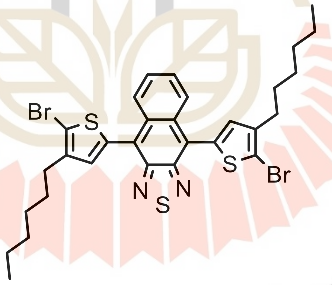

A mixture of 4, 9-bis(4-hexylthiophen-2-yl)naphtho[2,3-c][1,2,5]thiadiazole (**78**) (200 mg, 1.02 mmol) were added *N*-bromosuccinimide (0.11 mg, 0.63 mmol), THF (15 mL). The mixture was stirred at the room temperature for 4 hr. Then the mixture was poured in water 100 mL the aqueous layer was extracted with DCM dry over Na_2SO_4. The solvent was removed and the residue was extracted with CH_2Cl_2/brine. The residue was purified through column chromatography (silica gel, hexane/dichloromethane, (100/20, v/v). afforded compound **79** with the yield of (93 mg, 0.14 mmol). ^{1}H NMR (600 MHz,

$CDCl_3$) : δ 8.31-8.32 (q, 2H, H_{Ar}), 7.40-7.42 (q, 2H, H_{Ar}), 7.28 (s, 2H, H_{Ar}), 7.25 (s, 2H, H_{Ar}), 2.75-2.77 (t, 4H, $H_{aliphatic}$), 1.73-1.76 (t, 4H, $H_{aliphatic}$), 1.44 (s, 4H, $H_{aliphatic}$), 1.35 (m, 10H, $H_{aliphatic}$), 0.91 (t, 2 × CH_3, $H_{aliphatic}$).

4,9-bis(3,4'-dihexyl-[2,2'-bithiophen]-5-yl)naphtho[2,3-c][1,2,5]thiadiazole (**80**)

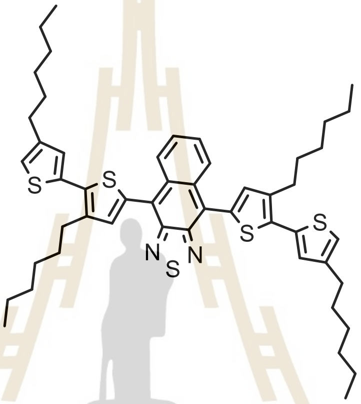

A mixture of 4, 9-bis(5-bromo-4-hexylthiophen-2-yl)naphtho[2,3-c][1,2,5]thia diazole (**79**) (200 mg, 1.02 mmol), 4-Hexyl-2-(4,4,5,5-tetrametyl-1,3,2-dioxaborolan-2-yl) thiophene (2.5 equiv, 7.40 mmol.), $Pd(PPh_3)_4$ (0.2 mmol), 2M Na_2CO_3 and THF (25 mL) was purged with nitrogen. The reaction mixture was stirred and reflux for 24 hr. After cooling, the product was extracted with CH_2Cl_2, washed with water, dried over Na_2SO_4. The solvent was evaporated to afford a crude product. The crude product was purified by silica gel column chromatography using the eluent mixture of hexane/CH_2Cl_2, (8:2, v/v) to obtain **80** as orang solid with the yield of (480 mg, 0.32 mmol) (84%). ^1H NMR (600 MHz, $CDCl_3$) : δ 8.30-8.32 (q, 2H, H_{Ar}), 7.42-7.44 (q, 2H, H_{Ar}), 7.14 (s, 2H, H_{Ar}), 6.75 (s, 2H, H_{Ar}), 2.69-2.71 (t, 4H, $H_{aliphatic}$), 2.47-2.49 (m, 2H, $H_{aliphatic}$), 1.73-1.76 (t, 4H, $H_{aliphatic}$), 1.44 (s, 4H, $H_{aliphatic}$), 1.35 (m, 10H, $H_{aliphatic}$), 0.91 (t, 4 × CH_3, $H_{aliphatic}$).

4,9-bis(5'-bromo-3,4'-dihexyl-[2,2'-bithiophen]-5-yl)naphtho[2,3-c][1,2,5] thiadiazole (**81**)

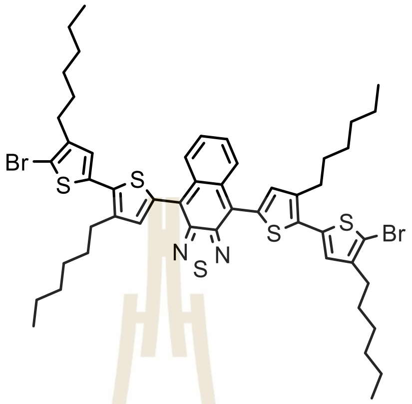

A mixture of 4,9-bis(3,4'-dihexyl-[2,2'-bithiophen]-5-yl)naphtho[2,3-c][1,2,5]thia- diazole (**80**) (200 mg, 1.02 mmol), were added *N*-bromosuccinimide (0.11 mg, 0.63 mmol), THF (20 mL). The mixture was stirred at the room temperature for 4 hr. Then the mixture was poured in water 100 mL the aqueous layer was extracted with DCM dry over Na_2SO_4. The solvent was removed and the residue was extracted with CH_2Cl_2/brine. The residue was purified through column chromatography (silica gel, hexane/dichloromethane, (100/20, v/v). afforded compound **81** with the yield of (93 mg, 0.14 mmol). ^{1}H NMR (600 MHz, $CDCl_3$) : δ 8.55 (s, 1H, H_{Ar}), 7.07-7.05 (d, 2H, *J* = 7.70 Hz, H_{Ar}), 3.17-3.15 (t, 2H, $H_{aliphatic}$), 2.63-2.60. MALDI-TOF (m/z) calcd for $C_{50}H_{60}Br_2N_2S_5$: 1006.17, found 1,006.3066 (M^+).

4,4'-(naphtho[2,3-c][1,2,5]thiadiazole-4,9-diylbis(3',4-dihexyl-[2,2'-bithiophene]-5',5-diyl))bis(N,N-diphenylaniline) (**67**)

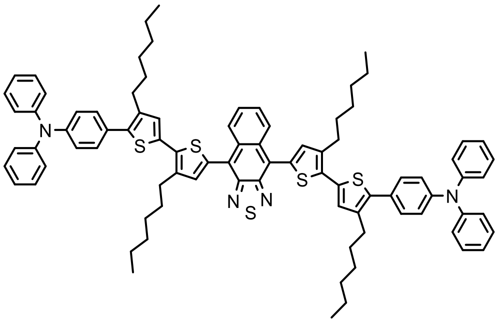

A mixture of 4, 9-bis(5-bromo-4-hexylthiophen-2-yl)naphtho[2,3-c][1,2,5] thiadiazole (**81**) (1.0 equiv, 0.14 mmol.), 4-(diphenylamino)phenylboronic acid (**72**) (2.5 equiv, 0.37 mmol) $Pd(PPh_3)_4$ (0.2 mmol), 2M Na_2CO_3 and THF (25 mL) was purged with nitrogen. The reaction mixture was stirred and reflux for 24 hr. After cooling, the product was extracted with CH_2Cl_2, washed with water, dried over Na_2SO_4. The solvent was evaporated to afford a crude product. The crude product was purified by silica gel column chromatography using the eluent mixture of hexane/CH_2Cl_2, (8:2, v/v) to obtain **67** as orang solid with the yield of (250 mg, 0.18 mmol) (54%). ^1H NMR (600 MHz, $CDCl_3$) : ^1H NMR (600 MHz, $CDCl_3$) : δ 8.49 - 8.48 (d, 2 H, J = 6.42 Hz, H_{Ar}), 7.45 - 7.44 (d, 6H, J = 7.62 Hz, H_{Ar}), 7.36 (s, 2H, H_{Ar}), 7.30 - 7.27 (t, 9H, H_{Ar}), 7.17 - 7.15 (d, 8H, H_{Ar}), 7.13 -7.12 (d, 4H, H_{Ar}), 7.06 - 7.04 (t, 4H, , H_{Ar}), 2.8, 8H, $H_{aliphatic}$), 3 - 2.81 (t, 6H, $H_{aliphatic}$), 1.74 – 1.72 (t, 6H, $H_{aliphatic}$), 1.42 - 1.40 (bs, 8H, $H_{aliphatic}$), 1.32 - 1.28 (m, 18H, $H_{aliphatic}$), 1.25 (m, 14H, $H_{aliphatic}$), 0.89 -0.87 (t, 18H, $H_{aliphatic}$); ^{13}C NMR (600 MHz, $CDCl_3$) δ 151.47, 143.69, 139.42, 135.45, 134.10, 134.04, 133.61, 132.77, 127.63, 126.91, 123.22, 120.35, 31.70, 30.65, 30.42, 29.45, 29.31, 22.66, 22.62, 14.08; MALDI-TOF (m/z) calcd for $C_{86}H_{88}N_4S_5$: 1336.56, found 1348.4917 (M^+).

4,9-bis(3,4',4''-trihexyl-[2,2':5',2''-terthiophen]-5-yl)naphtho[2,3-c][1,2,5] thiadiazole (**82**)

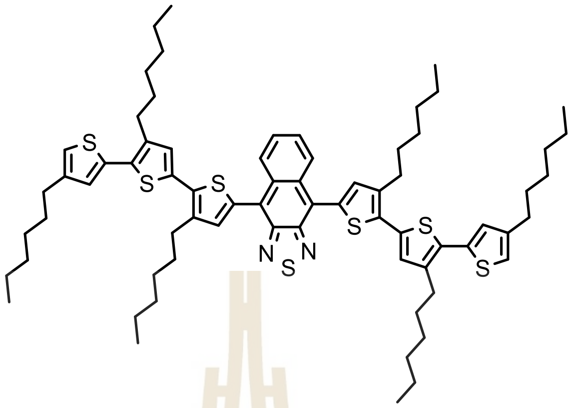

A mixture of 4,9-bis(4-hexylthiophen-2-yl)naphtho[2,3-c][1,2,5] thiadiazole (**81**) (200 mg, 1.02 mmol), were added *N*-bromosuccinimide (0.11 mg, 0.63 mmol), THF (20 mL). The mixture was stirred at the room temperature for 4 hr. Then the mixture was poured in water 100 mL the aqueous layer was extracted with DCM dry over Na_2SO_4. The solvent was removed and the residue was extracted with CH_2Cl_2/brine. The residue was purified through column chromatography (silica gel, hexane/dichloromethane, (100/20, v/v). afforded compound **82** with the yield of (56 mg, 0.32 mmol) (40%). ^{1}H NMR (600 MHz, $CDCl_3$) : δ 8.55 : δ 8.31-8.32 (q, 2H, H_{Ar}), 7.40-7.42 (q, 2H, H_{Ar}), 7.28 (s, 2H, H_{Ar}), 7.25 (s, 2H, H_{Ar}), 2.75-2.77 (t, 4H, $H_{aliphatic}$), 1.73-1.76 (t, 4H, $H_{aliphatic}$), 1.44 (s, 4H, $H_{aliphatic}$), 1.35 (m, 10H, $H_{aliphatic}$), 0.91 (t, 2 × CH_3, $H_{aliphatic}$). MALDI-TOF (m/z) calcd for $C_{86}H_{88}N_4S_7$: 1182.51, found 11182.4550 (M^+).

4,9-bis(5''-bromo-3,4',4''-trihexyl-[2,2':5',2''-terthiophen]-5-yl)naphtho[2,3-c] [1,2,5]thiadiazole (**83**)

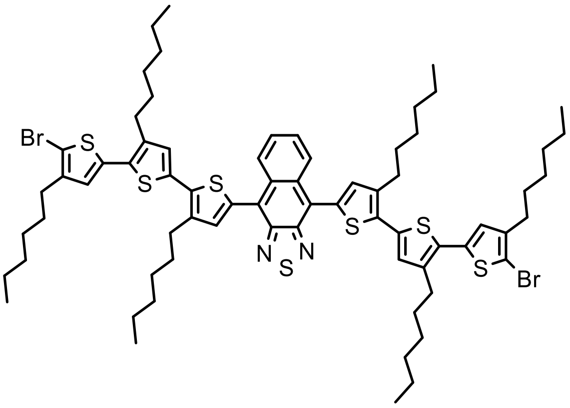

A mixture of 4,9-bis(4-hexylthiophen-2-yl)naphtho[2,3-c][1,2,5] thiadiazole (**82**) (200 mg, 1.02 mmol), were added *N*-bromosuccinimide (0.11 mg, 0.63 mmol), THF (20 mL). The mixture was stirred at the room temperature for 4 hr. Then the mixture was poured in water 100 mL the aqueous layer was extracted with DCM dry over Na_2SO_4. The solvent was removed and the residue was extracted with CH_2Cl_2/brine. The residue was purified through column chromatography (silica gel, hexane/dichloromethane, (100/20, v/v). afforded compound **83** with the yield of (93 mg, 0.14 mmol) (67%). MALDI-TOF (m/z) calcd for $C_{70}H_{88}Br_2N_2S_7$: 1338.34, found 1339.4917 (M^+).

4,4'-(naphtho[2,3-c][1,2,5]thiadiazole-4,9-diylbis(3',3",4-trihexyl-[2,2':5',2"-terthio phene]-5",5-diyl))bis(N,N-diphenylaniline) (**68**)

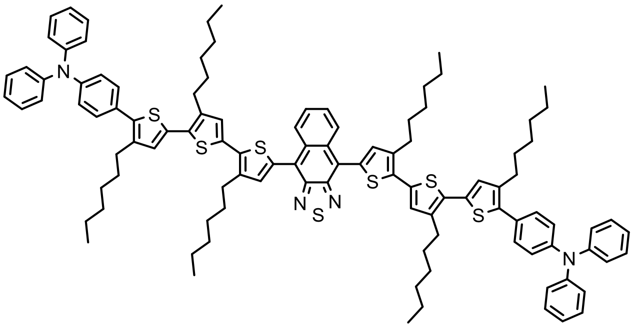

A mixture of 4, 9-bis(5-bromo-4-hexylthiophen-2-yl)naphtho[2,3-c][1,2,5] thiadiazole (**83**) (1.0 equiv, 0.09 mmol.), 4-(diphenylamino)phenylboronic acid (2.2 equiv, 0.19 mmol) $Pd(PPh_3)_4$ (0.2 mmol), 2M Na_2CO_3 and THF (30 mL) was purged with nitrogen. The reaction mixture was stirred and reflux for 24 hr. After cooling, the product was extracted with CH_2Cl_2, washed with water, dried over Na_2SO_4. The solvent was evaporated to afford a crude product. The crude product was purified by silica gel column chromatography using the eluent mixture of hexane/CH_2Cl_2, (8:2 v/v) to obtain **68** as orang solid 35%. ^{1}H NMR (600 MHz, $CDCl_3$) : δ 8.49 - 8.48 (dd, 2 H, H_{Ar}), 7.45 - 7.44 (d, 6H, *J* = 8.60 Hz, H_{Ar}), 7.36 (s, 2H, H_{Ar}), 7.30 - 7.27 (t, 9H, H_{Ar}), 7.17 - 7.15 (d, 8H, *J* = 7.74 Hz, H_{Ar}), 7.13 -7.12 (d, 4H, *J* = 8.64 Hz, H_{Ar}), 7.06 - 7.04 (t, 4H, , H_{Ar}), 2.8, 8H, $H_{aliphatic}$), 3 - 2.81 (t, 6H, $H_{aliphatic}$), 1.74 – 1.72 (t, 6H, $H_{aliphatic}$), 1.42 - 1.40 (bs, 8H, $H_{aliphatic}$), 1.32 - 1.28 (m, 18H, $H_{aliphatic}$), 1.25 (m, 14H, $H_{aliphatic}$), 0.89 -0.87 (t, 18H, $H_{aliphatic}$); ^{13}C NMR (600 MHz, $CDCl_3$) δ 151.53, 147.59, 147.25, 140.73, 138.42, 133.91, 133.29, 132.78, 130.04, 129.34, 128.19, 127.27, 126.77, 124.71, 123.16, 123.09, 31.70, 31.00,29.70, 29.01, 22.64, 14.10; MALDI-TOF (m/z) calcd for $C_{106}H_{116}N_4S_7$: 1664.72, found 1665.7152 (M^+).

6.3 Expected results

The expected results of the proposed thesis work will be as follows:

1 The novel OLEDs based on 1,8- naphthalimide derivatives as emissive hole transporting material with high performance will be achieved.

2 A research report will be published in an international journal.

REFERENCES

REFERENCES

Adachi, C. (2014). Third-generation organic electroluminescence materials. **Japanese Journal of Applied Physics**. 53(6): 060101-1-060101-11.

Arunchai, R., Sudyoadsuk, T., Prachumrak, N., Namuangruk, S., Promarak, V., Sukwattanasinitta, M. and Rashatasakhon, P. (2015). Synthesis and characterization of new triphenylamino-1,8-naphthalimides for organic light-emitting diode applications. **New Journal of Chemistry**. 39: 2807-2814.

Bagher, S. M. (2014). OLED display technology. **American Journal of Optics and Photonics**. 2(3): 32-36.

Baleizão, C. and Berberan-Santos, M. N. (2008). Thermally activated delayed fluorescence in fullerenes. **Annals of the New York Academy of Sciences**. 1130(1): 224-234.

Berberan-Santos, M. N. and Garcia, J. M. M. (1996). Unusually strong delayed fluorescence of C_{70}. **Journal of the American Chemical Society**. 118(39): 9391-9394.

Blasse, G. and McMillin, D. R. (1980). **Chemical Physics Letters**. 70: 1-3.

Burn, P. L., Lo, S. C. and Samuel, I. D. W. (2007). The development of light-emitting dendrimers for displays. **Advanced Materials**. 19(13): 1675-1688.

Chihaya, A., Marc, A. B., Mark, E. T. and Stephen, R. F. (2011). Nearly 100 % internal phosphorescence efficiency in an organic light-emitting device. **Journal of Applied Physics**. 90: 5048-5051.

Endo, A., Ogasawara, M., Takahashi, A., Yokoyama, D., Kato, Y. and Adachi, C. (2009). Thermally activated delayed fluorescence from Sn^{4+}-porphyrin complexes and their application to organic light-emitting diodes - a novel mechanism for electroluminescence. **Advanced Materials**. 21(47): 4802-4806.

Endo, A., Sato, K., Yoshimura, K., Kai, T., Kawada, A., Miyazaki, H. and Adachi, C. (2011). Efficient up-conversion of triplet excitons into a singlet state and its application for organic light emitting diodes. **Applied Physics Letters**. 98(8): 083302-1-083302-3.

Gaj, M. P., Hernandez, C. F., Zhang, Y., Marder, S. R. and Kippelen, B. (2015). Highly efficient organic light-emitting diodes from thermally activated delayed fluorescence using a sulfone-carbazole host material. **Organic Electronics**. 16: 109-112.

Graham, K. R., Yang, Y., Sommer, J. R., Shelton, A. H., Schanze, K. S., Xue, J. and Reynolds, J. R. (2011). Extended conjugation platinum(II) porphyrins for use in near-infrared emitting organic light emitting diodes. **Chemistry of Materials**. 23(24): 5305-5312.

Goushi, K., Yoshida, K., Sato, K. and Adachi, C. (2012). Organic light-emitting diodes employing efficient reverse intersystem crossing for triplet-to-singlet state conversion. **Nature Photonics**. 6(4): 253-258.

Gudeika, D., Grazulevicius, J. V., Sini, G., Bucinskas, A., Jank, V. and Miasojedovas, A., (2014). New derivatives of triphenylamine and naphthalimide as ambipolar organic semiconductors: Experiment and theoretical approach. **Dyes and Pigments**. 106: 58-70.

Gudeika, D., Sini, G., Jankauskas, V., Sych, G. and Grazulevicius, J. V. (2016). Synthesi and properties of the derivatives of triphenylamine and 1,8-naphthalimide with the olefinic linkages between chromophores **The Royal Society of ChemistryAdvances** 6: 2191-2201.

Heeger, A. J., MacDiarmid, A. G., Shirakawa, H., Louis, E. J. and Chiang, C. K. (1987). Synthesis of electrically conducting organic polymers: Halogen derivatives of polyacetylene, $(CH)_x$. **Journal of the Chemical Society, Chemical Communications**. 16: 578-580.

Hung, S. L and Chen, H. C. (2002). Recent progress of molecular organic electroluminescent materials and devices. **Materials Science and Engineering R**. 39: 143-222.

Hidayath, U., Raveendra, K., Bhadrachar, G. and Satyanrayan, N. (2014) Blue organic light emitting materials: Synthesis and characterization of novel 1,8-naphthalimide derivatives. **Optical Materials** 36: 704-711.

Ishiyama, T., Miyaura, N. and Suzuki, A. (1991) Synthesis of functionalized organotin compounds via palladium-catalyzed cross-coupling reaction of aryl or 1-alkenyl halides with 9-(ω-Stannylalkyl)-9-borabicyclo [3.3.1] nonanes. **Synthesis letter**, 10: 687-688.

Kallmann, H. and Pope, M. (1960). Bulk conductivity in organic crystals. **Nature**. 186: 31-33.

Kawamura, Y., Goushi, K., Brooks, J., Brown, J. J., Sasabe, H. and Adachi, C. (2005). 100 % phosphorescence quantum efficiency of Ir(III) complexes in organic semiconductor films. **Applied Physics Letters**. 86(7): 071104-1-071104-3.

Klajnert, B. and Bryszewska, M. (2001). Dendrimers: Properties and applications. **Acta Biochimica Polonica**. 48(1): 199-208.

Kohn, W. and Sham, L. (1965). Self-consistent equations including exchange and correlation effects. **American Physical Society**. 140: A1133.

Lee, G. H. and Kim, Y. S. (2016). High-efficiency diphenylsulfone derivative based organic light- emitting diode exhibiting thermally- activated delayed fluorescence. **Journal of the Korean Physical Society**. 69(3): 398-401.

Lee, S. B., Park, K. H., Joo, C. W., Lee, J. and Kim, Y. (2016). Highly twisted pyrene derivatives for non-doped blue OLEDs. **Dyes and Pigments**. 128: 19-25.

Li, J., Liao, X., Xu, H., Li, L., Zhang, J., Wang, H. and Xu, B. (2017). Deep-blue thermally activated delayed fluorescence dendrimers with reduced singlet-triplet energy gap for low roll-off non-doped solution-processed organic light-emitting diodes. **Dyes and Pigments**. 140: 79-86.

Li, W. S. and Aida, T. (2009). Dendrimerporphyrins and phthalocyanines. **Chemical Reviews**. 109(11): 6047-6076.

Lussem, B., Riede, M. and Leo, K. (2013). Doping of organic semiconductors. **Physica status solidi (a)**. 210(1): 9-43.

Nakagawa, T., Ku, S. Y., Wong, K. T. and Adachi, C. (2012). Electroluminescence based on thermally activated delayed fluorescence generated by a spirobifluorene donor-acceptor structure. **Chemical Communications**. 48(77): 9580-9582.

Mi-Seon, S., Quynh, B. N., Chang, H. S., Duckhee, L.and Kyu, Y. C. (2013). Synthesis of Some Green Dopants for OLEDs Based on Arylamine 2, 3-disubstituted Bithiophene Derivatives. **Molecules**. 18: 14033-14041

Miyaura, N., Yanagi, T. and Suzuki, A. (1981). The palladium-catalyzed coss-coupling reaction of phenylboronic acid with haloarenes in the presence of bases. **Synthetic Communication**. 11(7): 513-519.

Meng, L., Wang, H., Wei, X., Liu, J., Chen, Y., Kong, X., Lv, X., Wang, P. and Wang, Y. (2016). Highly efficient non doped organic light emitting diodes based on thermally activated delayed fluorescence emitter with quantum-well structure. **ACS Applied Materials & Interfaces**. 8: 20955-20961.

Monçalves, M., Rampon, D. S., Schneider, P. H., Rodembusch, F. S. and Silveira, C. C. (2013). Divinyl sulfides/sulfones-based D-π-A-π-D dyes as efficient non-aromatic bridges for π-conjugated compounds. **Dyes and Pigments**. 102: 71-78.

Muangpaisal, R., Ho, C. M., Huang, H. T., Chen, H. C. and Tsai, C. (2014), Tetrasubstitued-pyrene derivatives for electroluminescent application. **Organic Electronic**. 15: 2148-2157.

Quirino, W. G, Legnani, C., Cremona, M, Lima, P. P, Junior, S. A. and Malta, O. L. (2009). White OLED using β-diketones rare earth binuclear complex as emitting layer. **Thin Solid Film.** 494: 23-27.

Rajamalli, P., Senthilkumar, N., Gandeepan, P., Huang, P. Y., Huang, M. J., Wu, C. Z., Yang, C. Y., Chiu, M. J., Chu, L. K., Lin, H. W. and Cheng, C. H. (2016). A new molecular design based on thermally activated delayed fluorescence for highly efficient organic light emitting diodes. **Journal of the American Chemical Society**.138: 628-634.

Reghu, R. R., Simokaitiene, J., Grazulevicius, V. J., Raisys, S., Kazlauskas, K., Jursenas, S., Jankauskas, V.and Reina, A. (2015). Synthesis and properties if hole transporting triphenylamine- derived dendritic compounds. **Dyes and Pigments**. 115: 135-142.

Scheuble, M., Goll, M. And Ludwigs, S. (2015). Branched terthiophenes in organic electronics: From small molecules to polymers. **Macro molecular Rapid Communications**. 36(2): 115-137.

Schlaf, R., Murata, H. and Kafafi, Z. H. (2001). Work function measurements on indium tin oxide films. **Journal of Electron Spectroscopy and Related Phenomena**. 120(1): 149-154.

Schmidbauer, S., Hohenleutner, A. and König, B. (2013). Studies on the photodegradation of red, green and blue phosphorescent OLED emitters. **Beilste in Journal of Organic Chemistry**. 9: 2088-2096.

Segura, J. L. (1998). The chemistry of electroluminescent organic materials. **Acta Polymerica**. 49(7): 319-344.

Sharma, G. D., Reddy, M. A., Ganesh, K. Singh, S.P. and Chandrasekharam, M. (2014). Indole and triisopropyl phenyl as capping units for a diketopyrrolopyrrole (DPP) acceptor central unit: an efficient D-A-D type small molecule for organic solar cells. **The Royal Society of Chemistry Advances**. 4: 732-742.

Shinde, K. N., Dhoble, S. J., Swart, H. C. and Park, K. (2012). Phosphate phosphors for solid-state lighting. **Springer-Verlag Berlin Heidelberg**.

Shirota, Y. (2000). Organic materials for electronic and optoelectronic devices. **Journal of Materials Chemistry C**. 10: 1-25.

Shuai, L. F., Li, Y., Wang, X. L., Chengjian, Z. and Yixiang, C. (2017). Circularly polarized luminescence of chiral 1,8-naphthalimide-based pyrene fluorophore induced via supramolecular self-assembly. **Journal of Materials Chemistry C**. 5: 6030-6036.

Suzuki, A. (2004) Organoborane coupling reactions (Suzuki coupling). **Proceeding of the Japan Academy, Series B**. 80(8): 359-371.

Tanaka, H., Shizu, K., Miyazaki, H. and Adachi, C. (2012). Efficient green thermally activated delayed fluorescence (TADF) from a phenoxazine-triphenyltriazine (PXZ-TRZ) derivative. **Chemical Communications**. 48(93): 11392-11394.

Tang, T. W. and VanSlyke, S. A. (1987). Organic electroluminescent diodes. **Applied Physics Letters**. 51(12): 913-915.

Tao, Y., Yuan, K., Chen, T., Xu, P., Li, H., Chen, R., Zheng, C., Zhang, L. and Huang, W. (2014). Thermally activated delayed fluorescence materials towards the breakthrough of organo electronics. **Advanced Materials**. 26(47): 7931-7958.

Thejokalyani, T. and Dhoble, S. J. (2014). Novel approaches for energy efficient solid state lighting by RGB organic light emitting diodes - A review. **Renewable and Sustainable Energy Reviews**. 32: 448-467.

Thejokalyani, T. and Dhoble, S. J. (2015). Novel materials for fabrication and encapsulation of OLEDs. **Renewable and Sustainable Energy Reviews**. 44: 319-347.

Thirion, D., Berthelot, J. R., Vignau, L. and Poriel, C. (2011). Synthesis and properties of a blue bipolarindeno fluorene emitter based on a D-π-A Design. **Organic Letters**. 13(16): 4418-4421.

Tsujimura, T. (2012). **OLED displays: fundamentals and applications**. Singapore: John Wiley & Sons, Inc.

Uoyama1, H., Goushi, K., Shizu1, K., Nomura1, H. and Adachi, C. (2012). Highly efficient organic light-emitting diodes from delayed fluorescence. **Nature**. 492: 234-238.

Valeur, B. (2001). **Molecular fluorescence principles and applications**. Germany: Wiley-VCH Verlag GmbH.

Valeur, B. and Berberan-Santos, M. N. (2011). A brief history of fluorescence and phosphorescence before the emergence of quantum theory. **Journal of Chemical Education**. 88: 731-738.

Wang, H., Xie, L., Peng, Q., Meng, L., Wang, Y., Yi, Y. and Wang, P. (2014). Novel thermally activated delayed fluorescence materials-thioxanthone derivatives and their applications for highly efficient OLEDs. **Advanced Materials**. 26(30): 5198-5204.

Wyckhoff, R. (1963). Crystal structures. **NewYork Wiley**. 1: 28.

Wong, M. Y., Hedley, G. J., Xie, G., Kölln, L. S., Samuel, I. D. W., Pertegás, A., Bolink, H. J. and Colman, E. Z. (2015). Light-emitting electrochemical cells and solution-processed organic light-emitting diodes using small molecule organic thermally activated delayed fluorescence emitters. **Chemistry of Materials.** 27(19): 6535-6542.

Wu, S., Aonuma, M., Zhang, Q., Huang, S., Nakagawa, T., Kuwabara, K. and Adachi, C. (2014). High-efficiency deep-blue organic light-emitting diodes based on a thermally activated delayed fluorescence emitter. **Journal of Materials Chemistry C**. 2(3): 421-424.

Zhang, Q., Li, B. Huang, S., Nomura, H., Tanaka, H. and Adachi, C. (2014). Efficient blue organic light-emitting diodes employing thermally activated delayed fluorescence. **Nature Photonics**. 8(4): 326-332.

Zhang, Q., Li, J., Shizu, K., Huang, S., Hirata, S., Miyazaki, H. and Adachi, C. (2012). Design of efficient thermally activated delayed fluorescence materials for pure blue organic light emitting diodes. **Journal of the American Chemical Society**. 134(36): 14706-14709.

Zhong, C., Duan, C., Huang, F., Wu, H. and Cao, Y. (2011). Materials and devices toward fully solution processable organic light-emitting diodes. **Chemistry of Materials**. 23(3): 326-340.

APPENDICES

APPENDIX A

DSC ANALYSIS OF COMPOUND 49

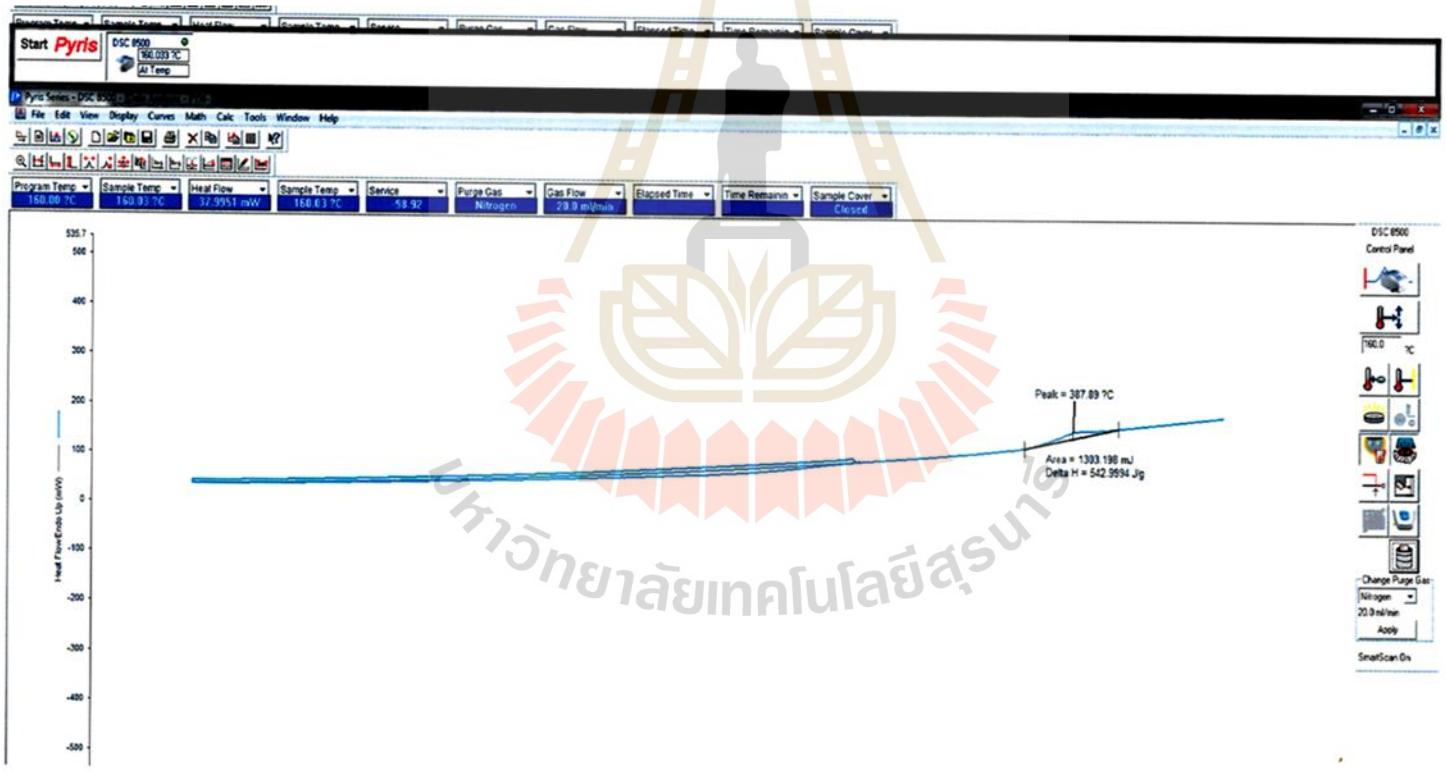

DSC 8500: 160.033 °C, At Temp

Program Temp: 160.00 °C

Sample Temp: 160.03 °C

Heat Flow: 37.9951 mW

Sample Temp: 160.03 °C

Service: 58.92

Purge Gas: Nitrogen

Gas Flow: 20.0 ml/min

Elapsed Time:

Time Remainin:

Sample Cover: Closed

Peak = 387.89 °C

Area = 1303.198 mJ

Delta H = 542.9994 J/g

Control Panel temperature: 160.0 °C

Change Purge Gas: Nitrogen, 20.0 ml/min

SmartScan On

APPENDIX B

DSC ANALYSIS OF COMPOUND 50

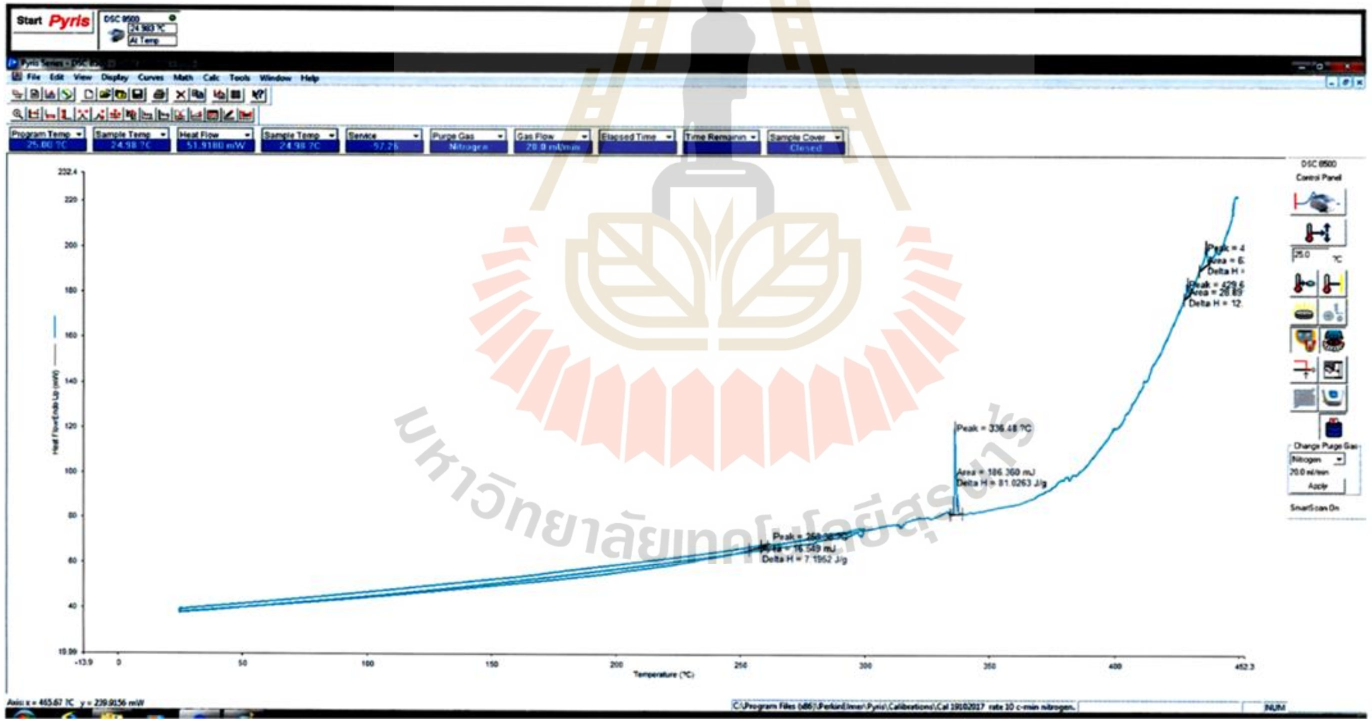

Program Temp 25.00 °C

Sample Temp 24.98 °C

Heat Flow 51.9180 mW

Sample Temp 24.98 °C

Service 57.25

Purge Gas Nitrogen

Gas Flow 20.0 ml/min

Elapsed Time

Time Remainin

Sample Cover Closed

Peak = 260.38 °C
Area = 16.549 mJ
Delta H = 7.1962 J/g

Peak = 336.48 °C
Area = 186.360 mJ
Delta H = 81.0263 J/g

Peak = 429.6
Area = 28.89
Delta H = 12.

Peak = 4
Area = 6.
Delta H =

Axis: x = 463.67 °C y = 239.9156 mW

C:\Program Files (x86)\PerkinElmer\Pyris\Calibrations\Cal 19102017 rate 10 c-min nitrogen.

APPENDIX C

DSC ANALYSIS OF COMPOUND 51

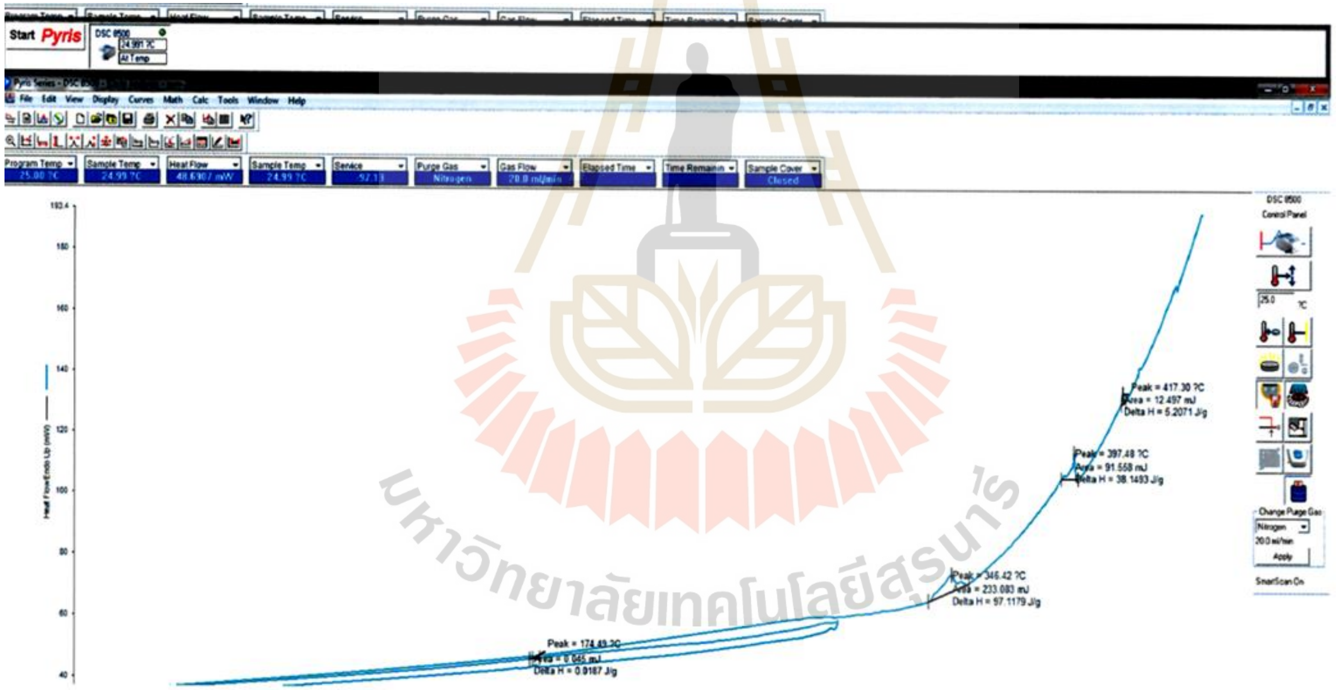

Program Temp: 25.00 ?C
Sample Temp: 24.99 ?C
Heat Flow: 48.6907 mW
Sample Temp: 24.99 ?C
Service: 57.13
Purge Gas: Nitrogen
Gas Flow: 20.0 ml/min
Elapsed Time:
Time Remainin:
Sample Cover: Closed

Peak = 174.49 ?C
Area = 0.045 mJ
Delta H = 0.0187 J/g

Peak = 346.42 ?C
Area = 233.083 mJ
Delta H = 97.1179 J/g

Peak = 397.48 ?C
Area = 91.558 mJ
Delta H = 38.1493 J/g

Peak = 417.30 ?C
Area = 12.497 mJ
Delta H = 5.2071 J/g

CURRICULUM VITAE

Name	Miss sumita boonnab
Date of Birth	2 April 1978
Place of Birth	Nakhon Ratchasima
Education	1 July 2014
Grants and Fellowships	National Science and Technology Development Agency (NSTDA) scholarship scheme and Nakhonratchasima Ratjabhat University
Position and Place of Work	Nakhonratchasima Ratjabhat University Suranarai Road, Nai Mueang Sub-district Mueang District,Nakhon Ratchasima Province 30000 Tel. 0-4400-9009 Fax 0-4424-4739